

CREEP OF NEXTEL 720/A CERAMIC MATRIX COMPOSITE WITH LASER DRILLED EFFUSION HOLES AT 1200°C IN AIR AND IN STEAM

THESIS

Savannah N. Minor, 2nd Lieutenant, USAF

AFIT-ENY-MS-18-M-279

DEPARTMENT OF THE AIR FORCE
AIR UNIVERSITY

AIR FORCE INSTITUTE OF TECHNOLOGY

Wright-Patterson Air Force Base, Ohio

DISTRIBUTION STATEMENT A:
APPROVED FOR PUBLIC RELEASE; DISTRIBUTION UNLIMITED.

The views expressed in this thesis are those of the author and do not reflect the official policy or position of the United States Air Force, Department of Defense, or the United States Government. This material is declared a work of the U.S. Government and is not subject to copyright protection in the United States.

AFIT-ENY-18-M-279

CREEP OF NEXTEL 720A CERAMIC MATRIX COMPOSITE WITH LASER DRILLED EFFUSION HOLES AT 1200°C IN AIR AND IN STEAM

THESIS

Presented to the Faculty

Department of Aeronautics and Astronautics

Graduate School of Engineering and Management

Air Force Institute of Technology

Air University

Air Education and Training Command

In Partial Fulfillment of the Requirements for the

Degree of Master of Science in Aeronautical Engineering

Savannah N. Minor, BS

2nd Lieutenant, USAF

March 2018

DISTRIBUTION STATEMENT A.
APPROVED FOR PUBLIC RELEASE; DISTRIBUTION UNLIMITED.

AFIT-ENY-18-M-279

CREEP OF NEXTEL 720/A CERAMIC MATRIX COMPOSITE WITH LASER DRILLED EFFUSION HOLES AT 1200°C IN AIR AND IN STEAM

Savannah N. Minor, BS
2nd Lieutenant, USAF

Committee Membership:

Dr. Marina B. Ruggles-Wrenn
Chair

Dr. Eric L. Jones
Member

Dr. Craig P. Przybyla
Member

Abstract

Creep behavior of an oxide-oxide ceramic matrix composite (CMC) containing an array of effusion holes was investigated at 1200ºC in laboratory air and in steam. The composite (N720/A) consisted of a porous alumina matrix reinforced with alumina-mullite Nextel™ 720 fibers. Test specimens had an array of 17 effusion holes with 0.5-mm diameter. The effusion holes were drilled through the specimen thickness normal to the specimen surface using a CO_2 laser. Effect of the effusion holes on tensile properties was evaluated in a tension test to failure at 1200°C in air. In addition, unnotched specimens were also tested in tension to failure to ensure the tensile properties of the current composite panel were consistent with those from previous work. Creep of specimens with effusion holes at 1200°C was studied for creep stresses ranging from 40 to 100 MPa in air and from 30 to 90 MPa in steam. Creep run-out was defined as 100 h at creep stress. All specimens that achieved run-out were then subjected to a tensile test to failure at 1200°C to evaluate retained tensile strength. Effect of the laser-drilled effusion holes on creep was assessed by comparing the results of the present study with the results from prior work on unnotched N720/A specimens. The presence of laser-drilled holes significantly reduced creep lifetimes in both air and steam. Degradation in creep performance due to steam for specimens with holes was similar to that reported for the unnotched specimens in prior work. Post-test microstructure of the composite was examined; damage and failure mechanisms were assessed. Dramatic loss of creep resistance in specimens with holes is due to extensive composite degradation caused by laser drilling.

Acknowledgments

I would like to thank my advisor, Dr. Marina Ruggles-Wrenn. She was an exceptional mentor and an excellent professor. I have learned much more than I thought possible through every class, every hour in the lab, and every moment spent working on my research. I would also like to thank my sponsors for allowing me to work on a project that I developed a great passion for. To the lab technicians thank you for your hours of patience and willingness to help me work through any piece of malfunctioning equipment. I would also like to thank my parents. Their love for education and continued support in every trial I face has gotten me where I am today. To my fiancée, your love and encouragement through hours of work has not gone unnoticed. Know that I have deeply appreciated every dinner made when I was too distracted to worry about it. Finally, thank you to my little puppy. Her constant companionship through hours of writing made it much more bearable.

Savannah N. Minor

Table of Contents

Abstract v

Table of Contents vii

List of Figures ix

List of Tables xxix

I. Introduction and Background 1

1.1 Ceramic Matrix Composites 2

1.2 Oxide/Oxide Ceramic Matrix Composites 5

1.2.1 Fibers 6

1.2.2 Matrix Materials 6

1.3 Background on Laser Drilling 6

1.4 Oxide-Oxide CMCs - Previous Efforts 7

1.4.1 Mechanical Behavior 7

1.4.2 Notch Sensitivity of CMCs 8

II. Material and Test Specimen 12

2.1 Material 12

2.2 Test Specimen Geometry 12

III. Experimental Arrangements and Procedures 16

3.1 Testing Equipment 16

3.2 Test Procedures 24

IV. Results and Discussion 32

4.1 Thermal Expansion 32

4.2 Monotonic Tensile Tests 34

4.3 Creep Rupture Tests at 1200 ºC 34

4.4 Retained Properties 40

4.5 Effect of Laser Drilled Holes on Creep Performance of N720/A at 1200°C in Air and in Steam 40
4.6 Composite Microstructure 43
V. Conclusions and Recommendations 53
5.1 Concluding Remarks 53
5.2 Recommendations 54
Appendix A. Optical Images 55
Appendix B. Scanning Electron Microscope Images 119
Appendix C. Exploration of Hi-Nicalon™ SiC/SiC CMC with an EBC 141
C.1 Material and Test Specimen 141
C.2 Monotonic Tensile Tests 142
C.3 Pre-Testing Optical Images 143
Bibliography 153

List of Figures

Figure 1: Maximum Material Service Temperature for Polymer Matrix Composites, Metals, and Ceramic Matrix Composites [1, p. 5] 2

Figure 2: Difference of crack propagation between a strong and weak interface [1, p. 170] ... 3

Figure 3: Illustration of (a) weak interface concept commonly achieved through fiber coating and (b) porous matrix concept used to achieve damage tolerance in CMCs. After Zok [3] 4

Figure 4: Test specimen (dimensions in mm). 13

Figure 5: Drawing sent to New Tech Precision in order to laser drill the effusion holes 14

Figure 6: Specimen with completed effusion holes 14

Figure 7: MTS 810 Material Test System 17

Figure 8: AMTECO Hot-Rail Furnace 18

Figure 9: MTS Temperature Controller 19

Figure 10: AMTECO Steam System 20

Figure 11: Alumina susceptor mounted around a test specimen 21

Figure 12: Zeiss optical microscope utilized for pre-test and post-test examination of specimens 22

Figure 13: EMS Quorum sputtering machine. 23

Figure 14: Quanta FEG 650 Scanning Electron Microscope 23

Figure 15: Temperature calibration specimen instrumented with R-type thermocouples secured using alumina pieces and high temperature wire. 25

Figure 16: Test specimen with tabs 26

Figure 17: Monotonic Tensile Test Procedure 29

Figure 18: Creep Rupture Test Procedure 30

Figure 19: Cut and mounted specimen prepared for SEM examination..... 31
Figure 20: Creep strain vs. time curves obtained for N720/A specimens with laser drilled effusion holes in air at 1200ºC. Figure a) is a shorter time scale for clarity while Figure b) shows time until runout. 36
Figure 21: Creep strain vs. time curves obtained for N720/A specimens with laser drilled effusion holes in steam at 1200ºC. Figure a) is a shorter time scale for clarity while Figure b) shows time until runout..... 37
Figure 22: Creep stress vs. time to rupture for N720/A specimens with laser drilled effusion holes in air and steam at 1200ºC..... 38
Figure 23: Minimum creep rate vs. creep stress for N720/A specimens with laser drilled effusion holes tested in air and steam at 1200ºC. 39
Figure 24: Creep stress vs. time to rupture for N720/A specimens with and without laser drilled effusion holes in air and in steam at 1200°C..... 41
Figure 25: Creep stress vs. creep strain rate for N720/A specimens with laser drilled effusion holes and without at 1200ºC in air and steam..... 43
Figure 26: Pre-Test optical micrographs of N720/A specimens with effusion holes showing material in the vicinity of randomly selected holes. 44
Figure 27: Optical micrograph of the N720/A specimen with effusion holes tested in tension to failure at 1200ºC showing material in the vicinity of a hole. 45
Figure 28: Optical micrograph of the N720/A specimen with effusion holes tested in tension to failure following 100 h of creep at 40 MPa at 1200°C in air. Formation of glassy phase and lack of fiber pull-out around effusion holes are clearly visible. 45

Figure 29: Optical micrograph of the N720/A specimen with effusion holes tested in creep at 1200ºC in air (σ_{cr} = 65 MPa, t_f = 58.4 h). Fusing of fiber and matrix as well as lack of fiber pull-out in the vicinity of the hole are clearly visible. 46

Figure 30: Optical micrograph of the N720/A specimen with effusion holes tested in tension to failure following 100 h of creep at 30 MPa at 1200°C in steam. Formation of glassy phase and lack of fiber pull-out around effusion holes are clearly visible. 46

Figure 31: Fracture surfaces obtained for N720/A specimens with effusion holes in creep tests conducted at 1200 °C in air: (a) σ_{cr} = 40 MPa, (b) σ_{cr} = 65 MPa, and (c) σ_{cr} = 100 MPa..... 47

Figure 32: Fracture surfaces obtained for N720/A specimens with effusion holes in creep tests conducted at 1200 °C in steam: (a) σ_{cr} = 40 MPa, (b) σ_{cr} = 65 MPa, and (c) σ_{cr} = 100 MPa..... 47

Figure 33: Fracture surface of a N720/A specimen tested in creep in laboratory air at 1200ºC (σ_{cr} = 65 MPa, t_f = 58.4 h). a) Edge of the hole and the glassy phase found in the interior of the hole are clearly visible. (b) Higher magnification view showing edge of the hole and glassy phase in the interior of the hole. 50

Figure 34: Fracture surface of a N720/A specimen tested in creep in steam at 1200ºC (σ_{cr} = 65 MPa, t_f = 12.4 h). Correlated fiber fracture and fiber/matrix bonding in the vicinity of the hole (top half of the image). Glassy phase in the hole interior (bottom half of the image). 51

Figure 35: Fracture surface of a N720/A specimen tested in creep in steam at 1200ºC (σ_{cr} = 65 MPa, t_f = 12.4 h). Correlated fiber fracture, fiber/matrix bonding and absence of fiber pull-out are apparent. 51

Figure 36: Fracture surface of a N720/A specimen tested in tension to failure following 100 h of creep at 40 MPa in laboratory air at 1200ºC. 52

Figure A. 1: Pre-test optical image of the hole pattern in a specimen. 55

Figure A. 2: Pre-test optical image of a randomly selected hole. 55

Figure A. 3: Pre-test optical image of a randomly selected hole. 56

Figure A. 4: Pre-test optical image of a randomly selected hole. 56

Figure A. 5: Pre-test optical image of a randomly selected hole. 57

Figure A. 6: Pre-test optical image of a randomly selected hole. 57

Figure A. 7: Pre-test optical image of a randomly selected hole. 58

Figure A. 8: Pre-test optical image of a randomly selected hole. 58

Figure A. 9: Pre-test optical image of a randomly selected hole. 59

Figure A. 10: Pre-test optical image of a randomly selected hole. 59

Figure A. 11: Fracture surface obtained for an unnotched N720/A specimen in tension to failure at 1200ºC in air. 60

Figure A. 12: Fracture surface obtained for an unnotched N720/A specimen in tension to failure at 1200ºC in air. 60

Figure A. 13: Fracture surface obtained for an unnotched N720/A specimen in tension to failure at 1200ºC in air. 61

Figure A. 14: Fracture surface obtained for an unnotched N720/A specimen in tension to failure at 1200ºC in air. 61

Figure A. 15: Fracture surface obtained for an unnotched N720/A specimen in tension to failure at 1200ºC in air. 62

Figure A. 16: Fracture surface obtained for an unnotched N720/A specimen in tension to failure at 1200ºC in air. 62
Figure A. 17: Fracture surface obtained for an unnotched N720/A specimen in tension to failure at 1200ºC in air. 63
Figure A. 18: Fracture surface obtained for an unnotched N720/A specimen in tension to failure at 1200ºC in air. 63
Figure A. 19: Fracture surface obtained for a N720/A specimen with effusion holes in tension to failure at 1200ºC in air. 64
Figure A. 20: Fracture surface obtained for a N720/A specimen with effusion holes in tension to failure at 1200ºC in air. 64
Figure A. 21: Fracture surface obtained for a N720/A specimen with effusion holes in tension to failure at 1200ºC in air. 65
Figure A. 22: Fracture surface obtained for a N720/A specimen with effusion holes in tension to failure at 1200ºC in air. 65
Figure A. 23: Fracture surface obtained for a N720/A specimen with effusion holes in tension to failure at 1200ºC in air. 66
Figure A. 24: Fracture surface obtained for a N720/A specimen with effusion holes in tension to failure at 1200ºC in air. 66
Figure A. 25: Fracture surface obtained for a N720/A specimen with effusion holes in tension to failure at 1200ºC in air. 67
Figure A. 26: Fracture surface obtained for a N720/A specimen with effusion holes in tension to failure at 1200ºC in air. 67

Figure A. 27: Fracture surface obtained for a N720/A specimen with effusion holes in tension to failure at 1200ºC in air. 68
Figure A. 28: Fracture surface obtained for a N720/A specimen with effusion holes in tension to failure at 1200ºC in air. 68
Figure A. 29: Fracture surface obtained for a N720/A specimen with effusion holes in tension to failure at 1200ºC in air. 69
Figure A. 30: Fracture surface obtained for a N720/A specimen with effusion holes in tension to failure following 100 h of creep at 40 MPa at 1200ºC in air. 69
Figure A. 31: Fracture surface obtained for a N720/A specimen with effusion holes in tension to failure following 100 h of creep at 40 MPa at 1200ºC in air. 70
Figure A. 32: Fracture surface obtained for a N720/A specimen with effusion holes in tension to failure following 100 h of creep at 40 MPa at 1200ºC in air. 70
Figure A. 33: Fracture surface obtained for a N720/A specimen with effusion holes in tension to failure following 100 h of creep at 40 MPa at 1200ºC in air. 71
Figure A. 34: Fracture surface obtained for a N720/A specimen with effusion holes in tension to failure following 100 h of creep at 40 MPa at 1200ºC in air. 71
Figure A. 35: Fracture surface obtained for a N720/A specimen with effusion holes in tension to failure following 100 h of creep at 40 MPa at 1200ºC in air. 72
Figure A. 36: Fracture surface obtained for a N720/A specimen with effusion holes in tension to failure following 100 h of creep at 40 MPa at 1200ºC in air. 72
Figure A. 37: Fracture surface obtained for a N720/A specimen with effusion holes in creep at 1200ºC in air (σcr = 65 MPa, t_f = 58.4 h). 73

Figure A. 38: Fracture surface obtained for a N720/A specimen with effusion holes in creep at 1200ºC in air (σ_{cr} = 65 MPa, t_f = 58.4 h). 73
Figure A. 39: Fracture surface obtained for a N720/A specimen with effusion holes in creep at 1200ºC in air (σ_{cr} = 65 MPa, t_f = 58.4 h). 74
Figure A. 40: Fracture surface obtained for a N720/A specimen with effusion holes in creep at 1200ºC in air (σ_{cr} = 65 MPa, t_f = 58.4 h). 74
Figure A. 41: Fracture surface obtained for a N720/A specimen with effusion holes in creep at 1200ºC in air (σ_{cr} = 65 MPa, t_f = 58.4 h). 75
Figure A. 42: Fracture surface obtained for a N720/A specimen with effusion holes in creep at 1200ºC in air (σ_{cr} = 65 MPa, t_f = 58.4 h). 75
Figure A. 43: Fracture surface obtained for a N720/A specimen with effusion holes in creep at 1200ºC in air (σ_{cr} = 65 MPa, t_f = 58.4 h). 76
Figure A. 44: Fracture surface obtained for a N720/A specimen with effusion holes in creep at 1200ºC in air (σ_{cr} = 65 MPa, t_f = 58.4 h). 76
Figure A. 45: Fracture surface obtained for a N720/A specimen with effusion holes in creep at 1200ºC in air (σ_{cr} = 65 MPa, t_f = 58.4 h). 77
Figure A. 46: Fracture surface obtained for a N720/A specimen with effusion holes in creep at 1200ºC in air (□cr = 80 MPa, tf = 30.4 h). 77
Figure A. 47: Fracture surface obtained for a N720/A specimen with effusion holes in creep at 1200ºC in air (σ_{cr} = 80 MPa, t_f = 30.4 h). 78
Figure A. 48: Fracture surface obtained for a N720/A specimen with effusion holes in creep at 1200ºC in air (σ_{cr} = 80 MPa, t_f = 30.4 h). 78

Figure A. 49: Fracture surface obtained for a N720/A specimen with effusion holes in creep at 1200ºC in air (σ_{cr} = 80 MPa, t_f = 30.4 h). 79
Figure A. 50: Fracture surface obtained for a N720/A specimen with effusion holes in creep at 1200ºC in air (σ_{cr} = 80 MPa, t_f = 30.4 h). 79
Figure A. 51: Fracture surface obtained for a N720/A specimen with effusion holes in creep at 1200ºC in air (σ_{cr} = 80 MPa, t_f = 30.4 h). 80
Figure A. 52: Fracture surface obtained for a N720/A specimen with effusion holes in creep at 1200ºC in air (σ_{cr} = 80 MPa, t_f = 30.4 h). 80
Figure A. 53: Fracture surface obtained for a N720/A specimen with effusion holes in creep at 1200ºC in air (σ_{cr} = 80 MPa, t_f = 30.4 h). 81
Figure A. 54: Fracture surface obtained for a N720/A specimen with effusion holes in creep at 1200ºC in air (σ_{cr} = 80 MPa, t_f = 30.4 h). 81
Figure A. 55: Fracture surface obtained for a N720/A specimen with effusion holes in creep at 1200ºC in air (σ_{cr} = 80 MPa, t_f = 30.4 h). 82
Figure A. 56: Fracture surface obtained for a N720/A specimen with effusion holes in creep at 1200ºC in air (σ_{cr} = 80 MPa, t_f = 30.4 h). 82
Figure A. 57: Fracture surface obtained for a N720/A specimen with effusion holes in creep at 1200ºC in air (σ_{cr} = 90 MPa, t_f = 9.65 h). 83
Figure A. 58: Fracture surface obtained for a N720/A specimen with effusion holes in creep at 1200ºC in air (σ_{cr} = 90 MPa, t_f = 9.65 h). 83
Figure A. 59: Fracture surface obtained for a N720/A specimen with effusion holes in creep at 1200ºC in air (σ_{cr} = 90 MPa, t_f = 9.65 h). 84

Figure A. 60: Fracture surface obtained for a N720/A specimen with effusion holes in creep at 1200ºC in air (σ_{cr} = 90 MPa, t_f = 9.65 h). 84
Figure A. 61: Fracture surface obtained for a N720/A specimen with effusion holes in creep at 1200ºC in air (σ_{cr} = 90 MPa, t_f = 9.65 h). 85
Figure A. 62: Fracture surface obtained for a N720/A specimen with effusion holes in creep at 1200ºC in air (□cr = 90 MPa, tf = 9.65 h). 85
Figure A. 63: Fracture surface obtained for a N720/A specimen with effusion holes in creep at 1200ºC in air (σ_{cr} = 100 MPa, t_f = 0.538 h). 86
Figure A. 64: Fracture surface obtained for a N720/A specimen with effusion holes in creep at 1200ºC in air (σ_{cr} = 100 MPa, t_f = 0.538 h). 86
Figure A. 65: Fracture surface obtained for a N720/A specimen with effusion holes in creep at 1200ºC in air (σ_{cr} = 100 MPa, t_f = 0.538 h). 87
Figure A. 66: Fracture surface obtained for a N720/A specimen with effusion holes in creep at 1200ºC in air (σ_{cr} = 100 MPa, t_f = 0.538 h). 87
Figure A. 67: Fracture surface obtained for a N720/A specimen with effusion holes in creep at 1200ºC in air (σ_{cr} = 100 MPa, t_f = 0.538 h). 88
Figure A. 68: Fracture surface obtained for a N720/A specimen with effusion holes in creep at 1200ºC in air (σ_{cr} = 100 MPa, t_f = 0.538 h). 88
Figure A. 69: Fracture surface obtained for a N720/A specimen with effusion holes in creep at 1200ºC in air (σ_{cr} = 100 MPa, t_f = 0.538 h). 89
Figure A. 70: Fracture surface obtained for a N720/A specimen with effusion holes in creep at 1200ºC in air (σ_{cr} = 100 MPa, t_f = 0.538 h). 89

Figure A. 71: Fracture surface obtained for a N720/A specimen with effusion holes in creep at 1200ºC in air (σ_{cr} = 150 MPa, t_f = 0.0038 h). 90
Figure A. 72: Fracture surface obtained for a N720/A specimen with effusion holes in creep at 1200ºC in air (σ_{cr} = 150 MPa, t_f = 0.0038 h). 90
Figure A. 73: Fracture surface obtained for a N720/A specimen with effusion holes in creep at 1200ºC in air (σ_{cr} = 150 MPa, t_f = 0.0038 h). 91
Figure A. 74: Fracture surface obtained for a N720/A specimen with effusion holes in creep at 1200ºC in air (σ_{cr} = 150 MPa, t_f = 0.0038 h). 91
Figure A. 75: Fracture surface obtained for a N720/A specimen with effusion holes in creep at 1200ºC in air (σ_{cr} = 150 MPa, t_f = 0.0038 h). 92
Figure A. 76: Fracture surface obtained for a N720/A specimen with effusion holes in creep at 1200ºC in air (σ_{cr} = 150 MPa, t_f = 0.0038 h). 92
Figure A. 77: Fracture surface obtained for a N720/A specimen with effusion holes in creep at 1200ºC in air (σ_{cr} = 150 MPa, t_f = 0.0038 h). 93
Figure A. 78: Fracture surface obtained for a N720/A specimen with effusion holes in creep at 1200ºC in air (σ_{cr} = 150 MPa, t_f = 0.0038 h). 93
Figure A. 79: Fracture surface obtained for a N720/A specimen with effusion holes in creep at 1200ºC in air (σ_{cr} = 150 MPa, t_f = 0.0038 h). 94
Figure A. 80: Fracture surface obtained for a N720/A specimen with effusion holes in creep at 1200ºC in air (σ_{cr} = 150 MPa, t_f = 0.0038 h). 94
Figure A. 81: Fracture surface obtained for a N720/A specimen with effusion holes in tension to failure following 100 h of creep at 30 MPa at 1200ºC in steam. 95

Figure A. 82: Fracture surface obtained for a N720/A specimen with effusion holes in tension to failure following 100 h of creep at 30 MPa at 1200ºC in steam. 95
Figure A. 83: Fracture surface obtained for a N720/A specimen with effusion holes in tension to failure following 100 h of creep at 30 MPa at 1200ºC in steam. 96
Figure A. 84: Fracture surface obtained for a N720/A specimen with effusion holes in tension to failure following 100 h of creep at 30 MPa at 1200ºC in steam. 96
Figure A. 85: Fracture surface obtained for a N720/A specimen with effusion holes in tension to failure following 100 h of creep at 30 MPa at 1200ºC in steam. 97
Figure A. 86: Fracture surface obtained for a N720/A specimen with effusion holes in tension to failure following 100 h of creep at 30 MPa at 1200ºC in steam. 97
Figure A. 87: Fracture surface obtained for a N720/A specimen with effusion holes in tension to failure following 100 h of creep at 30 MPa at 1200ºC in steam. 98
Figure A. 88: Fracture surface obtained for a N720/A specimen with effusion holes in tension to failure following 100 h of creep at 30 MPa at 1200ºC in steam. 98
Figure A. 89: Fracture surface obtained for a N720/A specimen with effusion holes in tension to failure following 100 h of creep at 30 MPa at 1200ºC in steam. 99
Figure A. 90: Fracture surface obtained for a N720/A specimen with effusion holes in creep at 1200ºC in steam (σ_{cr} = 40 MPa, t_f = 98.79 h). 99
Figure A. 91: Fracture surface obtained for a N720/A specimen with effusion holes in creep at 1200ºC in steam (σ_{cr} = 40 MPa, t_f = 98.79 h). 100
Figure A. 92: Fracture surface obtained for a N720/A specimen with effusion holes in creep at 1200ºC in steam (σ_{cr} = 40 MPa, t_f = 98.79 h). 100

Figure A. 93: Fracture surface obtained for a N720/A specimen with effusion holes in creep at 1200ºC in steam (σ_{cr} = 40 MPa, t_f = 98.79 h). 101
Figure A. 94: Fracture surface obtained for a N720/A specimen with effusion holes in creep at 1200ºC in steam (σ_{cr} = 40 MPa, t_f = 98.79 h). 101
Figure A. 95: Fracture surface obtained for a N720/A specimen with effusion holes in creep at 1200ºC in steam (σ_{cr} = 40 MPa, t_f = 98.79 h). 102
Figure A. 96: Fracture surface obtained for a N720/A specimen with effusion holes in creep at 1200ºC in steam (σ_{cr} = 40 MPa, t_f = 98.79 h). 102
Figure A. 97: Fracture surface obtained for a N720/A specimen with effusion holes in creep at 1200ºC in steam (σ_{cr} = 40 MPa, t_f = 98.79 h). 103
Figure A. 98: Fracture surface obtained for a N720/A specimen with effusion holes in creep at 1200ºC in steam (σ_{cr} = 65 MPa, t_f = 12.44 h). 103
Figure A. 99: Fracture surface obtained for a N720/A specimen with effusion holes in creep at 1200ºC in steam (σ_{cr} = 65 MPa, t_f = 12.44 h). 104
Figure A. 100: Fracture surface obtained for a N720/A specimen with effusion holes in creep at 1200ºC in steam (σ_{cr} = 65 MPa, t_f = 12.44 h). 104
Figure A. 101: Fracture surface obtained for a N720/A specimen with effusion holes in creep at 1200ºC in steam (σ_{cr} = 65 MPa, t_f = 12.44 h). 105
Figure A. 102: Fracture surface obtained for a N720/A specimen with effusion holes in creep at 1200ºC in steam (σ_{cr} = 65 MPa, t_f = 12.44 h). 105
Figure A. 103: Fracture surface obtained for a N720/A specimen with effusion holes in creep at 1200ºC in steam (σ_{cr} = 65 MPa, t_f = 12.44 h). 106

Figure A. 104: Fracture surface obtained for a N720/A specimen with effusion holes in creep at 1200ºC in steam (σ_{cr} = 80 MPa, t_f = 1.605 h). 106
Figure A. 105: Fracture surface obtained for a N720/A specimen with effusion holes in creep at 1200ºC in steam (σ_{cr} = 80 MPa, t_f = 1.605 h). 107
Figure A. 106: Fracture surface obtained for a N720/A specimen with effusion holes in creep at 1200ºC in steam (σ_{cr} = 80 MPa, t_f = 1.605 h). 107
Figure A. 107: Fracture surface obtained for a N720/A specimen with effusion holes in creep at 1200ºC in steam (σ_{cr} = 80 MPa, t_f = 1.605 h). 108
Figure A. 108: Fracture surface obtained for a N720/A specimen with effusion holes in creep at 1200ºC in steam (σ_{cr} = 80 MPa, t_f = 1.605 h). 108
Figure A. 109: Fracture surface obtained for a N720/A specimen with effusion holes in creep at 1200ºC in steam (σ_{cr} = 80 MPa, t_f = 1.605 h). 109
Figure A. 110: Fracture surface obtained for a N720/A specimen with effusion holes in creep at 1200ºC in steam (σ_{cr} = 80 MPa, t_f = 1.605 h). 109
Figure A. 111: Fracture surface obtained for a N720/A specimen with effusion holes in creep at 1200ºC in steam (σ_{cr} = 80 MPa, t_f = 1.605 h). 110
Figure A. 112: Fracture surface obtained for a N720/A specimen with effusion holes in creep at 1200ºC in steam (σ_{cr} = 80 MPa, t_f = 1.605 h). 110
Figure A. 113: Fracture surface obtained for a N720/A specimen with effusion holes in creep at 1200ºC in steam (σ_{cr} = 90 MPa, t_f = 0.572 h). 111
Figure A. 114: Fracture surface obtained for a N720/A specimen with effusion holes in creep at 1200ºC in steam (σ_{cr} = 90 MPa, t_f = 0.572 h). 111

Figure A. 115: Fracture surface obtained for a N720/A specimen with effusion holes in creep at 1200ºC in steam (σ_{cr} = 90 MPa, t_f = 0.572 h). 112
Figure A. 116: Fracture surface obtained for a N720/A specimen with effusion holes in creep at 1200ºC in steam (σ_{cr} = 90 MPa, t_f = 0.572 h). 112
Figure A. 117: Fracture surface obtained for a N720/A specimen with effusion holes in creep at 1200ºC in steam (σ_{cr} = 90 MPa, t_f = 0.572 h). 113
Figure A. 118: Fracture surface obtained for a N720/A specimen with effusion holes in creep at 1200ºC in steam (σ_{cr} = 90 MPa, t_f = 0.572 h). 113
Figure A. 119: Fracture surface obtained for a N720/A specimen with effusion holes in creep at 1200ºC in steam (σ_{cr} = 90 MPa, t_f = 0.572 h). 114
Figure A. 120: Fracture surface obtained for a N720/A specimen with effusion holes in creep at 1200ºC in steam (σ_{cr} = 90 MPa, t_f = 0.572 h). 114
Figure A. 121: Fracture surface obtained for a N720/A specimen with effusion holes in creep at 1200ºC in steam (σ_{cr} = 100 MPa, t_f = 0.141 h). 115
Figure A. 122: Fracture surface obtained for a N720/A specimen with effusion holes in creep at 1200ºC in steam (σ_{cr} = 100 MPa, t_f = 0.141 h). 115
Figure A. 123: Fracture surface obtained for a N720/A specimen with effusion holes in creep at 1200ºC in steam (σ_{cr} = 100 MPa, t_f = 0.141 h). 116
Figure A. 124: Fracture surface obtained for a N720/A specimen with effusion holes in creep at 1200ºC in steam (σ_{cr} = 100 MPa, t_f = 0.141 h). 116
Figure A. 125: Fracture surface obtained for a N720/A specimen with effusion holes in creep at 1200ºC in steam (σ_{cr} = 100 MPa, t_f = 0.141 h). 117

Figure A. 126: Fracture surface obtained for a N720/A specimen with effusion holes in creep at 1200ºC in steam (σ_{cr} = 100 MPa, t_f = 0.141 h). 117
Figure A. 127: Fracture surface obtained for a N720/A specimen with effusion holes in creep at 1200ºC in steam (σ_{cr} = 100 MPa, t_f = 0.141 h). 118

Figure B. 1: Fracture surface obtained for an unnotched N720/A specimen in tension to failure at 1200ºC in air. 119
Figure B. 2: Fracture surface obtained for an unnotched N720/A specimen in tension to failure at 1200ºC in air. 119
Figure B. 3: Fracture surface obtained for an unnotched N720/A specimen in tension to failure at 1200ºC in air. 120
Figure B. 4: Fracture surface obtained for an unnotched N720/A specimen in tension to failure at 1200ºC in air. 120
Figure B. 5: Fracture surface obtained for an unnotched N720/A specimen in tension to failure at 1200ºC in air. 121
Figure B. 6: Fracture surface obtained for a N720/A specimen with effusion holes in tension to failure at 1200ºC in air. 121
Figure B. 7: Fracture surface obtained for a N720/A specimen with effusion holes in tension to failure at 1200ºC in air. 122
Figure B. 8: Fracture surface obtained for a N720/A specimen with effusion holes in tension to failure at 1200ºC in air. 122
Figure B. 9: Fracture surface obtained for a N720/A specimen with effusion holes in tension to failure at 1200ºC in air. 123

Figure B. 10: Fracture surface obtained for a N720/A specimen with effusion holes in tension to failure at 1200ºC in air. 123
Figure B. 11: Fracture surface obtained for a N720/A specimen with effusion holes in tension to failure at 1200ºC in air. 124
Figure B. 12: Fracture surface obtained for a N720/A specimen with effusion holes in tension to failure at 1200ºC in air. 124
Figure B. 13: Fracture surface obtained for a N720/A specimen with effusion holes in tension to failure at 1200ºC in air. 125
Figure B. 14: Fracture surface obtained for a N720/A specimen with effusion holes in tension to failure at 1200ºC in air. 125
Figure B. 15: Fracture surface obtained for a N720/A specimen with effusion holes in creep at 1200ºC in air (σ_{cr} = 65 MPa, t_f = 58.4 h). 126
Figure B. 16: Fracture surface obtained for a N720/A specimen with effusion holes in creep at 1200ºC in air (σ_{cr} = 65 MPa, t_f = 58.4 h). 126
Figure B. 17: Fracture surface obtained for a N720/A specimen with effusion holes in creep at 1200ºC in air (σ_{cr} = 65 MPa, t_f = 58.4 h). 127
Figure B. 18: Fracture surface obtained for a N720/A specimen with effusion holes in creep at 1200ºC in air (σ_{cr} = 65 MPa, t_f = 58.4 h). 127
Figure B. 19: Fracture surface obtained for a N720/A specimen with effusion holes in creep at 1200ºC in air (σ_{cr} = 65 MPa, t_f = 58.4 h). 128
Figure B. 20: Fracture surface obtained for a N720/A specimen with effusion holes in creep at 1200ºC in air (σ_{cr} = 65 MPa, t_f = 58.4 h). 128

Figure B. 21: Fracture surface obtained for a N720/A specimen with effusion holes in creep at 1200ºC in steam (σ_{cr} = 65 MPa, t_f = 12.44 h). 129
Figure B. 22: Fracture surface obtained for a N720/A specimen with effusion holes in creep at 1200ºC in steam (σ_{cr} = 65 MPa, t_f = 12.44 h). 129
Figure B. 23: Fracture surface obtained for a N720/A specimen with effusion holes in creep at 1200ºC in steam (σ_{cr} = 65 MPa, t_f = 12.44 h). 130
Figure B. 24: Fracture surface obtained for a N720/A specimen with effusion holes in creep at 1200ºC in steam (σ_{cr} = 65 MPa, t_f = 12.44 h). 130
Figure B. 25: Fracture surface obtained for a N720/A specimen with effusion holes in creep at 1200ºC in steam (σ_{cr} = 65 MPa, t_f = 12.44 h). 131
Figure B. 26: Fracture surface obtained for a N720/A specimen with effusion holes in creep at 1200ºC in steam (σ_{cr} = 65 MPa, t_f = 12.44 h). 131
Figure B. 27: Fracture surface obtained for a N720/A specimen with effusion holes in tension to failure following 100 h of creep at 40 MPa at 1200ºC in air. 132
Figure B. 28: Fracture surface obtained for a N720/A specimen with effusion holes in tension to failure following 100 h of creep at 40 MPa at 1200ºC in air. 132
Figure B. 29: Fracture surface obtained for a N720/A specimen with effusion holes in tension to failure following 100 h of creep at 40 MPa at 1200ºC in air. 133
Figure B. 30: Fracture surface obtained for a N720/A specimen with effusion holes in tension to failure following 100 h of creep at 40 MPa at 1200ºC in air. 133
Figure B. 31: Fracture surface obtained for a N720/A specimen with effusion holes in tension to failure following 100 h of creep at 40 MPa at 1200ºC in air. 134

Figure B. 32: Fracture surface obtained for a N720/A specimen with effusion holes in tension to failure following 100 h of creep at 40 MPa at 1200ºC in air..... 134
Figure B. 33: Fracture surface obtained for a N720/A specimen with effusion holes in tension to failure following 100 h of creep at 40 MPa at 1200ºC in air..... 135
Figure B. 34: Fracture surface obtained for a N720/A specimen with effusion holes in tension to failure following 100 h of creep at 40 MPa at 1200ºC in air..... 135
Figure B. 35: Fracture surface obtained for a N720/A specimen with effusion holes in tension to failure following 100 h of creep at 40 MPa at 1200ºC in air..... 136
Figure B. 36: Fracture surface obtained for a N720/A specimen with effusion holes in tension to failure following 100 h of creep at 30 MPa at 1200ºC in steam 136
Figure B. 37: Fracture surface obtained for a N720/A specimen with effusion holes in tension to failure following 100 h of creep at 30 MPa at 1200ºC in steam 137
Figure B. 38: Fracture surface obtained for a N720/A specimen with effusion holes in tension to failure following 100 h of creep at 30 MPa at 1200ºC in steam 137
Figure B. 39: Fracture surface obtained for a N720/A specimen with effusion holes in tension to failure following 100 h of creep at 30 MPa at 1200ºC in steam. 138
Figure B. 40: Fracture surface obtained for a N720/A specimen with effusion holes in tension to failure following 100 h of creep at 30 MPa at 1200ºC in steam. 138
Figure B. 41: Fracture surface obtained for a N720/A specimen with effusion holes in tension to failure following 100 h of creep at 30 MPa at 1200ºC in steam. 139
Figure B. 42: Fracture surface obtained for a N720/A specimen with effusion holes in tension to failure following 100 h of creep at 30 MPa at 1200ºC in steam. 139

Figure B. 43: Fracture surface obtained for a N720/A specimen with effusion holes in tension to failure following 100 h of creep at 30 MPa at 1200ºC in steam. 140
Figure B. 44: Fracture surface obtained for a N720/A specimen with effusion holes in tension to failure following 100 h of creep at 30 MPa at 1200ºC in steam. 140

Figure C. 1: Specimen geometry for SiC/SiC CMC. All dimensions are in mm. 141
Figure C. 2: Coated SiC/SiC composite 142
Figure C. 3: Pre-Test optical image of coated SiC/SiC. 143
Figure C. 4: Pre-Test optical image of coated SiC/SiC. 143
Figure C. 5: Pre-Test optical image of coated SiC/SiC. 143
Figure C. 6: Pre-Test optical image of coated SiC/SiC. 144
Figure C. 7: Pre-Test optical image of coated SiC/SiC. 144
Figure C. 8: Pre-Test optical image of coated SiC/SiC. 144
Figure C. 9: Pre-Test optical image of coated SiC/SiC. 145
Figure C. 10: Pre-Test optical image of coated SiC/SiC. 145
Figure C. 11: Pre-Test optical image of coated SiC/SiC. 145
Figure C. 12: Pre-Test optical image of coated SiC/SiC. 146
Figure C. 13: Pre-Test optical image of coated SiC/SiC. 146
Figure C. 14: Pre-Test optical image of coated SiC/SiC. 146
Figure C. 15: Pre-Test optical image of coated SiC/SiC. 147
Figure C. 16: Pre-Test optical image of coated SiC/SiC. 147
Figure C. 17: Pre-Test optical image of coated SiC/SiC. 147
Figure C. 18: Pre-Test optical image of coated SiC/SiC. 148

Figure C. 19: Pre-Test optical image of coated SiC/SiC. 148
Figure C. 20: Pre-Test optical image of coated SiC/SiC. 148
Figure C. 21: Pre-Test optical image of coated SiC/SiC. 149
Figure C. 22: Pre-Test optical image of coated SiC/SiC. 149
Figure C. 23: Pre-Test optical image of coated SiC/SiC. 149
Figure C. 24: Pre-Test optical image of coated SiC/SiC. 150
Figure C. 25: Pre-Test optical image of coated SiC/SiC. 150
Figure C. 26: Pre-Test optical image of coated SiC/SiC. 150
Figure C. 27: Pre-test optical image of an SiC/SiC specimen without grit blasting. 151
Figure C. 28: Pre-test optical image of an SiC/SiC specimen without grit blasting. 151
Figure C. 29: Pre-test optical image of an SiC/SiC specimen with grit blasting. 152
Figure C. 30: Pre-test optical image of an SiC/SiC specimen with grit blasting. 152
Figure C. 31: Pre-test optical image of an SiC/SiC specimen with grit blasting. 152

List of Tables

Table 1: Physical Properties of N720/A Panels Supplied by COI [14] 12

Table 2: Specimen dimensions 15

Table 3: Temperature Set-Points (ºC) 26

Table 4: Testing Matrix 32

Table 5: Thermal strain and coefficients of linear thermal expansion for N720/A specimens. 33

Table 6: Creep stress values and time until failure. 39

Table 7: Summary of minimum creep strain rates obtained for the N720/A specimens with laser drilled effusion holes at 1200ºC in laboratory air and in steam environments. 40

I. Introduction and Background

Ceramic materials are known for their ability to withstand elevated temperatures. However, due to their brittle nature, monolithic ceramics exhibit a catastrophic mode of failure. Ceramic-matrix composites (CMCs) are capable of enduring high temperatures while maintaining excellent strength and fracture toughness. Early efforts on SiC fiber-reinforced SiC matrix composites revealed that SiC/SiC CMC's failed by oxidation embrittlement. The need to improve the thermodynamic stability and oxidation resistance of CMCs motivated the development of composites based on environmentally stable oxide fibers and oxide matrix materials.

The key advantage of the CMCs over monolithic ceramics is their superior toughness, flaw tolerance and non-catastrophic mode of failure. These desirable properties are achieved through a specific design of the fiber-matrix interphase, which provides for crack deflection around the fibers. It is widely recognized that the same flaw tolerant behavior in CMCs can be achieved by means of a finely distributed porosity in the matrix. The concept of a porous matrix has been successfully employed in the development on oxide/oxide composites, which combine excellent damage tolerance with inherent oxidation resistance.

This effort aims to characterize the creep behavior of the N720/A oxide-oxide ceramic-matrix composite with an array of laser drilled effusion holes. Tensile creep tests are performed at various creep stress levels at 1200ºC in laboratory air and in steam. Composite microstructure is examined before and after testing in order to assess damage and failure mechanisms.

1.1 Ceramic Matrix Composites

Ceramic matrix composites are ideal materials for operating in aggressive environments. Figure 1 compares the operating temperatures of CMCs to other common composites. The ability for CMCs to operate at very high temperatures opens many doors that were previously closed due to the operating temperature limits of other materials.

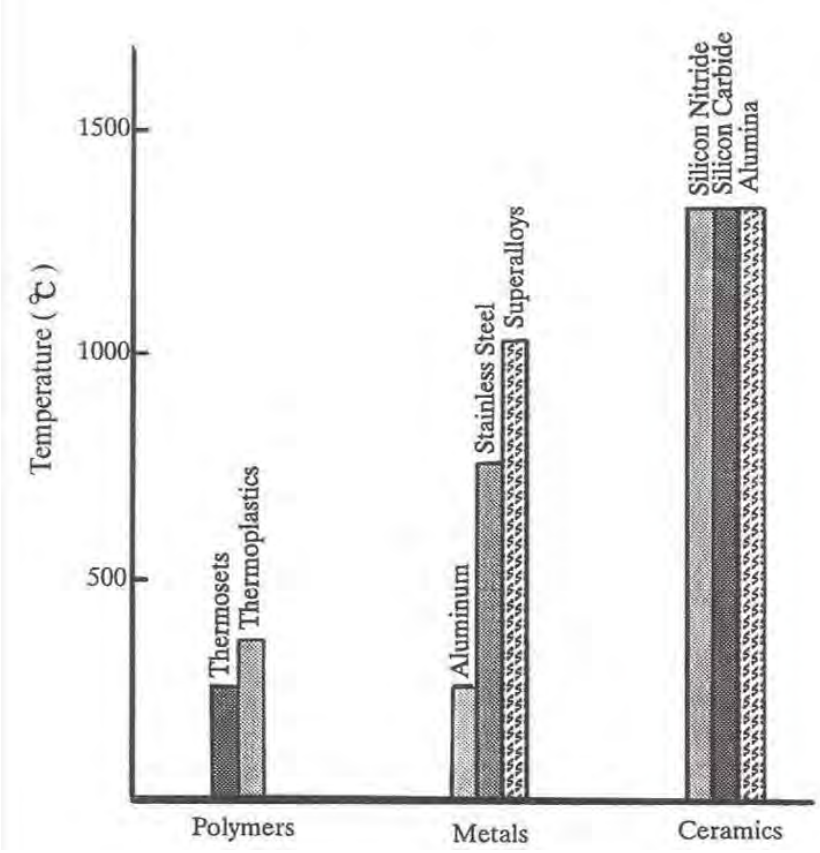


Figure 1: Maximum Material Service Temperature for Polymer Matrix Composites, Metals, and Ceramic Matrix Composites [1, p. 5]

Though structural ceramics have the ability to operate at much higher temperatures than other common composites, they lack fracture toughness, damage tolerance, and the ability to achieve a non-catastrophic failure. Ceramic matrix composites were developed specifically to address these shortcomings. Ceramic matrix composites are designed to exhibit toughness, tolerance to the presence of defects and cracks, and to fail gracefully. These desirable traits are

achieved by a proper design of the fiber/matrix interphase [1, p. 169]. If the fiber/matrix interphase is too strong, it will not stop a crack from propagating through the load-bearing fibers [1, p. 169]. The desired interface for a CMC is a weak fiber/matrix bond that will dissipate the energy of a crack propagating through the composite. Weak fiber/matrix interphase permits the fiber-reinforced CMCs their ability to undergo "inelastic" deformation and fail gracefully. Deformation proceeds through matrix cracking and the associated debonding and sliding along the fiber-matrix interfaces. Matrix cracks are thus deflected around the fibers. The fibers continue to carry the load and fail progressively at different locations within the composite. As a result, the CMC exhibits a non-catastrophic failure mode. Figure 2 depicts the difference between a strong interface and a weak interface [1, p. 170].

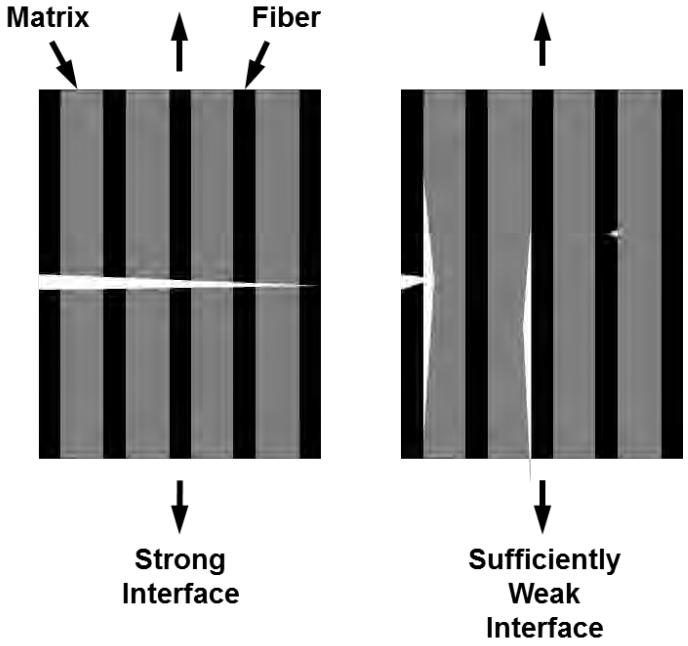


Figure 2: Difference of crack propagation between a strong and weak interface [1, p. 170]

The method of fiber coating has been utilized to combat the strong interface between fiber and matrix in CMCs. Fiber coating prevents the matrix from chemically bonding with the

fiber and results in the ability of the fiber to debond from the matrix and to move separately. For this method to work as desired, the matrix must be dense with as few flaws as possible to avoid crack initiation sites [2]. This method is successful for non-oxide materials such as silicon carbide fiber-silicon carbide matrix CMCs with boron nitride fiber coatings [1, p. 170]. Figure 3 (a) demonstrates the failure of a CMC seen when a fiber coating is used to create a weak fiber-matrix interface.

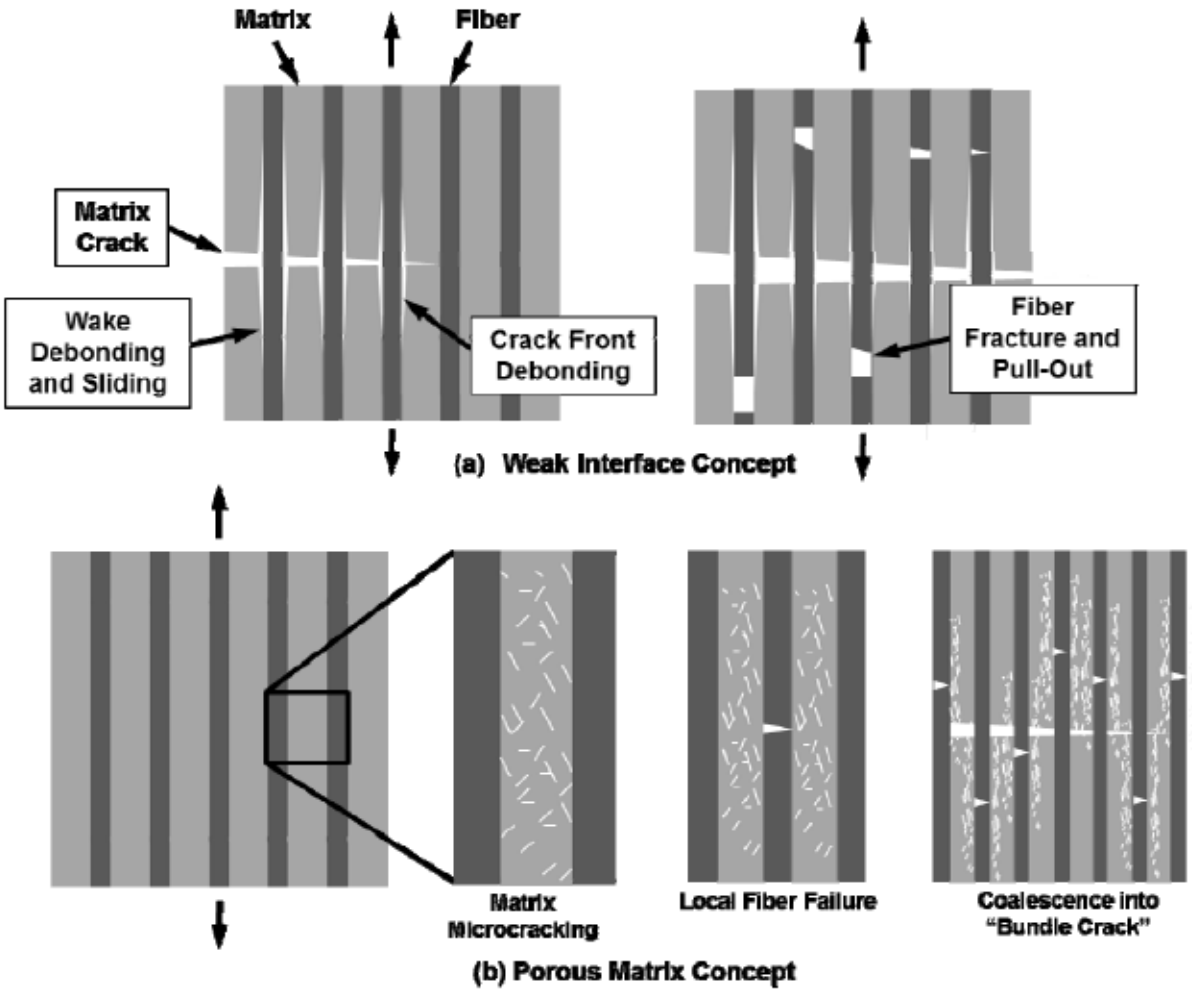


Figure 3: Illustration of (a) weak interface concept commonly achieved through fiber coating and (b) porous matrix concept used to achieve damage tolerance in CMCs. After Zok [3].

As CMCs have been studied further, the need for composites with improved

thermodynamic stability and oxidation resistance was recognized. Oxide/oxide CMCs based on environmentally stable oxide constituents were developed.

1.2 Oxide/Oxide Ceramic Matrix Composites

Oxide/oxide CMCs were developed to combat the oxidation embrittlement of non-oxide CMCs at high temperatures in oxidizing environments. Though oxide/oxide composites have superior environmental stability, there is a small reduction in their mechanical properties and performance compared to the non-oxide composites [2].

Development of oxide/oxide CMCs encountered a new problem that had not been seen before. At first, the traditional method of fiber coating with a dense matrix was used in order to create the weak interface between fiber and matrix to avoid catastrophic failure. When put in demanding environments, the fiber coating oxidized causing a strong interface between matrix and fiber to form. Without the coating, a crack would propagate straight through the entire composite with no energy dissipating phenomenon to stop it. This led to catastrophic failure and a need for a new processing method [2].

Because the traditional fiber coating system demonstrated the inability to work in the case of oxide/oxide CMCs, the focus was shifted to the matrix. The new microstructural design philosophy implicitly accepts strong fiber/matrix interfaces and aims to combat the unavoidable strong interface with a weak and porous matrix. The crack-deflecting behavior of a CMC is achieved by means of a finely distributed porosity in the matrix instead of a separate interface between matrix and fibers. In porous-matrix composites the cracks would propagate through the matrix and around the fibers [2]. Figure 3 (b) illustrates a porous-matrix concept developed for oxide/oxide CMCs.

1.2.1 Fibers

Common fibers used in oxide/oxide CMCs are Nextel^{TM} fibers. Of the Nextel fibers (312, 440, 550, 610, and 720), only Nextel 610 and 720 are designed for use at high temperatures due to their composition. Nextel 610 fibers are alumina fibers and have superior tensile strength to Nextel 720 fibers which are made of alumina-mullite. However, Nextel 720 fibers exhibit improved creep resistance which allows the material to perform for longer periods of time at elevated temperatures [2].

1.2.2 Matrix Materials

Porous matrix oxide/oxide CMCs untilize three main matrix materials: aluminosilicate, alumina-mullite, and alumina. Aluminosilicate matrices are mainly alumina with a silica binder. When fired, the silica produces a porous phase in-between the alumina particles. This matrix starts to degrade at temperatures above 1000ºC due to the molten silica causing densification of the matrix. Alumina matrices were developed to combat the densification caused by aluminosilicate. In the absence of silica, the alumina matrices did not exhibit adverse densification effects at temperatures up to 1100-1200ºC. Alumina-mullite matrices are the most stable of the three materials. Using mullite as the main constituent and alumina as the binder created a matrix that experienced little, if any, shrinkage [3].

1.3 Background on Laser Drilling

As mentioned above, one of the attractive features of the fiber-reinforced CMCs in their ability to exhibit “inelastic” deformation. A key task of the “inelastic” deformation is to relieve stress concentration occurring around geometric discontinuities in the CMC components, making them relatively notch-insensitive. In this effort, we investigate the discontinuities in the form of laser-drilled effusion holes. Laser drilling can be accomplished using several

techniques. The most common and direct method is to use a single laser pulse of high energy to puncture through the material. Percussion drilling is another technique where multiple, short-duration pulses are used to produce the desired hole. Percussion drilling is typically used to produce holes of smaller diameters [4]. A third technique called trepanning employs multiple laser pulses, starting with a pilot hole and moving outward in a series of large circles. A fourth technique is helical drilling, which is similar to trepanning but without a drilled pilot hole. Single shot drilling is fast but lacks the precision that the other techniques can offer.

1.4 Oxide-Oxide CMCs - Previous Efforts

1.4.1 Mechanical Behavior

The first efforts put toward new materials involve characterizing their mechanical behavior. Many tests have been conducted for N720/A at different temperatures and environments. These tests were done in order to determine which conditions and which types of loading are the most damaging to the composite.

Braun investigated creep behavior of N720/A with 0/90 woven fibers at 1000 and 1100ºC. A defined run-out time was set to 100 h. It was found that run-out was achieved for all specimens tested at 1000ºC at 150 MPa. Once the temperature was raised to 1100ºC, run out was achieved at 150 MPa in air, but only at 100 MPa in steam. This result demonstrated that steam was a much more damaging environment. Additional sintering at elevated temperatures caused the matrix to lose some of its porosity. Additionally, depletion of the mullite phase from the N720 fibers further reduced creep resistance of the N720/A CMC [5]. Siegert investigated creep behavior of N720/A with a ±45º fiber orientation in air, steam, and argon at 1200ºC. As expected, the composite with the ±45º fiber orientation offered a reduced creep performance compared to the 0/90 cross-ply [6].

Mehrman tested N720/A in creep, fatigue, and fatigue with hold times. Tests were conducted at 1200ºC in air and in steam. In the case of cyclic loading with hold times in air, the CMC performance was between those obtained in creep tests and in fatigue tests. In steam, lifetimes produced in fatigue tests with hold times were similar to those obtained in creep tests. Furthermore, results revealed significant degradation of the material microstructure and performance due to steam [7].

Koutsoukos tested N720/AS in creep at 1200ºC in air, in argon, and in steam. It was found that a shorter creep life was achieved in the steam environment. It was also found that N720/A performed better than N720/AS under the same conditions [8].

Results of prior research at AFIT into the mechanical behavior of N720/A at elevated temperature in various environments provide a solid foundation for the current effort. Because creep was found to be the most damaging form of loading for N720/A, the current research examines the effect of effusion holes on creep behavior of N720/A.

1.4.2 Notch Sensitivity of CMCs

Flaw tolerance of high performing ceramic matrix composites is a desired trait. In order to use these materials in their desired applications, holes may need to be intentionally placed within the composite. These holes should not cause catastrophic failure. Traditional ceramics have poor flaw tolerance. Any flaw in the monolithic ceramic material can act as a crack initiation site resulting in rapid crack growth and ultimate failure. It is recognized that CMCs with a porous matrix exhibit an improved flaw tolerance.

However, recent studies offer conflicting conclusions regarding the effect of notches on high-temperature mechanical performance of oxide-oxide CMCs. Kramb et al [9] reported significant notch sensitivity of Nextel^{TM}610/aluminosilicate composite tested in tension at

950ºC. Notched fracture behavior of Nextel610/AS was investigated at 23 and 950ºC using optical microscopy, ultrasonic C-scans, and crack mouth opening displacement methods to characterize the crack growth after a tensile test was performed. A singe notch was cut with a diamond blade on one side of the specimen. It was found that at room temperature the failure was much more distributed through the matrix whereas at elevated temperature, self-similar crack growth was prevalent. It was concluded that crack propagation at elevated temperatures is through a different mode (self-similar crack growth versus extensive matrix cracking within the fiber tows) and is a much more damaging process. The load-bearing capacity of the composite was decreased after the peak load but the damage in the wake of the crack was not enough to cause catastrophic failure [9].

Subsequent investigations revealed that Nextel^{TM}720/aluminosilicate composite was highly notch sensitive under monotonic and sustained tensile loading at temperatures ≥ 1100°C. Buchanan et al. performed a series of tests on Nextel720/AS. In the first set of tests, the specimen was notched with a semicircular notch geometry and a saw-cut notch geometry. Both notches were of the same length. Tensile tests were performed in laboratory air at 23, 1000, 1100 and 1200ºC. It was found that at 1100ºC and above, the material began to show notch sensitivity. Below those temperatures, the material behaved as desired showing fiber pullout as the final failure mode. At 1100 and 1200ºC the materials exhibited much less fiber pullout but there was still some present. Overall, the material perform well without much difference in results for the two types of notches [10].

The second set of tests involved Nextel720/AS specimens notched in the same manner as described above and tested under tensile monotonic and sustained loading at 1100ºC. It was found that under tensile loading, the material exhibited slight notch sensitivity in that the

notched strength was about 15% lower than the unnotched strength. Once the material was tested at creep, it was found that there was a much higher notch sensitivity. The specimens put under creep displayed much more deformation and ruptured much quicker than the unnotched specimens resulting in a 40% decrease in strength. The type of notch did not make enough difference to cause note. Thus, it was concluded that creep behavior is much more damaging than tensile behavior [11].

The third set of tests examined the effect of small effusion holes in Nextel720/AS. Specimens containing and array of 0.5 mm diameter holes, were tested at 1100ºC in laboratory air under sustained loading. One-hole, two-hole, and five-hole arrays were considered. It was concluded that the holes did not have an adverse effect on the creep behavior of the material [12].

Similary, the Nextel^{TM}720/alumina composite was demonstrated to be notch insensitive under monotonic tensile, creep, and fatigue loading conditions at 1200ºC [13]. Mall and Sullivan [13] tested specimens with holes in tension to failure as well as in tension-tension fatigue at 1200ºC in laboratory air. The results of both tests concluded that the material was notch insensitive [13].

Notably the aforementioned studies focused on the mechanical performance of notched composites at elevated temperature in laboratory air. Mechanical performance at elevated temperature in steam was not considered. However, it is recognized that steam causes dramatic degradation of mechanical performance of oxide-oxide CMCs and their constituents at elevated temperature. The present effort investigates the behavior of an oxide-oxide CMC containing an array of small effusion holes under monotonic tension and creep loadings at 1200ºC in air and in steam. The composite consisting of a porous alumina matrix reinforced

with Nextel^{TM}720 alumina-mullite fibers is studied in this research.

II. Material and Test Specimen

2.1 Material

The material studied in this research effort was Nextel^{TM} 720/Alumina (N720/A), an oxide-oxide ceramic composite consisting of a porous alumina matrix reinforced with N720 alumina-mullite fibers. This CMC does not have a fiber coating and relies on the porous matrix for damage tolerance. The composite was manufactured by COI Ceramics, Inc. and supplied in the form of 12 in. x 9 in. panels. The panels were comprised of 12 0/90 plies woven in an eight harness satin weave (8HSW). Table 1 lists the physical properties of the composite panel as reported by COI [14].

Table 1: Physical Properties of N720/A Panels Supplied by COI [14]

Panel	Fiber Denier	Fiber Volume Fraction	Bulk Density	Open Porosity
P01006	1500	45.1 %	2.79 g/cc	23.6 %
P01008	1500	44.1%	2.73 g/cc	25.2 %

2.2 Test Specimen Geometry

Dog-bone shaped specimens were used in this work. The total specimen length was 150 mm and the width of the specimen gauge section was 10 mm. Specimens were machined using diamond grinding according to the specifications shown in Figure 4.

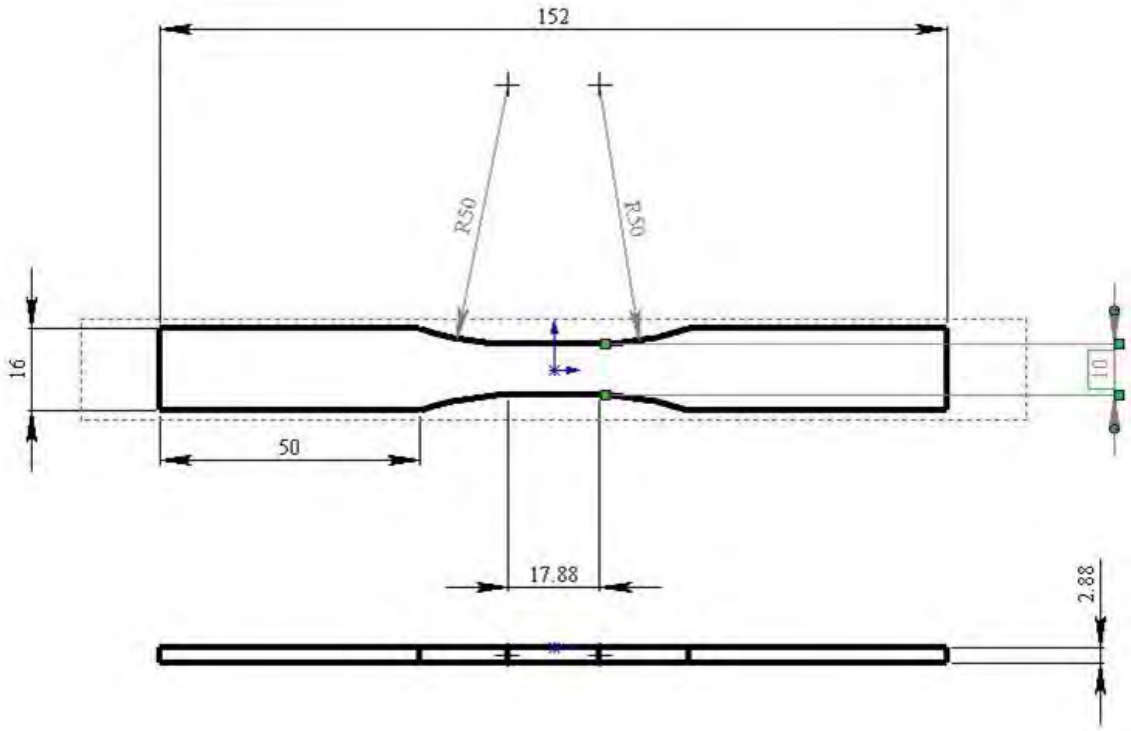


Figure 4: Test specimen (dimensions in mm).

In order to investigate the effect of effusion holes on creep behavior of the N720/A CMC, test specimens contained an array of 17 effusion holes in the gage section. The holes were 0.5 mm in diameter with the axis of the hole oriented at 90° to the specimen surface. The hole pattern is shown in Figure 5. The holes were drilled using a CO_2 laser set to 60 Hz with a 3.0 millisecond pulse length. The laser drilling was performed by New Tech Precision, Jupiter, Florida using a 100 Watt laser. Each hole was cut at 3 in/min (IPM). Figure 6 shows a specimen with the array of holes.

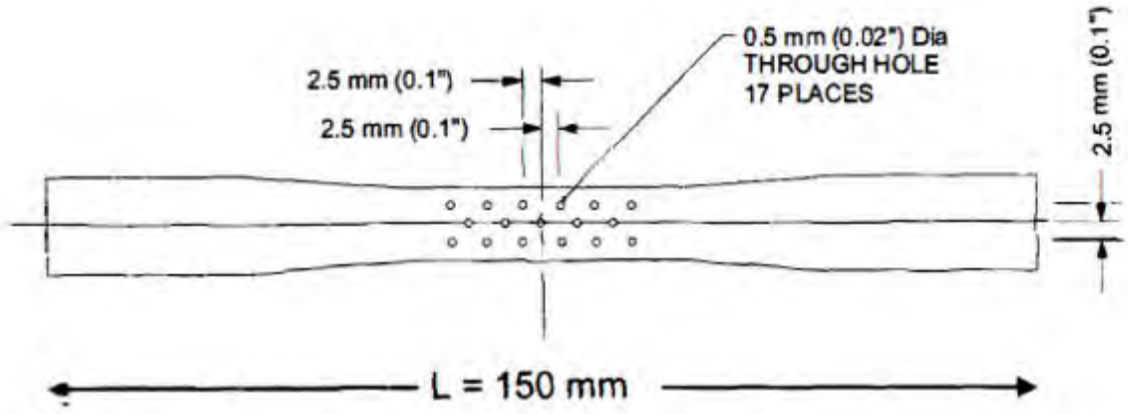


Figure 5: Drawing sent to New Tech Precision in order to laser drill the effusion holes

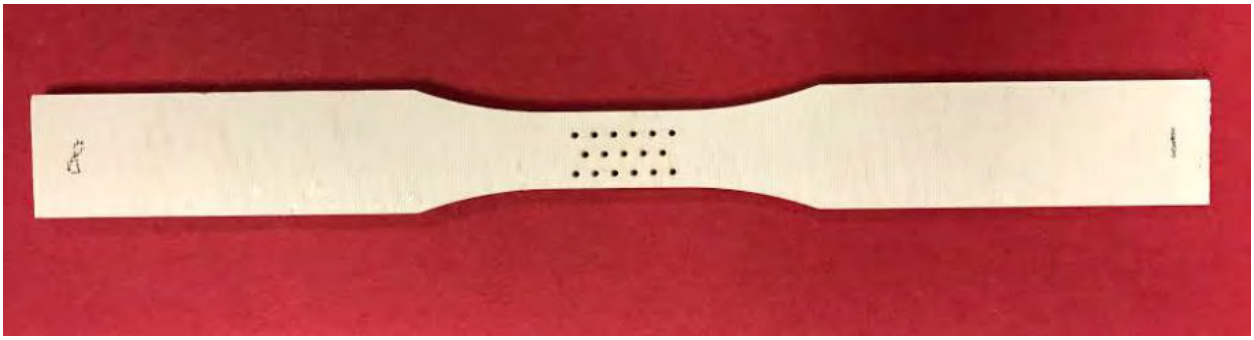


Figure 6: Specimen with completed effusion holes

Each specimen was measured. The width and thickness for each specimen were measured using Mitutoyo Corporation Digital Calipers. Each measurement was repeated five times, then an average dimension was calculated. The resulting specimen dimensions are reported in Table 2.

Table 2: Specimen dimensions

Panel	Specimen Number	Width (mm)	Thickness (mm)
P01006	6-1	10.020	2.690
P01006	6-2	10.026	2.670
P01006	6-3	10.018	2.728
P01006	6-4	9.772	2.666
P01006	6-5	9.768	2.680
P01006	6-6	10.034	2.706
P01006	6-7	10.022	2.666
P01008	8-1	9.984	2.824
P01008	8-2	10.036	2.690
P01008	8-3	10.012	2.698
P01008	8-4	10.020	2.642
P01008	8-5	9.998	2.692
P01008	8-6	9.996	2.634

III. Experimental Arrangements and Procedures

3.1 Testing Equipment

3.1.1 Mechanical Testing Equipment

A vertically actuated, servo-hydraulic MTS 810 Material Test System was used for all tests (see Figure 7). An MTS Flex Test 40 digital controller was used for input signal generation and data acquisition. MTS System Software and Multi-Purpose Testware (MPT) were used to program and execute all tests. MTS series 647 hydraulic wedge grips with a Surfalloy surface were used to grip specimens for testing. A grip pressure of 8 MPa was used for all tests. The grips were water cooled using a Neslab model RTE 7 chiller. The chiller continuously circulated water at a temperature of 15 ºC in order to keep the grips sufficiently cooled for the duration of testing.

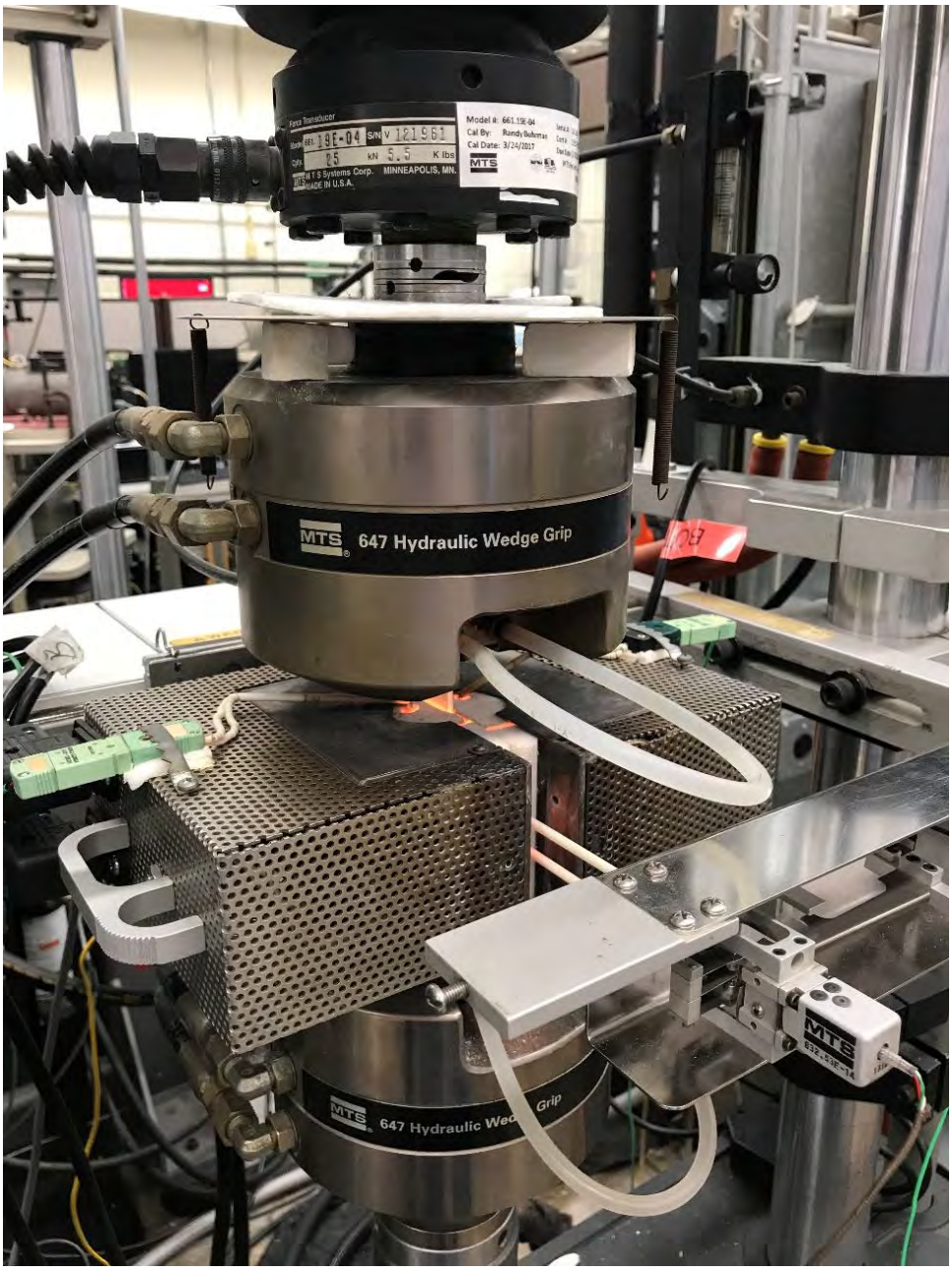


Figure 7: MTS 810 Material Test System

The test system had a capacity of 25 kN (5.5 kip). An MTS Force Transducer (Model 661.19E-04) was used for force measurement. An LDVT internal to the test station was used to measure displacement. A low contact force, uniaxial, high temperature MTS Extensometer (Model 632.53E-14) was used for strain measurement. The force transducer, top wedge grip, and extensometer are seen in Figure 7.

3.1.2 Environmental Testing Equipment

Additional equipment was required in order to conduct tests at 1200 ºC in both laboratory air and steam. The mechanical testing station was equipped with a compact, dual zone AMTECO Hot-Rail Furnace (Figure 8) controlled by an MTS (model 409.83) Temperature Controller (Figure 9).

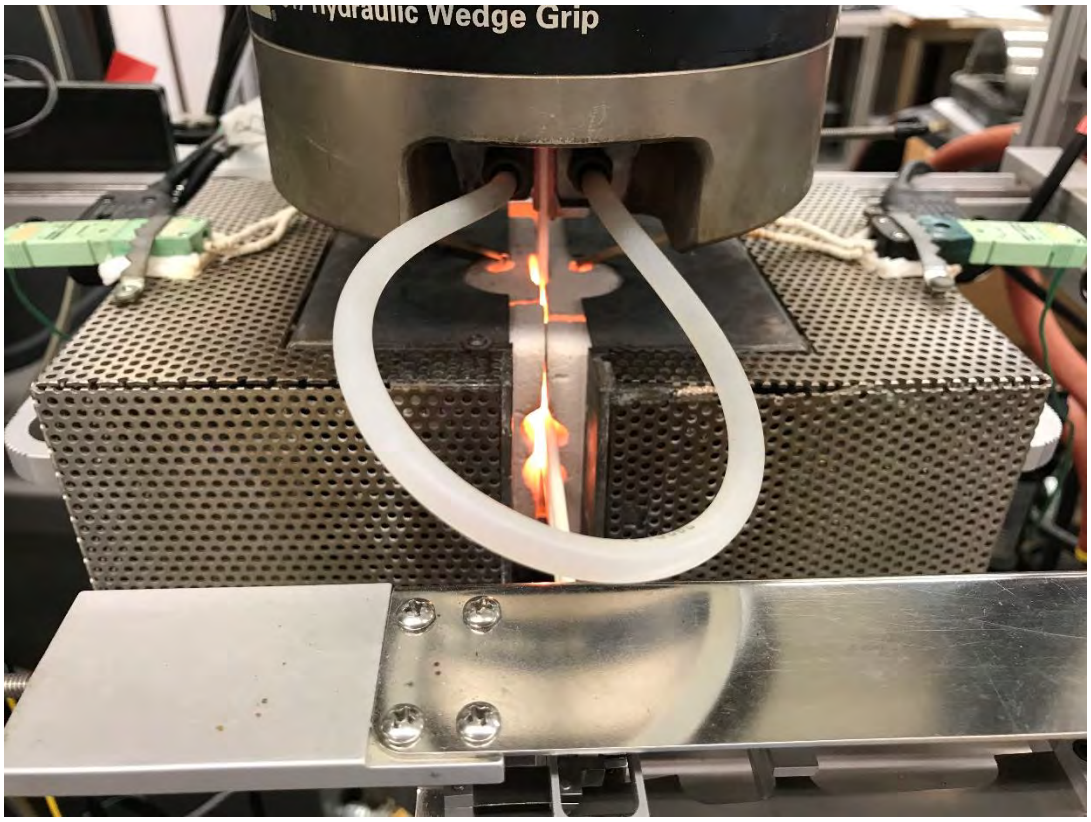


Figure 8: AMTECO Hot-Rail Furnace



Figure 9: MTS Temperature Controller

Each side of the furnace was fitted with an S-type control thermocouple in order to provide chamber temperature to the controller. Temperature set point was provided via the Flex Test 40 controller to the temperature controller, which applied a PID control algorithm to the furnace elements with a feedback loop from the control thermocouples. The temperature measured by the control thermocouples did not match the temperature of the specimen and was accounted for via temperature calibration discussed in section 3.2.1.

For testing in steam, a continuous steam environment was provided by an AMTECO HRFS-STMGEN Steam Generation System shown in Figure 10. In order to create a near 100% steam environment, an alumina susceptor was used. The susceptor is a cylinder with slots and end caps that fits inside the furnace. The specimen gauge section fits within the susceptor and the ends of the specimen pass through slots in the susceptor. Steam is introduced through a

feeding tube in a continuous stream with slight positive pressure which expels the dry air and creates a near 100% steam environment around the specimen gage section. The susceptor is shown in Figure 11.



Figure 10: AMTECO Steam System

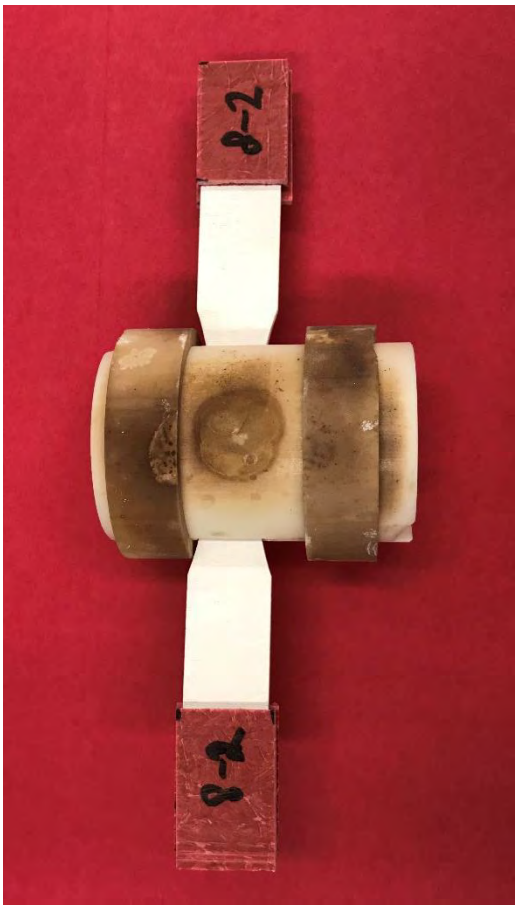


Figure 11: Alumina susceptor mounted around a test specimen

3.1.3 Microstructural Characterization

Test specimens were examined using an optical microscope before and after testing. A Zeiss optical microscope (serial number 2 12 05 5474) equipped with AxioCam HRc was used for this task. Figure 12 shows the optical microscope.



Figure 12: Zeiss optical microscope utilized for pre-test and post-test examination of specimens.

After testing, the fracture surfaces of the test specimens were examined with, a Quanta FEG 650 Scanning Electron Microscope (SEM). Fracture surfaces were cut off using a water-cooled saw and mounted for the SEM examination. Once mounted, the specimens were coated with gold-palladium (Au-Pd) using the EMS Quorum sputtering machine (see Figure 13). Figure 14 shows the Quanta FEG 650 SEM used in this work.



Figure 13: EMS Quorum sputtering machine.

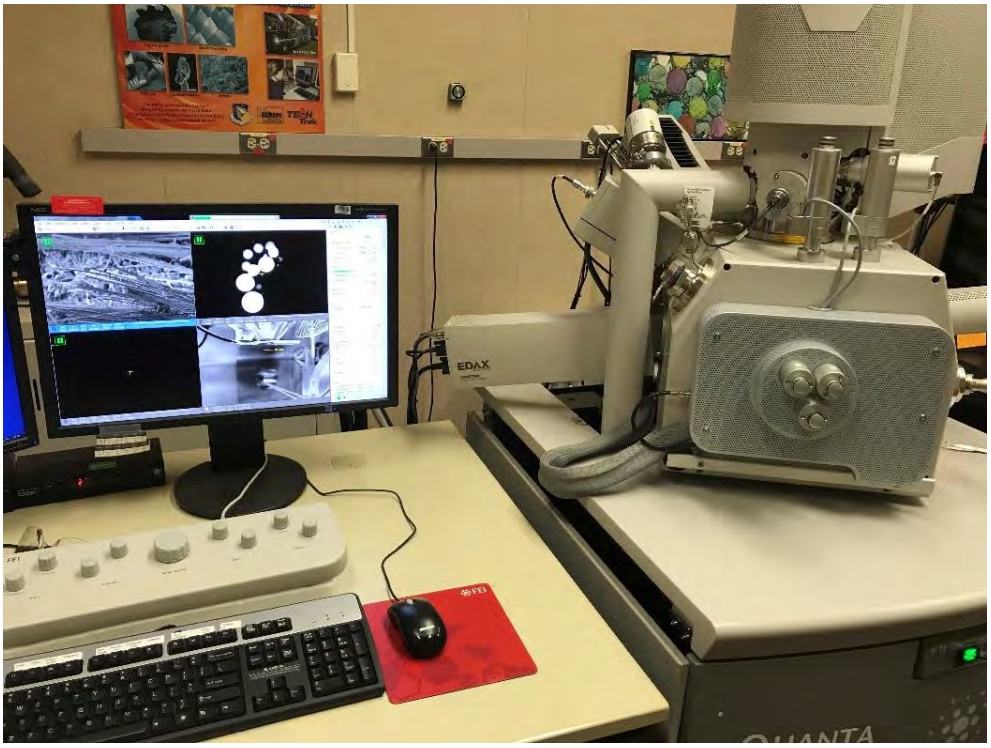


Figure 14: Quanta FEG 650 Scanning Electron Microscope.

3.2 Test Procedures

3.2.1 Mechanical Testing Equipment – Calibration

The MTS testing machine was aligned prior to testing using an MTS 609 Alignment Fixture, a specimen instrumented with 12 strain gauges and MTS 709 Alignment Software. The machine was tuned in displacement control with and in force control. Tuning of the force control mode required the use of an actual test specimen. The extensometer was calibrated using standard procedures.

The furnace temperature controller was calibrated to maintain a 1200ºC specimen temperature for all tests. A test specimen was fitted with two R-type thermocouples and used for temperature calibration in both air and steam. Two small pieces of alumina and high-temperature wire were used to fit the thermocouples on either side of the specimen. The temperature calibration specimen is shown in Figure 15.

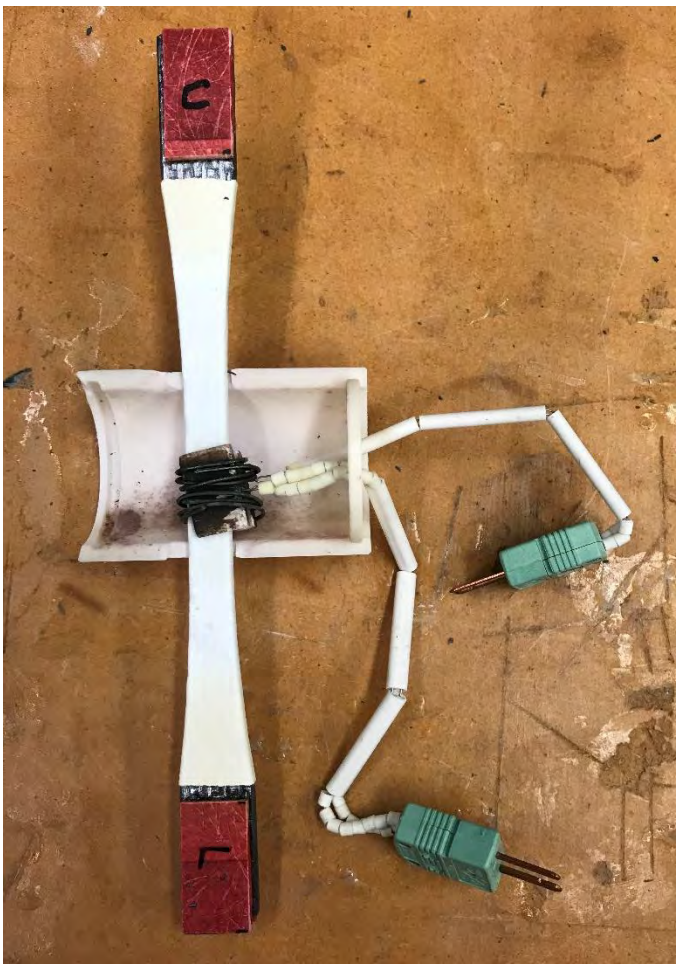


Figure 15: Temperature calibration specimen instrumented with R-type thermocouples secured using alumina pieces and high temperature wire.

The temperature calibration specimen was mounted in the MTS machine with the alumina susceptor in place and heated under zero load. The thermocouples were connected to an Omega® HH501BR handheld type R thermometer for readout.

Oven temperature was slowly raised until the desired temperature of the specimen was reached. Once the initial calibration was complete, a trial heat-up at a rate of 1ºC/s followed by a 45-min dwell was completed with the calibration specimen to ensure the correct target temperature was obtained and maintained. The same temperature calibration procedure was completed in steam. The temperature controller set points obtained during this process were then used in actual tests. Table 3 shows the set points obtained for testing in air and in steam.

Table 3: Temperature Set-Points (°C)

	Right	Left
Air	1245	1240
Steam	1285	1280

3.2.2 Mechanical Testing – Preparation

Before testing, each specimen was fitted with $^{1}/_{16}$-in. thick fiberglass tabs. The tabs were bonded to the specimens using M-Bond 200 adhesive. The tabs protected the specimen surface from damage caused by the grips of the MTS Machine. A tabbed specimen is shown in Figure 16.



Figure 16: Test specimen with tabs

The width and thickness of the specimen gauge section were measured with Mitutoyo Corporation Digital Micrometers (Model CD-S6”CT). Five measurements were taken and an average calculated. Based on these measurements, the cross-sectional area of each specimen was calculated. The effusion holes were taken into account by calculating an “effective area”. To calculate the effective area, first the nominal volume of the cross section (without holes) was calculated, then the volume removed by laser drilling of the 17 holes was subtracted from the nominal volume. The result of the subtraction was divided by the length of the gage section

to obtain the effective area. This effective cross-sectional area was used to calculate the load needed to attain the desired test stress level, using:

$$\sigma = \frac{P}{A} \tag{1}$$

where σ is stress in Pascals (Pa), P is load in Newtons (N), and A is the effective cross-sectional area in meters squared (m^2).

Before every test, the MTS machine was warmed up using the MTS function generator to cycle the actuator in displacement control mode at 0.1 Hz for 15 minutes. The Neslab chiller was turned on and given sufficient time to come to temperature. The temperature controller was verified to be in "enabled" mode with no error codes on its readouts. If the test required steam, the steam generator was turned on and allowed sufficient time to stabilize. The ceramic steam feeding tube was inserted into the front of the steam pump. The steam pump was turned on just before the start of the test.

A separate procedure was written for each test using the MPT Procedure Editor module. The MPT Procedure Editor allowed for multiple channel data acquisition, sampling rate, and file saving formats. Examples of each test procedure are located in the following sections outlining each test type.

To begin a test, the alumina susceptor was assembled around the specimen even if steam was not used in the test. If steam was used in the test, then the steam feeding tube was carefully fitted in to the back of the susceptor while the specimen was being placed in the grips. The specimen was first secured in the top grip while in displacement control mode. Then the control mode was switched to force, the force command set to 0 N, and the bottom grip closed. The extensometer was mounted on the test specimen with the extensometer extension rods contacting the specimen through the front face of the susceptor. Next, the ovens were slowly

moved into place ensuring the extensometer remained free floating. Care had to be taken not to damage the susceptor due to the brittle material and thin front and back faces.

Once the specimen was fully mounted in the MTS machine, the strain and displacement were both digitally zeroed with the MTS control software. The program was then locked in, ensuring all safety interlocks were active. All tests began with a heat up to the test temperature at 1 ºC/s followed by a 45-minute dwell at test temperature and zero load.

3.2.3 Monotonic Tensile Tests

All tensile tests were performed in laboratory air in displacement control with a constant displacement rate of 0.05 mm/s. Load, displacement, strain, time, and temperature setting for both right and left ovens were collected every 0.05 s and recorded. The data collected during the heat up to and dwell at test temperature were recorded every 1 s. The duration of all tensile tests to failure was approximately 10 s. A sample of the tensile test procedure is shown in Figure 17.

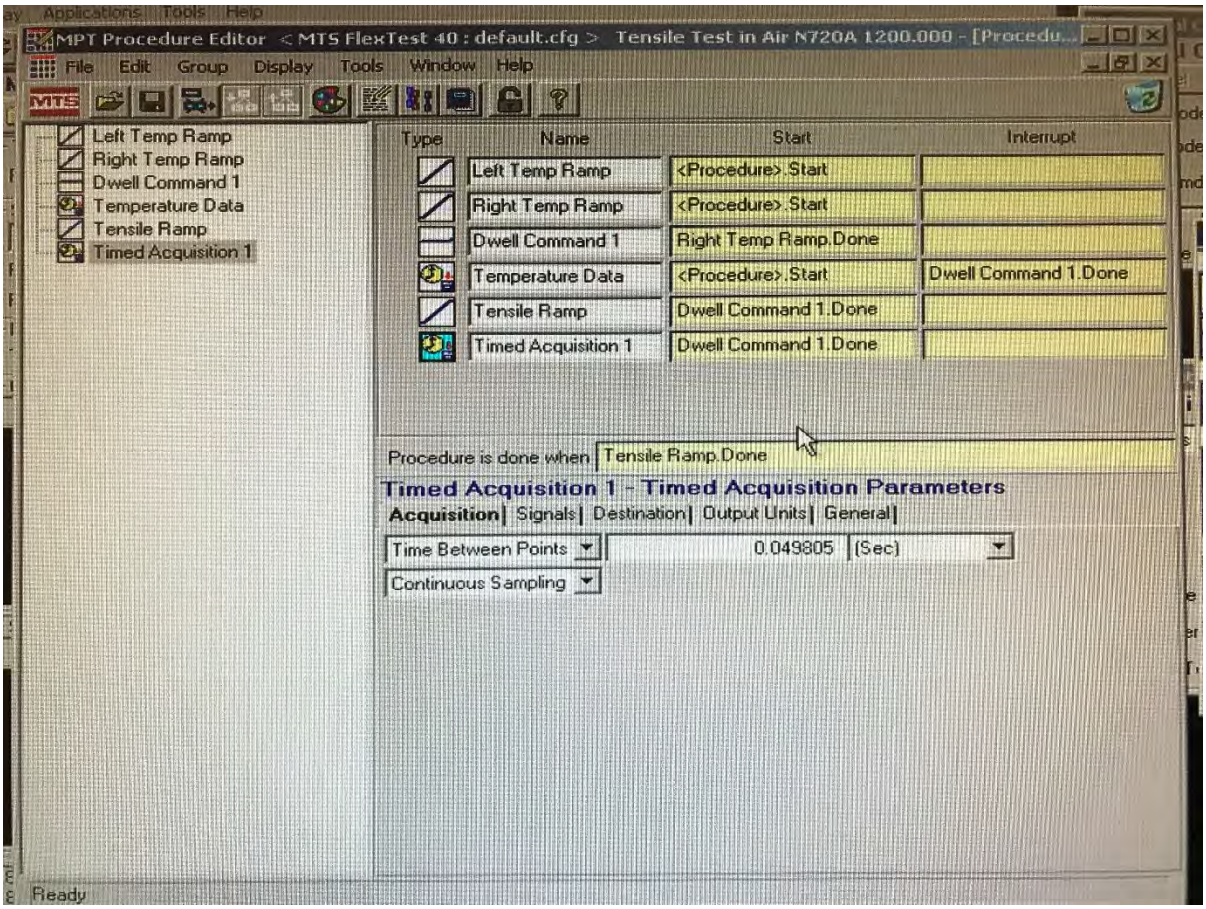


Figure 17: Monotonic Tensile Test Procedure

3.2.4 Creep-Rupture Tests

Creep rupture tests were conducted in force control. The loading to creep stress level was accomplished at 25 MPa/s. Data was sampled: (i) at 30 Hz during the first 8 min of the test, (ii) at 6.67 Hz during the remainder of the first hour of the test, (iii) once every 2 s during the second hour of the test, (iv) every 10 s during hours 3-5 of the test, and (v) every 3 min during the remaining 95 hours of the test. Creep run-out was defined as 100 h at creep stress. If run-out was achieved, the program automatically unloaded the specimen to zero load at 25 MPa/s and then performed a tensile test at 0.05 mm/s to failure in order to measure retained properties. It is noteworthy that in all tests reported herein failure occurred within the gauge section of the specimen. A sample procedure for creep rupture tests can be found in Figure 18.

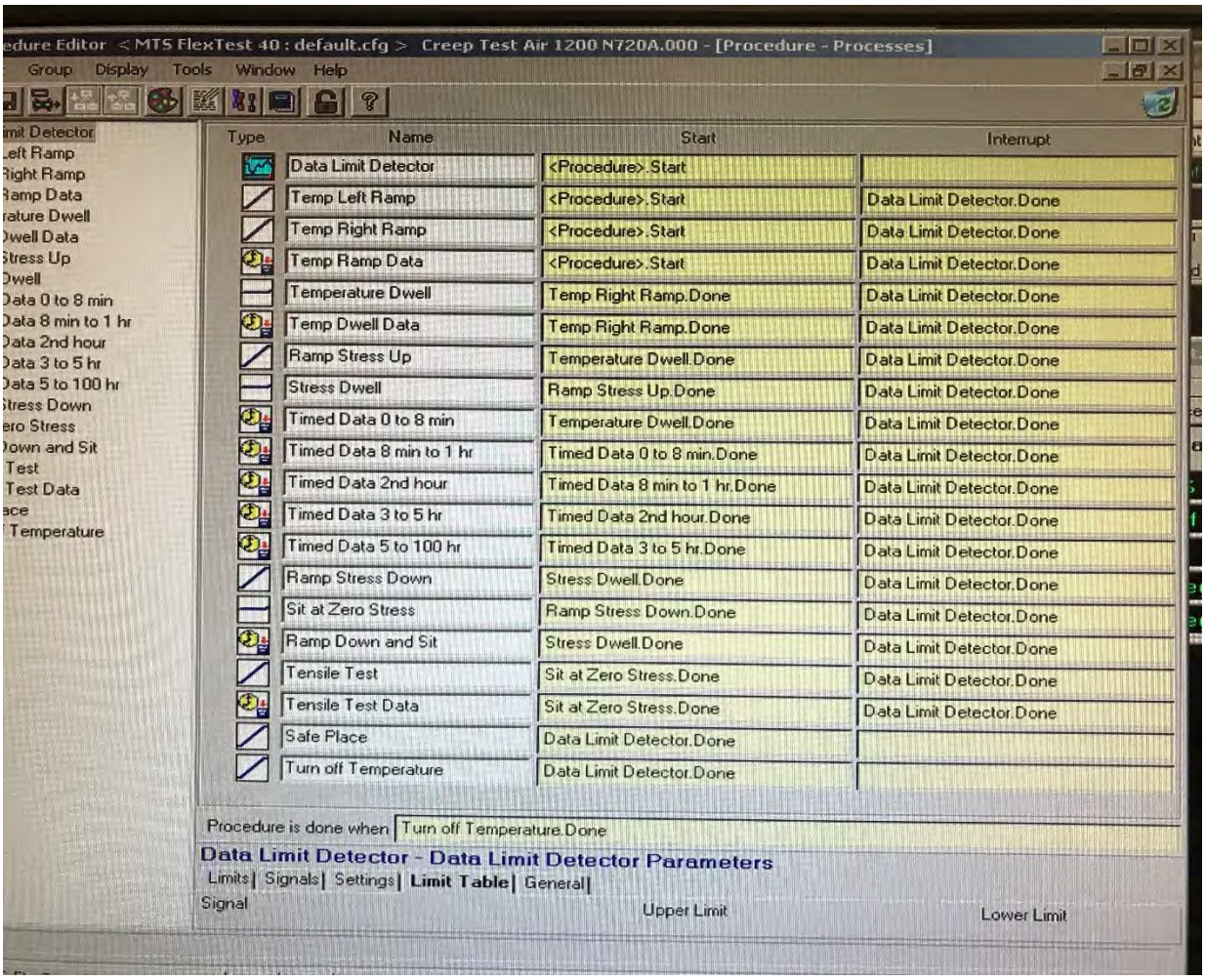


Figure 18: Creep Rupture Test Procedure

3.2.5 Microstructural Characterization – Specimen Preparation

Specimen preparation was not required for optical microscopy. Once all optical micrographs were completed, specimens were prepared for the SEM examination.

Each specimen chosen for post-test SEM examination had the tabbed portion removed using a water-cooled saw. Once shortened, the specimens were outfitted with a piece of copper tape down the side to ensure conductivity to the base. The specimens were then mounted on 90 degree platforms using carbon tape. Once mounted, the specimens were coated with gold-palladium (Au-Pd) in the sputtering machine. Coating thickness was targeted at 5 nm. Once mounted and coated, the specimens were ready for SEM examination. Figure 19 depicts a cut

and mounted specimen.

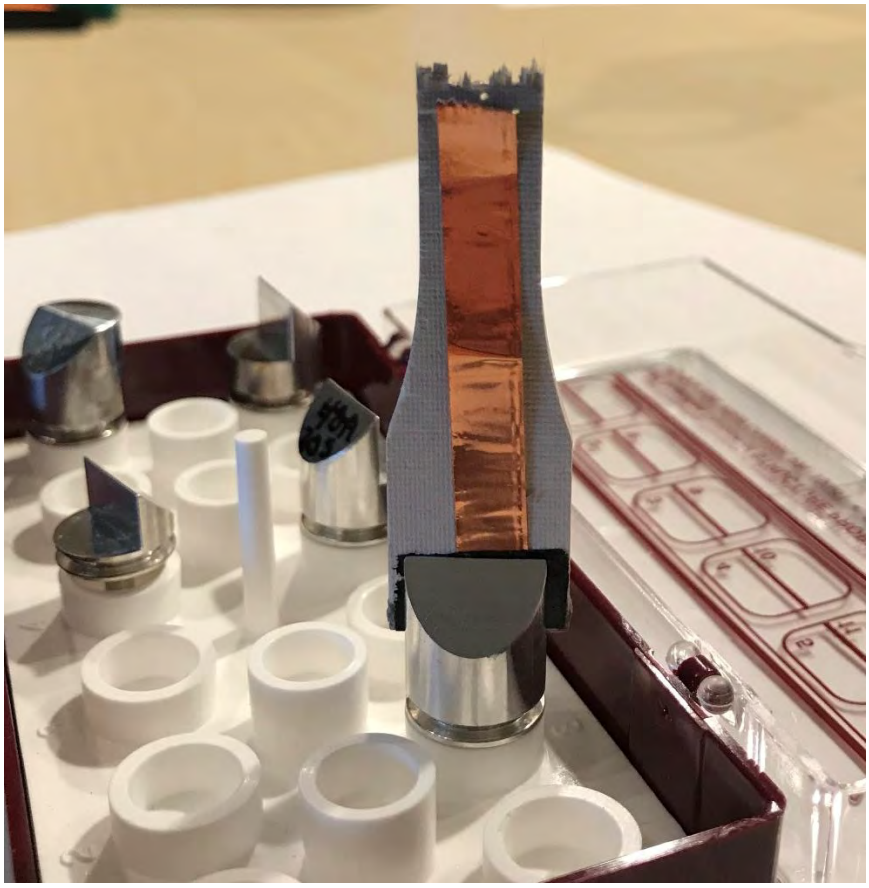


Figure 19: Cut and mounted specimen prepared for SEM examination

IV. Results and Discussion

Table 4 summarizes the tests performed during the course of this research. Panel ID, specimen number, test type, test environment, temperature, and maximum stress are provided. Note that specimen numbers also refer to the panel number. For example, P6-4 refers to specimen 4 from panel 6.

Table 4: Testing Matrix

Panel ID	Specimen Number	Test Type	Test Environment	Temperature (ºC)	Maximum Stress (MPa)
P01006	P6-1	Creep	Air	1200	150
P01006	P6-2	Creep	Air	1200	65
P01006	P6-3	Creep	Air	1200	80
P01006	P6-4	Creep	Steam	1200	65
P01006	P6-5	Creep	Steam	1200	80
P01006	P6-6	Creep	Steam	1200	30
P01006	P6-7	Tensile	Air	1200	174
P01008	P8-1	Creep	Air	1200	100
P01008	P8-2	Creep	Air	1200	40
P01008	P8-3	Creep	Air	1200	90
P01008	P8-4	Creep	Steam	1200	40
P01008	P8-5	Creep	Steam	1200	100
P01008	P8-6	Creep	Steam	1200	90
	T-1	Tensile	Air	1200	208
	T-2	Tensile	Air	1200	201

4.1 Thermal Expansion

Strain-temperature data recorded during the heat-up to test temperature were used to determine the coefficient of linear thermal expansion. The linear portion of the strain-temperature cure was assumed to behave according to the linear relationship

$$\varepsilon_{th} = \alpha * \Delta T \quad (2)$$

where ε_{th} is the thermal strain, α is the coefficient of linear thermal expansion, and ΔT is the temperature change from room temperature (nominally taken to be 23ºC) to test temperature.

Expansion coefficients were similar for air and steam environments. Table 5 presents thermal strains and coefficients of linear thermal expansion obtained for each test specimen.

Table 5: Thermal strain and coefficients of linear thermal expansion for N720/A specimens.

Specimen	Thermal Strain (%)	Thermal Coefficient (x 10^{-6}/ºC)
P6_1	0.56	4.758
P6_2	0.72	6.117
P6_3	0.73	6.202
P6_4	0.68	5.777
P6_5	0.711	6.041
P6_6	0.722	6.132
P6_7	0.72	6.117
P8_1	0.72	6.117
P8_2	0.7	5.947
P8_3	0.72	6.117
P8_4	0.68	5.777
P8_5	0.718	6.100
P8_6	0.69	5.862
T1	0.8	6.797
T-2	0.52	4.418
	Average	5.885

Average values of 7.20, 7.66, and 7.57 10^{-6} K^{-1} were reported by Harlan [15], Mehrman

[7], and Hetrick [16] respectively. These reported values are slightly higher than that found in this effort. This difference is most likely due to the fusing of fibers and matrix caused by the laser drilling of holes. The fibers and matrix material around each hole were fused together impeding thermal expansion of the CMC and thus reducing the overall thermal expansion coefficient. Fiber/matrix fusing due to laser drilling is discussed in detail in section 4.6.

4.2 Monotonic Tensile Tests

Two specimens without holes were tested in tension to failure at 1200ºC. The first specimen had an Ultimate Tensile Strength (UTS) of 207 MPa and a Modulus of Elasticity (E) of 77 GPa. The second specimen had a UTS of 200 MPa and a modulus of 75 GPa. Harlan [15], Mehrman [7], and COI [14] reported a UTS of 192, 186, and 219 MPa respectively. Harlan [15], Mehrman [7], and COI [14] also reported elastic moduli of 74.7, 77.7, and 76.1 GPa. We conclude that the UTS found in this effort are consistent with those reported previously.

One specimen containing laser drilled holes was tested in tension to failure at 1200ºC. The specimen with holes produced a UTS of 174 MPa, which is 13% lower than the UTS values produced by undrilled specimens without holes. The specimen with holes also produced a modulus of 63 GPa which is 16% lower than the specimen without holes. This reduction in UTS and modulus is attributed to the degradation of the CMC by fusing of fibers and matrix around the holes caused by the high temperature of the laser drilling. A more in depth discussion of the composite microstructure around the laser drilled holes is given in section 4.6.

4.3 Creep Rupture Tests at 1200 ºC

Creep tests were conducted at stress levels of 40, 65, 80, 90, 100, and 150 MPa in

laboratory air and at stress levels of 30, 40, 65, 80, 90, and 100 MPa in steam. All tests were conducted at 1200ºC. Figure 20 and Figure 21 show the creep curves obtained in air and steam, respectively, for N720/A specimens with laser drilled holes. It can be seen that creep curves produced in air and in steam appear similar in nature. All creep curves obtained in this work exhibit primary and secondary creep. In all tests primary creep transitions rapidly to secondary creep. Some specimens exhibited tertiary creep before failure. Though creep life times are much shorter in steam, the qualitative characteristics of the creep curves are little affected by steam.

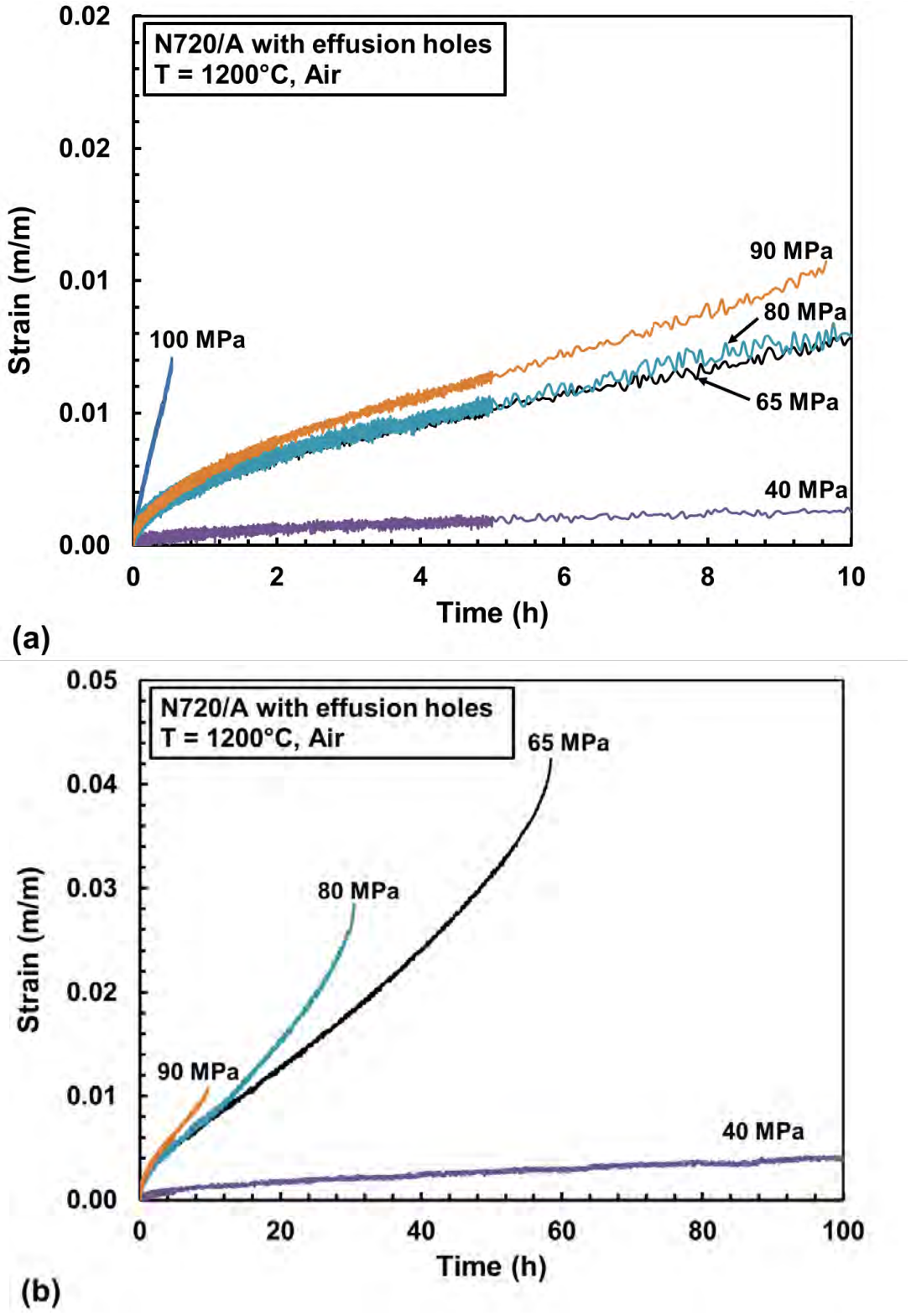


Figure 20: Creep strain vs. time curves obtained for N720/A specimens with laser drilled effusion holes in air at 1200ºC. Figure a) is a shorter time scale for clarity while Figure b) shows time until runout.

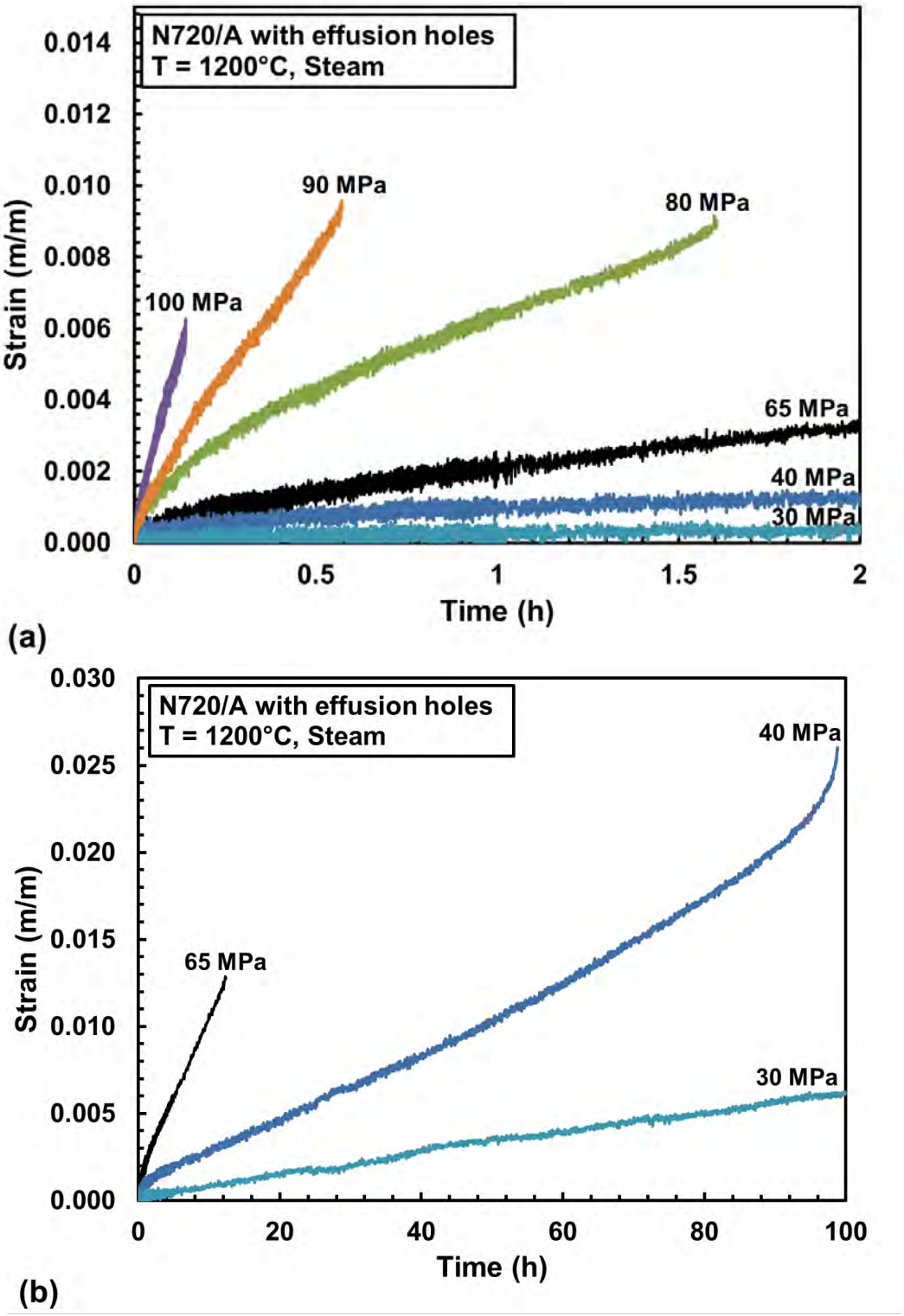


Figure 21: Creep strain vs. time curves obtained for N720/A specimens with laser drilled effusion holes in steam at 1200ºC. Figure a) is a shorter time scale for clarity while Figure b) shows time until runout.

Figure 22 depicts the creep stress versus time to rupture at 1200°C in air and in steam. Clearly, steam has a negative effect on creep lifetime. In air, creep run-out was achieved at 40 MPa while in steam run-out was achieved at 30 MPa. As seen in Figure 22, the presence of steam can reduce creep lifetime by as much as 90%. Creep-rupture results are also summarized in Table 6, where the values of creep stress are shown together with rupture time for tests performed in air and in steam.

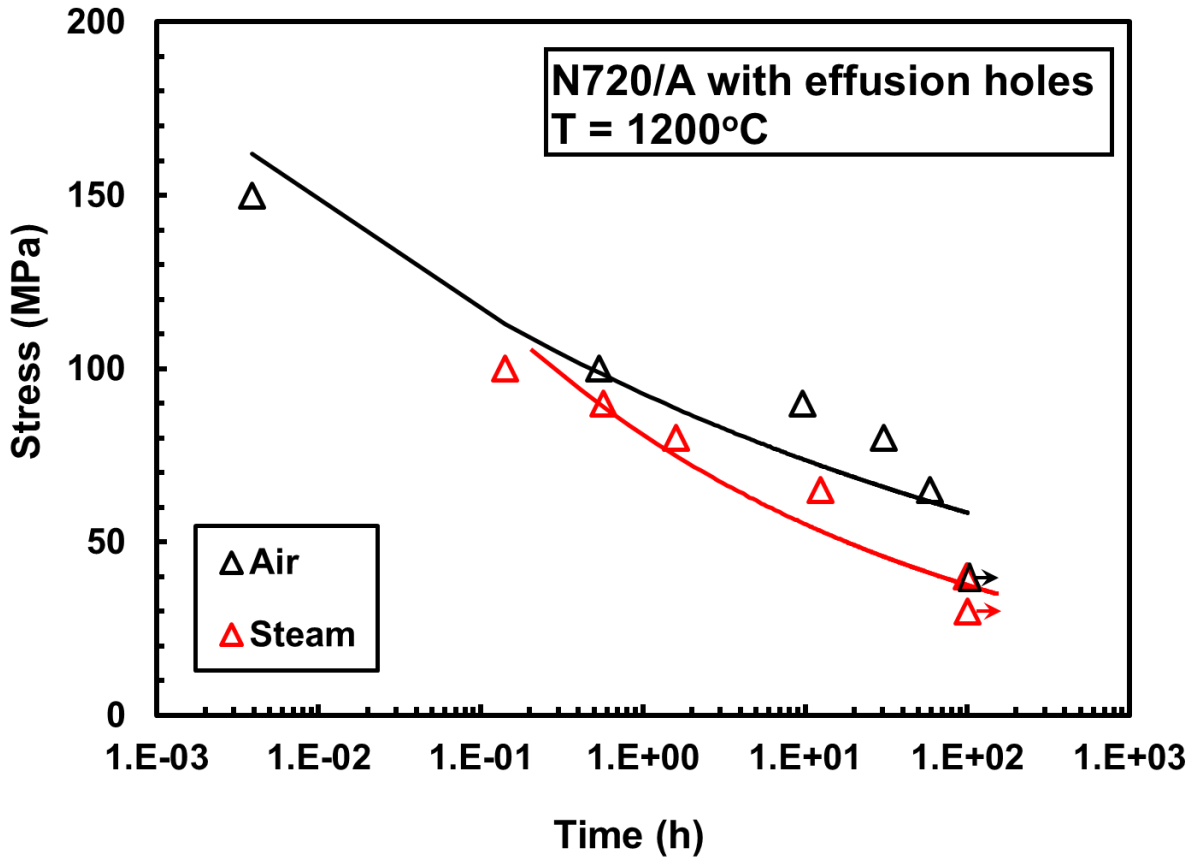


Figure 22: Creep stress vs. time to rupture for N720/A specimens with laser drilled effusion holes in air and steam at 1200°C.

Table 6: Creep stress values and time until failure.

Creep Stress (MPa)	Air Lifetime (h)	Steam Lifetime (h)
30	N/A	100
40	100	98.79
65	58.45	12.45
80	30.45	1.61
90	9.65	0.57
100	0.54	0.14
150	0.0039	N/A

Minimum creep rate was measured in all tests. Minimum creep strain rate as a function of applied stress is presented in Figure 23. Creep strain rates are also summarized in Table 7. Steam accelerates the minimum creep strain rates by a factor of 6-7 on average.

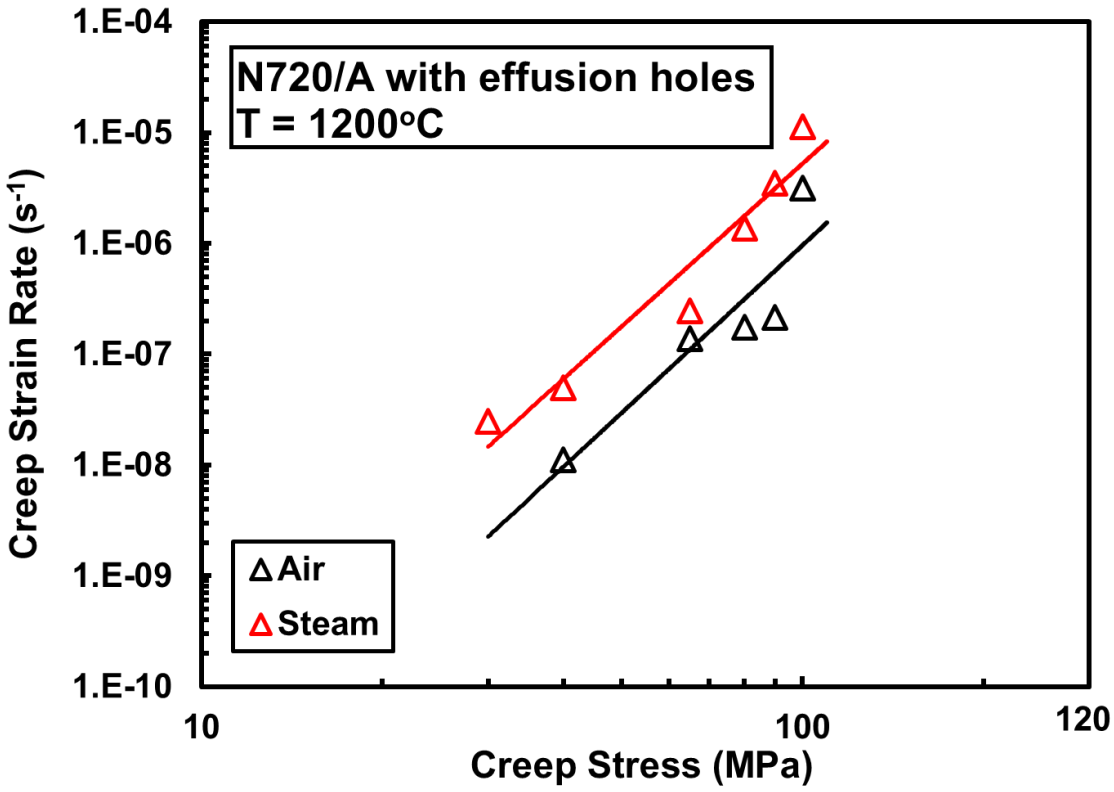


Figure 23: Minimum creep rate vs. creep stress for N720/A specimens with laser drilled effusion holes tested in air and steam at 1200°C.

Table 7: Summary of minimum creep strain rates obtained for the N720/A specimens with laser drilled effusion holes at 1200ºC in laboratory air and in steam environments.

Stress (MPa)	Air Creep Rate (1/s)	Steam Creep Rate (1/s)
30	N/A	2.5E-08
40	1.1E-08	5.0E-08
65	1.4E-07	2.4E-07
80	1.7E-07	1.4E-06
90	2.2E-07	3.5E-06
100	3.2E-06	1.1E-05

4.4 Retained Properties

Specimens that achieved run-out were then tested in tension to failure in order to assess retained tensile properties. The specimen that achieved run-out in air at 40 MPa had a retained tensile strength of 158 MPa and a modulus of 57 GPa. Evidently the specimen retained approximately 90% of its tensile strength and approximately 90% of its original stiffness. The specimen that achieved run-out at 30 MPa in steam had a retained tensile strength of 113 MPa and a modulus of 58.3 GPa. The specimens subjected to 100 h of prior creep in steam retained only 65% of its tensile strength and nearly 90% of its stiffness. These results demonstrate that prior creep in steam degrades the material much more than prior creep in air.

4.5 Effect of Laser Drilled Holes on Creep Performance of N720/A at 1200°C in Air and in Steam

The effect of laser drilled effusion holes on creep performance of N720/A at 1200°C in air and in steam was assessed by comparing the results of the current study with the results obtained for unnotched specimens by Harlan [15]. Figure 24 presents a comparison of the creep-rupture results obtained for specimens with effusion holes and those obtained for the

unnotched specimens. Results in Figure 24 reveal that the presence of laser drilled effusion holes dramatically degrades creep lifetime of N720/A composite. Specimens with laser drilled effusion holes produced significantly shorter creep lifetimes than the unnotched specimens. An average decrease in creep lifetime due to the presence of hole was ~80% in air and ~95% in steam.

Notably steam had a similar effect on creep performance of the specimens with and without laser drilled holes. An average decrease in creep lifetime due to steam was ~80% for specimens with laser drilled holes and ~90% for the unnotched specimens. These results suggest that the presence of effusion holes did neither increase nor lessen the detrimental effects of steam on creep lifetime of N720/A composite at 1200°C.

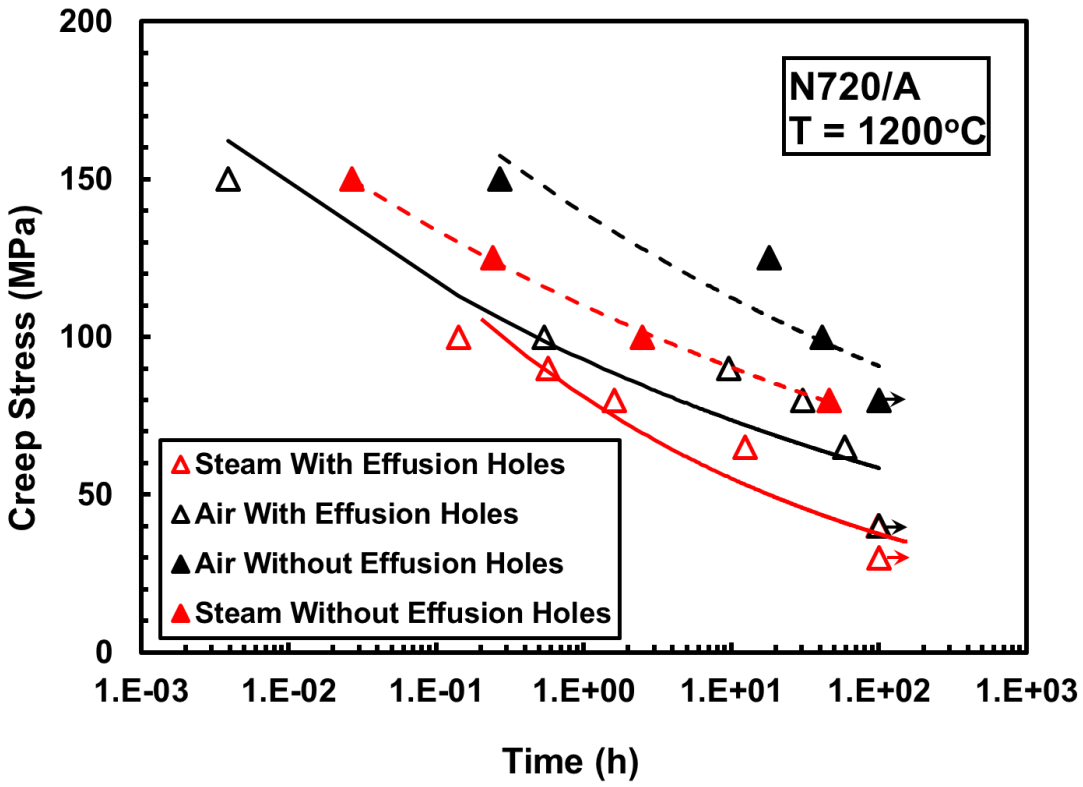


Figure 24: Creep stress vs. time to rupture for N720/A specimens with and without laser drilled effusion holes in air and in steam at 1200°C.

Minimum creep strain rate as a function of applied stress obtained for N720/A

specimens with and without laser drilled effusion holes at 1200°C in air and in steam is presented in Figure 25. It is seen that the presence of laser drilled effusion holes results in a significant increase in minimum creep rates of N720/A composite at 1200°C in air. Creep rates produced by specimens with effusion holes were approximately an order of magnitude higher than those produced by unnotched specimens. Notably, the presence of effusion holes had a less pronounced effect on minimum creep rates in steam. At 1200°C in steam, the presence of laser drilled effusion holes increased the minimum creep strain rates by a factor of 4-5 on average.

It is also noteworthy that at 1200°C steam has a considerably greater detrimental effect on creep rates for the unnotched N720/A specimens. As previously reported by Harlan [15], steam accelerates minimum creep rates by approximately an order of magnitude for the unnotched specimens. Recall that in the case of specimens with effusion holes, steam increased the minimum creep strain rates by a factor of 6-7 on average. The degradation of creep performance of N720/A unnotched specimens at 1200 °C in steam is due to (1) accelerated matrix densification and (2) loss of mullite phase in N720 fibers [17], [18]. We believe that laser drilling significantly alters composite microstructure around the holes. Both matrix densification and formation of glassy phase in the material surrounding each hole became evident when composite microstructure was examined under SEM. Matrix densification implies the loss of matrix porosity needed for N720/A composite to perform as designed. Formation of glassy phase indicates that mullite phase is being leached from N720 fibers thereby degrading creep resistance of the fibers. A detailed discussion of the composite microstructure and changes to microstructure due to laser drilling is presented in Section 4.6 below.

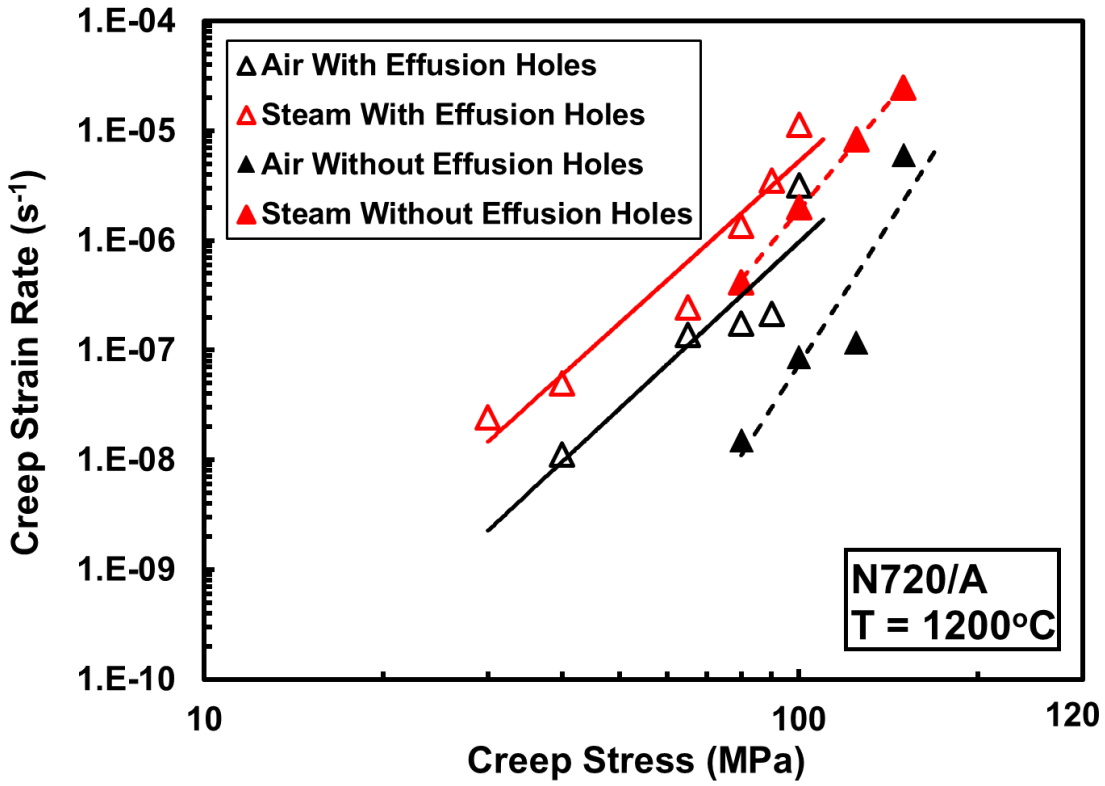


Figure 25: Creep stress vs. creep strain rate for N720/A specimens with laser drilled effusion holes and without at 1200°C in air and steam.

4.6 Composite Microstructure

Optical micrographs of the N720/A specimens with laser drilled holes were taken prior to testing. Representative optical micrographs showing composite microstructure in the vicinity of two randomly selected holes are presented in Figure 26 a) and b). A key feature seen in these micrographs is the formation of the glassy phase around the hole. While the matrix is alumina (α-Al_2O_3), N720 fibers contain both alumina and mullite. Chemical composition of N720 fiber is: ~ 85 wt.% Al_2O_3 and 15 wt.% SiO_2. Phase composition of N720 fiber is: ~ 60% mullite ($Al_6Si_2O_{13}$) and 40% (α-Al_2O_3). Glassy bubble-like features seen around the hole are believed to be SiO_2 glass, indicating the Si was leached from N720 fibers

to form SiO_2 glass. As a result, fibers and matrix in the vicinity of the hole are fused together by this glassy phase. The matrix porosity is lost and the material performance is degraded. Furthermore, leaching of Si from the fibers implies depletion of mullite phase in N720 fibers. It is widely accepted that the superior high-temperature creep resistance of N720 fibers is due to high mullite content. Depletion of mullite phase from the fibers results in further degradation of the creep performance of N720/A.

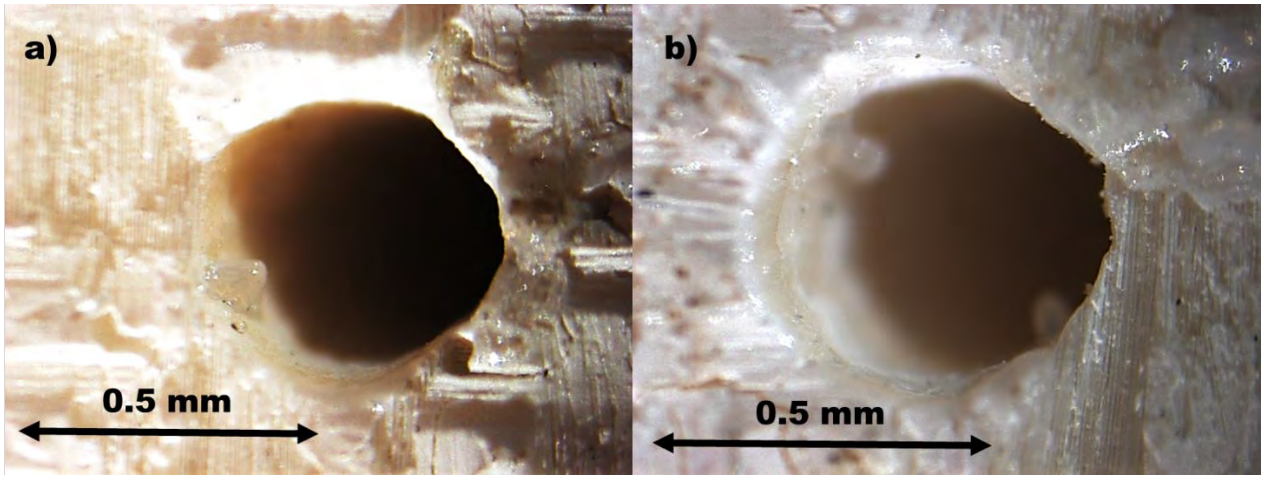


Figure 26: Pre-Test optical micrographs of N720/A specimens with effusion holes showing material in the vicinity of randomly selected holes.

Optical micrographs showing composite material in the vicinity of a hole in specimens subjected to various tests are presented in Figure 27, Figure 28, Figure 29, and Figure 30. As in the case of pre-test images, substantial amount of fiber/matrix fusing is seen in the material around the hole. Such fusing indicates loss of matrix porosity. Recall that N720/A composite relies on a porous matrix for crack deflection. Loss of matrix porosity leads to degradation of composite performance. Consequently, minimal fiber pull-out is seen in the vicinity of the holes; planar, non-fibrous fracture prevails.

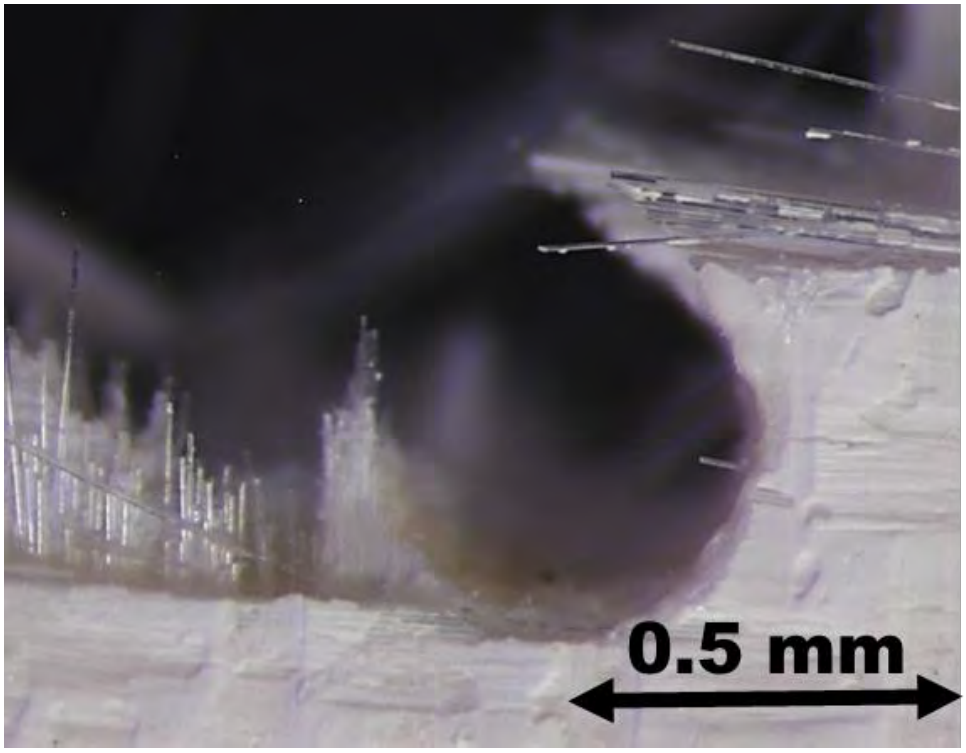


Figure 27: Optical micrograph of the N720/A specimen with effusion holes tested in tension to failure at 1200ºC showing material in the vicinity of a hole.

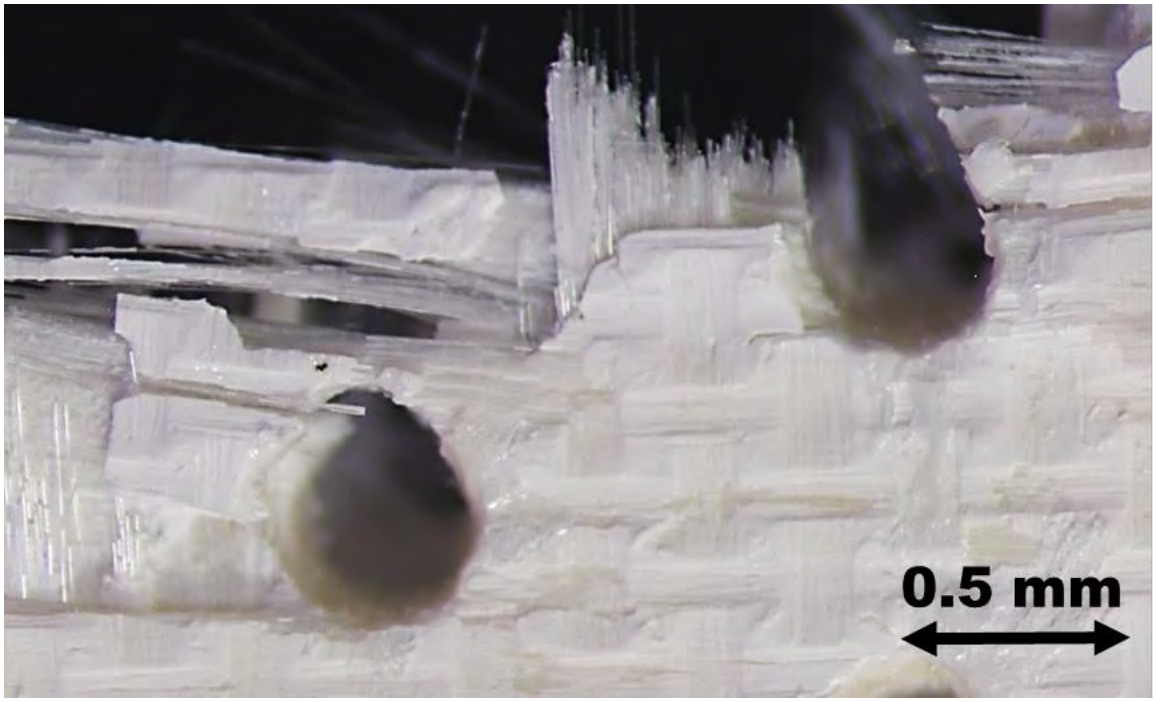


Figure 28: Optical micrograph of the N720/A specimen with effusion holes tested in tension to failure following 100 h of creep at 40 MPa at 1200°C in air. Formation of glassy phase and lack of fiber pull-out around effusion holes are clearly visible.

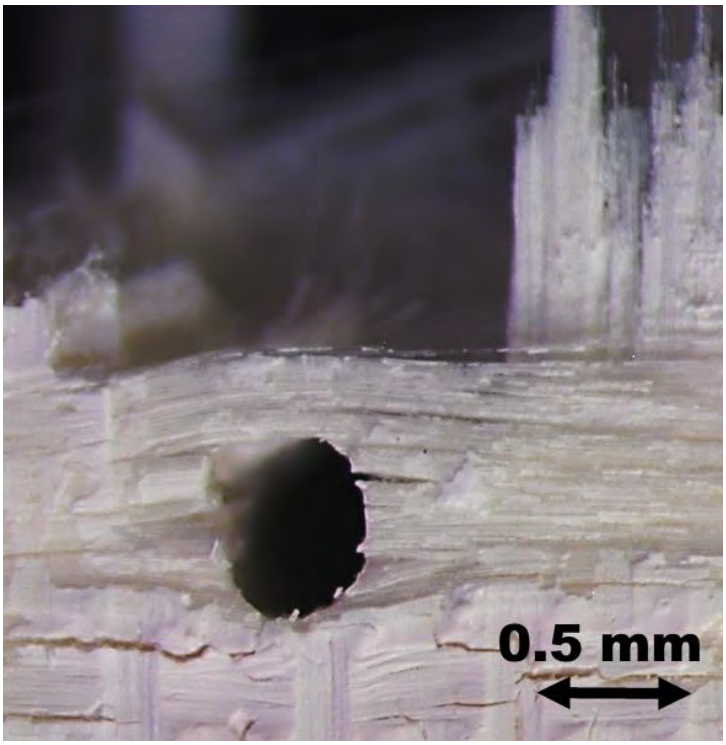


Figure 29: Optical micrograph of the N720/A specimen with effusion holes tested in creep at 1200ºC in air (σ_{cr} = 65 MPa, t_f = 58.4 h). Fusing of fiber and matrix as well as lack of fiber pull-out in the vicinity of the hole are clearly visible.

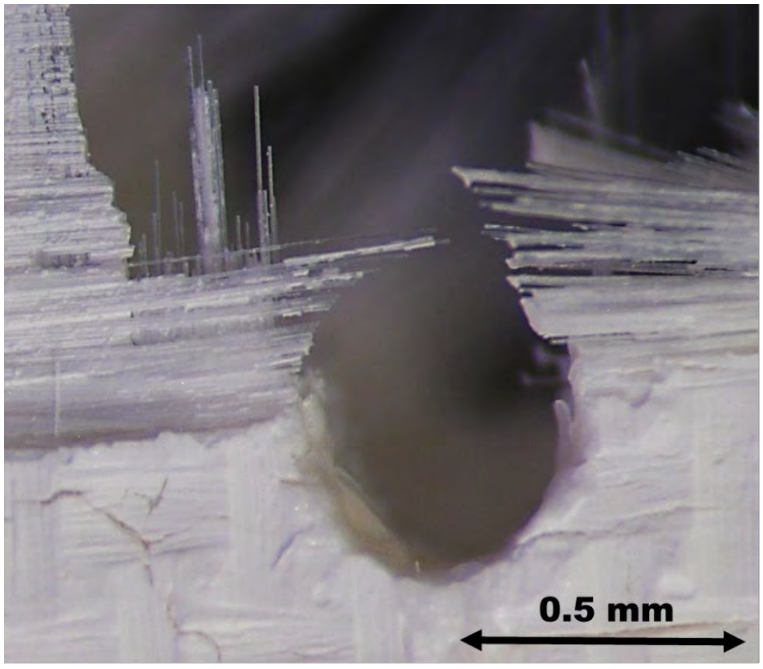


Figure 30: Optical micrograph of the N720/A specimen with effusion holes tested in tension to failure following 100 h of creep at 30 MPa at 1200°C in steam. Formation of glassy phase and lack of fiber pull-out around effusion holes are clearly visible.

Optical micrographs of fracture surfaces produced in creep tests performed in air and in steam are shown in Figure 31 and Figure 32, respectively. The specimens tested in air (Figure 31) show a slightly greater degree of uncorrelated fiber fracture than those tested in steam (Figure 32). The test environment appears to have a weak effect on the fracture surface topography. We believe that considerable damage to the composite occurred during laser drilling of the effusion holes. Creep performance of the composite is significantly degraded due to laser drilling. While steam has an additional degrading effect on creep of N720/A, this additional degradation is minor compared to that due to laser drilling.

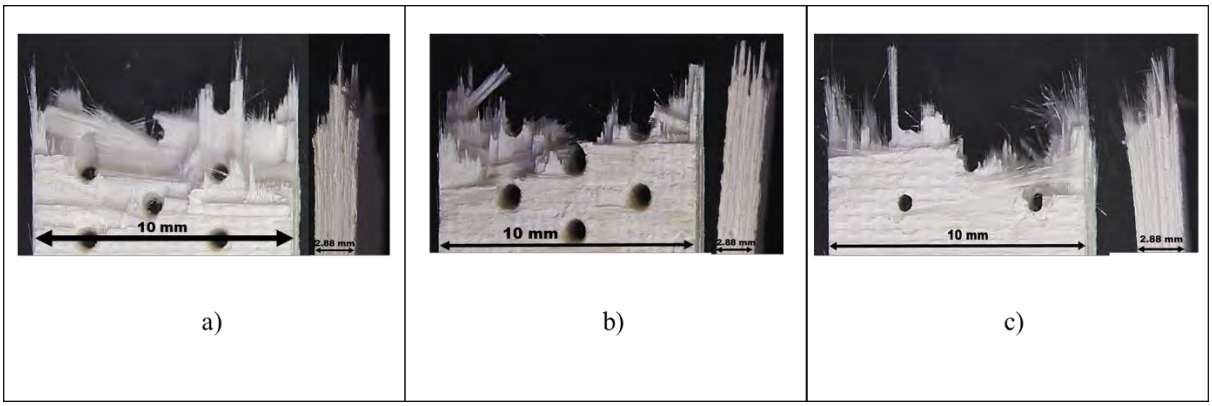


Figure 31: Fracture surfaces obtained for N720/A specimens with effusion holes in creep tests conducted at 1200 °C in air: (a) σ_{cr} = 40 MPa, (b) σ_{cr} = 65 MPa, and (c) σ_{cr} = 100 MPa.

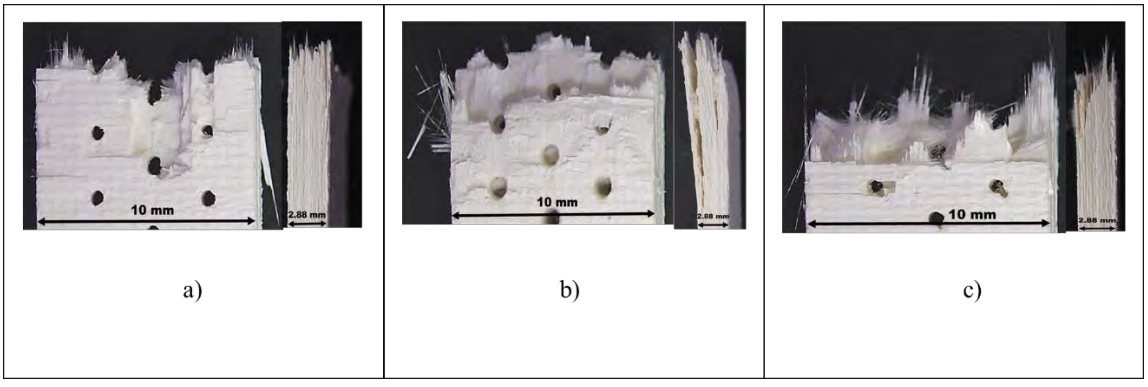


Figure 32: Fracture surfaces obtained for N720/A specimens with effusion holes in creep tests conducted at 1200 °C in steam: (a) σ_{cr} = 40 MPa, (b) σ_{cr} = 65 MPa, and (c) σ_{cr} = 100 MPa.

SEM micrographs of selected fracture surfaces obtained in this work are presented in Figure 33 to Figure 36. The extent of the damage done to the composite by the laser drilling is of particular interest. Hence, the focus of these SEM images is on regions in the vicinity of the holes. By examining the SEM images in Figure 33 to Figure 36 we can estimate the size of the damaged zone (DZ) surrounding a laser drilled hole. Consider, for example, the SEM images in Figure 33. The edge of the hole as well as the glassy phase found in the interior of the hole are clearly visible in Figure 33a. Note that the fibers in the area next to the hole have failed in a correlated fashion. Fiber bonding is apparent, while pull-out of individual filaments is not observed. Fracture surface in Figure 34 also exhibits correlated fiber fracture as well as fiber/matrix bonding in the vicinity of the hole, suggesting that considerable damage occurred to the composite during laser drilling. Glassy phase covering the hole interior is also visible (bottom half of the image). Another example of fiber/matrix bonding and noticeable absence of fiber pull-out is seen in Figure 35. It should be noted that SEM images in Figure 33 to Figure 36 are typical and representative of the fracture surfaces obtained in this work. Similar signs of damage were observed around the laser-drilled holes in all fracture surfaces obtained in this work. It is possible that a single laser drilled hole of 0.5-mm diameter would have little effect on creep performance of N720/A composite. However, damage zones produced by laser drilling an array of 17 holes consumed a considerable portion of the specimen gage section. Hence the dramatic effect of laser drilled effusion holes on creep performance. Using SEM images in Figure 33 to Figure 36, we are able to estimate the size of the damage zone surrounding a laser drilled hole. Recall that the diameter of the hole is 0.5 mm. Based on SEM images it appears that the diameter of the damage zone is close to 1mm. As a result a large portion of the specimen gage section is affected by damage due to laser drilling. The ability of

the material to perform as designed is noticeable reduced, creep resistance of the CMC is degraded.

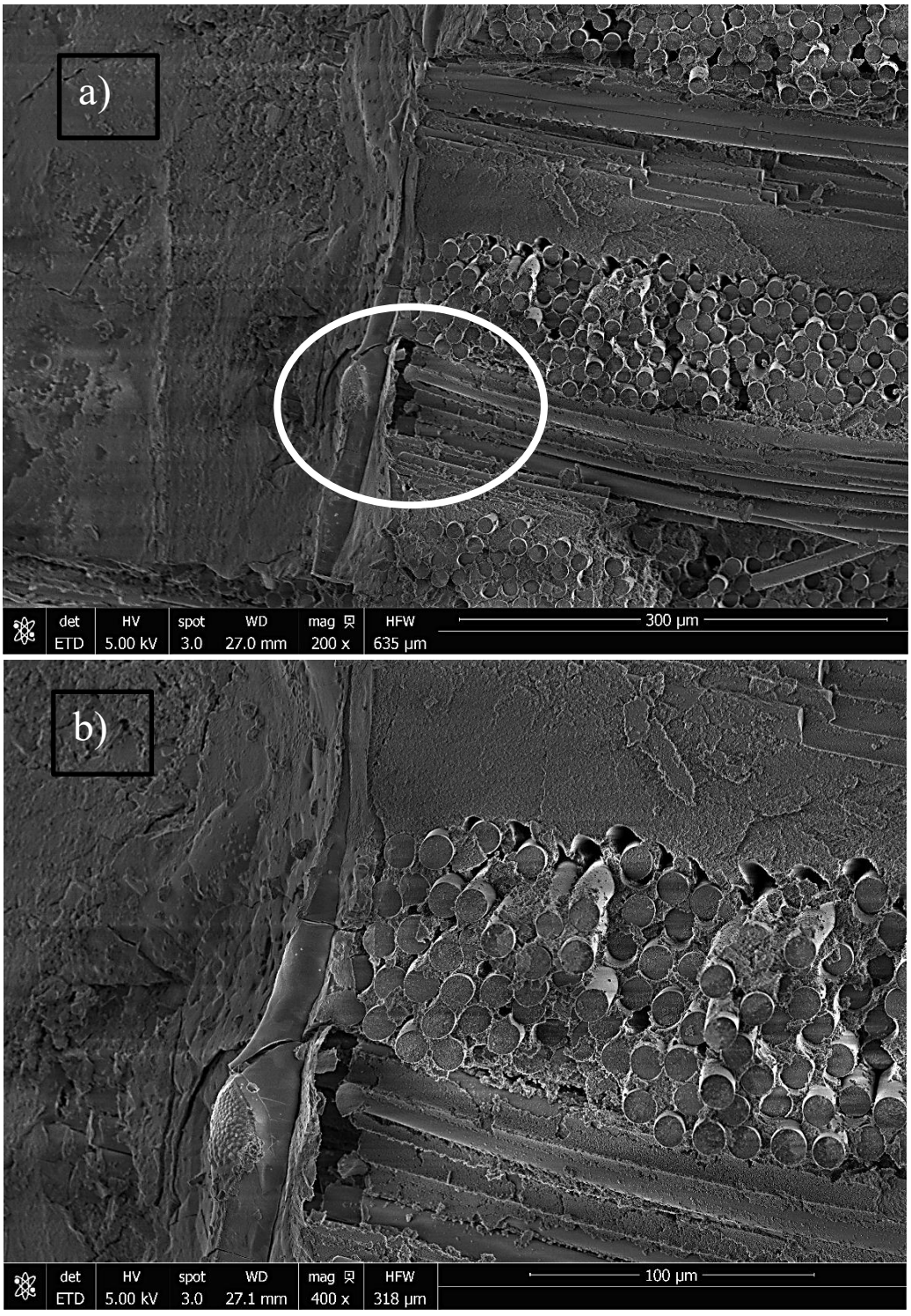


Figure 33: Fracture surface of a N720/A specimen tested in creep in laboratory air at 1200ºC (σ_{cr} = 65 MPa, t_f = 58.4 h). a) Edge of the hole and the glassy phase found in the interior of the hole are clearly visible. (b) Higher magnification view showing edge of the hole and glassy phase in the interior of the hole.

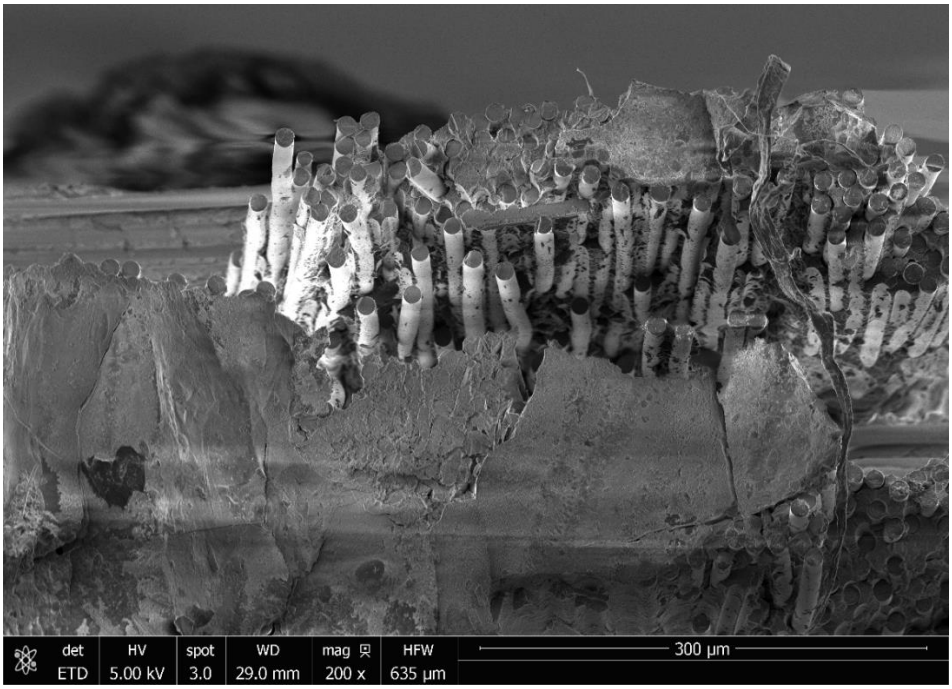


Figure 34: Fracture surface of a N720/A specimen tested in creep in steam at 1200ºC (σ_{cr} = 65 MPa, t_f = 12.4 h). Correlated fiber fracture and fiber/matrix bonding in the vicinity of the hole (top half of the image). Glassy phase in the hole interior (bottom half of the image).

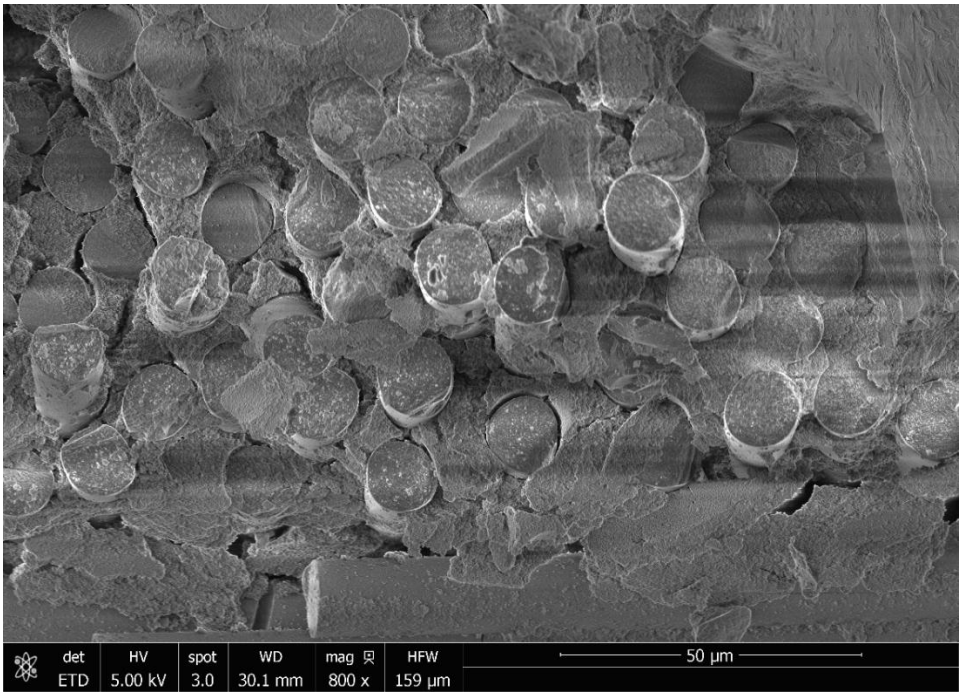


Figure 35: Fracture surface of a N720/A specimen tested in creep in steam at 1200ºC (σ_{cr} = 65 MPa, t_f = 12.4 h). Correlated fiber fracture, fiber/matrix bonding and absence of fiber pull-out are apparent.

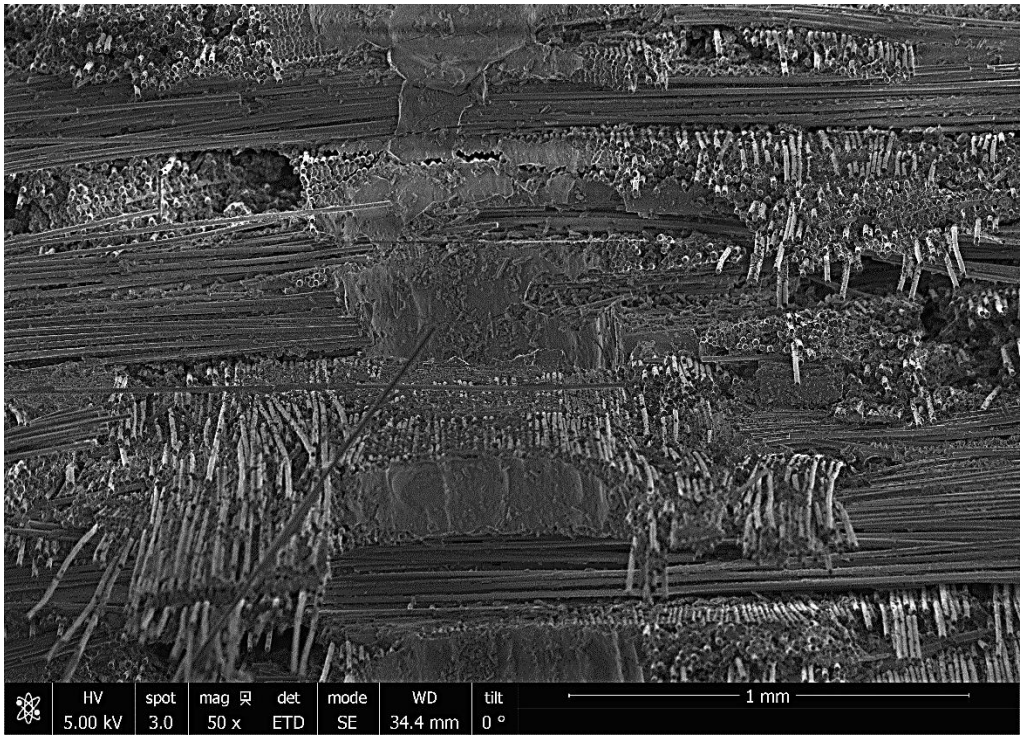


Figure 36: Fracture surface of a N720/A specimen tested in tension to failure following 100 h of creep at 40 MPa in laboratory air at 1200ºC.

V. Conclusions and Recommendations

5.1 Concluding Remarks

This research effort evaluated the creep-rupture behavior of Nextel^{TM} 720/A with laser drilled effusion holes at 1200°C in air and in steam environments. Mechanical tests were performed to determine the creep response of the CMC. Then, the composite microstructure was analyzed using an optical microscope and an SEM. Results of this research show that laser drilling cause significant damage to the composite microstructure leading to significant degradation of the creep resistance of N720/A CMC.

Monotonic tensile tests to failure were performed in order to determine the effect of laser drilled effusion holes on ultimate tensile strength of the composite. Results revealed that the presence of the effusion holes reduced the UTS by approximately 13% and reduced the modulus by 16%.

Creep-rupture tests were performed at 1200°C in laboratory air and in steam environments. Creep stress levels were 150, 100, 90, 80, 65, and 40 MPa in air, and 100, 90, 80, 65, 40, and 30 MPa in steam. Results revealed that the laser drilled holes had a strong detrimental effect on the creep performance of the composite. The presence of laser drilled effusion holes reduced creep lifetimes by 70-95% in air and by ~95% in steam.

Test specimens were examined with an optical microscope before and after mechanical testing. Optical micrographs obtained prior to testing showed a glassy phase surrounding the laser drilled holes, indicating that laser drilling caused considerable damage to both matrix and fibers. Optical micrographs of the fracture surfaces further confirmed considerable fusing of fibers and matrix as well as formation of the glassy SiO_2 phase in the vicinity of the holes.

These observations indicate the loss of porosity in the alumina matrix and depletion of the mullite phase from N720 fibers. Because N720/A composite relies on porous matrix for crack deflection, loss of matrix porosity is highly damaging. Furthermore, depletion of mullite phase from N720 fibers causes decrease of load bearing capacity of the fibers. As a result creep performance of the composite is severely reduced.

Fracture surfaces obtained in this work were examined with an SEM. The SEM images focused in the vicinity of the laser drilled holes showed damage zones produced by laser drilling. Based on careful examination of these SEM images, the average size of the damage zone was estimated to be ~1 mm in diameter. We believe that the damage to fibers and matrix is caused by intense localized heat that occurs during laser drilling.

5.2 Recommendations

This pilot study has opened many doors for further work. Results of this work show that laser drilling drastically degrades the microstructure and the mechanical performance of the composite. It is possible, that using a laser with a much shorter pulse length (for example, a nanolaser) may not cause such dramatic damage to the composite. On the other hand, hours would be required to drill a single hole in this material using a nanolaser. Hence, this is not an efficient solution if arrays of holes are to be drilled. Other drilling methods (such as diamond drilling) should be explored.

Appendix A. Optical Images

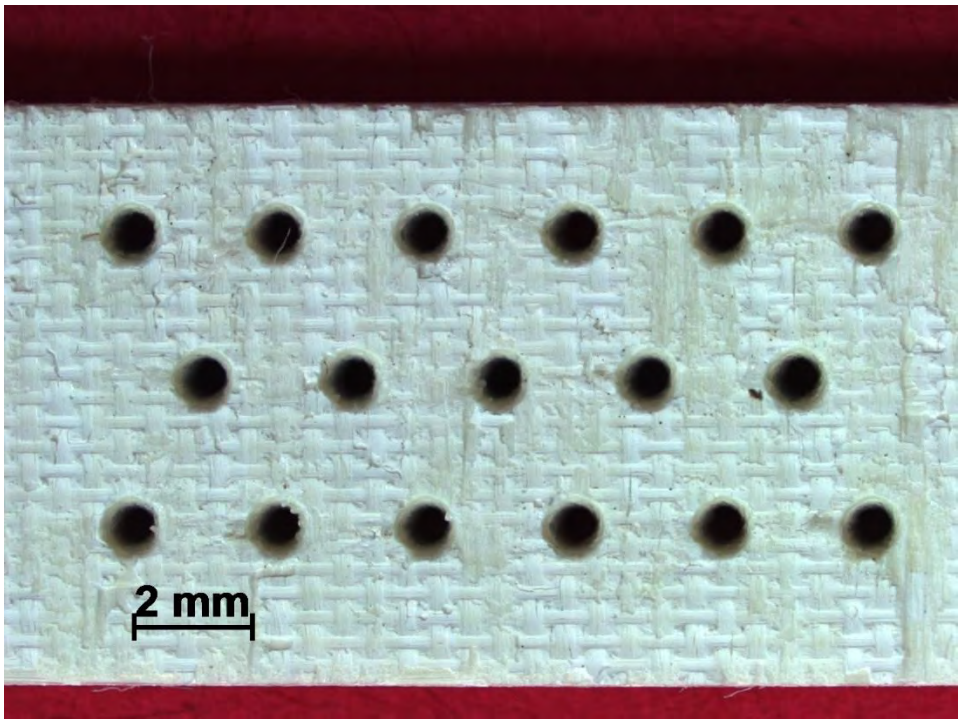


Figure A. 1: Pre-test optical image of the hole pattern in a specimen.

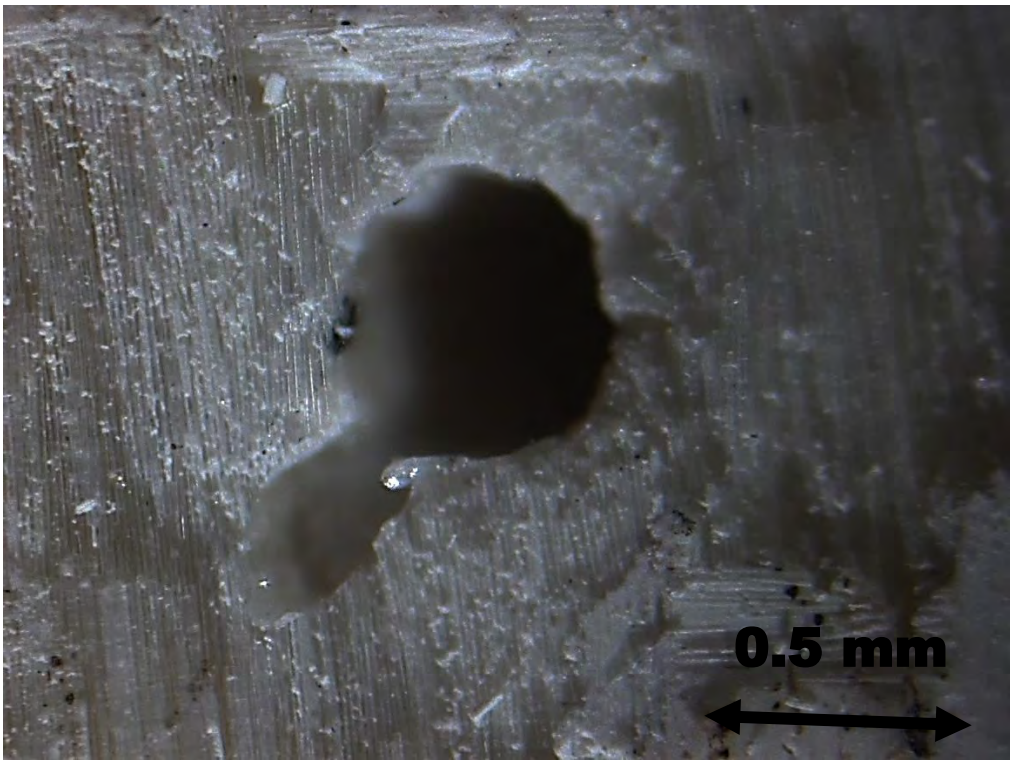


Figure A. 2: Pre-test optical image of a randomly selected hole.

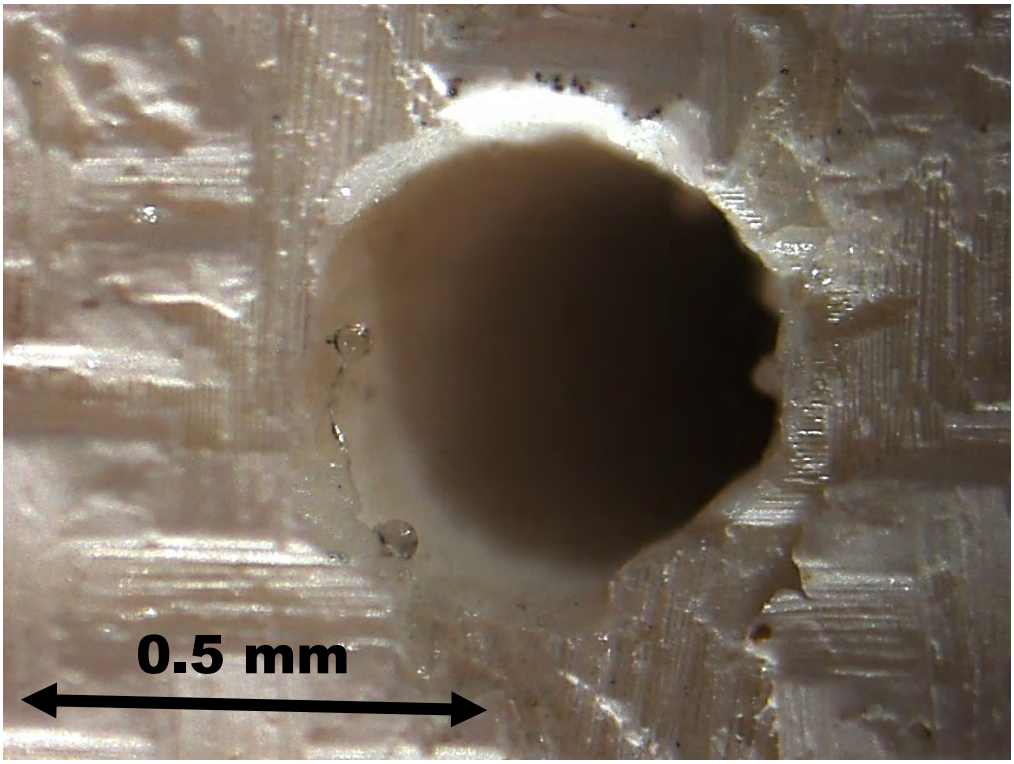


Figure A. 3: Pre-test optical image of a randomly selected hole.

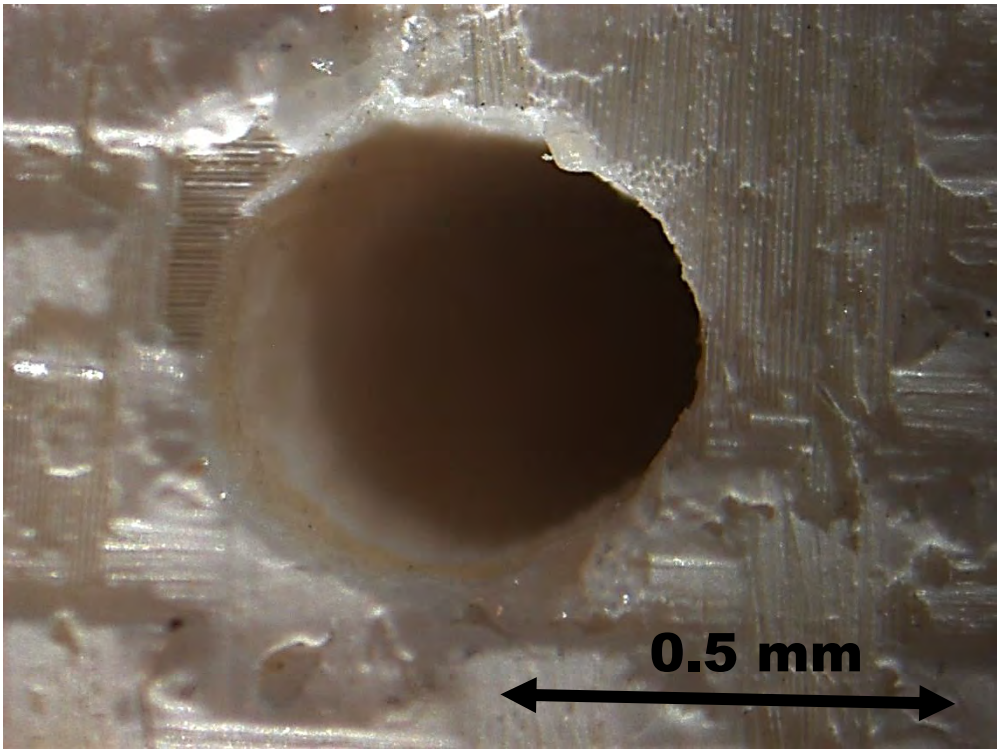


Figure A. 4: Pre-test optical image of a randomly selected hole.

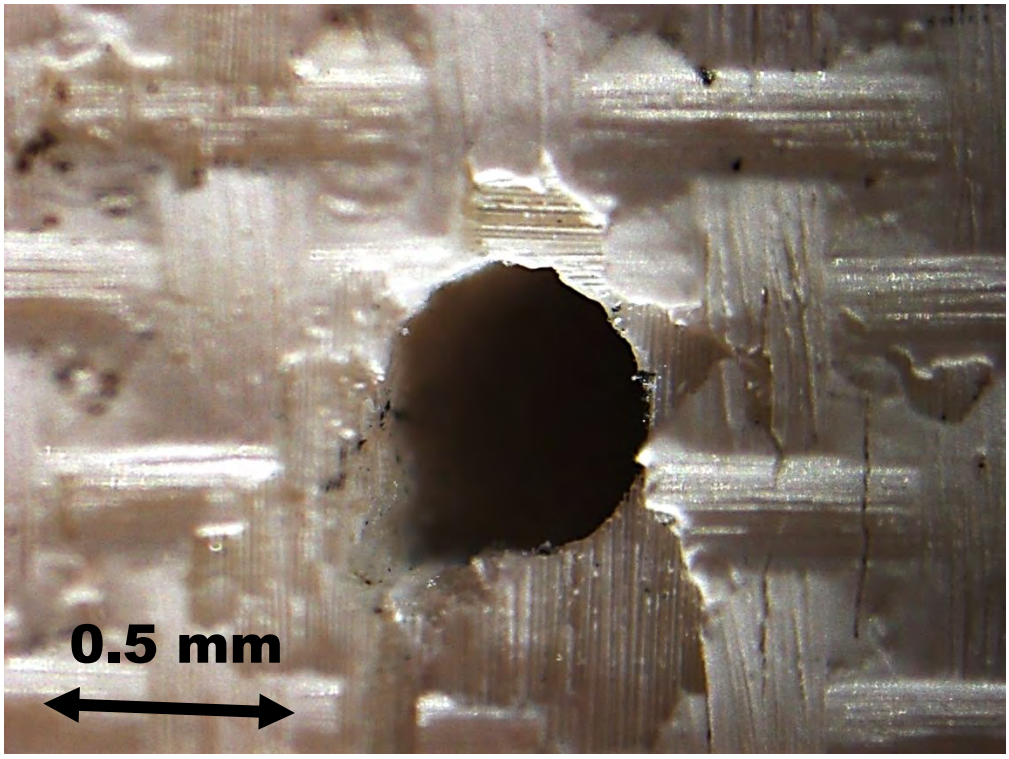


Figure A. 5: Pre-test optical image of a randomly selected hole.

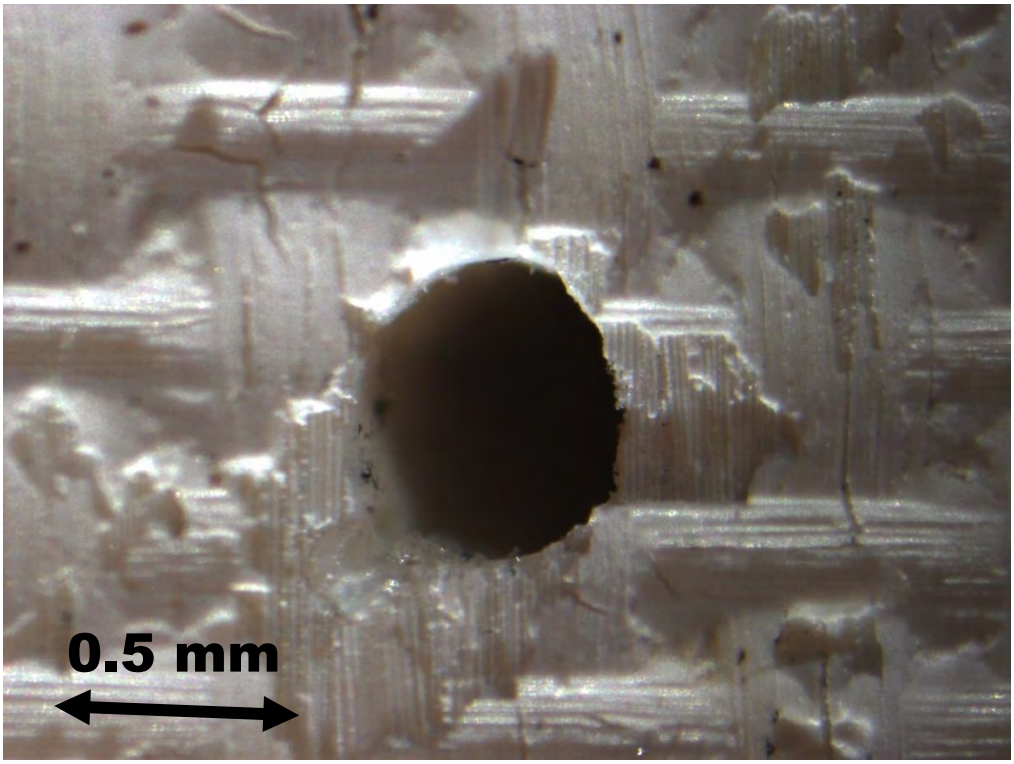


Figure A. 6: Pre-test optical image of a randomly selected hole.

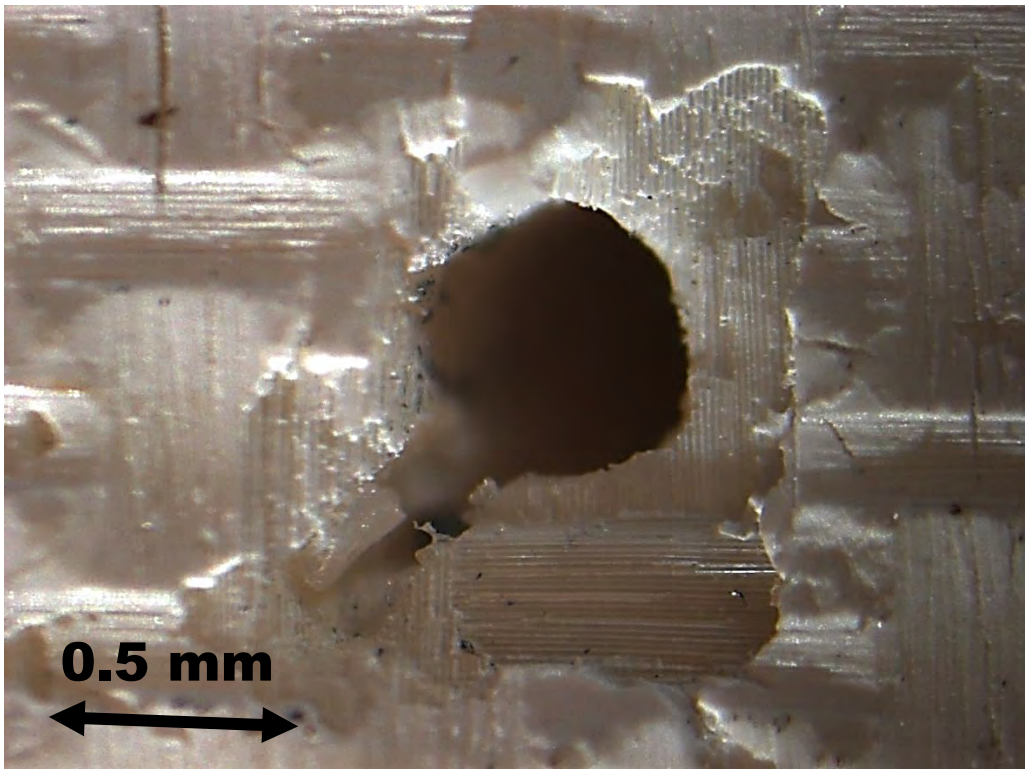


Figure A. 7: Pre-test optical image of a randomly selected hole.

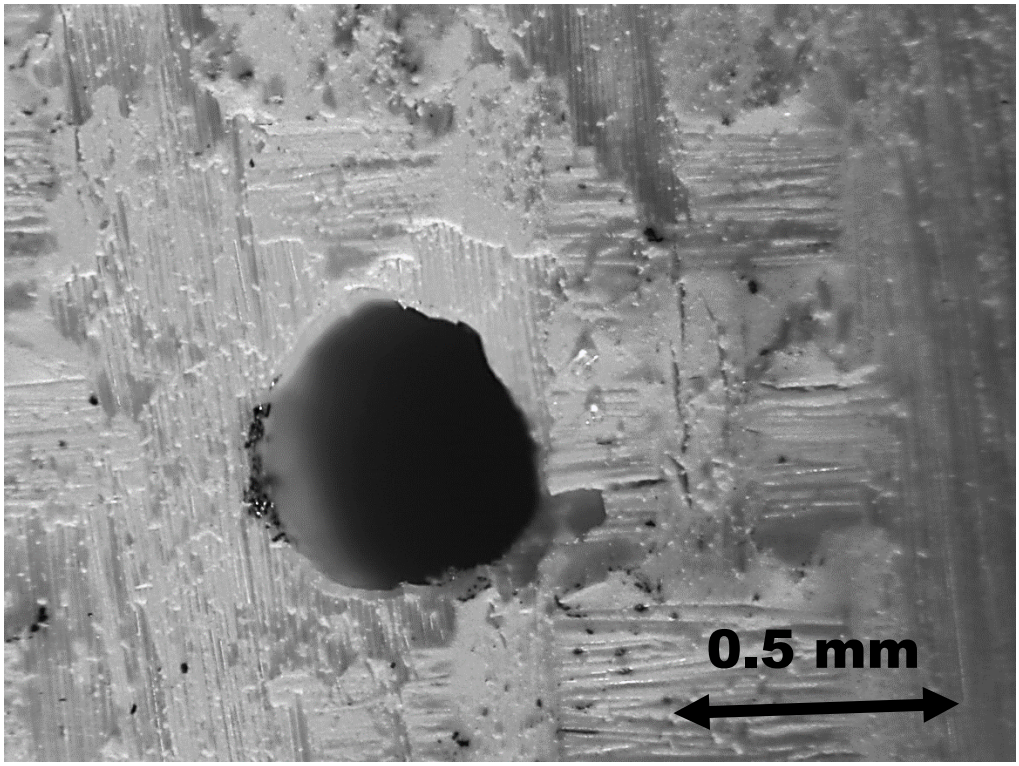


Figure A. 8: Pre-test optical image of a randomly selected hole.

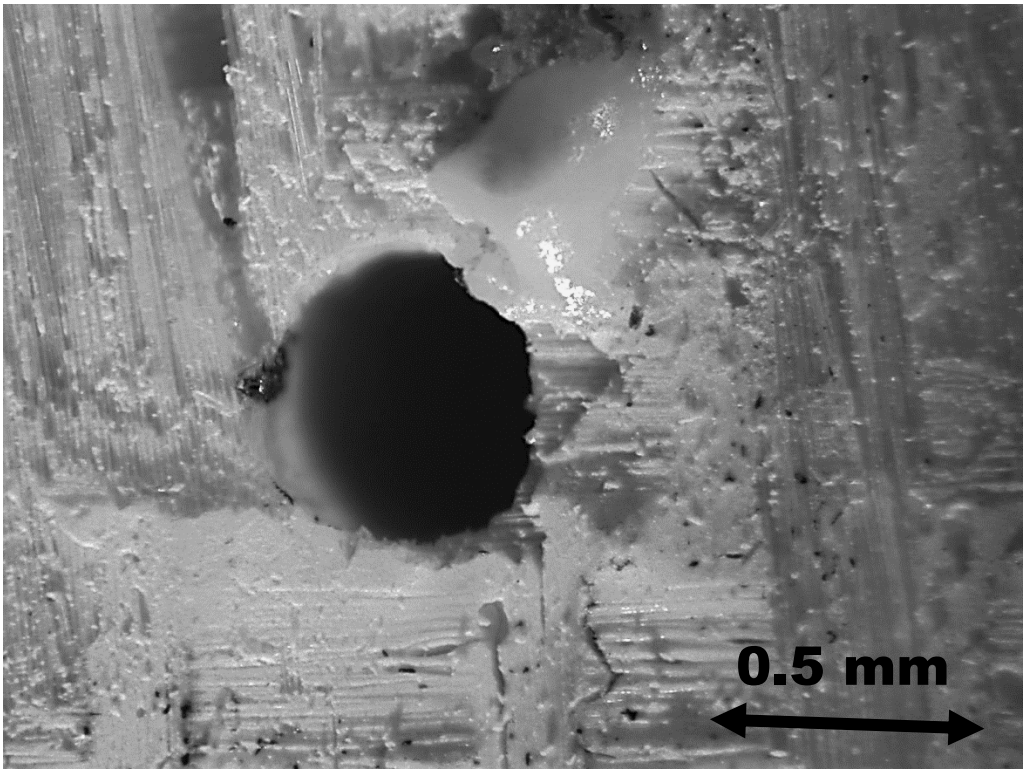


Figure A. 9: Pre-test optical image of a randomly selected hole.

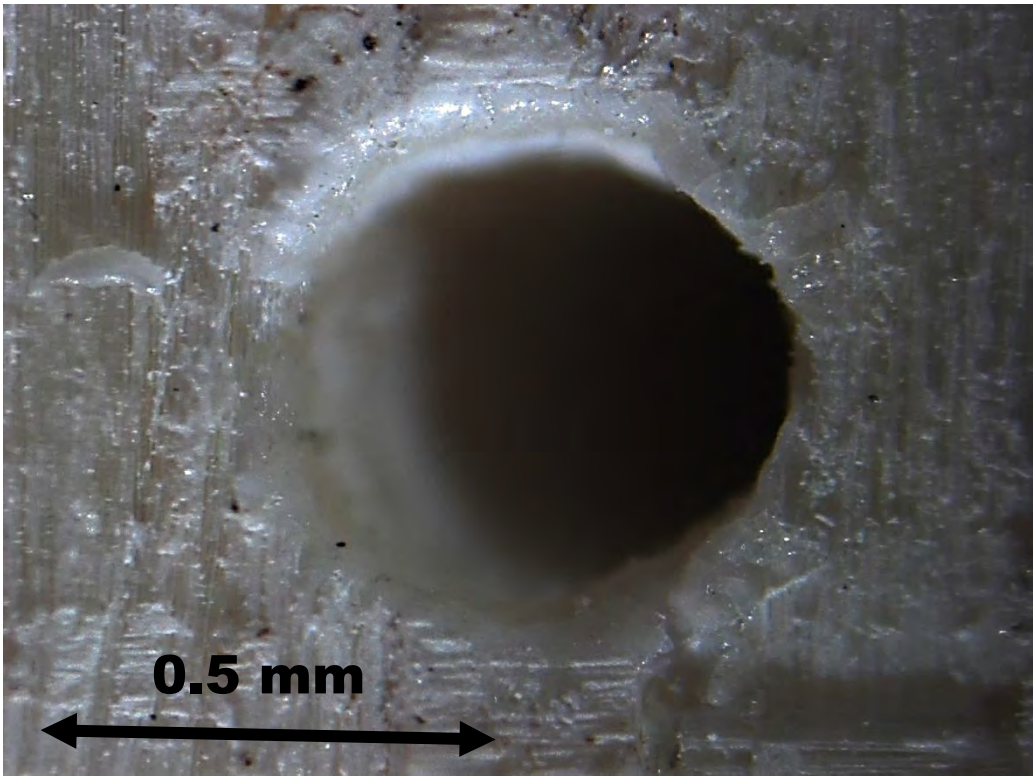


Figure A. 10: Pre-test optical image of a randomly selected hole.

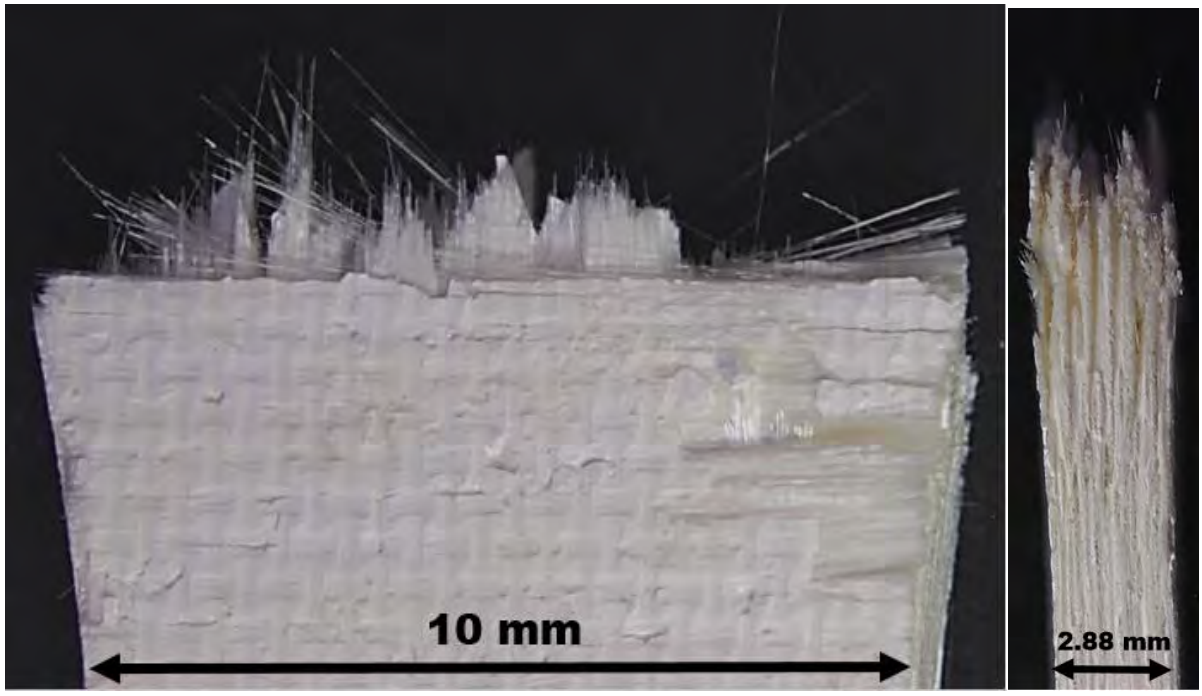


Figure A. 11: Fracture surface obtained for an unnotched N720/A specimen in tension to failure at 1200ºC in air.

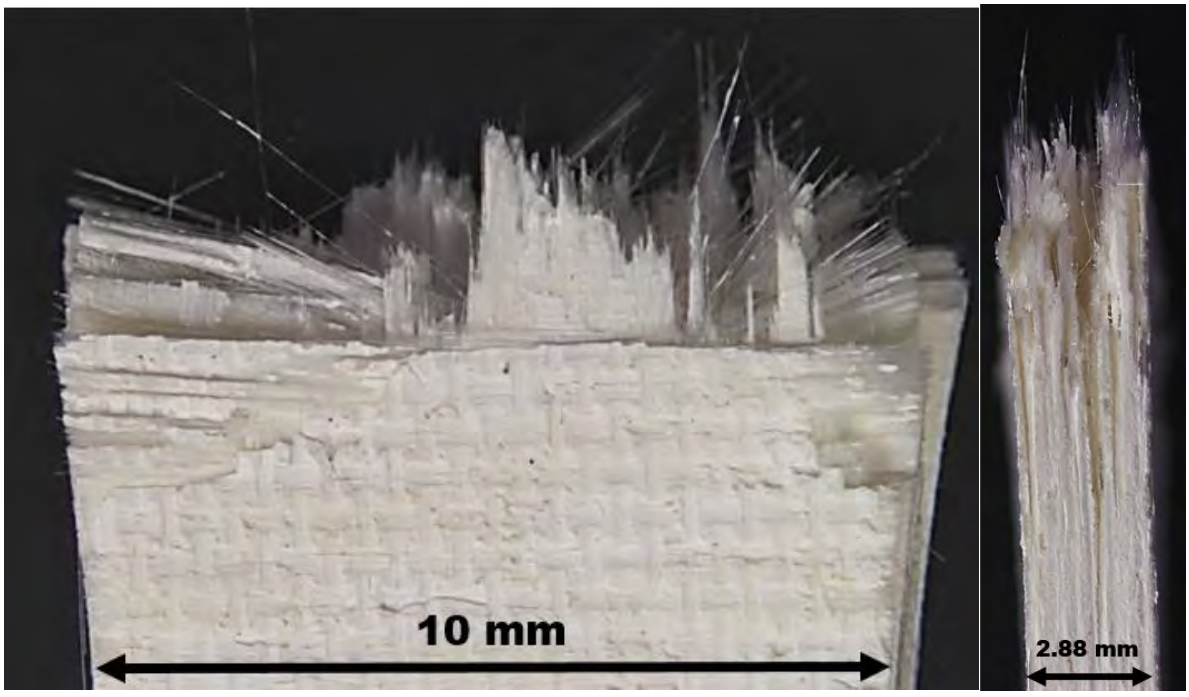


Figure A. 12: Fracture surface obtained for an unnotched N720/A specimen in tension to failure at 1200ºC in air.

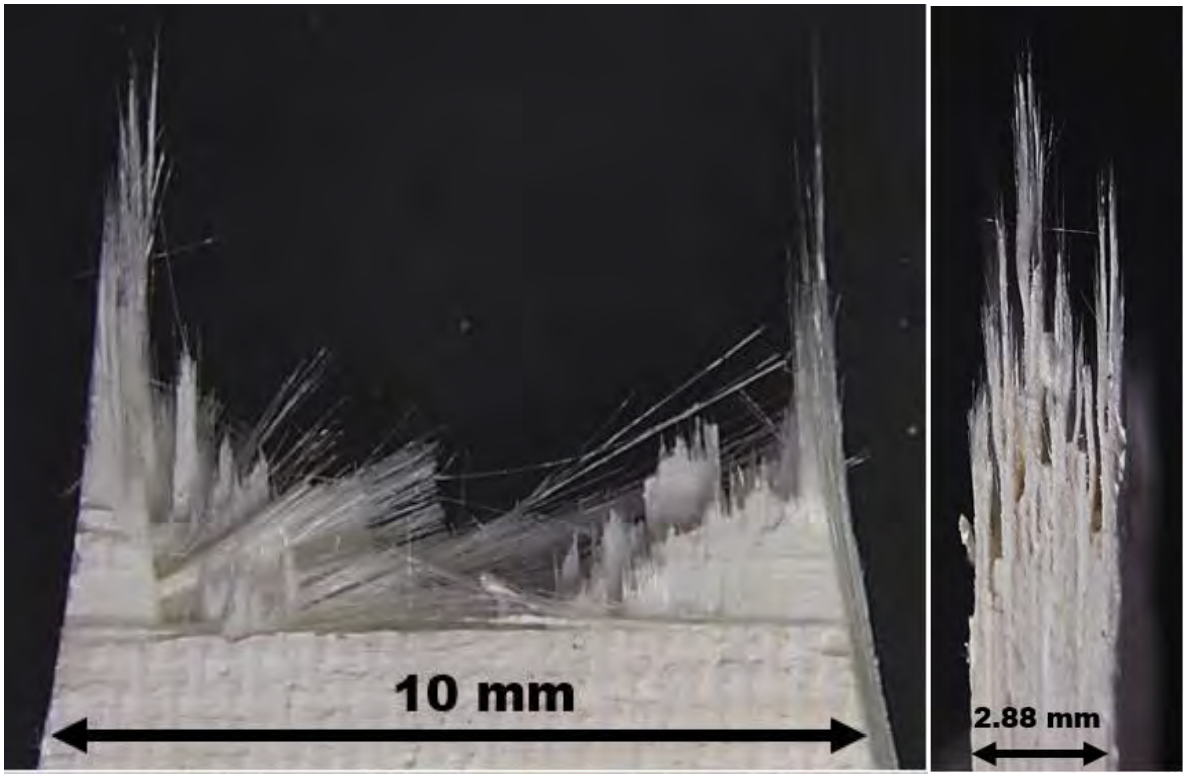


Figure A. 13: Fracture surface obtained for an unnotched N720/A specimen in tension to failure at 1200ºC in air.

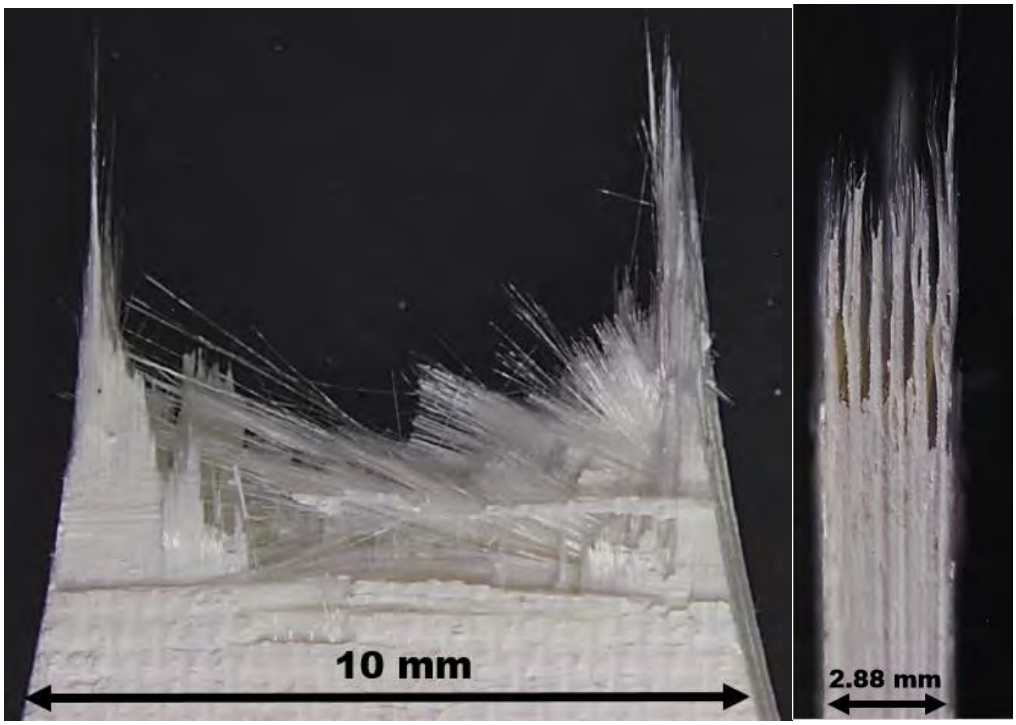


Figure A. 14: Fracture surface obtained for an unnotched N720/A specimen in tension to failure at 1200ºC in air.

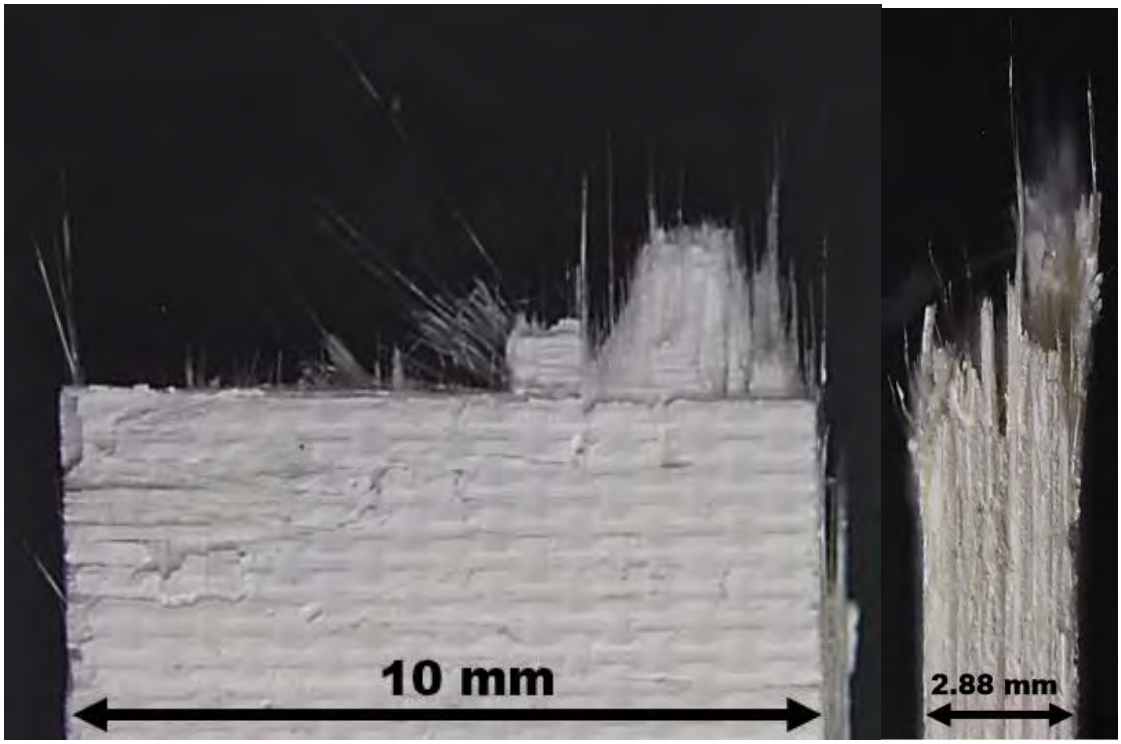


Figure A. 15: Fracture surface obtained for an unnotched N720/A specimen in tension to failure at 1200ºC in air.

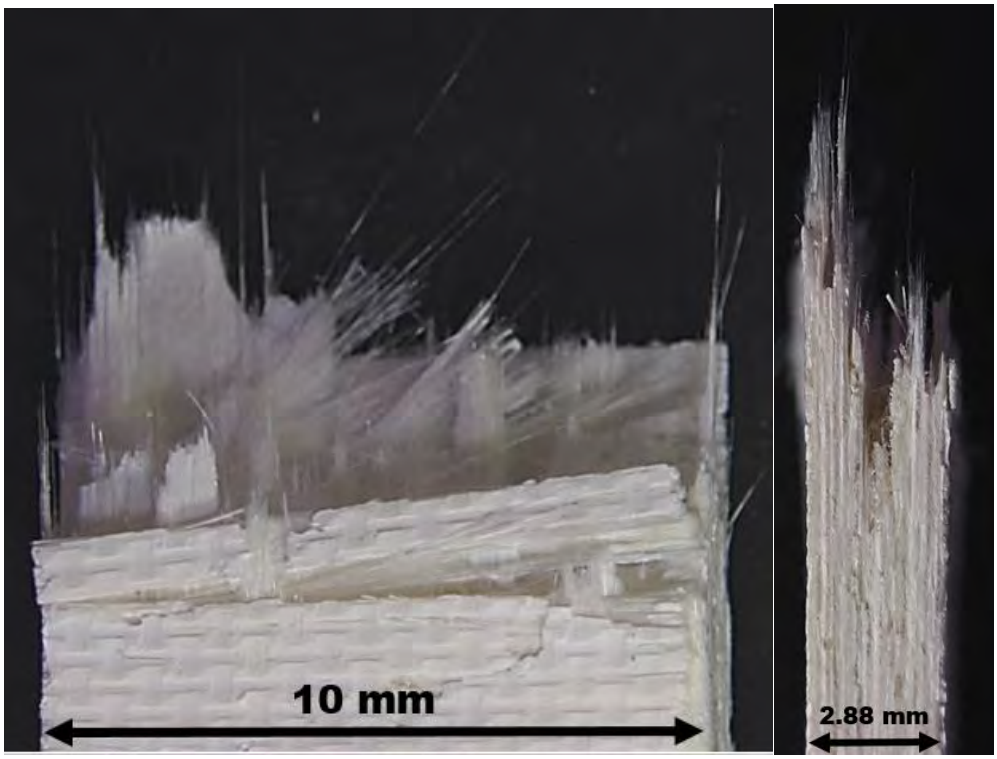


Figure A. 16: Fracture surface obtained for an unnotched N720/A specimen in tension to failure at 1200ºC in air.

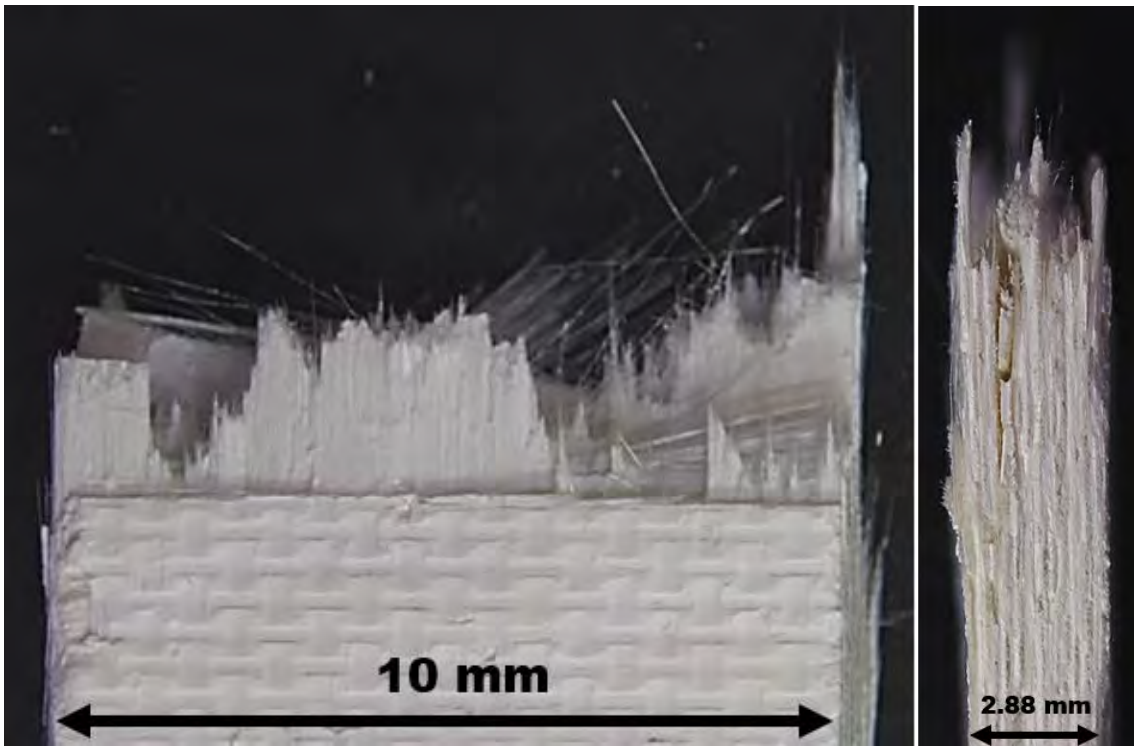


Figure A. 17: Fracture surface obtained for an unnotched N720/A specimen in tension to failure at 1200ºC in air.

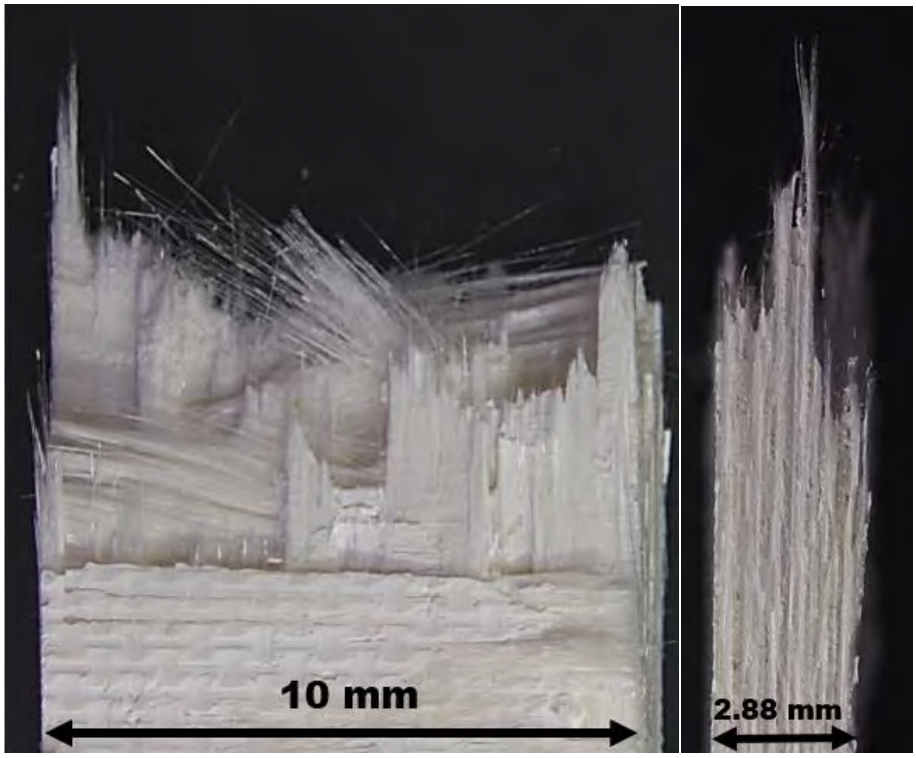


Figure A. 18: Fracture surface obtained for an unnotched N720/A specimen in tension to failure at 1200ºC in air.

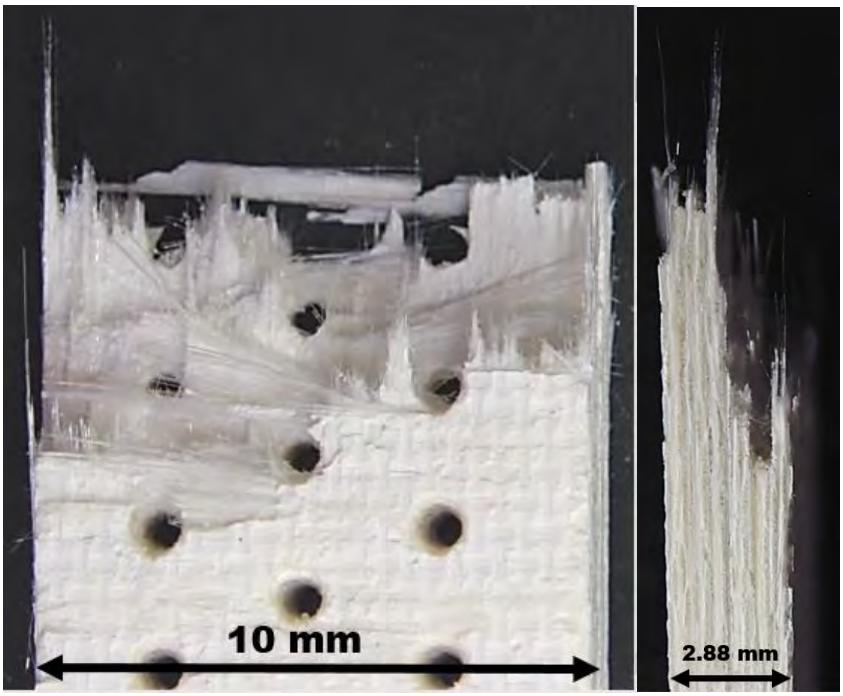


Figure A. 19: Fracture surface obtained for a N720/A specimen with effusion holes in tension to failure at 1200ºC in air.

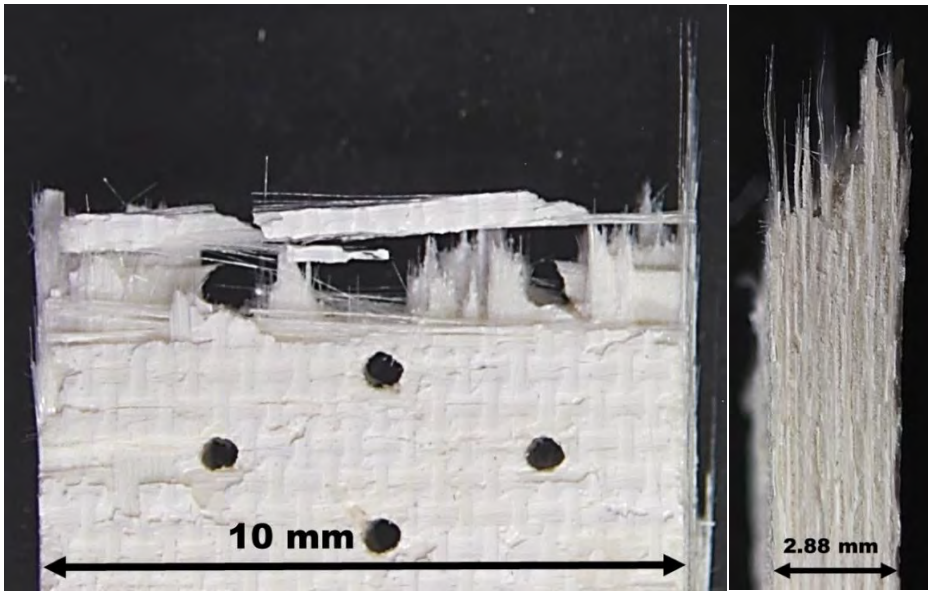


Figure A. 20: Fracture surface obtained for a N720/A specimen with effusion holes in tension to failure at 1200ºC in air.

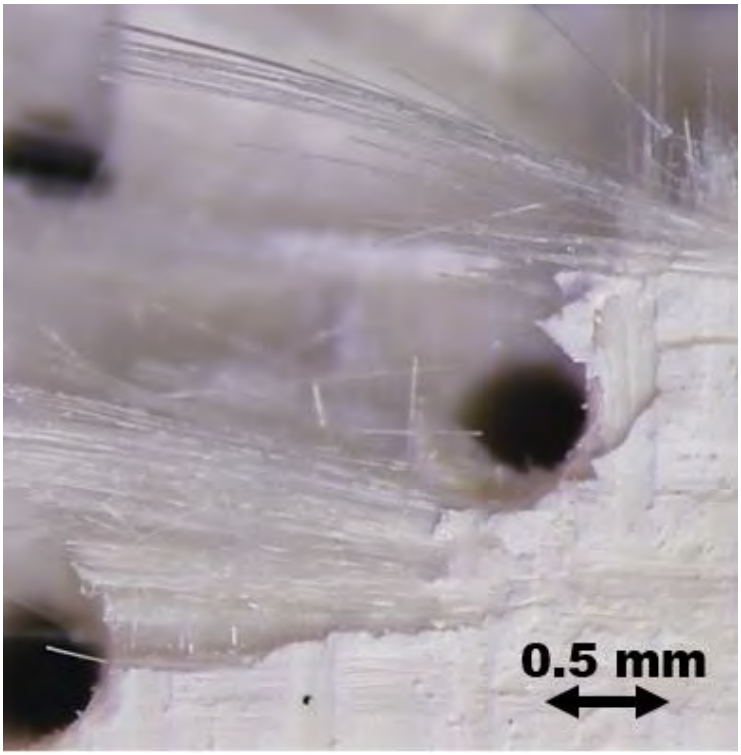


Figure A. 21: Fracture surface obtained for a N720/A specimen with effusion holes in tension to failure at 1200ºC in air.

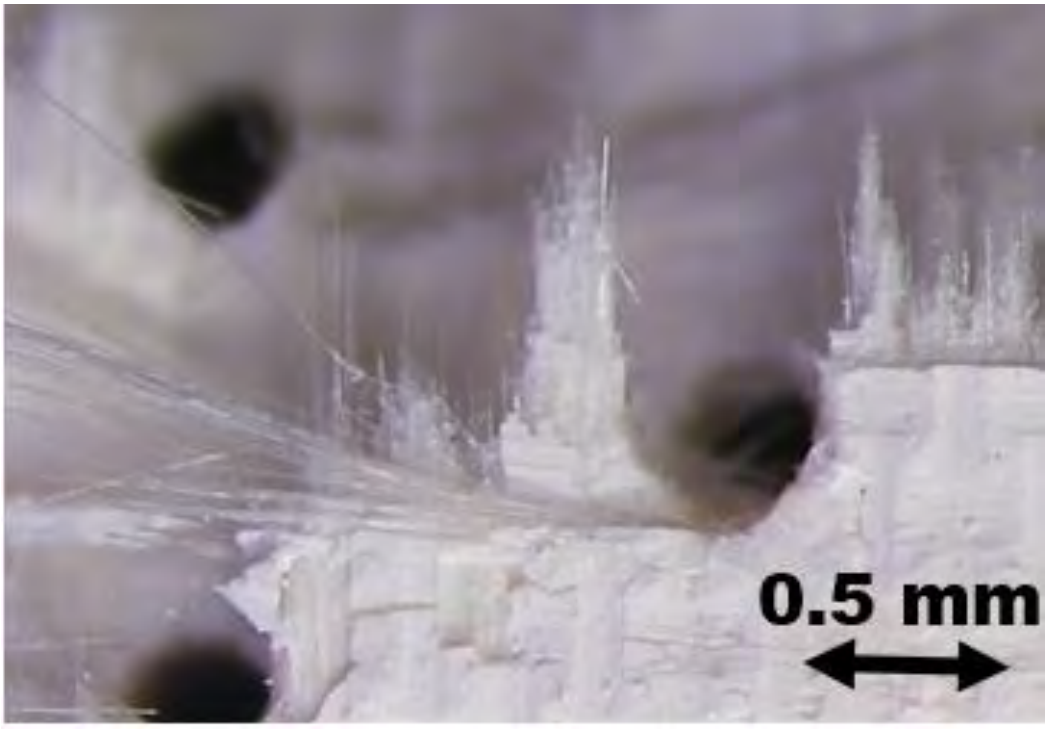


Figure A. 22: Fracture surface obtained for a N720/A specimen with effusion holes in tension to failure at 1200ºC in air.

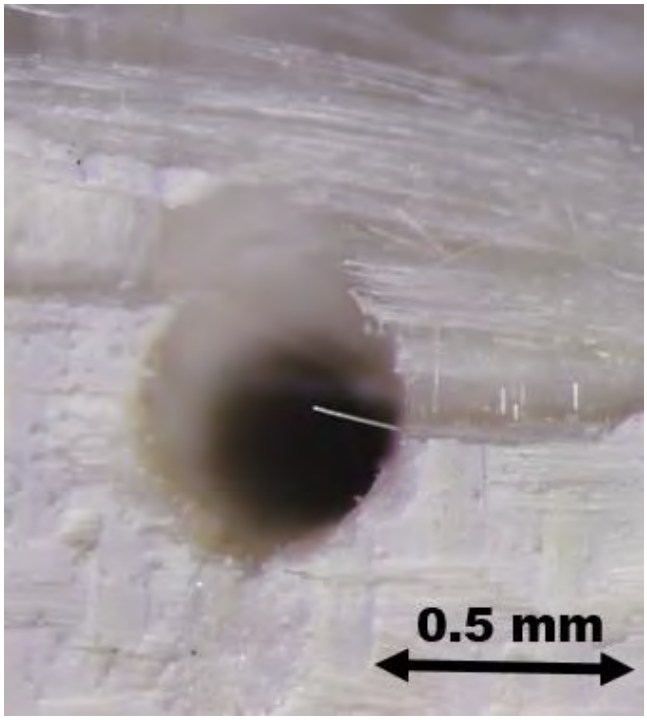


Figure A. 23: Fracture surface obtained for a N720/A specimen with effusion holes in tension to failure at 1200ºC in air.

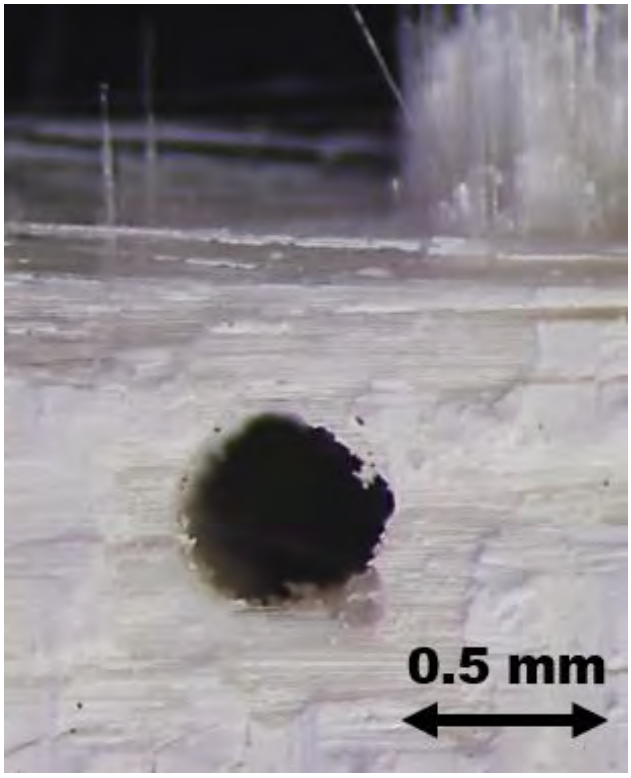


Figure A. 24: Fracture surface obtained for a N720/A specimen with effusion holes in tension to failure at 1200ºC in air.

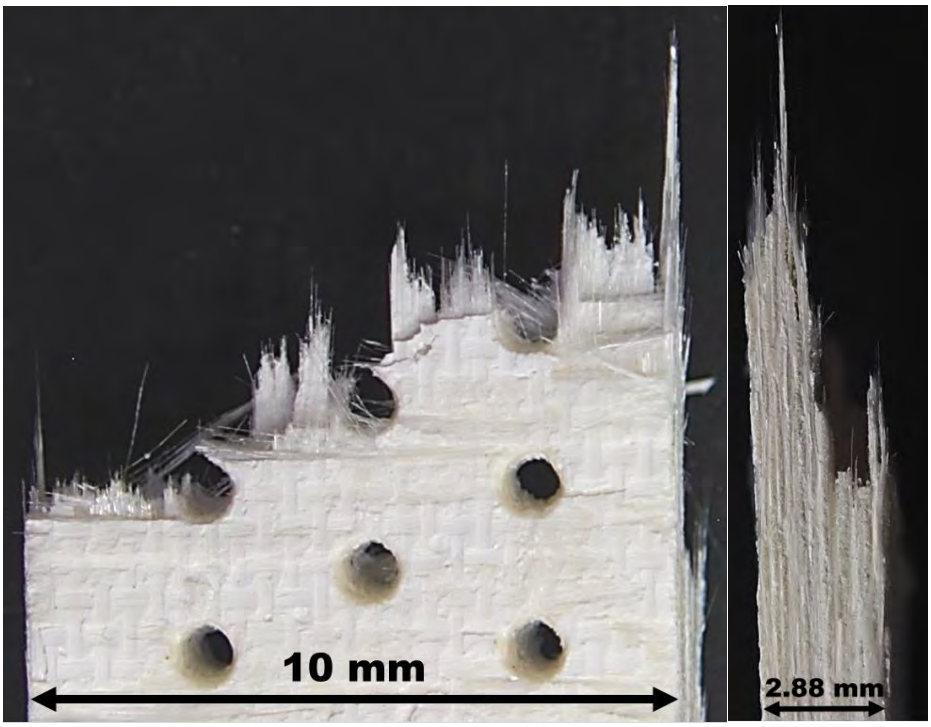


Figure A. 25: Fracture surface obtained for a N720/A specimen with effusion holes in tension to failure at 1200ºC in air.

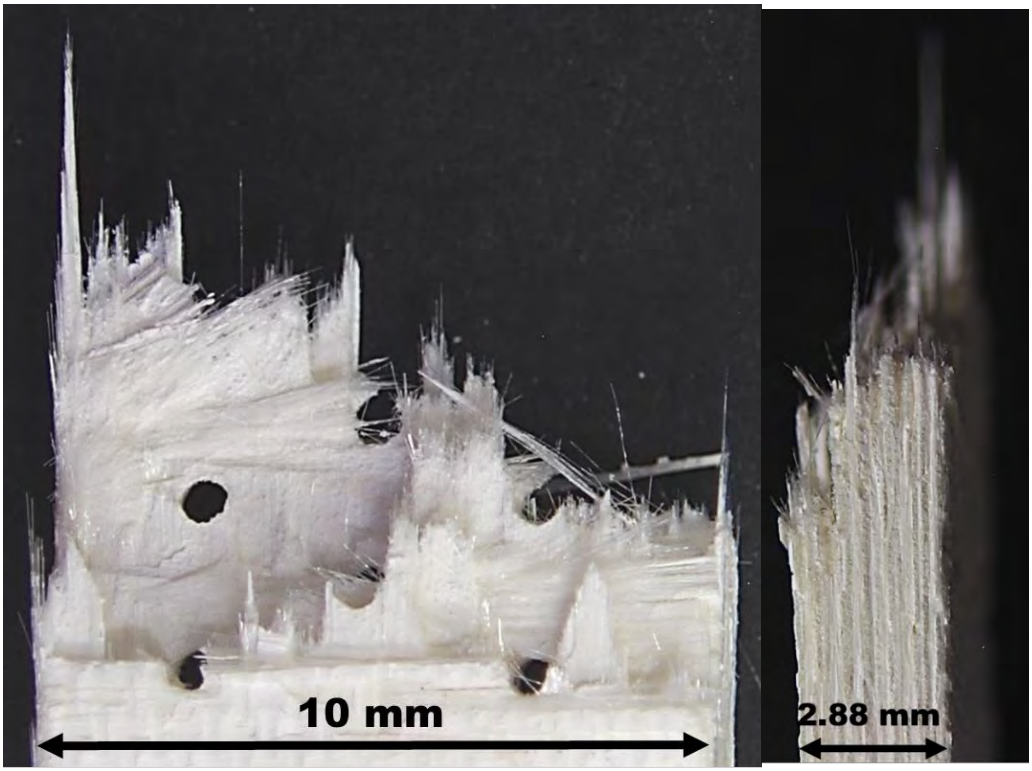


Figure A. 26: Fracture surface obtained for a N720/A specimen with effusion holes in tension to failure at 1200ºC in air.

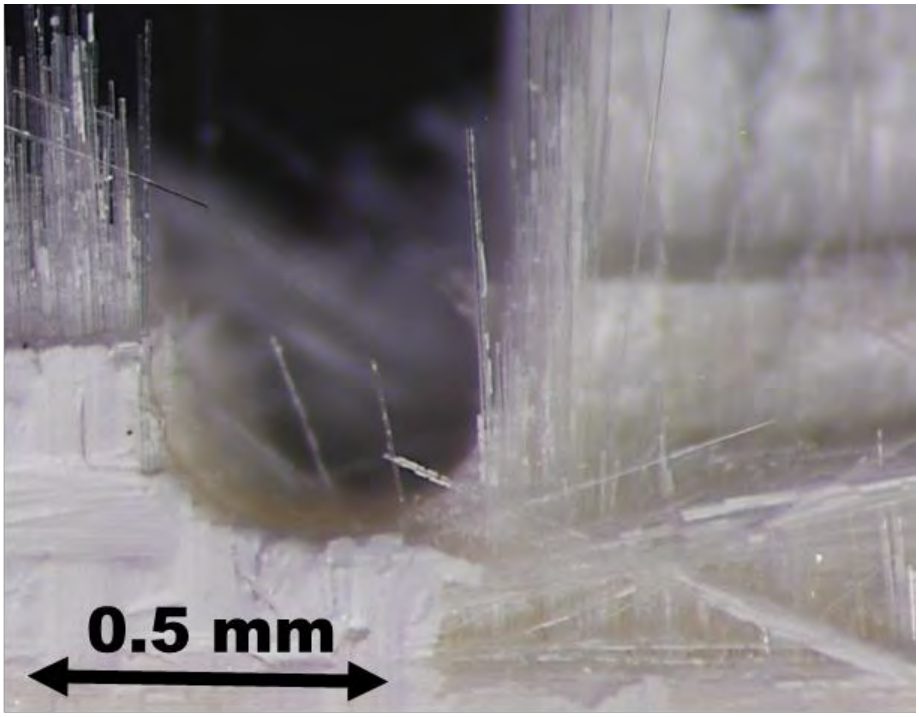


Figure A. 27: Fracture surface obtained for a N720/A specimen with effusion holes in tension to failure at 1200ºC in air.

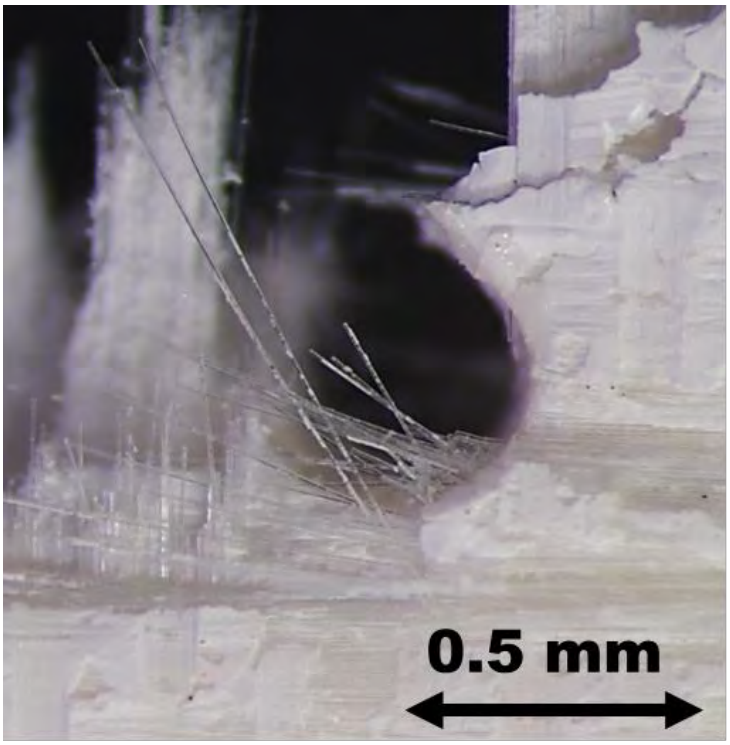


Figure A. 28: Fracture surface obtained for a N720/A specimen with effusion holes in tension to failure at 1200ºC in air.

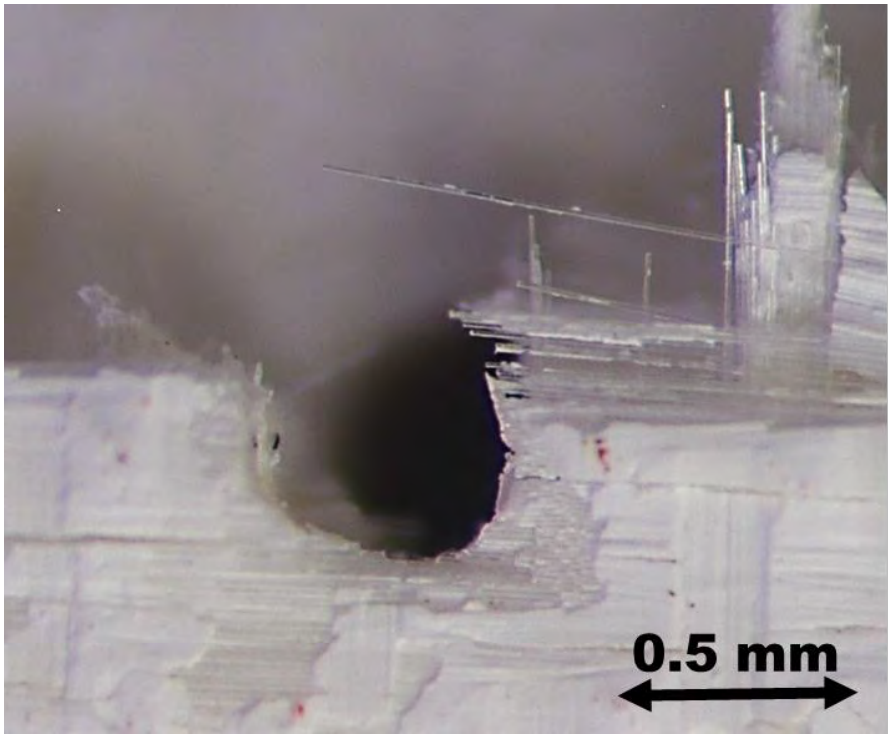


Figure A. 29: Fracture surface obtained for a N720/A specimen with effusion holes in tension to failure at 1200ºC in air.

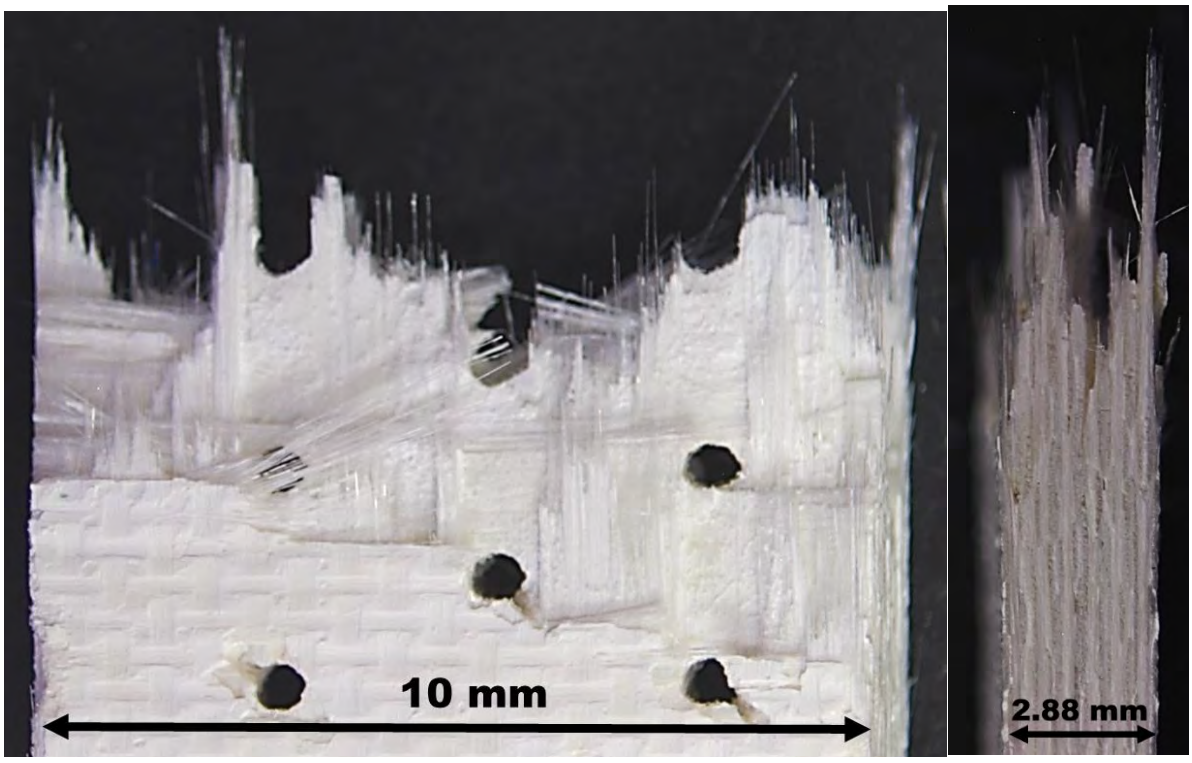


Figure A. 30: Fracture surface obtained for a N720/A specimen with effusion holes in tension to failure following 100 h of creep at 40 MPa at 1200ºC in air.

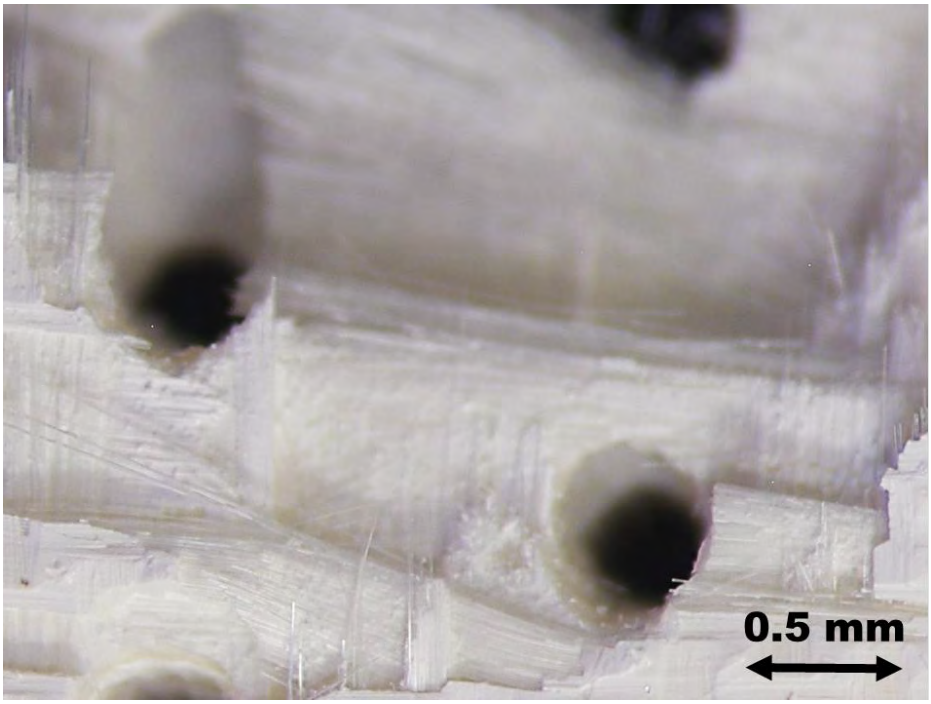


Figure A. 31: Fracture surface obtained for a N720/A specimen with effusion holes in tension to failure following 100 h of creep at 40 MPa at 1200ºC in air.

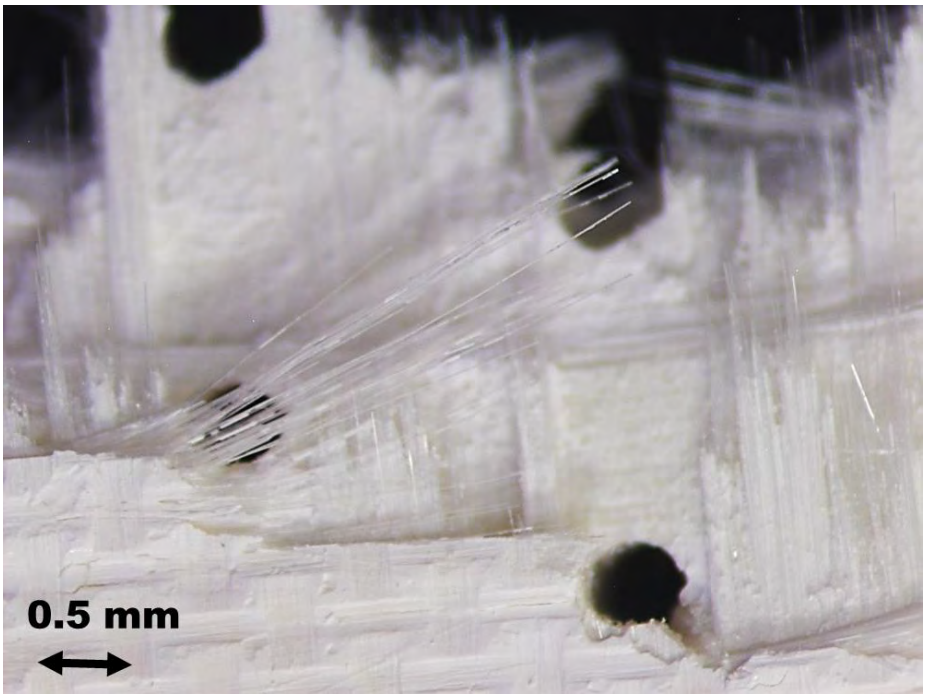


Figure A. 32: Fracture surface obtained for a N720/A specimen with effusion holes in tension to failure following 100 h of creep at 40 MPa at 1200ºC in air.

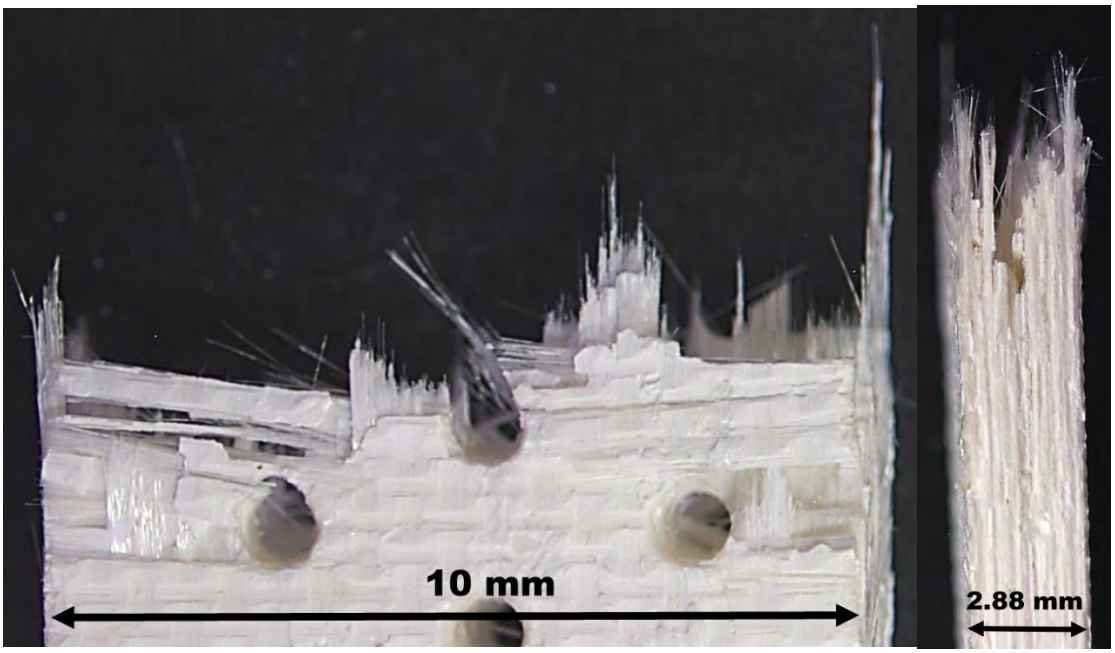


Figure A. 33: Fracture surface obtained for a N720/A specimen with effusion holes in tension to failure following 100 h of creep at 40 MPa at 1200ºC in air.

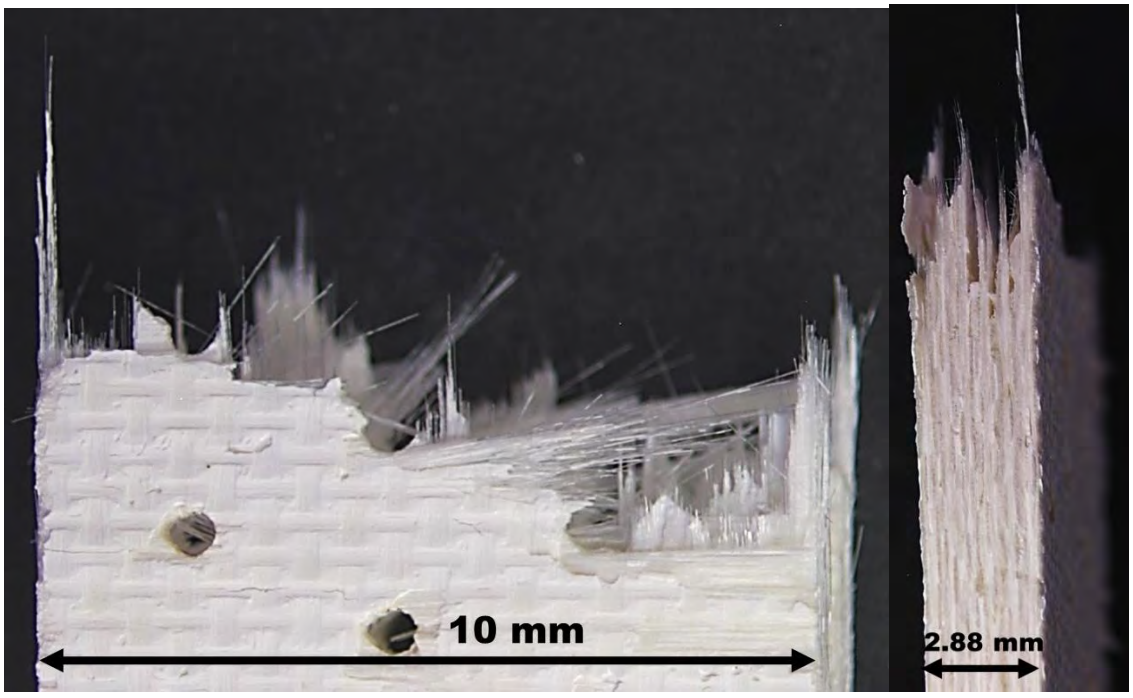


Figure A. 34: Fracture surface obtained for a N720/A specimen with effusion holes in tension to failure following 100 h of creep at 40 MPa at 1200ºC in air.



Figure A. 35: Fracture surface obtained for a N720/A specimen with effusion holes in tension to failure following 100 h of creep at 40 MPa at 1200ºC in air.

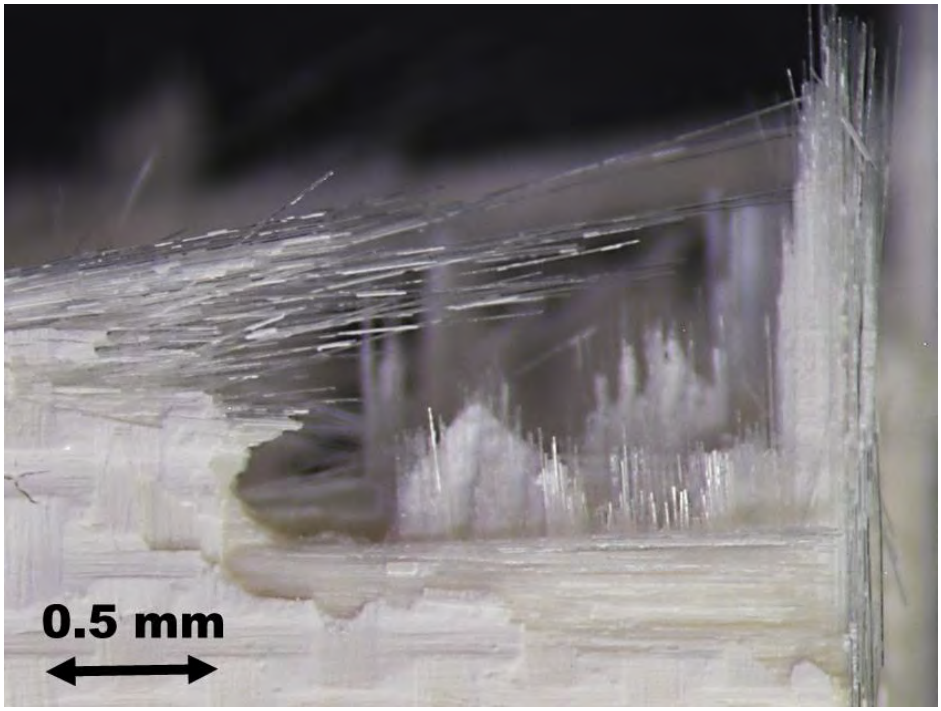


Figure A. 36: Fracture surface obtained for a N720/A specimen with effusion holes in tension to failure following 100 h of creep at 40 MPa at 1200ºC in air.

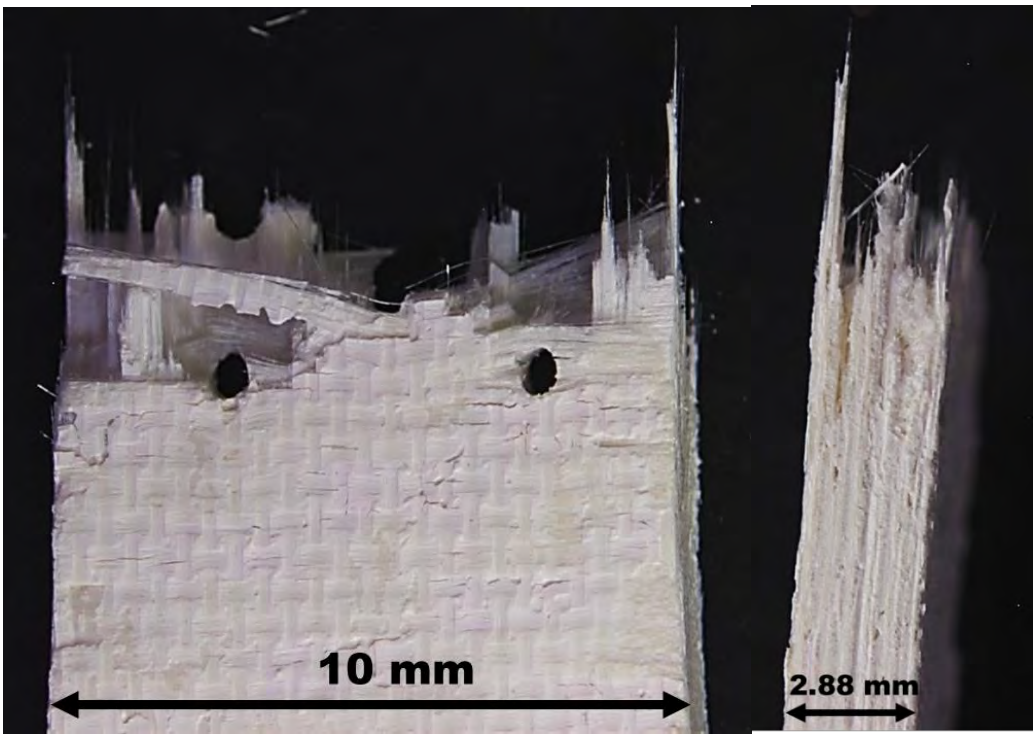


Figure A. 37: Fracture surface obtained for a N720/A specimen with effusion holes in creep at 1200ºC in air (σ_{cr} = 65 MPa, t_f = 58.4 h).

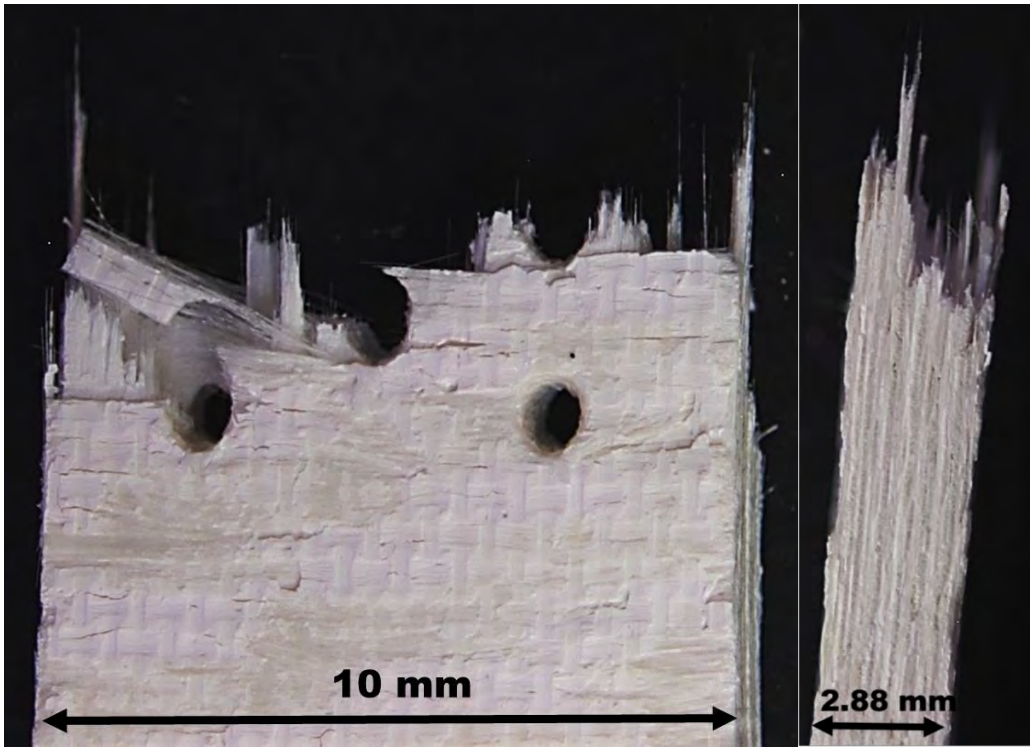


Figure A. 38: Fracture surface obtained for a N720/A specimen with effusion holes in creep at 1200ºC in air (σ_{cr} = 65 MPa, t_f = 58.4 h).

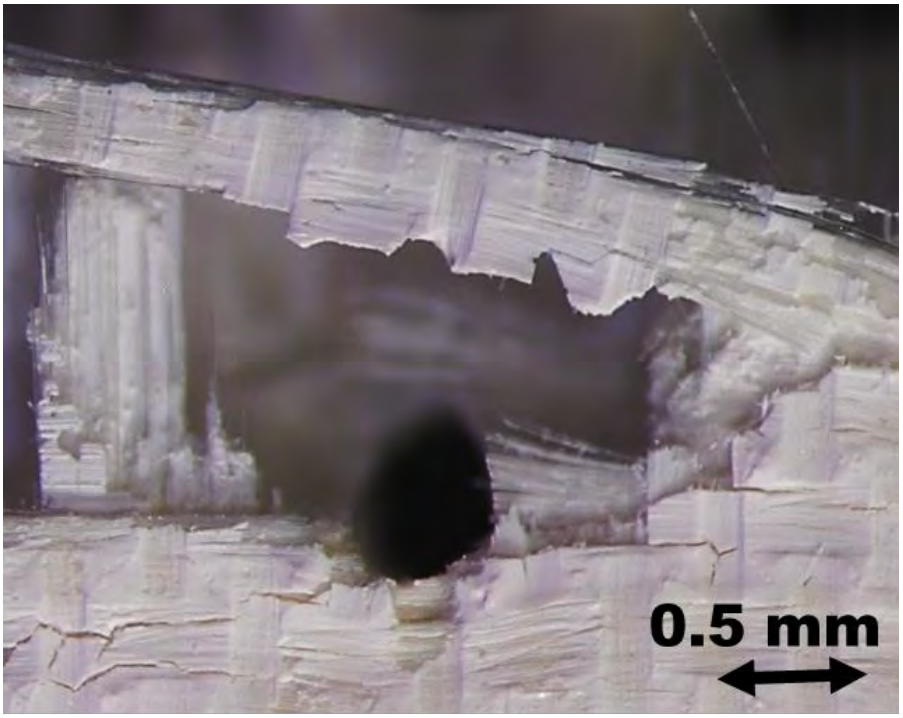


Figure A. 39: Fracture surface obtained for a N720/A specimen with effusion holes in creep at 1200ºC in air (σ_{cr} = 65 MPa, t_f = 58.4 h).

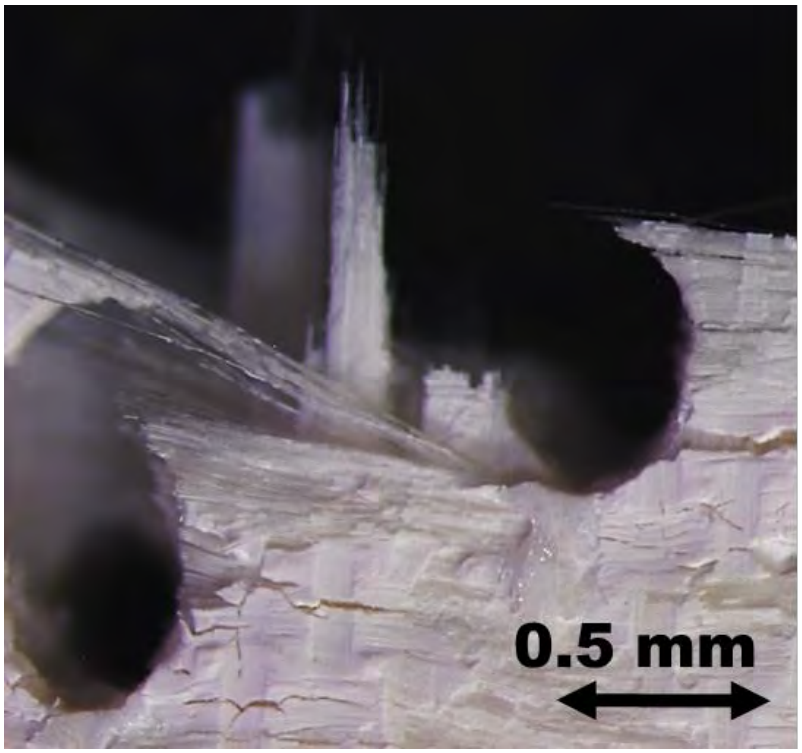


Figure A. 40: Fracture surface obtained for a N720/A specimen with effusion holes in creep at 1200ºC in air (σ_{cr} = 65 MPa, t_f = 58.4 h).

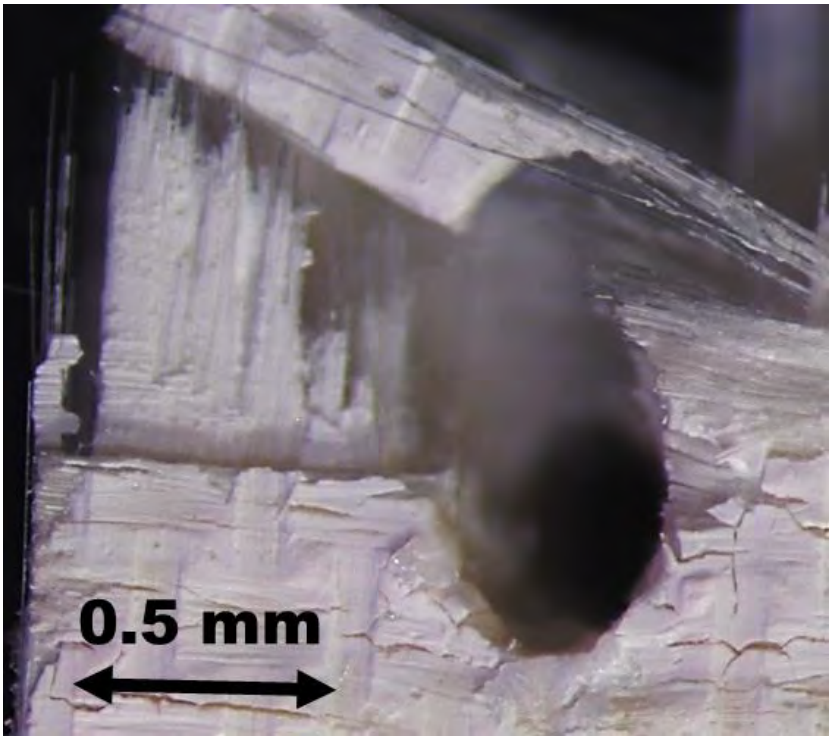


Figure A. 41: Fracture surface obtained for a N720/A specimen with effusion holes in creep at 1200ºC in air (σ_{cr} = 65 MPa, t_f = 58.4 h).

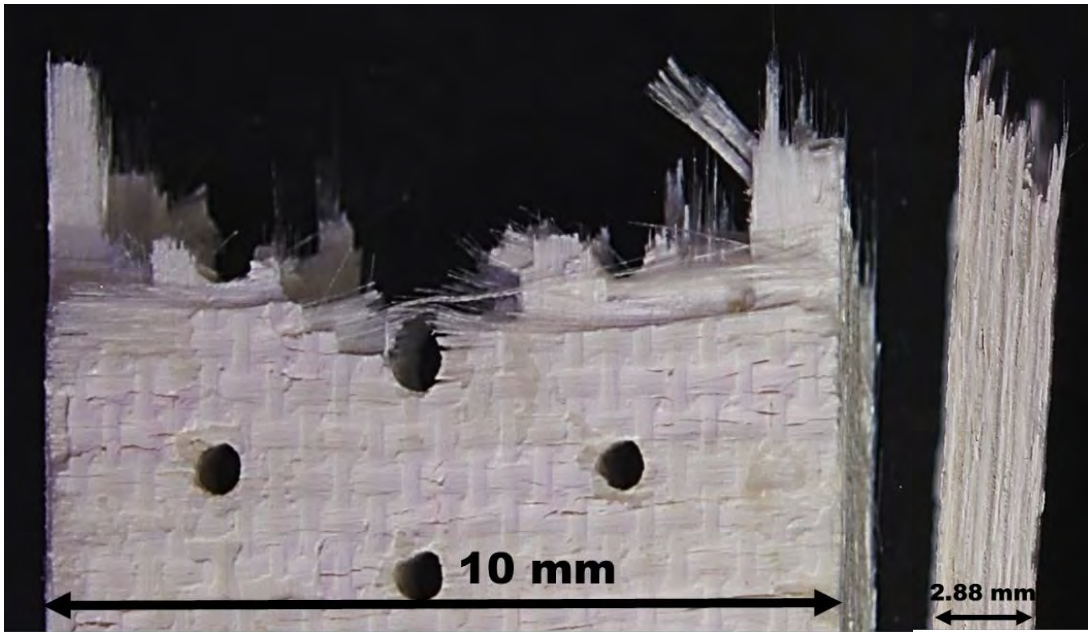


Figure A. 42: Fracture surface obtained for a N720/A specimen with effusion holes in creep at 1200ºC in air (σ_{cr} = 65 MPa, t_f = 58.4 h).

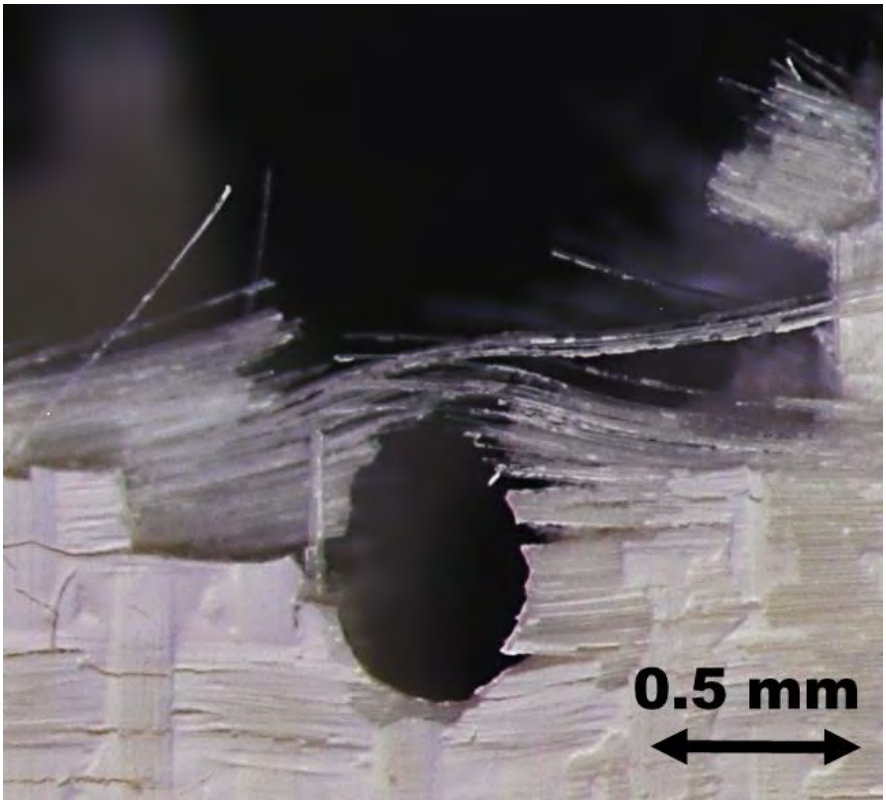


Figure A. 43: Fracture surface obtained for a N720/A specimen with effusion holes in creep at 1200ºC in air (σ_{cr} = 65 MPa, t_f = 58.4 h).

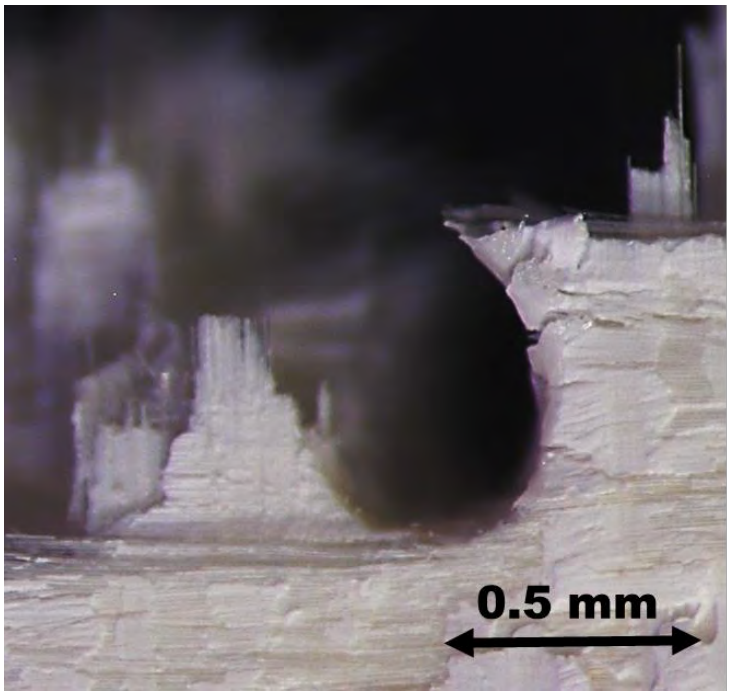


Figure A. 44: Fracture surface obtained for a N720/A specimen with effusion holes in creep at 1200ºC in air (σ_{cr} = 65 MPa, t_f = 58.4 h).

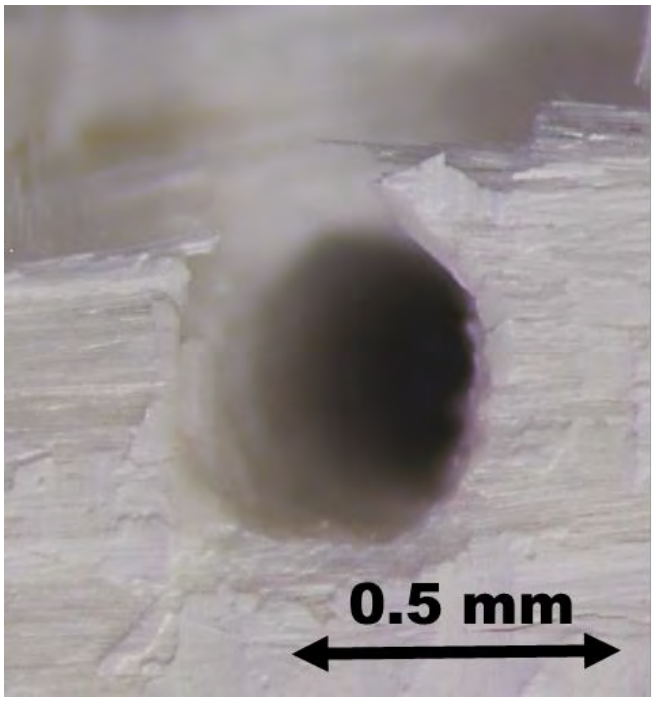


Figure A. 45: Fracture surface obtained for a N720/A specimen with effusion holes in creep at 1200ºC in air (σ_{cr} = 65 MPa, t_f = 58.4 h).

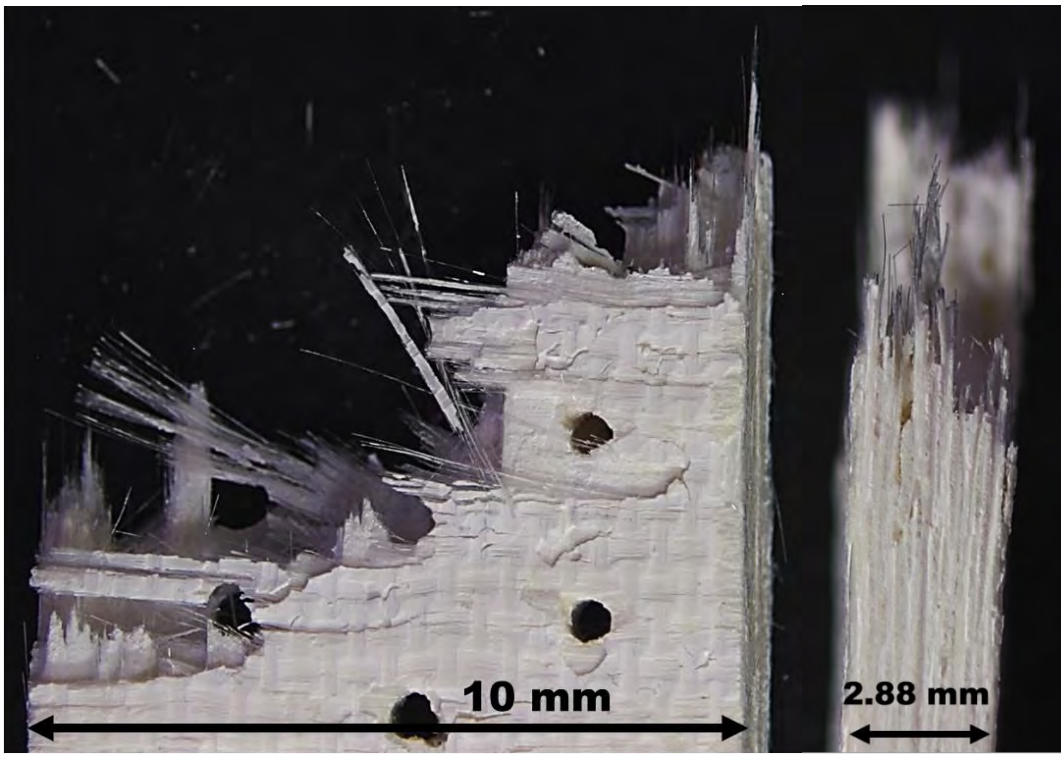


Figure A. 46: Fracture surface obtained for a N720/A specimen with effusion holes in creep at 1200ºC in air (□cr = 80 MPa, tf = 30.4 h).

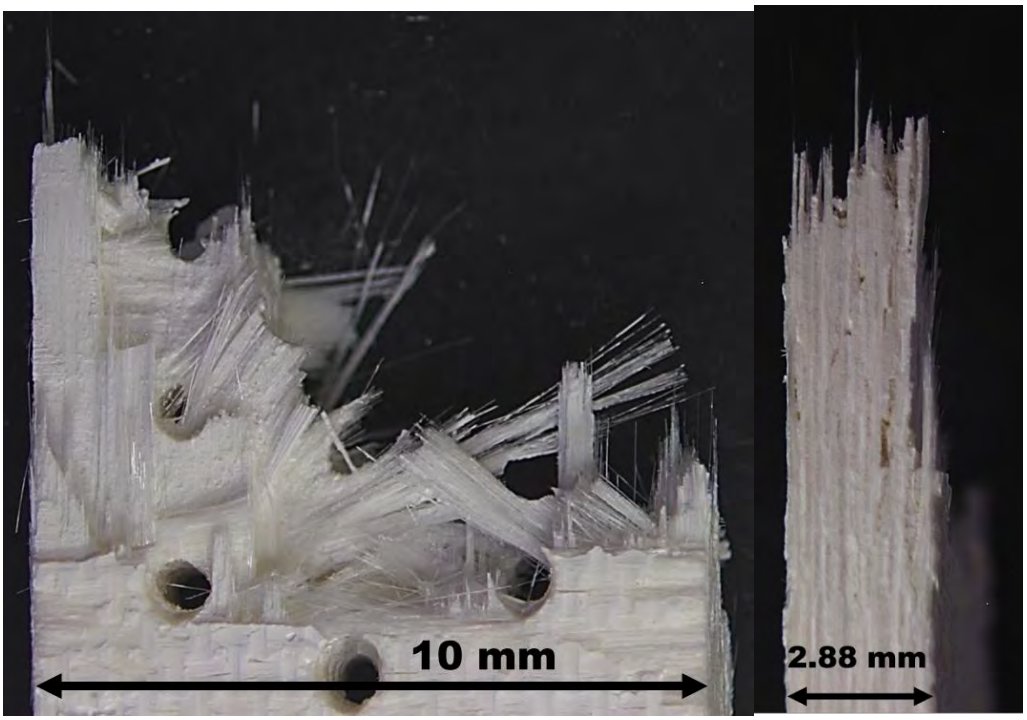


Figure A. 47: Fracture surface obtained for a N720/A specimen with effusion holes in creep at 1200ºC in air (σ_{cr} = 80 MPa, t_f = 30.4 h).

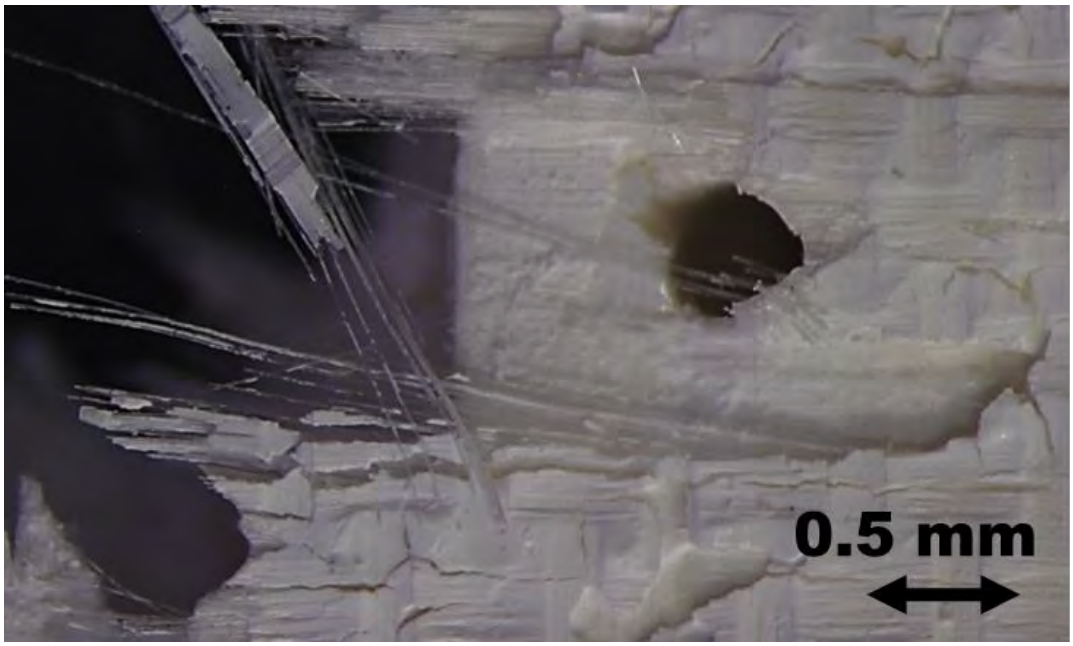


Figure A. 48: Fracture surface obtained for a N720/A specimen with effusion holes in creep at 1200ºC in air (σ_{cr} = 80 MPa, t_f = 30.4 h).

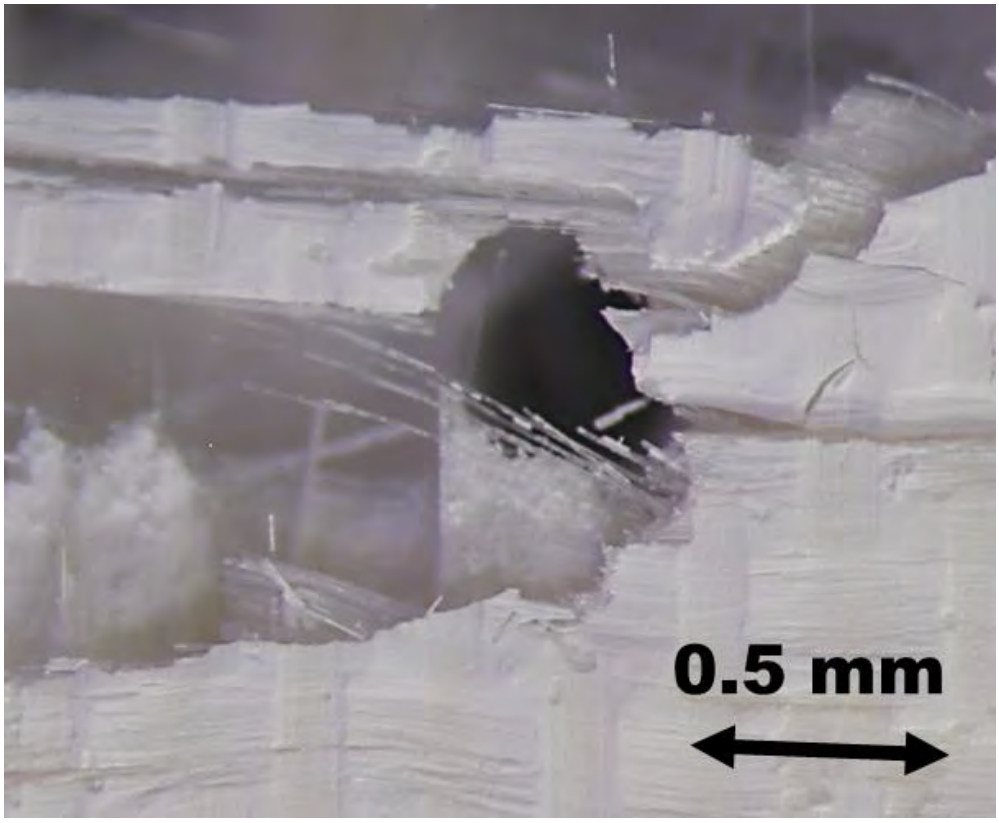


Figure A. 49: Fracture surface obtained for a N720/A specimen with effusion holes in creep at 1200ºC in air (σ_{cr} = 80 MPa, t_f = 30.4 h).

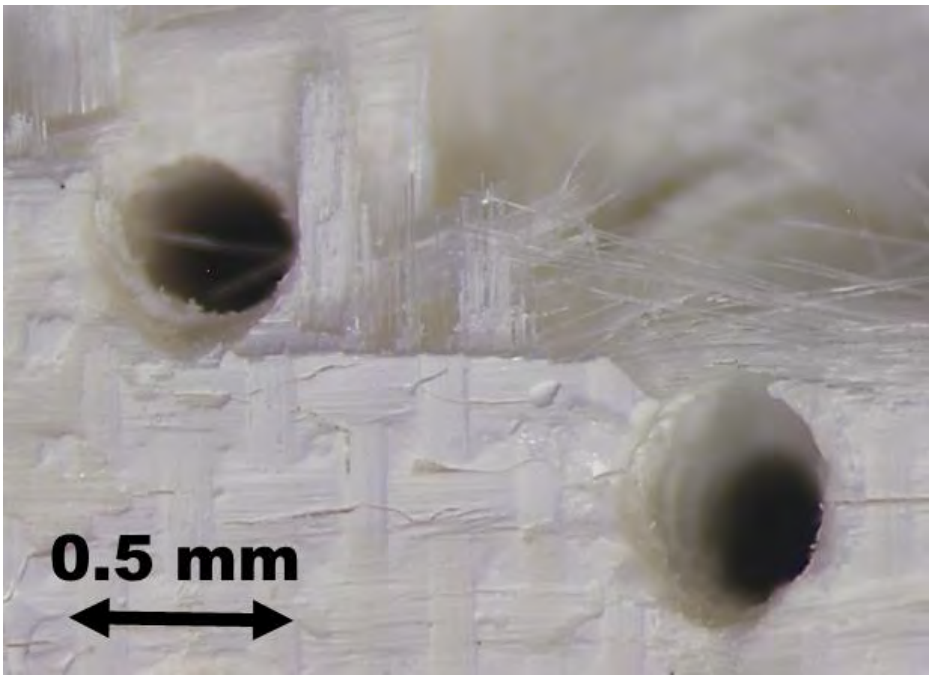


Figure A. 50: Fracture surface obtained for a N720/A specimen with effusion holes in creep at 1200ºC in air (σ_{cr} = 80 MPa, t_f = 30.4 h).

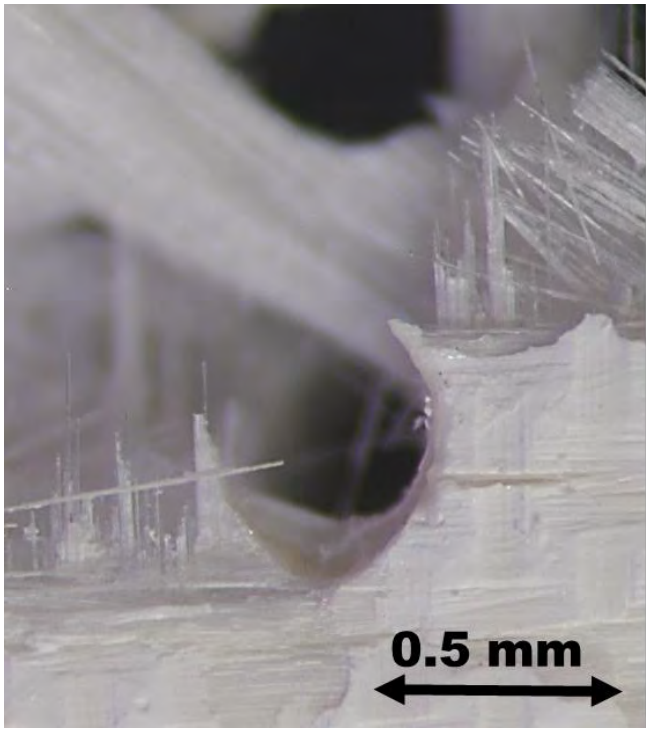


Figure A. 51: Fracture surface obtained for a N720/A specimen with effusion holes in creep at 1200ºC in air (σ_{cr} = 80 MPa, t_f = 30.4 h).

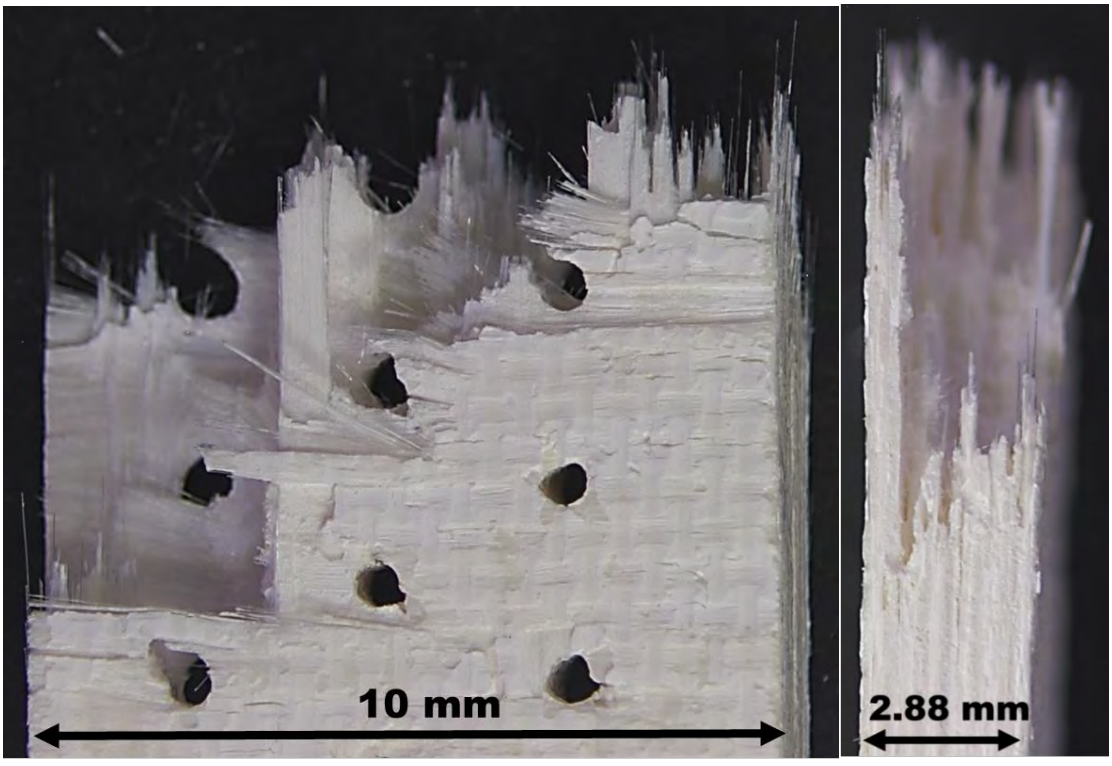


Figure A. 52: Fracture surface obtained for a N720/A specimen with effusion holes in creep at 1200ºC in air (σ_{cr} = 80 MPa, t_f = 30.4 h).

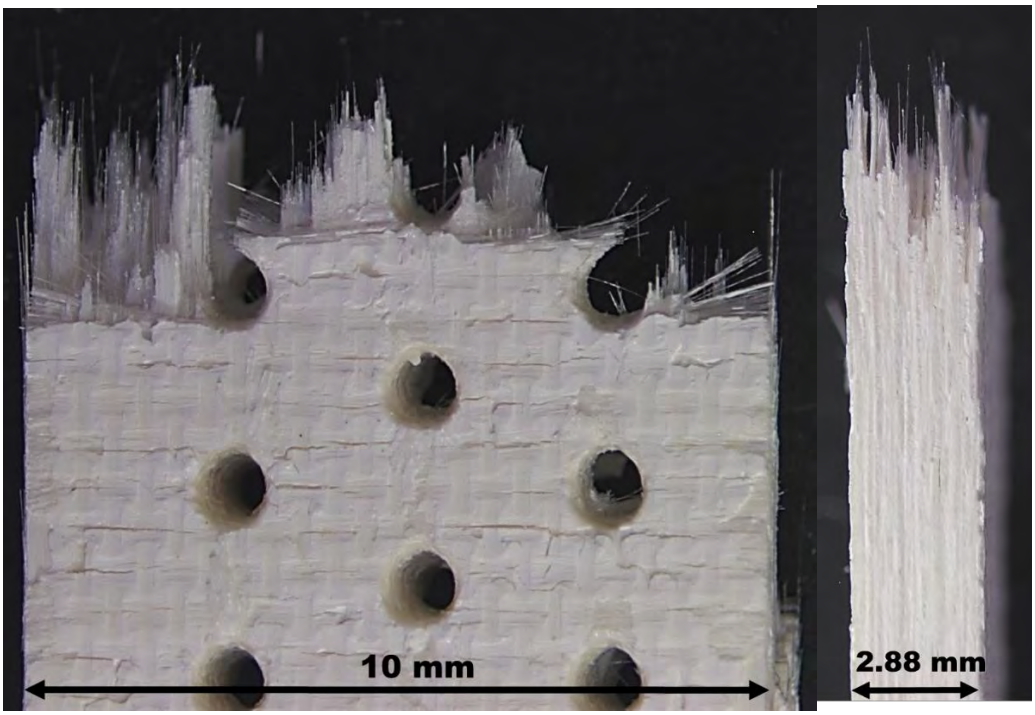


Figure A. 53: Fracture surface obtained for a N720/A specimen with effusion holes in creep at 1200ºC in air (σ_{cr} = 80 MPa, t_f = 30.4 h).

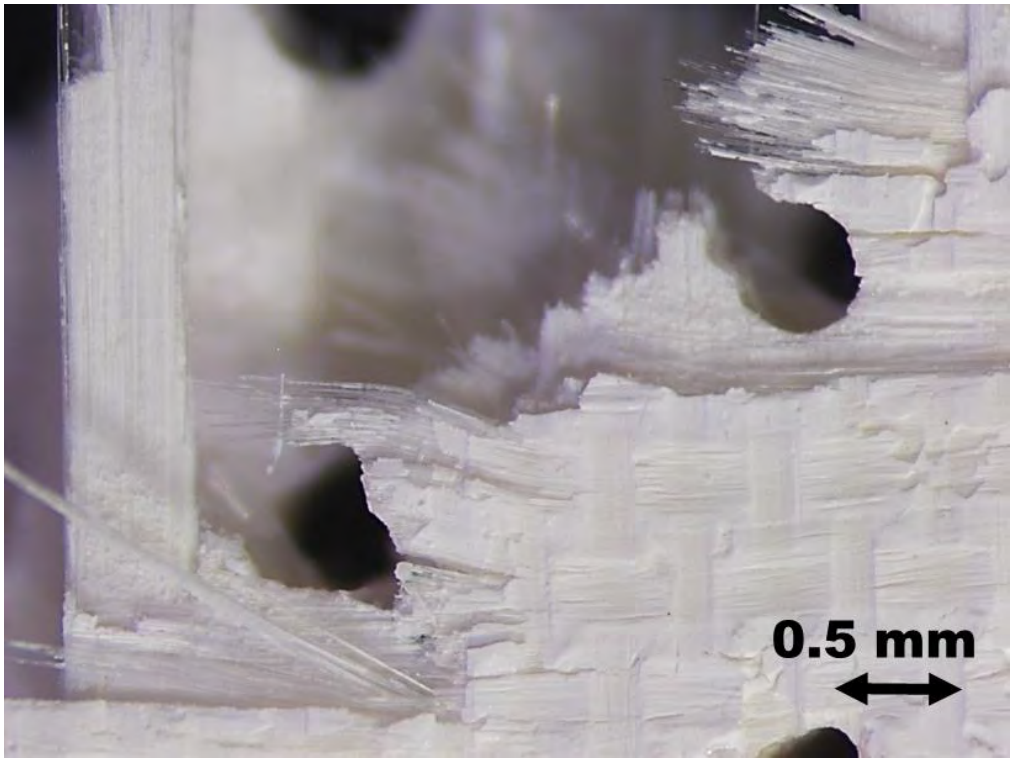


Figure A. 54: Fracture surface obtained for a N720/A specimen with effusion holes in creep at 1200ºC in air (σ_{cr} = 80 MPa, t_f = 30.4 h).

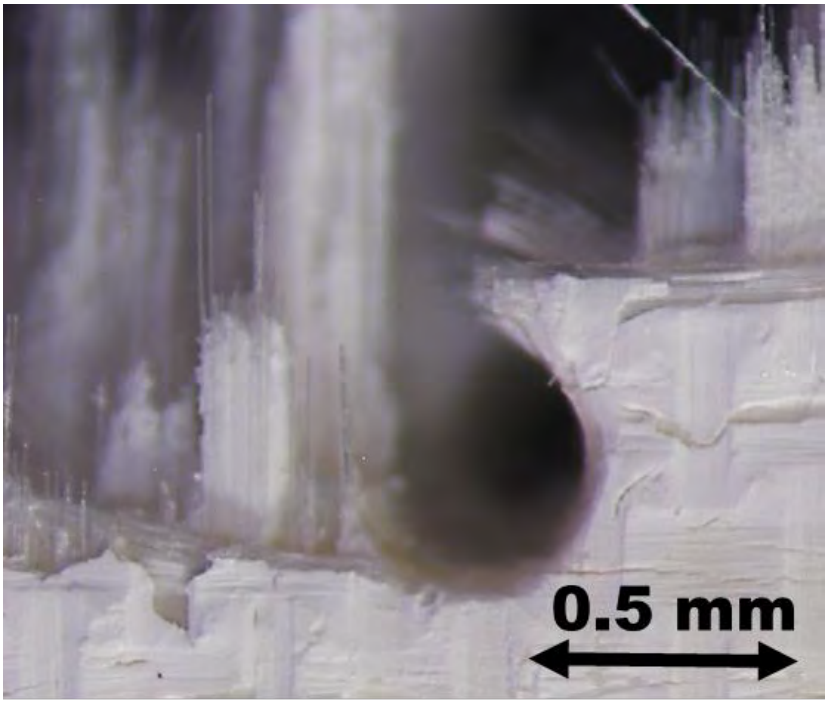


Figure A. 55: Fracture surface obtained for a N720/A specimen with effusion holes in creep at 1200ºC in air (σ_{cr} = 80 MPa, t_f = 30.4 h).

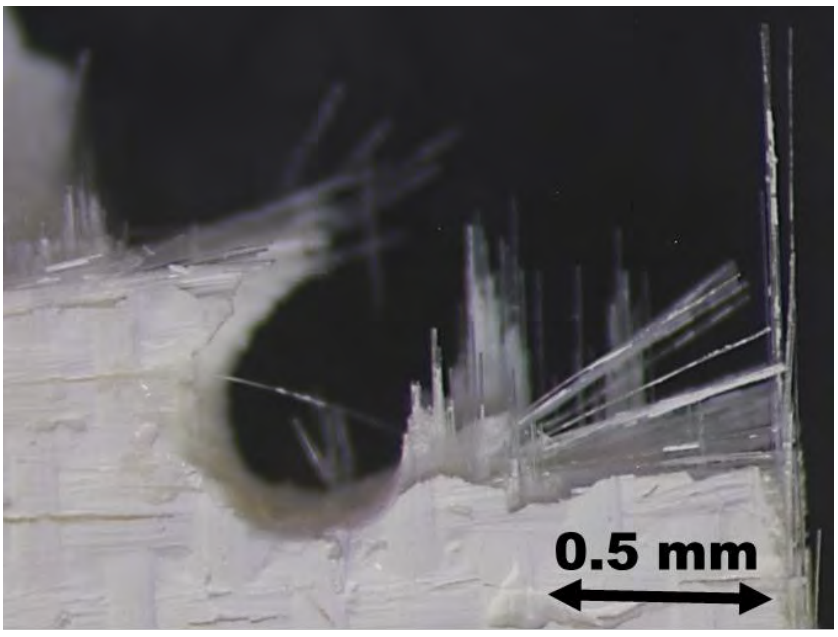


Figure A. 56: Fracture surface obtained for a N720/A specimen with effusion holes in creep at 1200ºC in air (σ_{cr} = 80 MPa, t_f = 30.4 h).

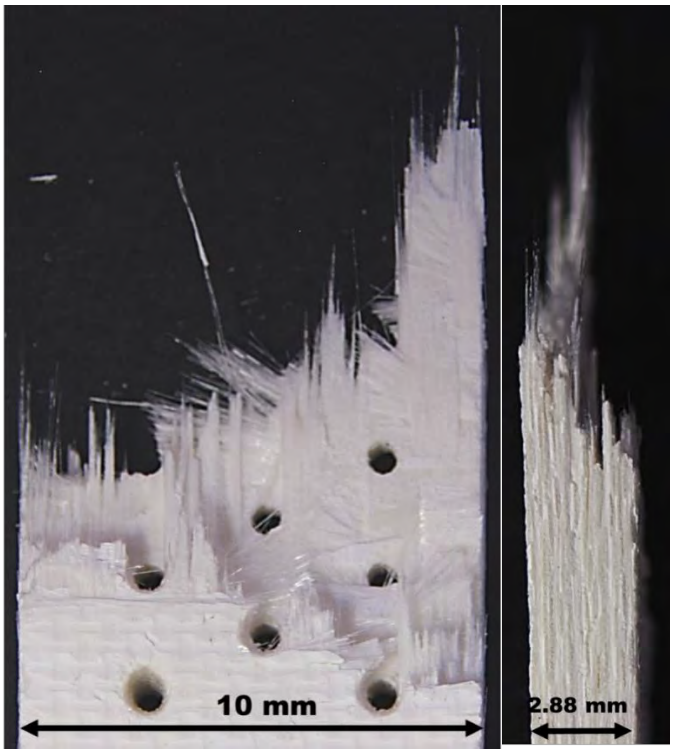


Figure A. 57: Fracture surface obtained for a N720/A specimen with effusion holes in creep at 1200ºC in air (σ_{cr} = 90 MPa, t_f = 9.65 h).

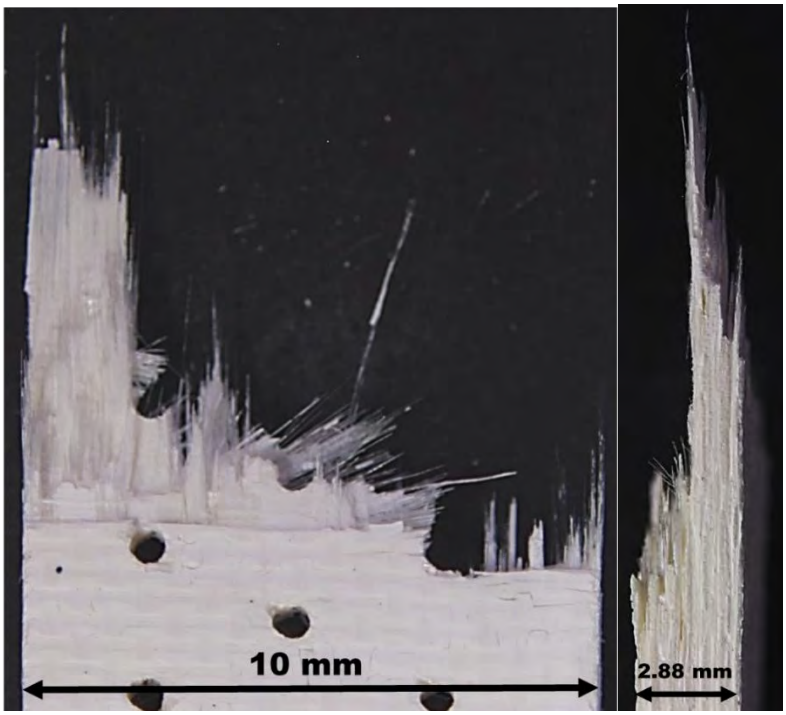


Figure A. 58: Fracture surface obtained for a N720/A specimen with effusion holes in creep at 1200ºC in air (σ_{cr} = 90 MPa, t_f = 9.65 h).

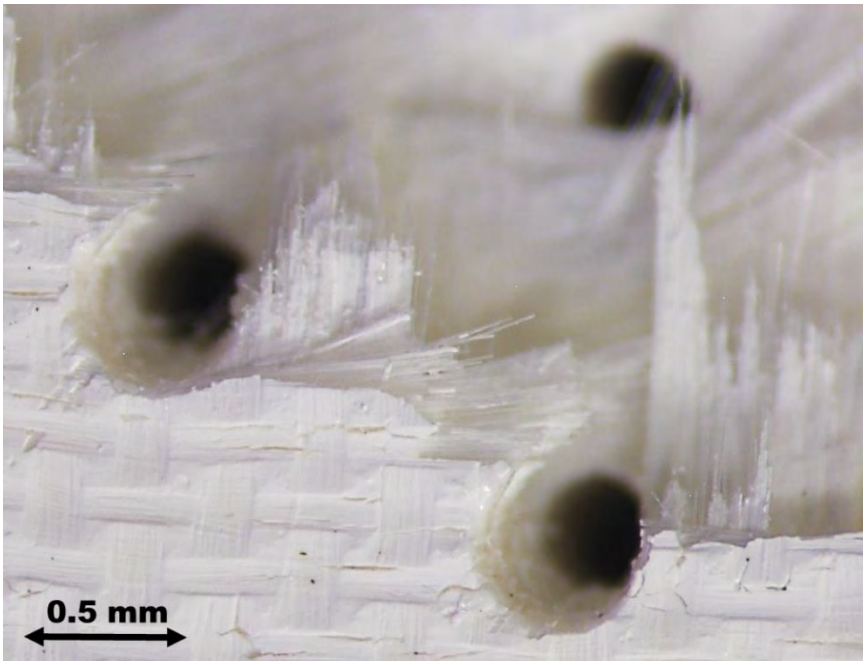


Figure A. 59: Fracture surface obtained for a N720/A specimen with effusion holes in creep at 1200ºC in air (σ_{cr} = 90 MPa, t_f = 9.65 h).

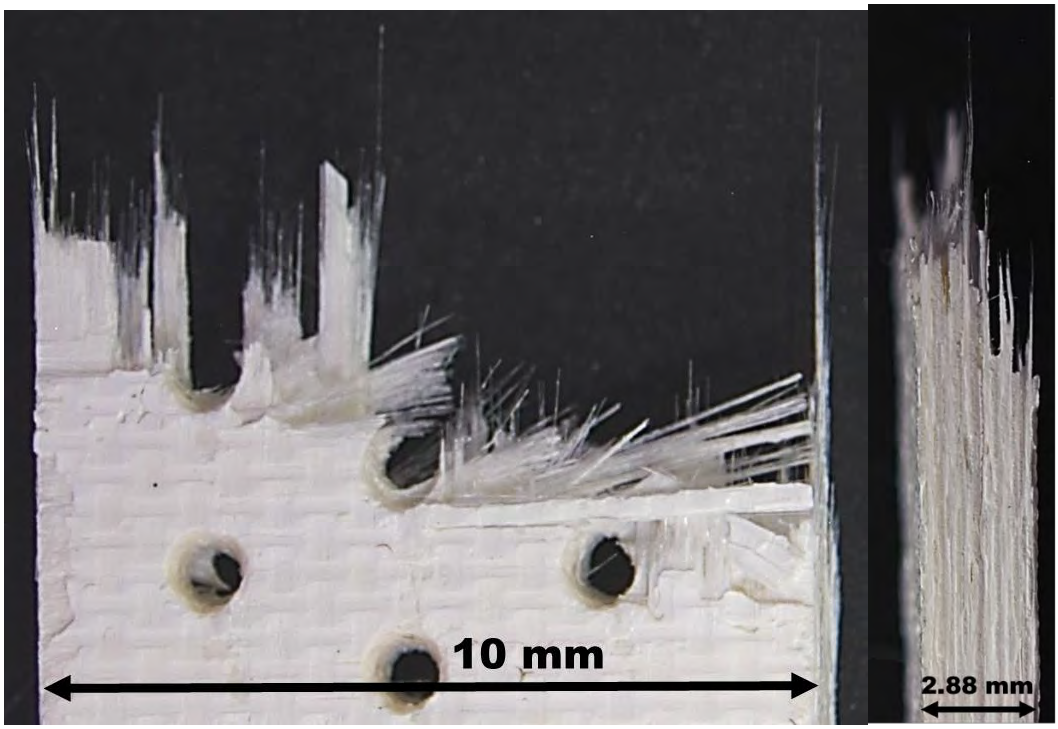


Figure A. 60: Fracture surface obtained for a N720/A specimen with effusion holes in creep at 1200ºC in air (σ_{cr} = 90 MPa, t_f = 9.65 h).

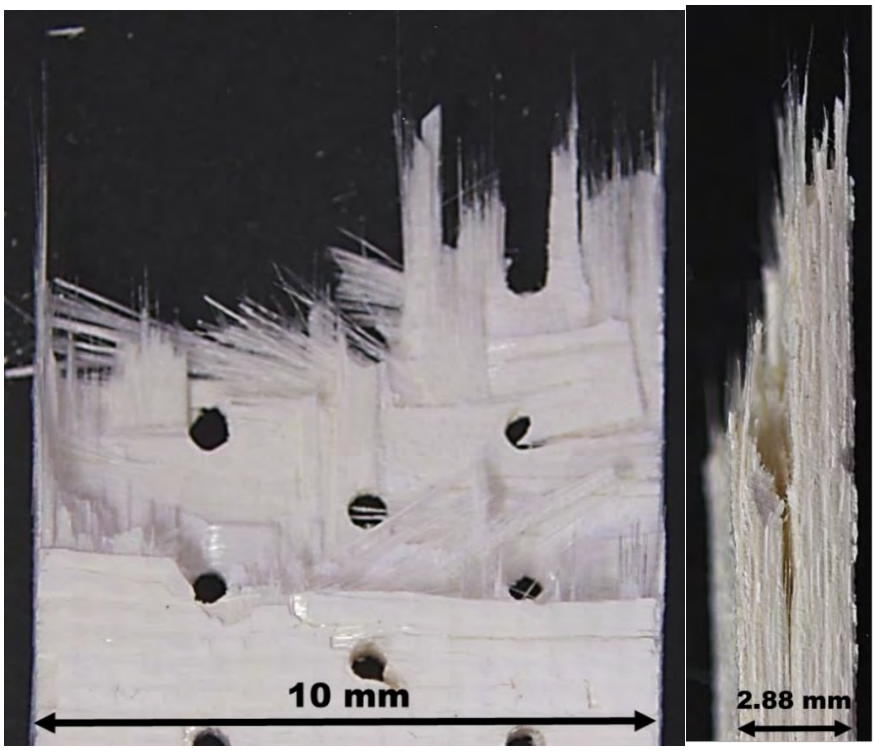


Figure A. 61: Fracture surface obtained for a N720/A specimen with effusion holes in creep at 1200ºC in air (σ_{cr} = 90 MPa, t_f = 9.65 h).

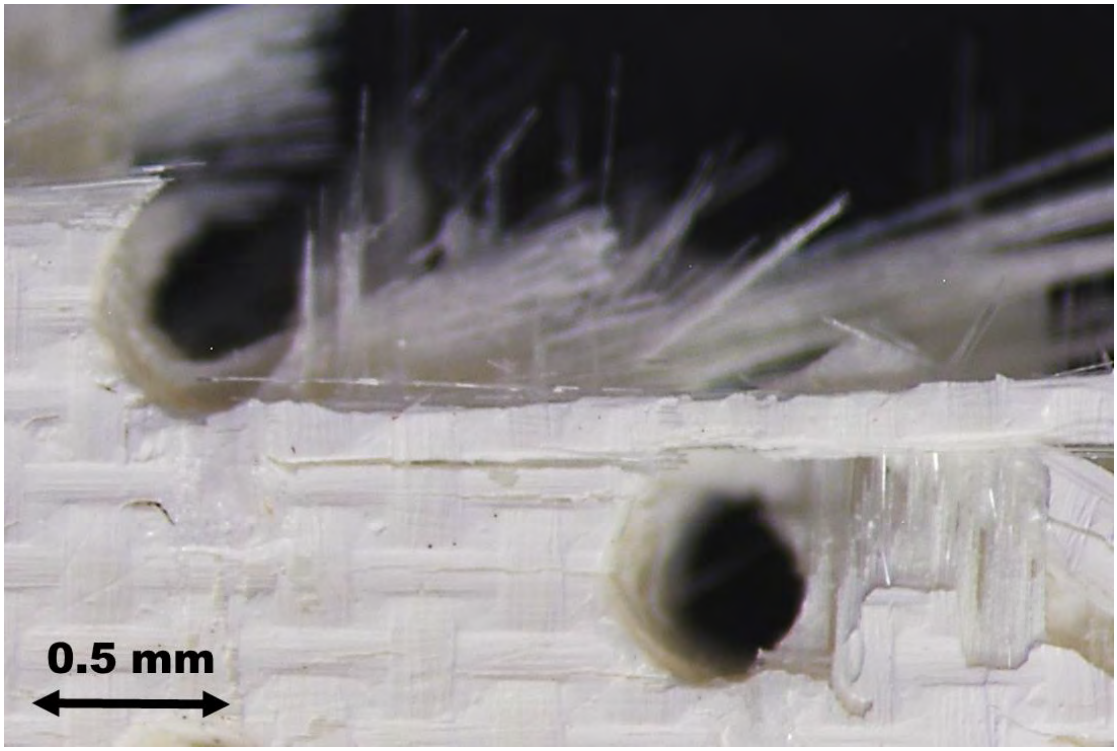


Figure A. 62: Fracture surface obtained for a N720/A specimen with effusion holes in creep at 1200ºC in air (□cr = 90 MPa, tf = 9.65 h).

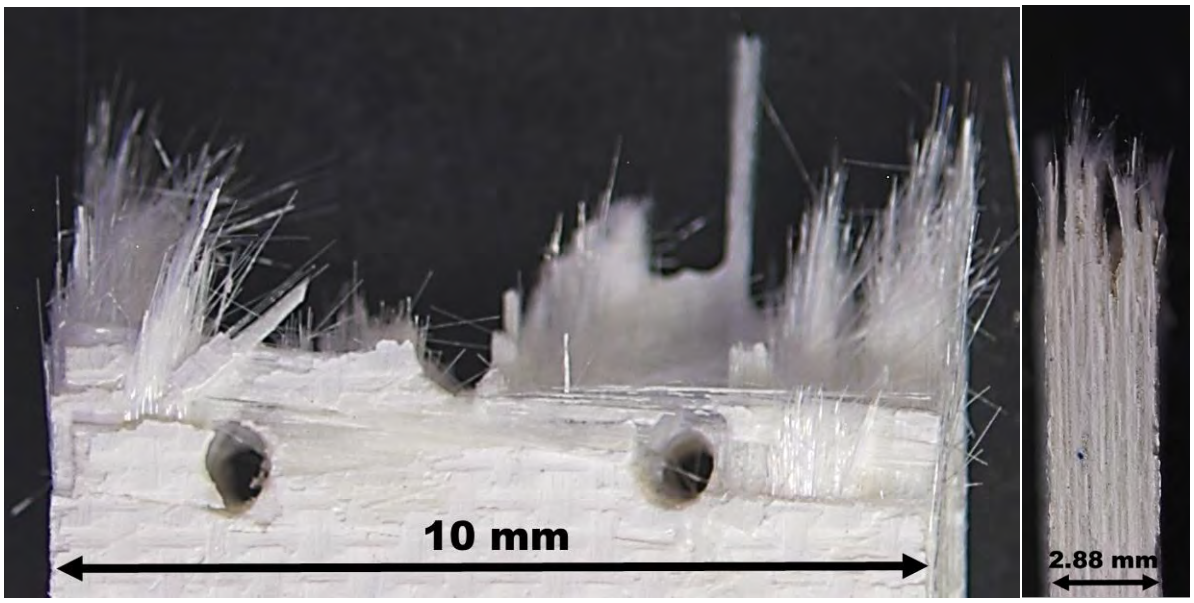


Figure A. 63: Fracture surface obtained for a N720/A specimen with effusion holes in creep at 1200ºC in air (σ_{cr} = 100 MPa, t_f = 0.538 h).

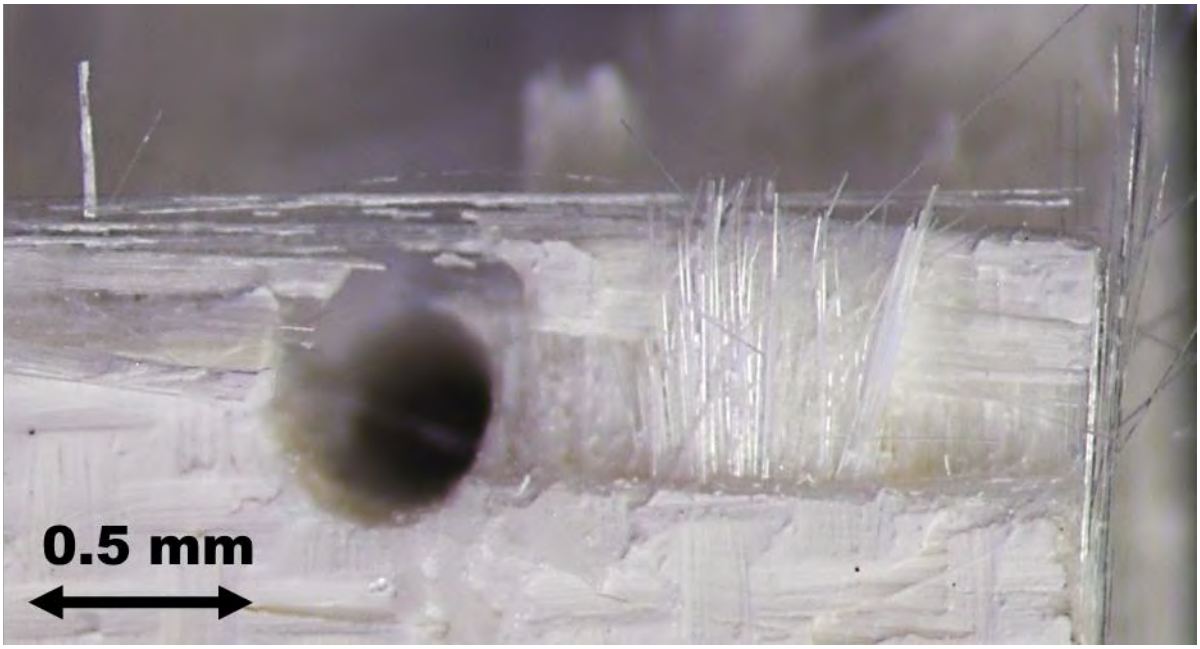


Figure A. 64: Fracture surface obtained for a N720/A specimen with effusion holes in creep at 1200ºC in air (σ_{cr} = 100 MPa, t_f = 0.538 h).

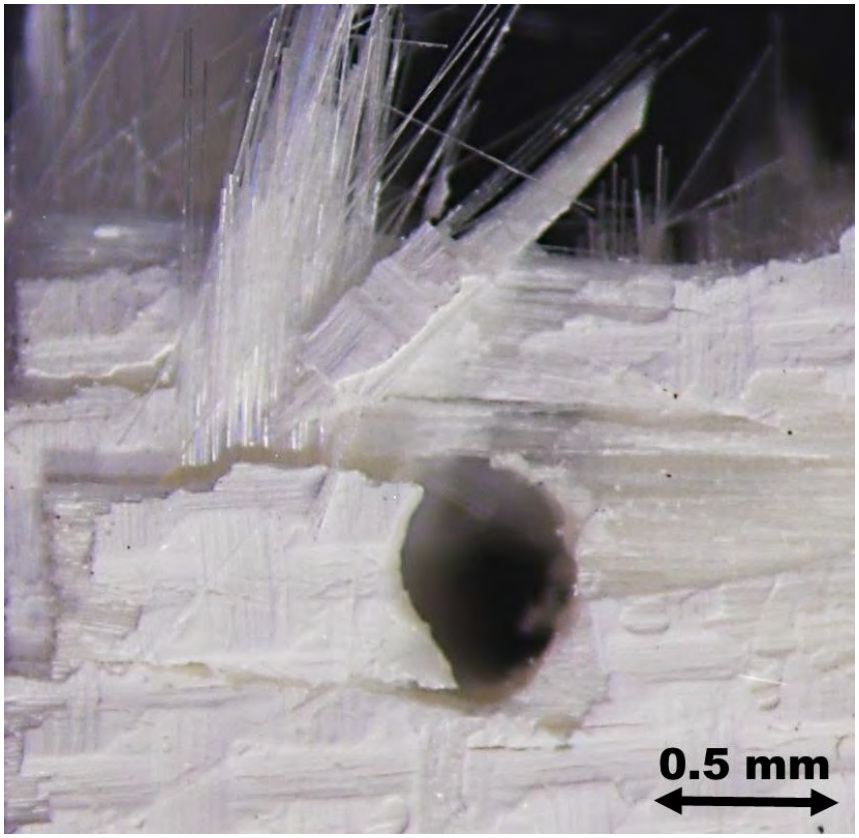


Figure A. 65: Fracture surface obtained for a N720/A specimen with effusion holes in creep at 1200°C in air (σ_{cr} = 100 MPa, t_f = 0.538 h).

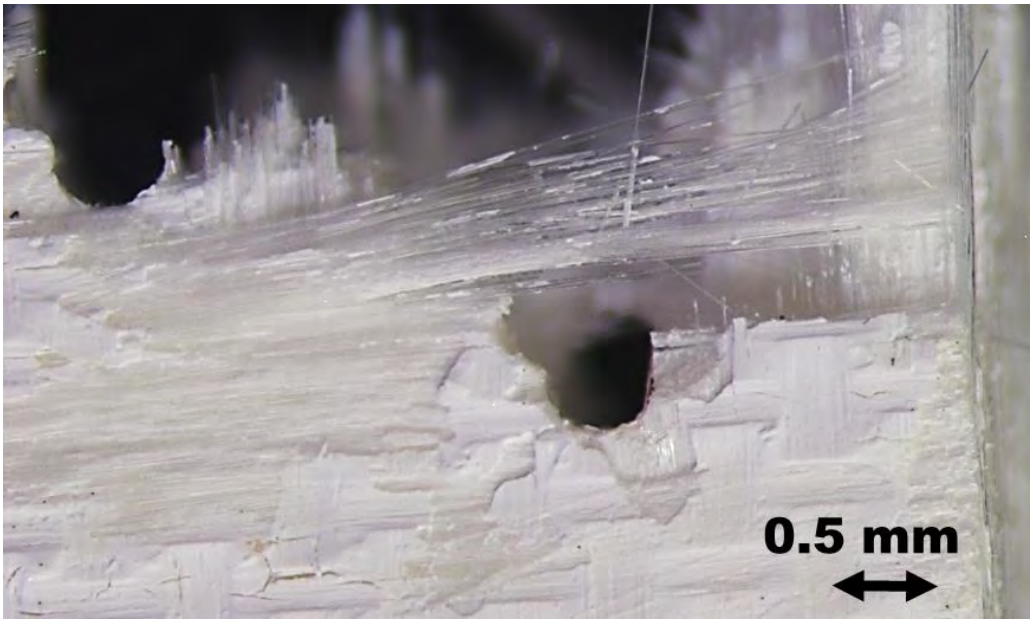


Figure A. 66: Fracture surface obtained for a N720/A specimen with effusion holes in creep at 1200°C in air (σ_{cr} = 100 MPa, t_f = 0.538 h).

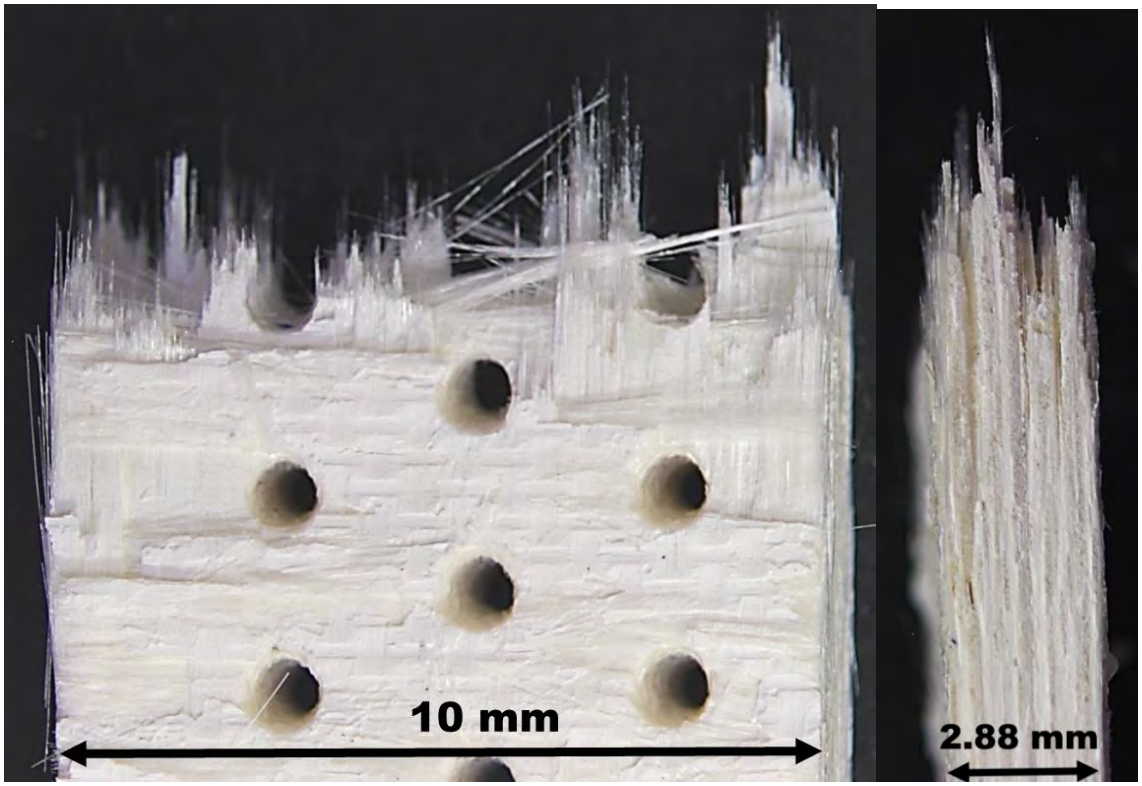


Figure A. 67: Fracture surface obtained for a N720/A specimen with effusion holes in creep at 1200ºC in air (σ_{cr} = 100 MPa, t_f = 0.538 h).

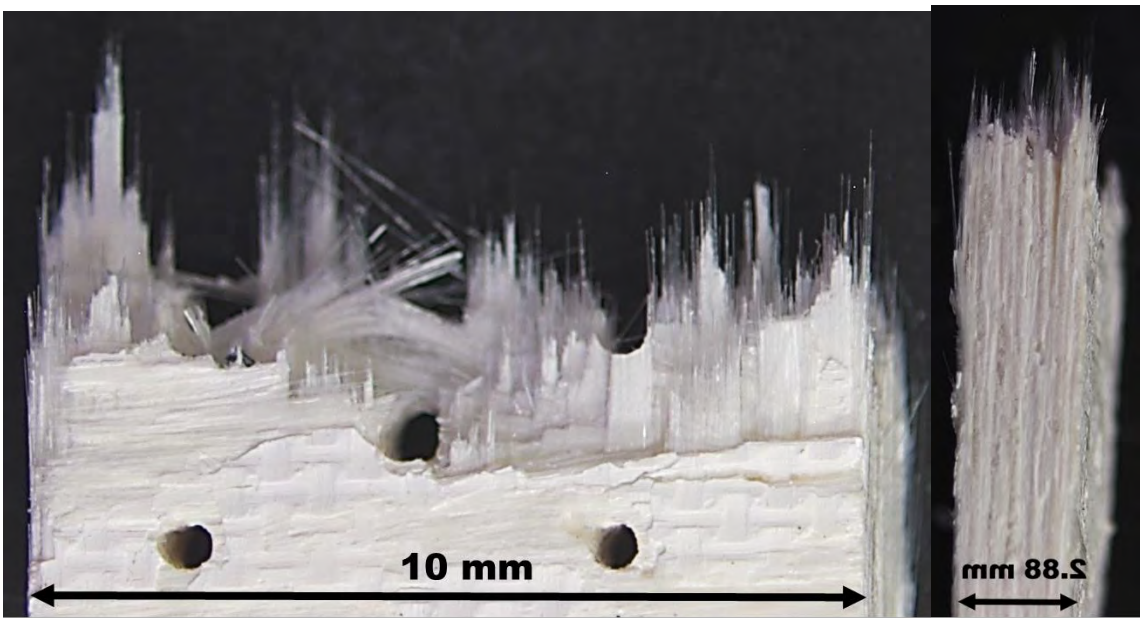


Figure A. 68: Fracture surface obtained for a N720/A specimen with effusion holes in creep at 1200ºC in air (σ_{cr} = 100 MPa, t_f = 0.538 h).

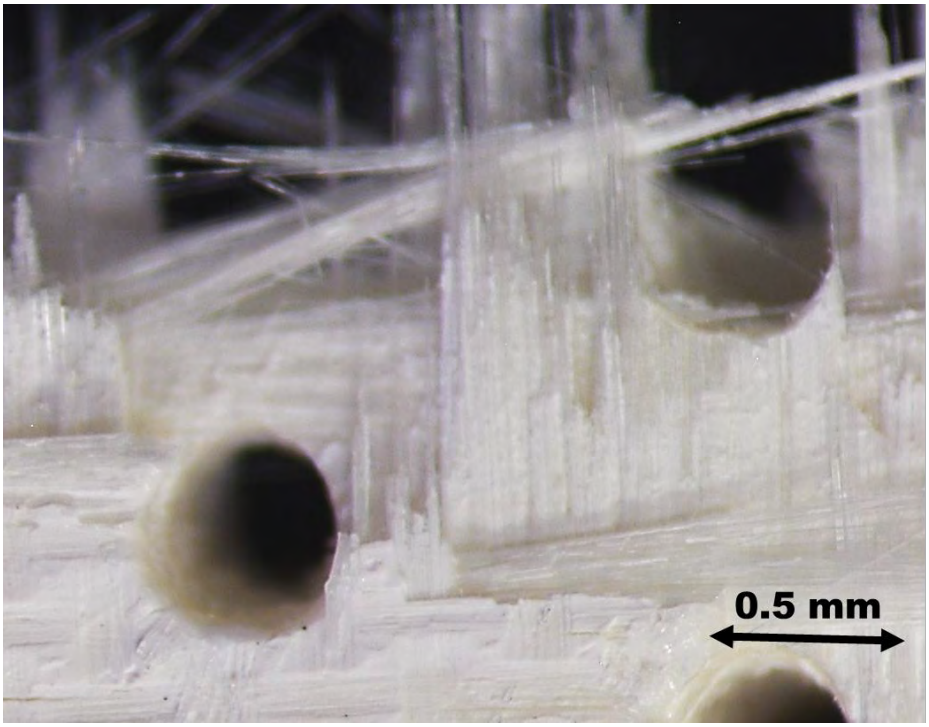


Figure A. 69: Fracture surface obtained for a N720/A specimen with effusion holes in creep at 1200°C in air (σ_{cr} = 100 MPa, t_f = 0.538 h).

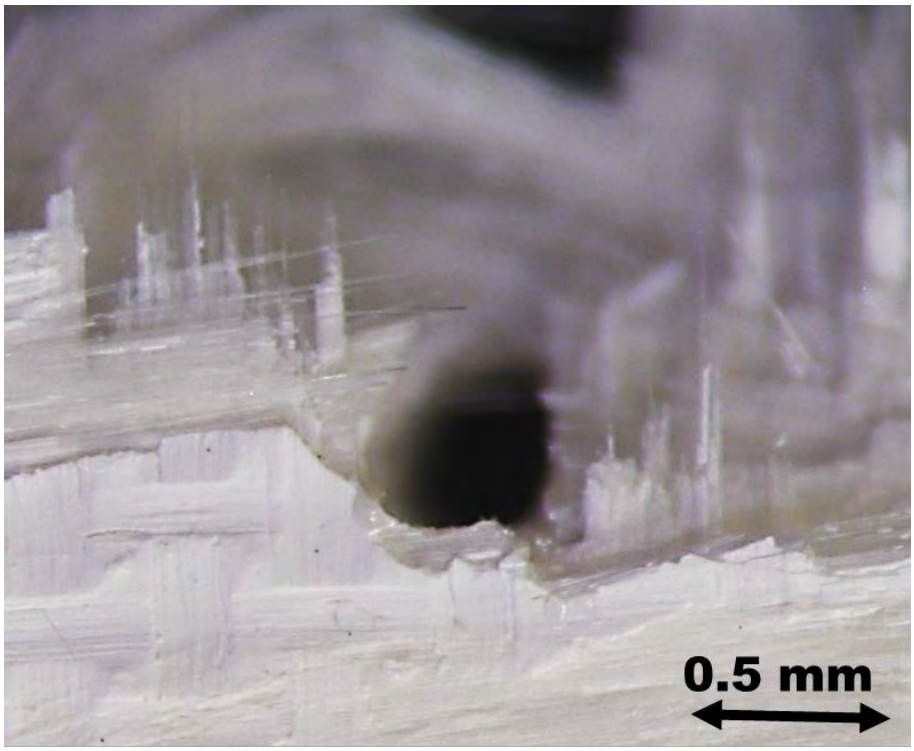


Figure A. 70: Fracture surface obtained for a N720/A specimen with effusion holes in creep at 1200°C in air (σ_{cr} = 100 MPa, t_f = 0.538 h).

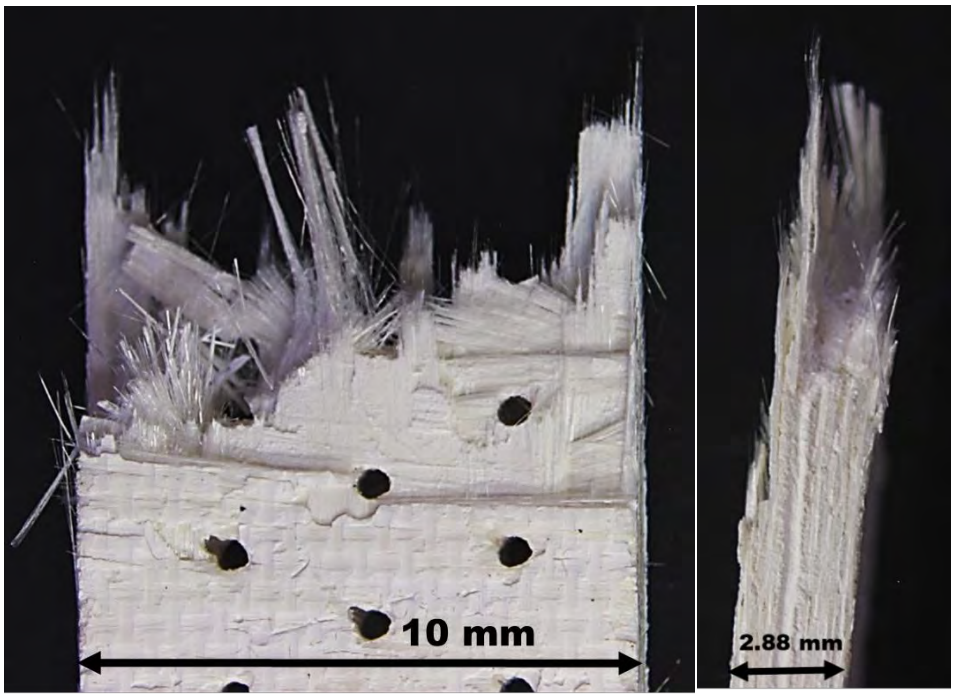


Figure A. 71: Fracture surface obtained for a N720/A specimen with effusion holes in creep at 1200ºC in air (σ_{cr} = 150 MPa, t_f = 0.0038 h).

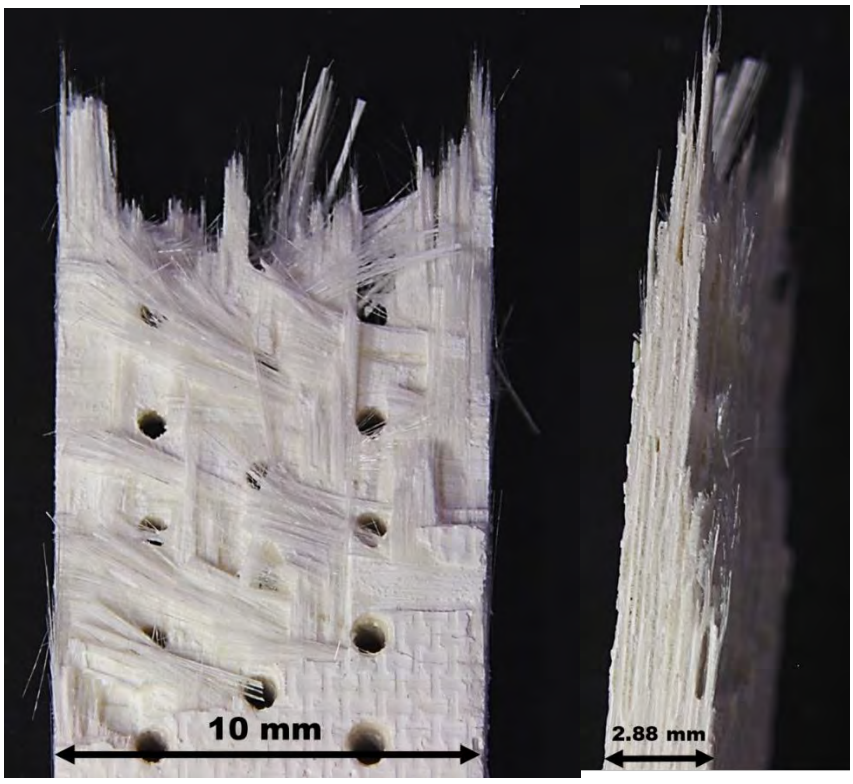


Figure A. 72: Fracture surface obtained for a N720/A specimen with effusion holes in creep at 1200ºC in air (σ_{cr} = 150 MPa, t_f = 0.0038 h).

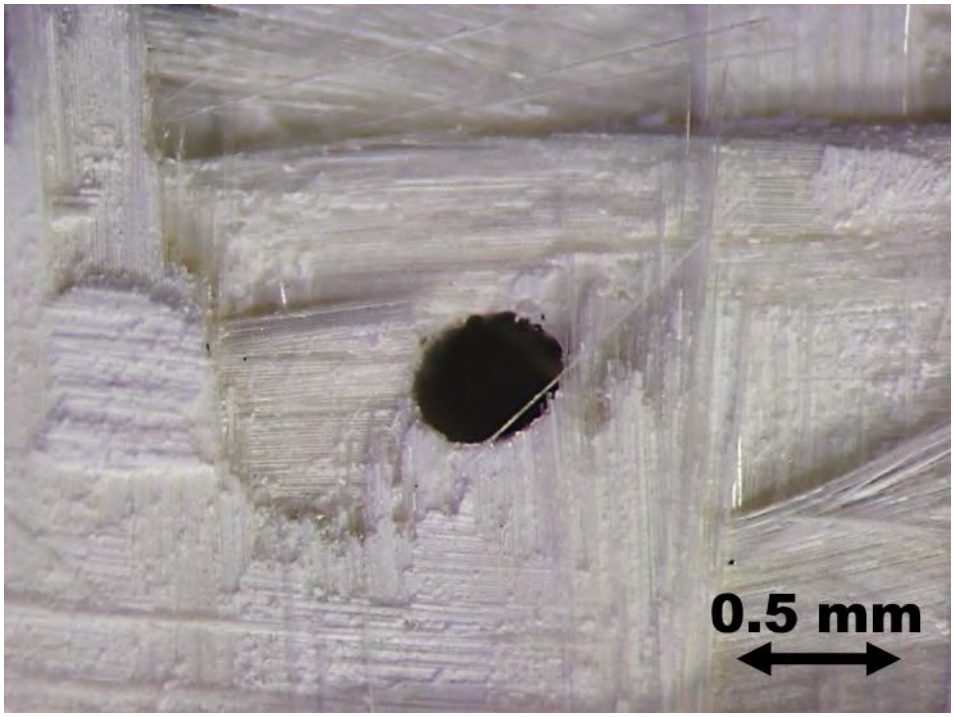


Figure A. 73: Fracture surface obtained for a N720/A specimen with effusion holes in creep at 1200ºC in air (σ_{cr} = 150 MPa, t_f = 0.0038 h).

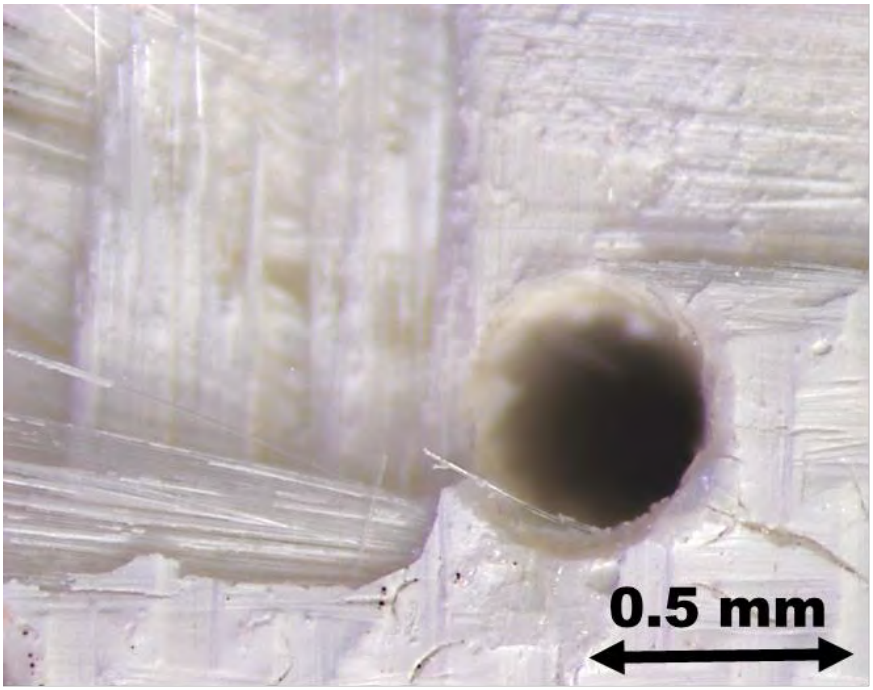


Figure A. 74: Fracture surface obtained for a N720/A specimen with effusion holes in creep at 1200ºC in air (σ_{cr} = 150 MPa, t_f = 0.0038 h).

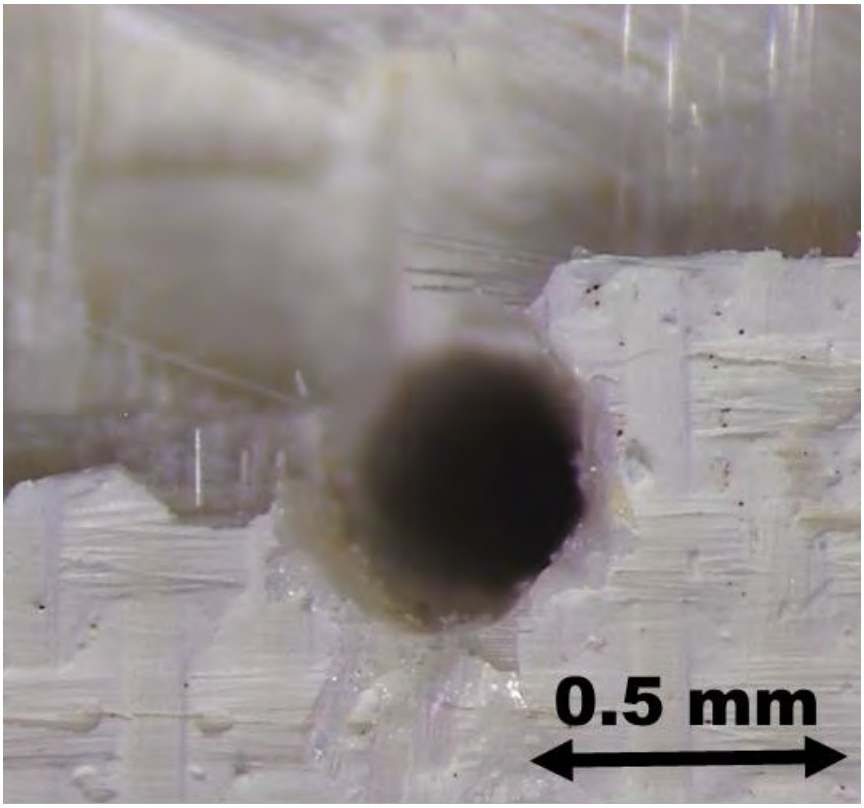


Figure A. 75: Fracture surface obtained for a N720/A specimen with effusion holes in creep at 1200ºC in air (σ_{cr} = 150 MPa, t_f = 0.0038 h).

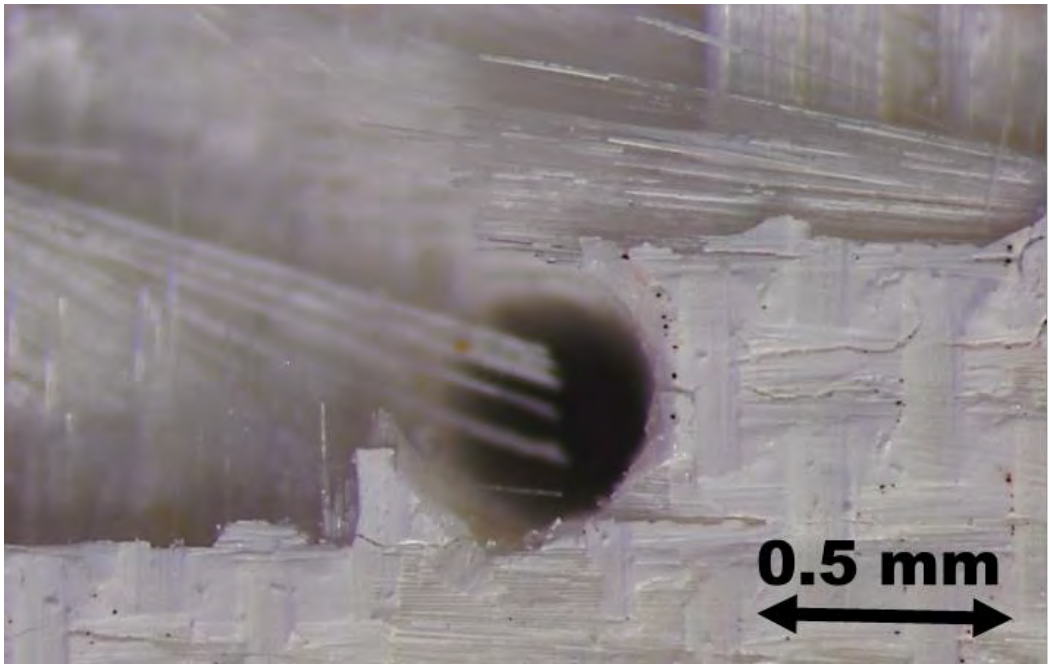


Figure A. 76: Fracture surface obtained for a N720/A specimen with effusion holes in creep at 1200ºC in air (σ_{cr} = 150 MPa, t_f = 0.0038 h).

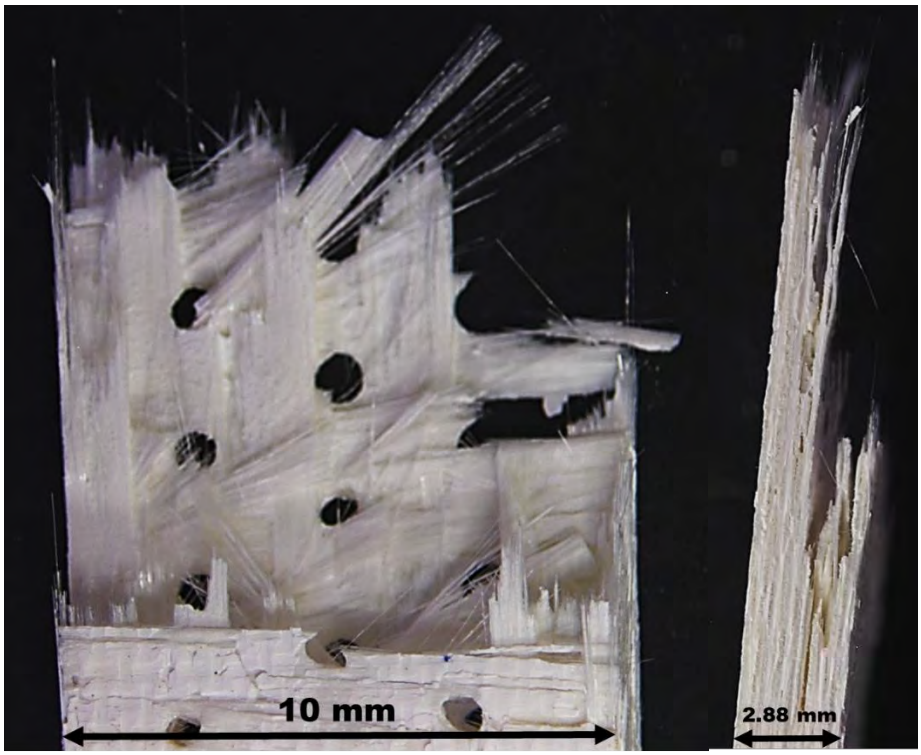


Figure A. 77: Fracture surface obtained for a N720/A specimen with effusion holes in creep at 1200ºC in air (σ_{cr} = 150 MPa, t_f = 0.0038 h).

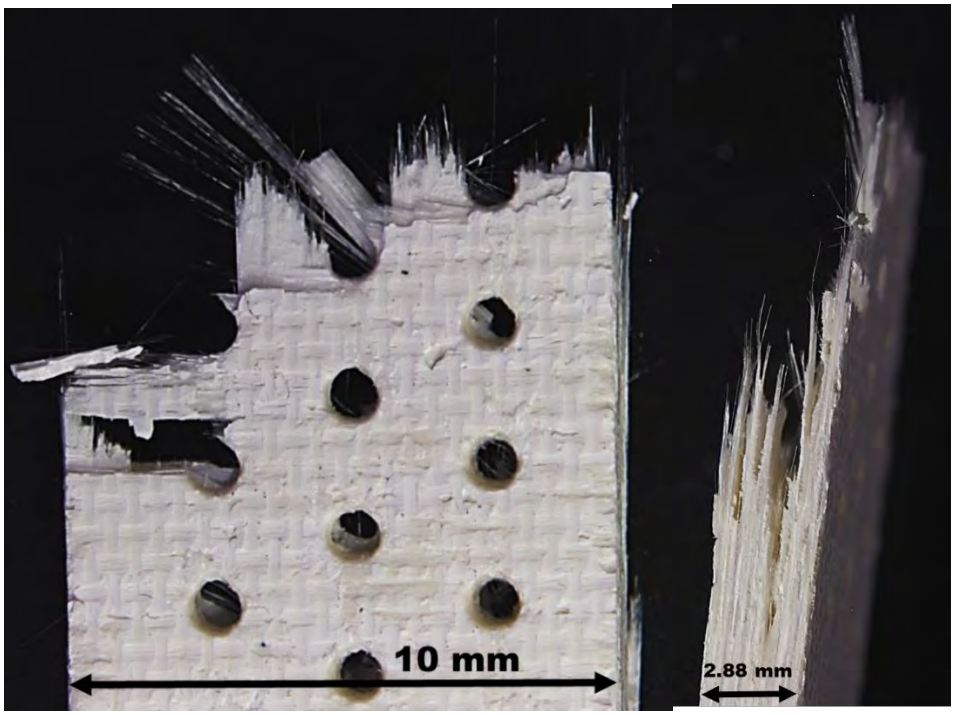


Figure A. 78: Fracture surface obtained for a N720/A specimen with effusion holes in creep at 1200ºC in air (σ_{cr} = 150 MPa, t_f = 0.0038 h).

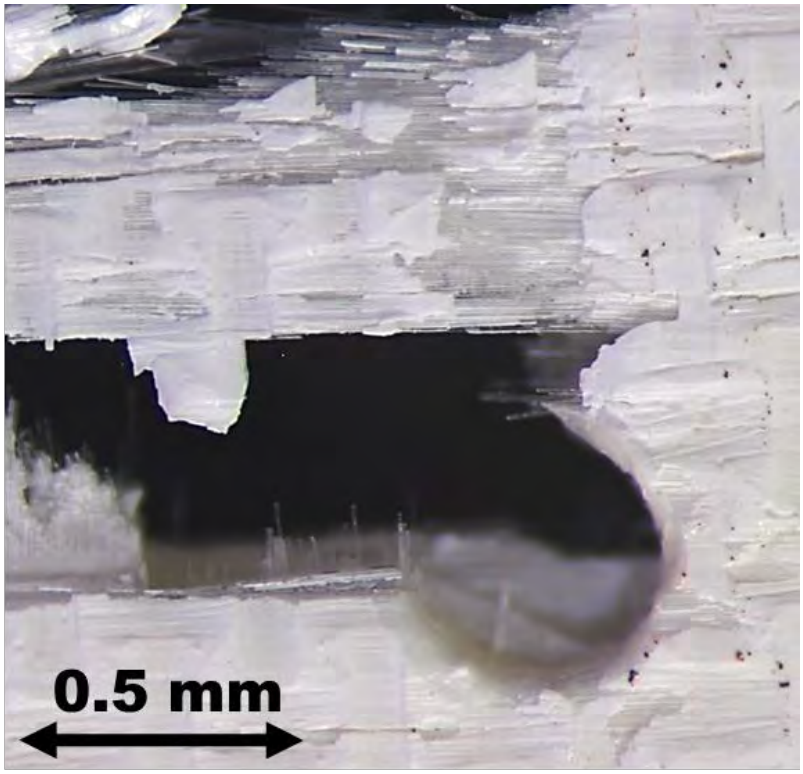


Figure A. 79: Fracture surface obtained for a N720/A specimen with effusion holes in creep at 1200ºC in air (σ_{cr} = 150 MPa, t_f = 0.0038 h).

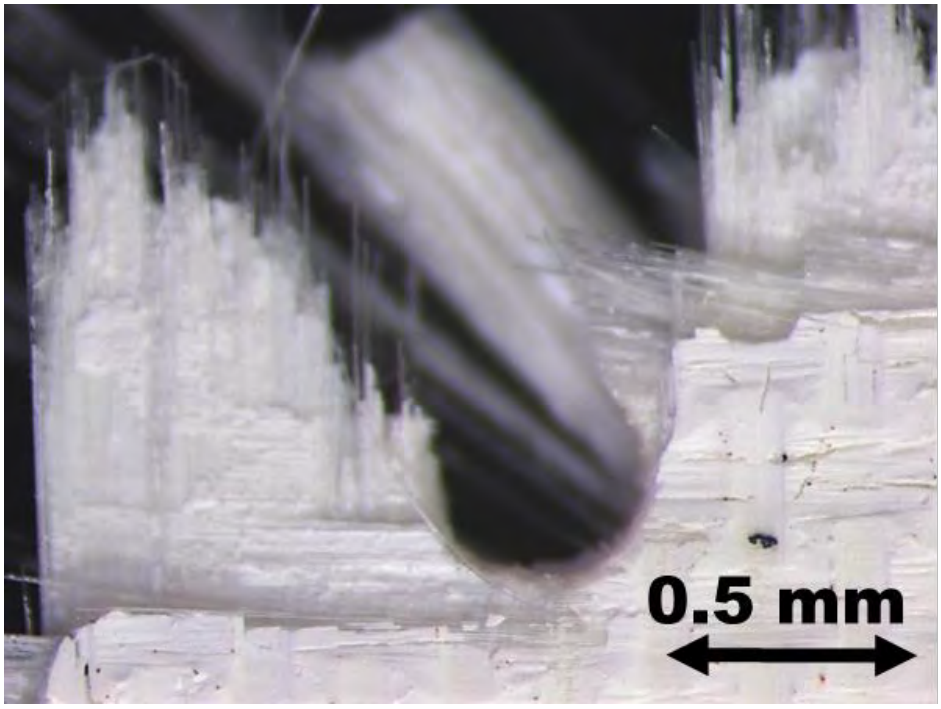


Figure A. 80: Fracture surface obtained for a N720/A specimen with effusion holes in creep at 1200ºC in air (σ_{cr} = 150 MPa, t_f = 0.0038 h).

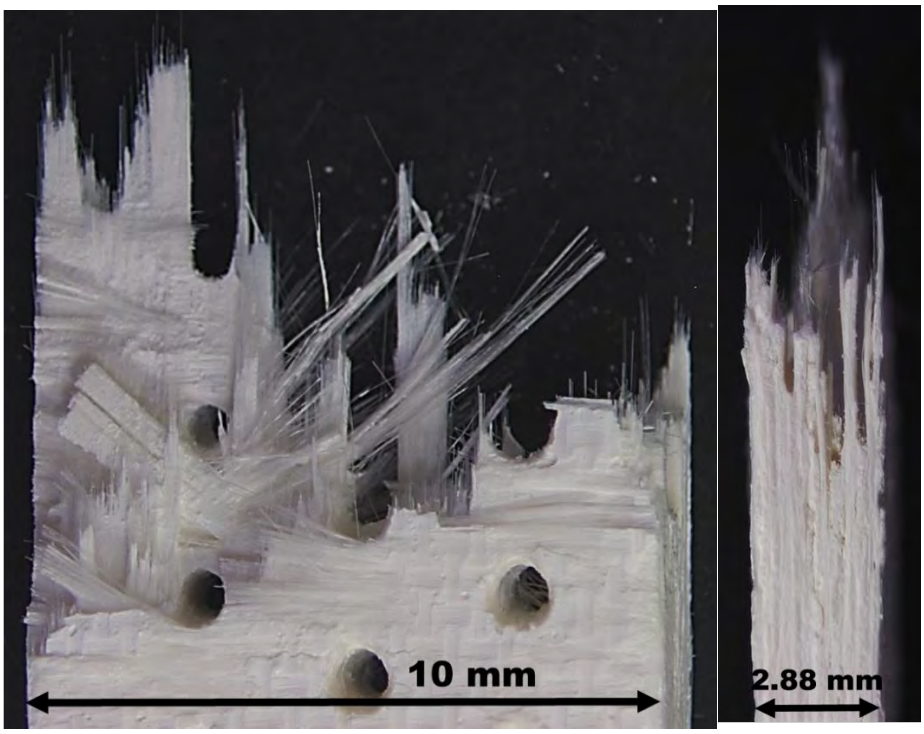


Figure A. 81: Fracture surface obtained for a N720/A specimen with effusion holes in tension to failure following 100 h of creep at 30 MPa at 1200ºC in steam.

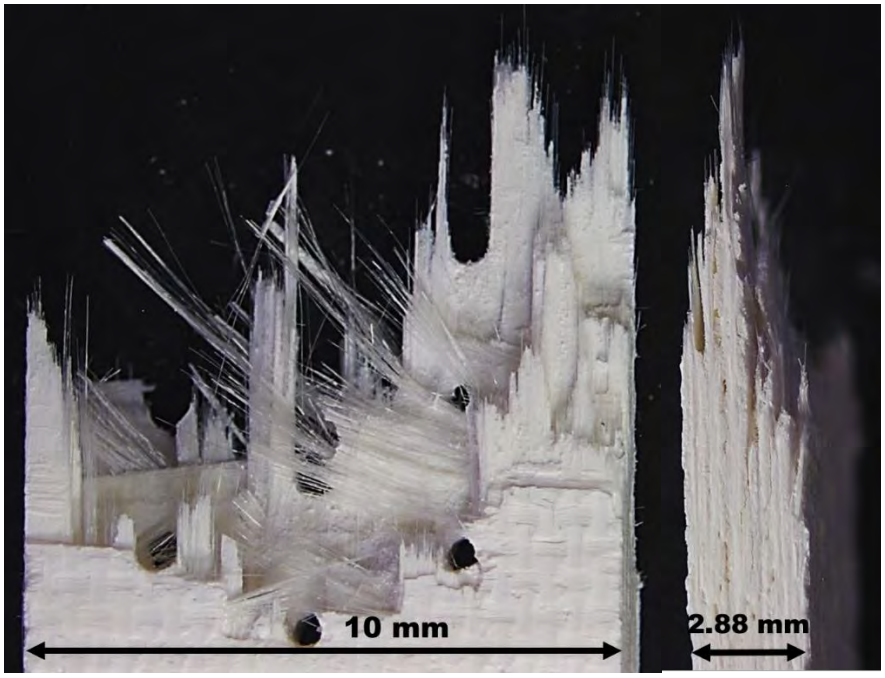


Figure A. 82: Fracture surface obtained for a N720/A specimen with effusion holes in tension to failure following 100 h of creep at 30 MPa at 1200ºC in steam.

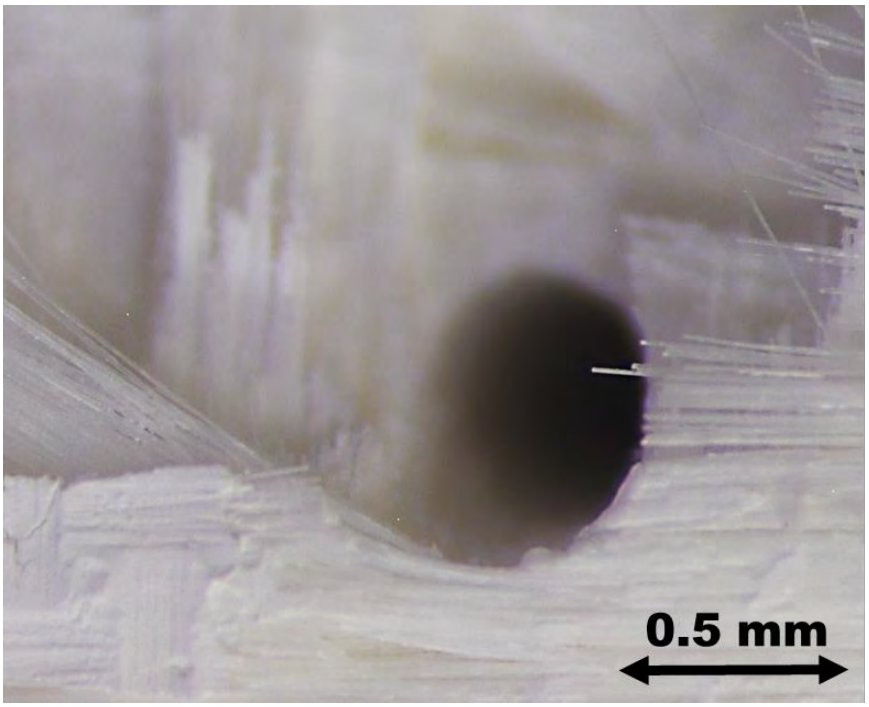


Figure A. 83: Fracture surface obtained for a N720/A specimen with effusion holes in tension to failure following 100 h of creep at 30 MPa at 1200ºC in steam.

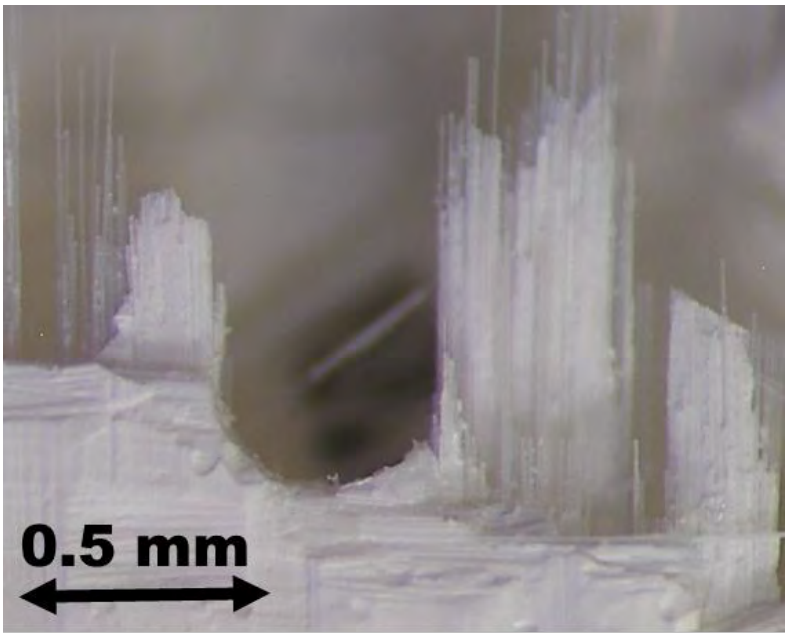


Figure A. 84: Fracture surface obtained for a N720/A specimen with effusion holes in tension to failure following 100 h of creep at 30 MPa at 1200ºC in steam.

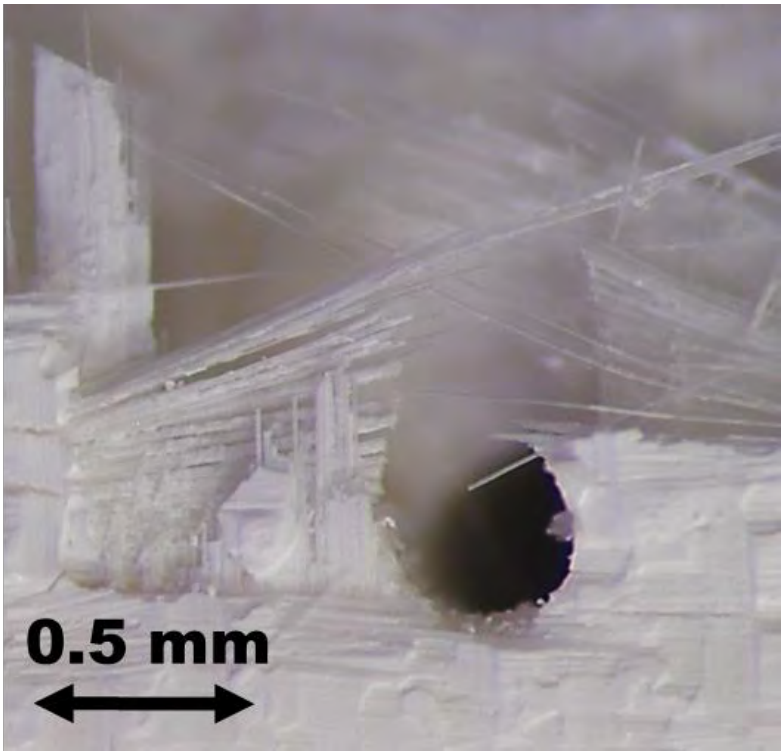


Figure A. 85: Fracture surface obtained for a N720/A specimen with effusion holes in tension to failure following 100 h of creep at 30 MPa at 1200ºC in steam.

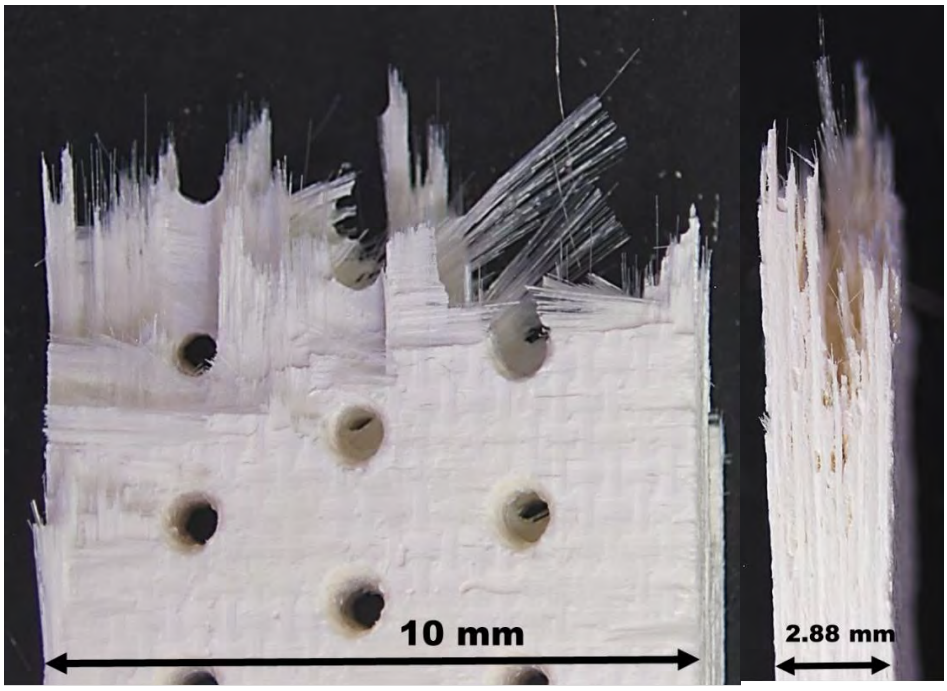


Figure A. 86: Fracture surface obtained for a N720/A specimen with effusion holes in tension to failure following 100 h of creep at 30 MPa at 1200ºC in steam.

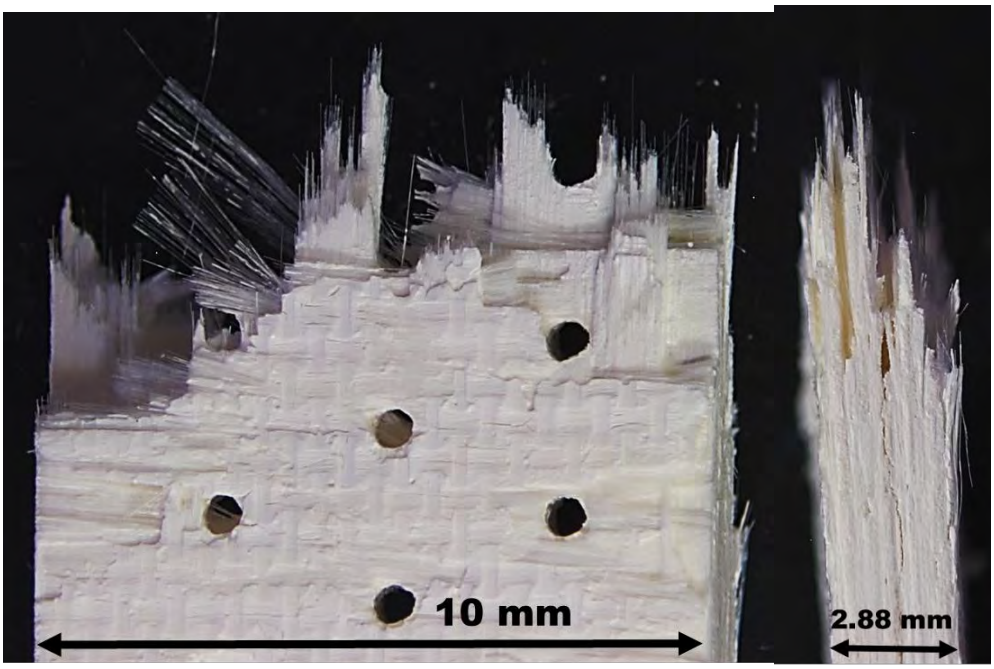


Figure A. 87: Fracture surface obtained for a N720/A specimen with effusion holes in tension to failure following 100 h of creep at 30 MPa at 1200ºC in steam.

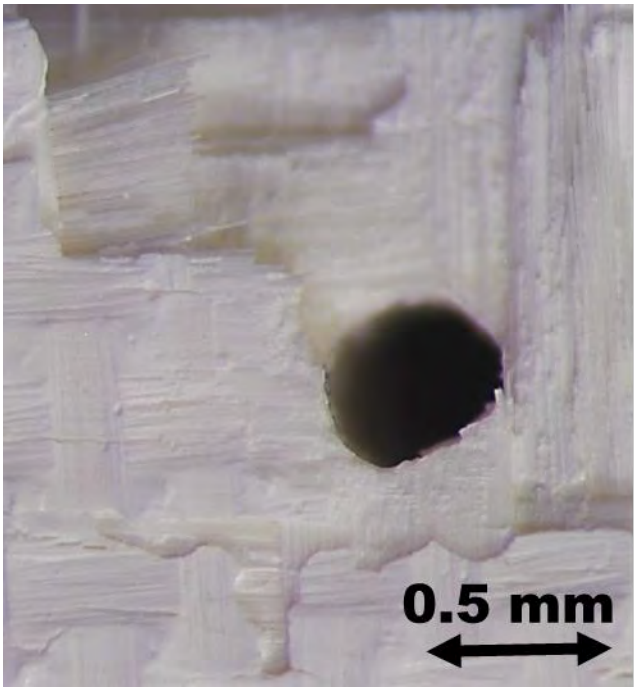


Figure A. 88: Fracture surface obtained for a N720/A specimen with effusion holes in tension to failure following 100 h of creep at 30 MPa at 1200ºC in steam.

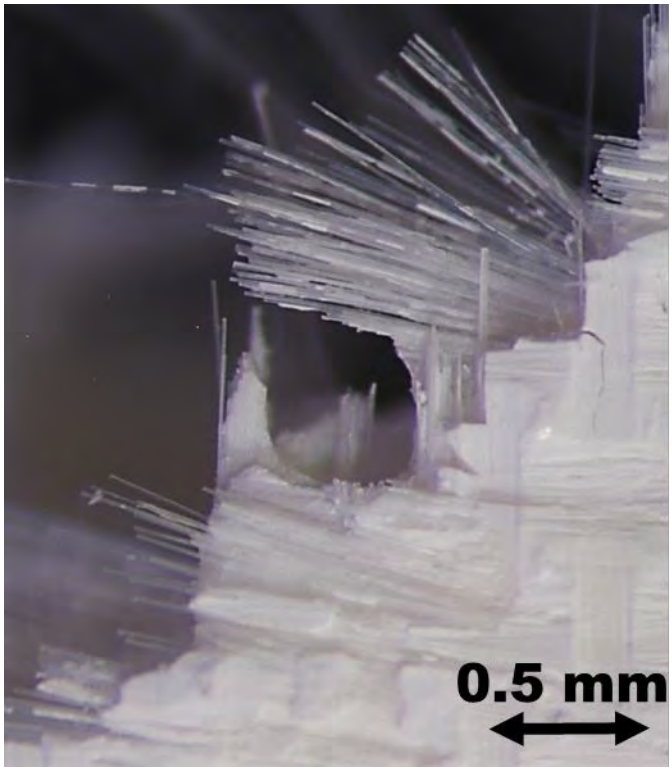


Figure A. 89: Fracture surface obtained for a N720/A specimen with effusion holes in tension to failure following 100 h of creep at 30 MPa at 1200ºC in steam.

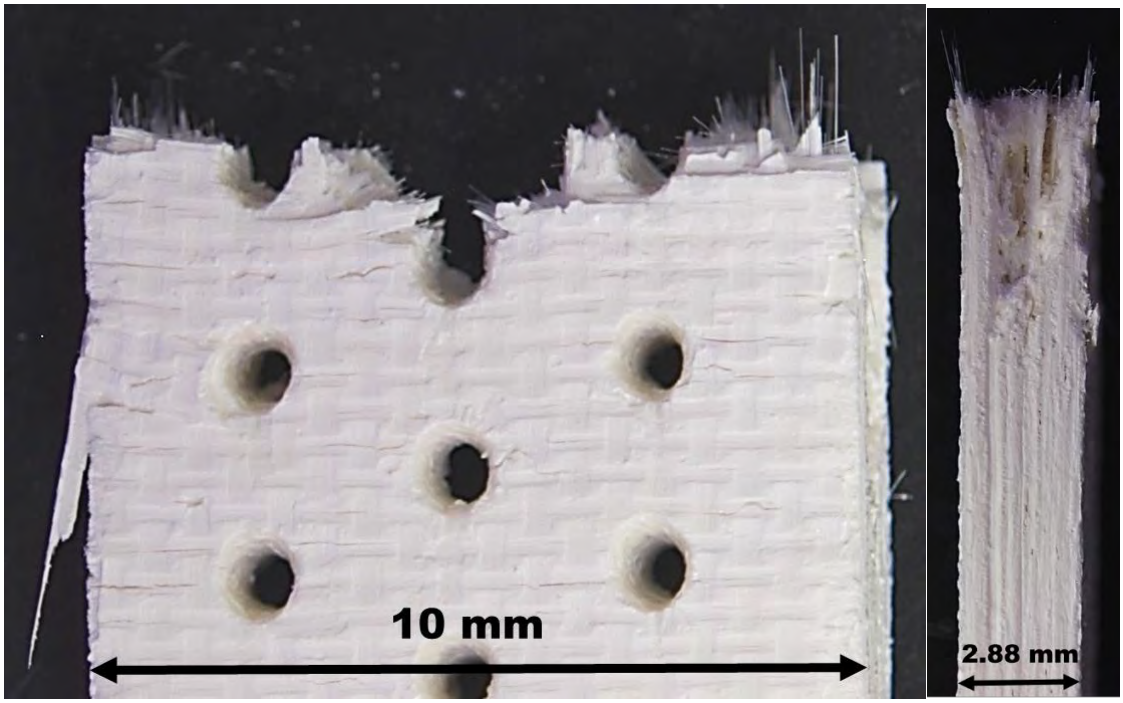


Figure A. 90: Fracture surface obtained for a N720/A specimen with effusion holes in creep at 1200ºC in steam (σ_{cr} = 40 MPa, t_f = 98.79 h).

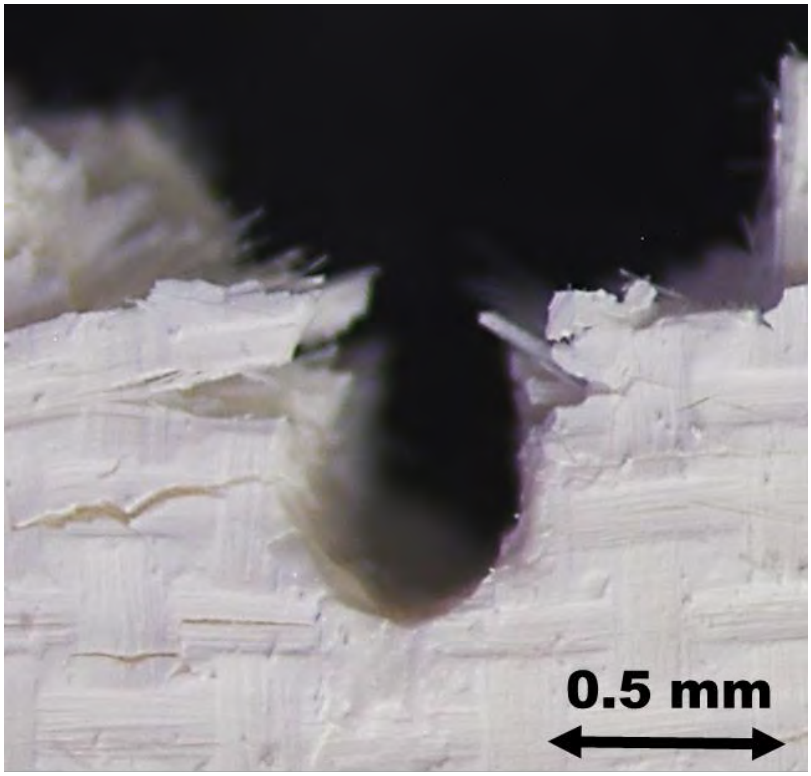


Figure A. 91: Fracture surface obtained for a N720/A specimen with effusion holes in creep at 1200ºC in steam (σ_{cr} = 40 MPa, t_f = 98.79 h).

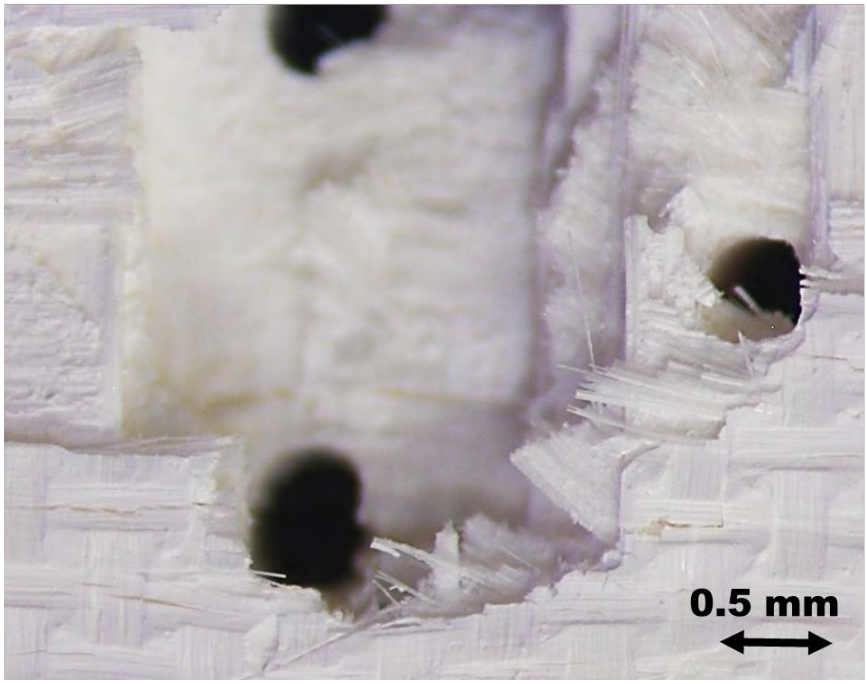


Figure A. 92: Fracture surface obtained for a N720/A specimen with effusion holes in creep at 1200ºC in steam (σ_{cr} = 40 MPa, t_f = 98.79 h).

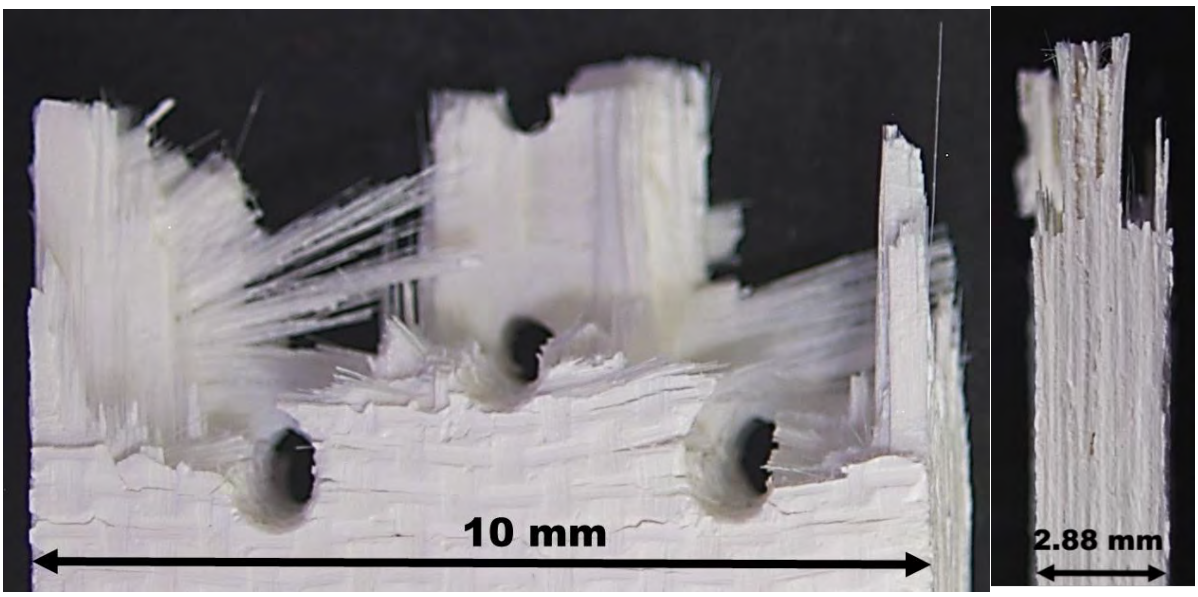


Figure A. 93: Fracture surface obtained for a N720/A specimen with effusion holes in creep at 1200ºC in steam (σ_{cr} = 40 MPa, t_f = 98.79 h).

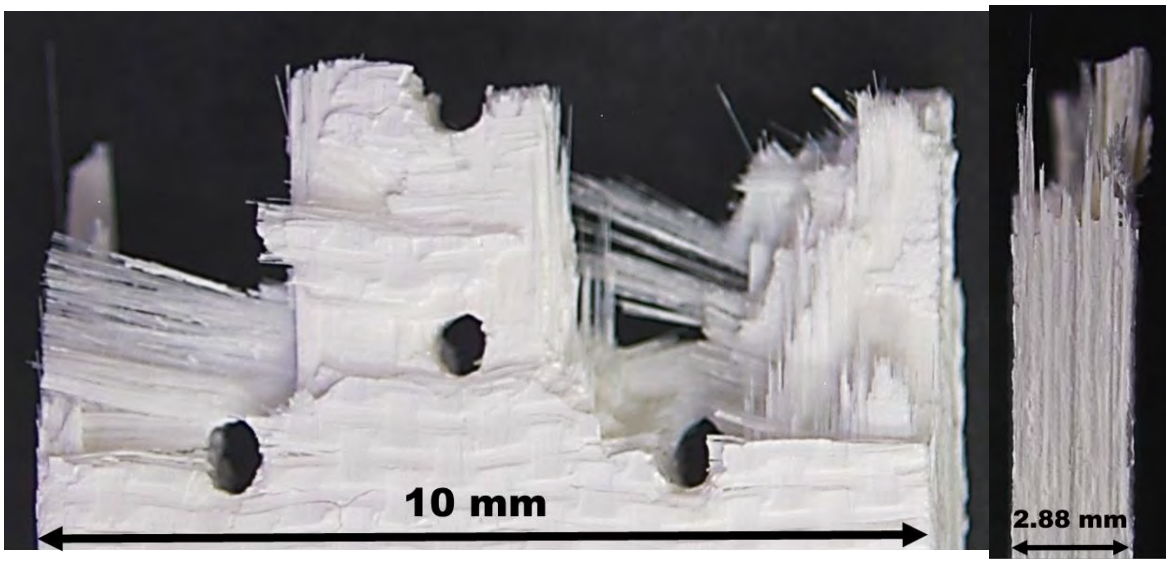


Figure A. 94: Fracture surface obtained for a N720/A specimen with effusion holes in creep at 1200ºC in steam (σ_{cr} = 40 MPa, t_f = 98.79 h).

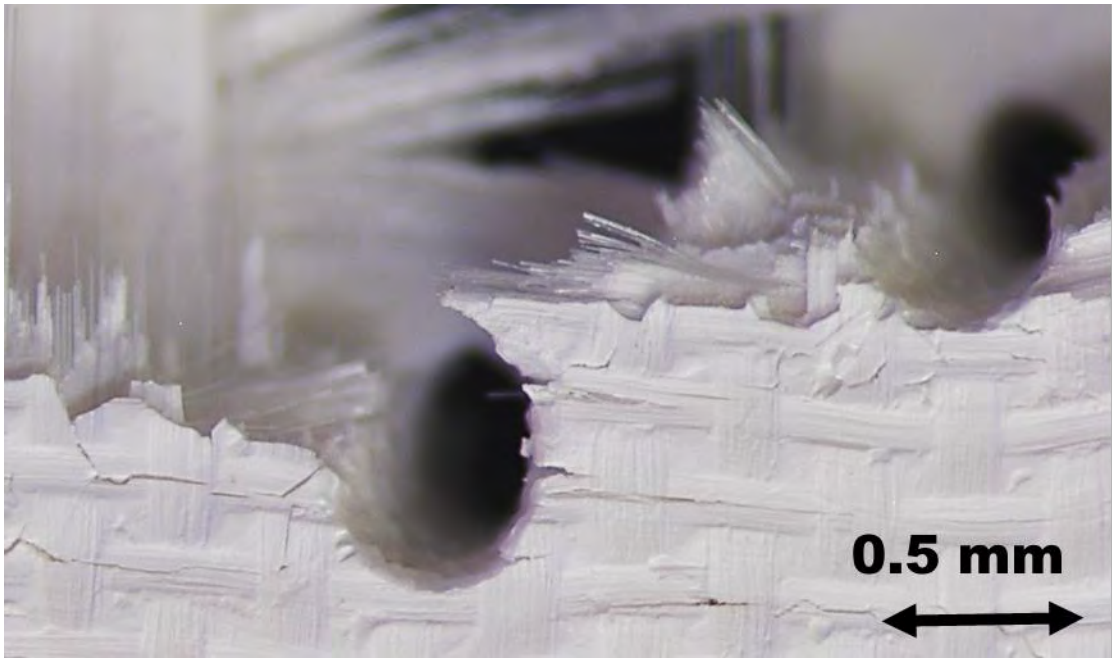


Figure A. 95: Fracture surface obtained for a N720/A specimen with effusion holes in creep at 1200ºC in steam (σ_{cr} = 40 MPa, t_f = 98.79 h).

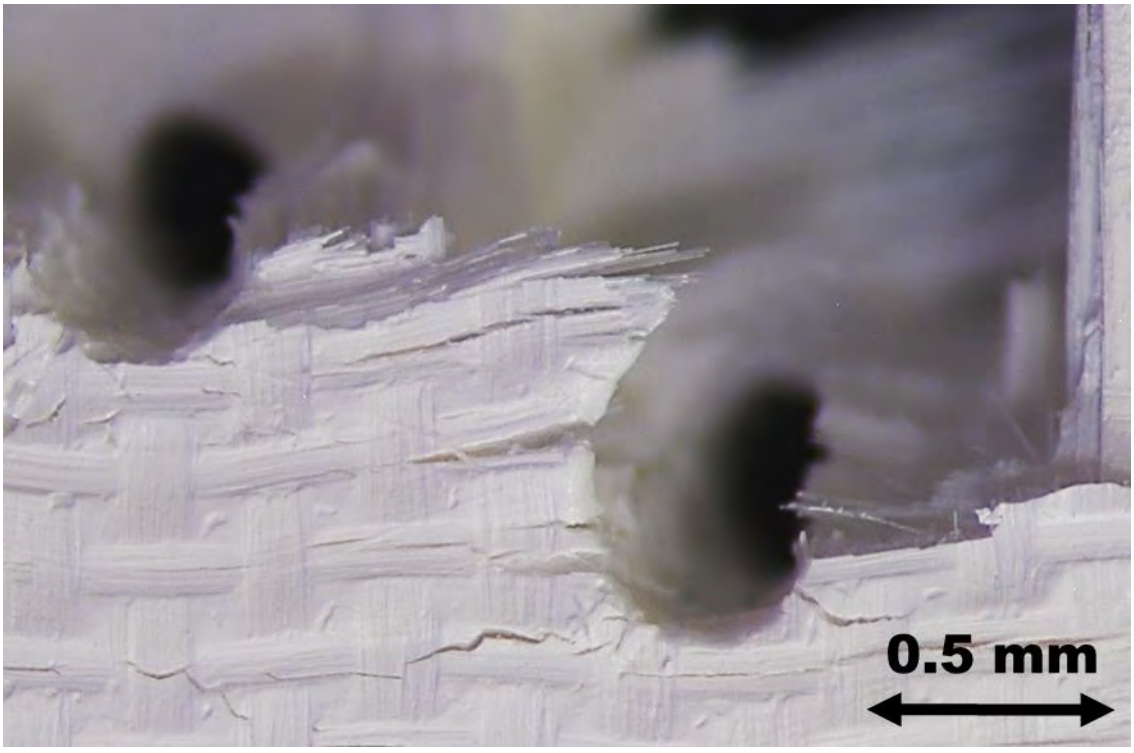


Figure A. 96: Fracture surface obtained for a N720/A specimen with effusion holes in creep at 1200ºC in steam (σ_{cr} = 40 MPa, t_f = 98.79 h).

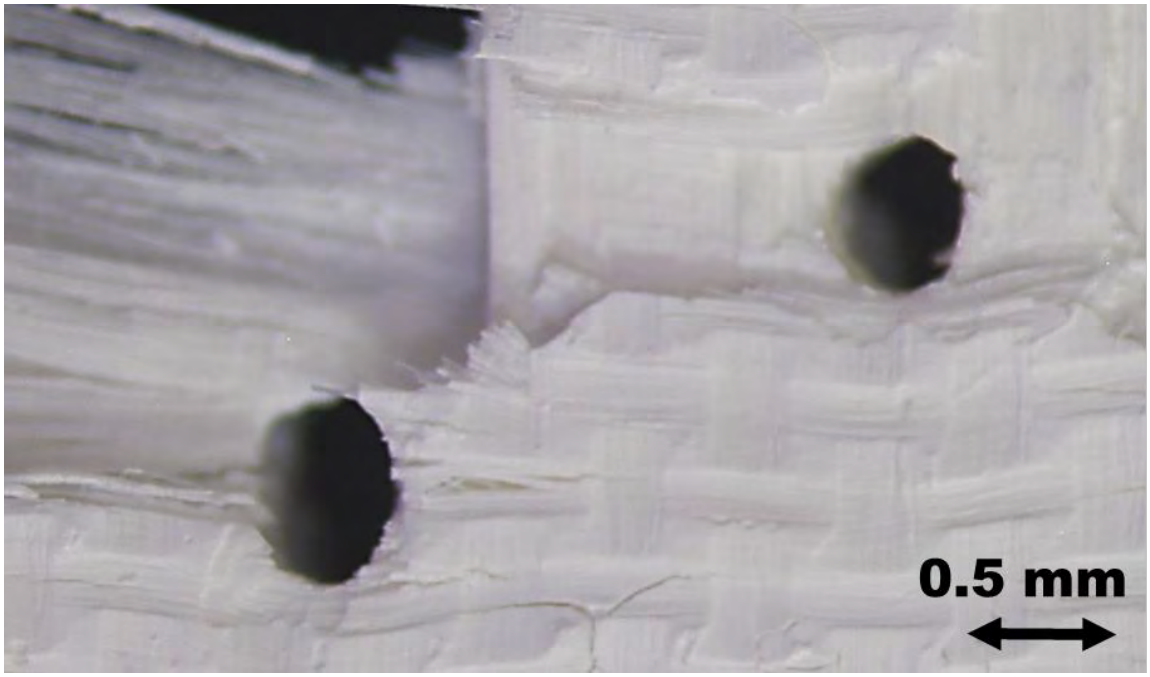


Figure A. 97: Fracture surface obtained for a N720/A specimen with effusion holes in creep at 1200ºC in steam (σ_{cr} = 40 MPa, t_f = 98.79 h).

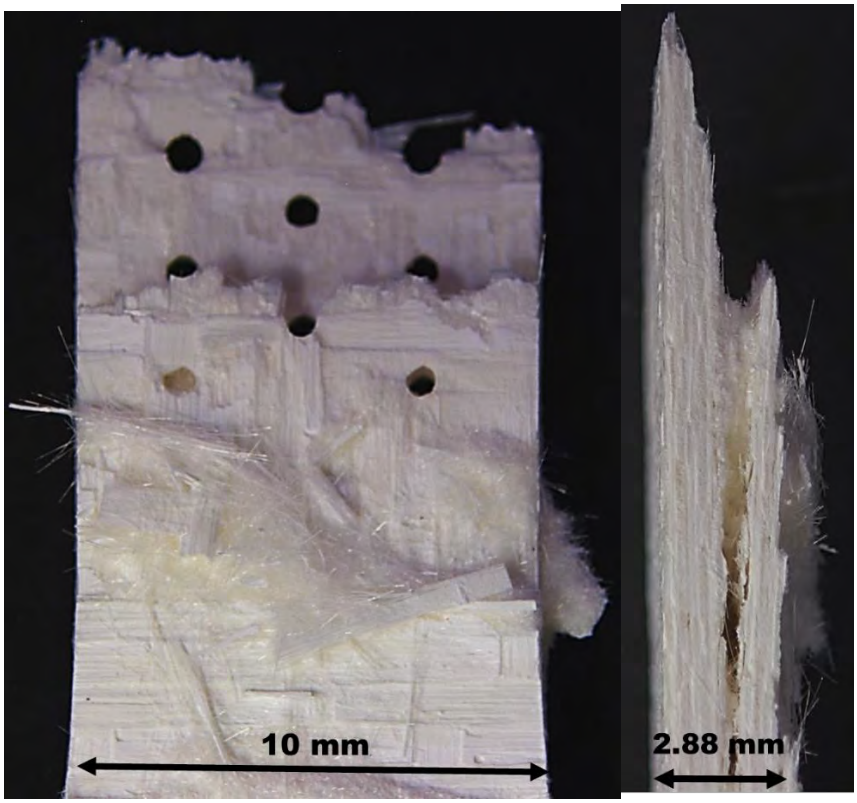


Figure A. 98: Fracture surface obtained for a N720/A specimen with effusion holes in creep at 1200ºC in steam (σ_{cr} = 65 MPa, t_f = 12.44 h).

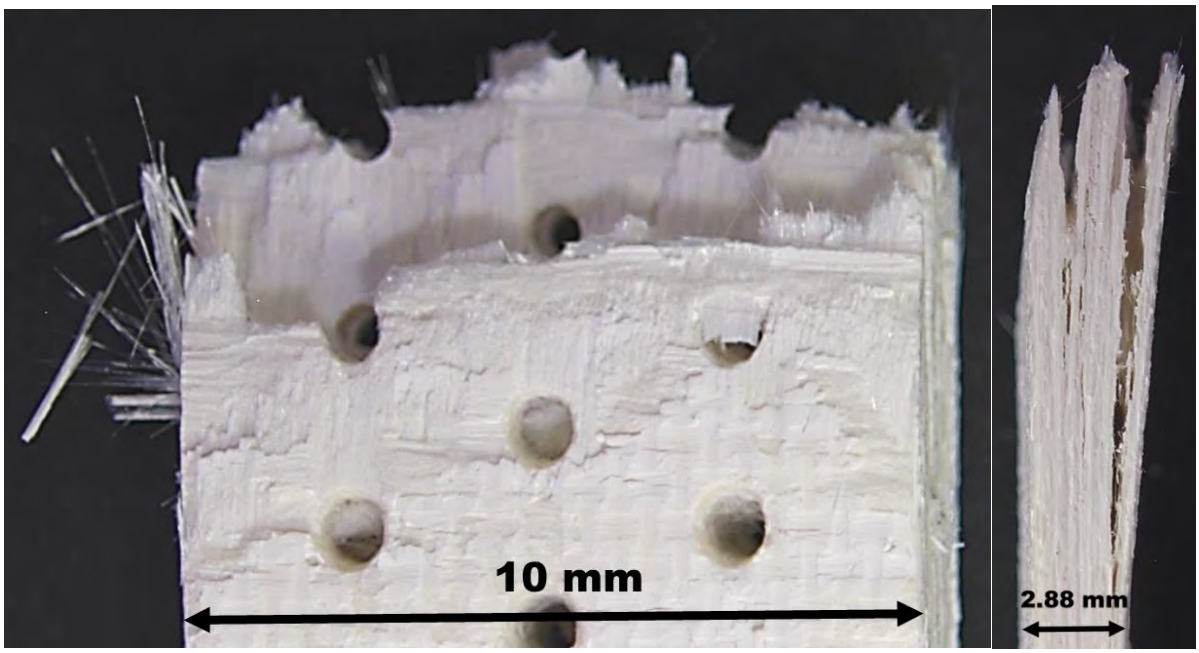


Figure A. 99: Fracture surface obtained for a N720/A specimen with effusion holes in creep at 1200ºC in steam (σ_{cr} = 65 MPa, t_f = 12.44 h).

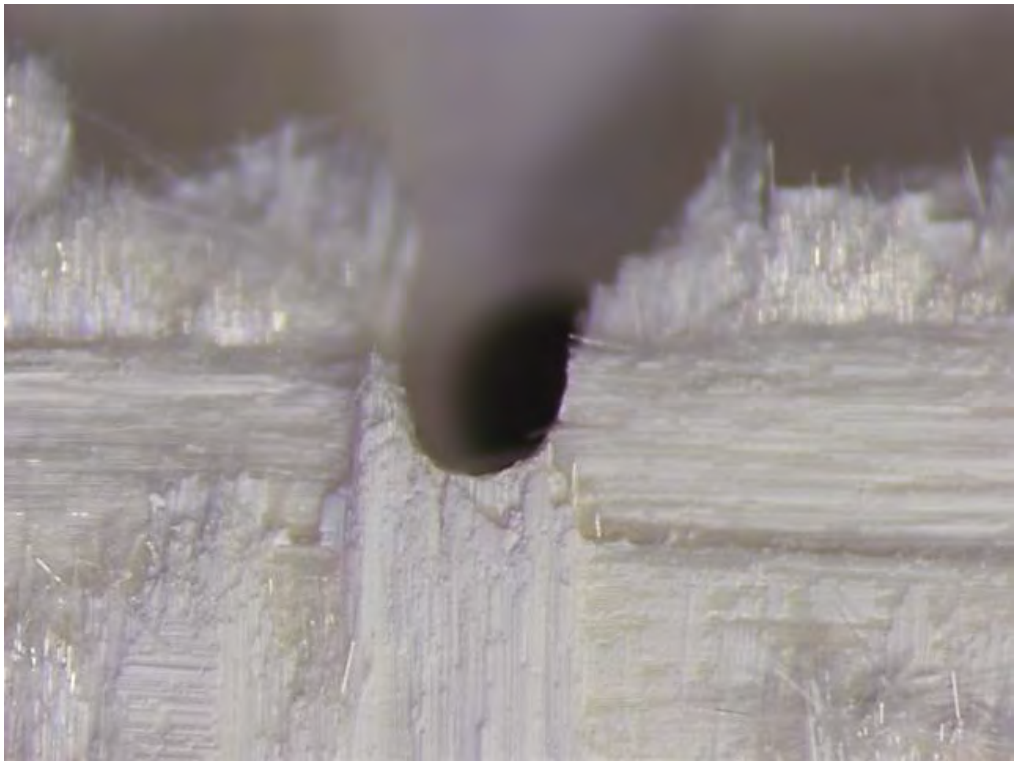


Figure A. 100: Fracture surface obtained for a N720/A specimen with effusion holes in creep at 1200ºC in steam (σ_{cr} = 65 MPa, t_f = 12.44 h).

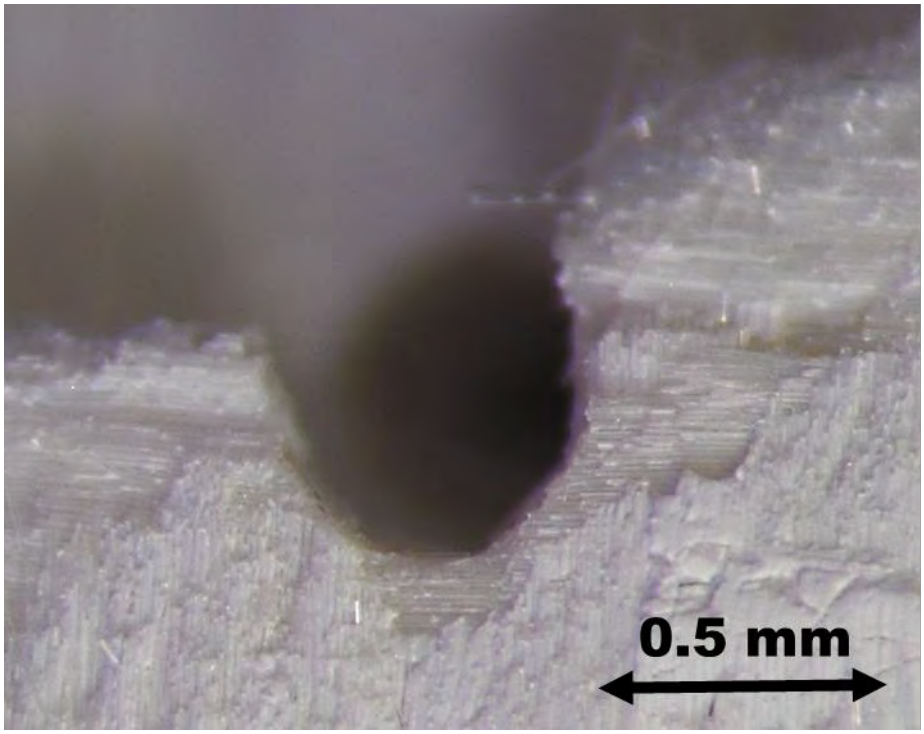


Figure A. 101: Fracture surface obtained for a N720/A specimen with effusion holes in creep at 1200ºC in steam (σ_{cr} = 65 MPa, t_f = 12.44 h).

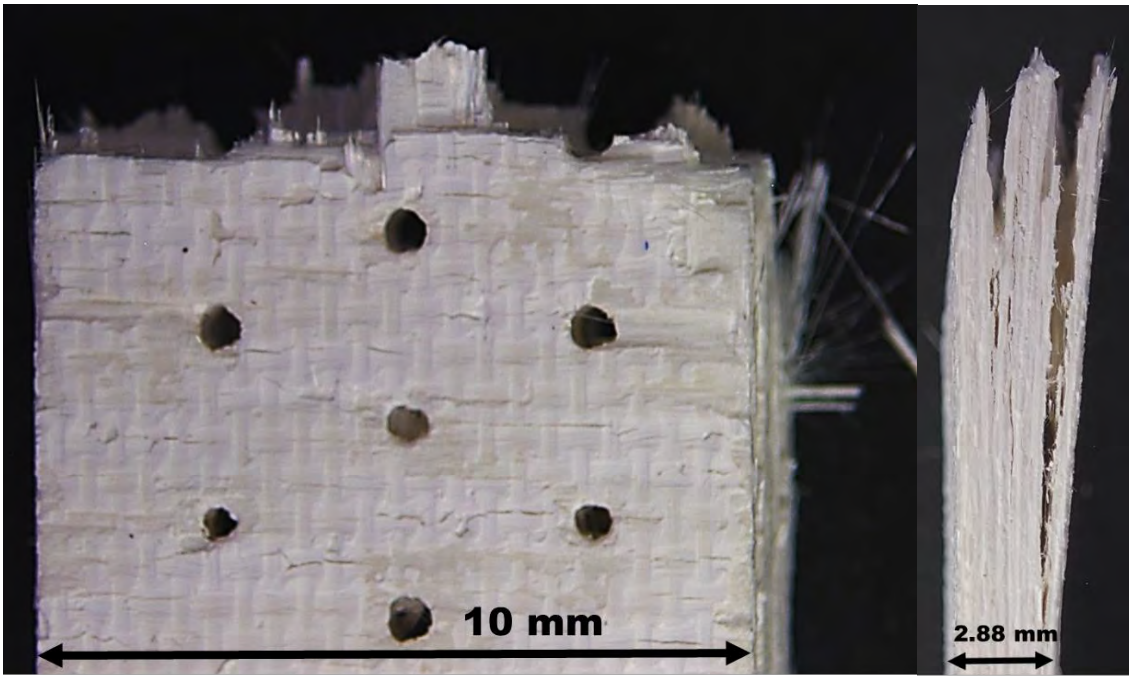


Figure A. 102: Fracture surface obtained for a N720/A specimen with effusion holes in creep at 1200ºC in steam (σ_{cr} = 65 MPa, t_f = 12.44 h).

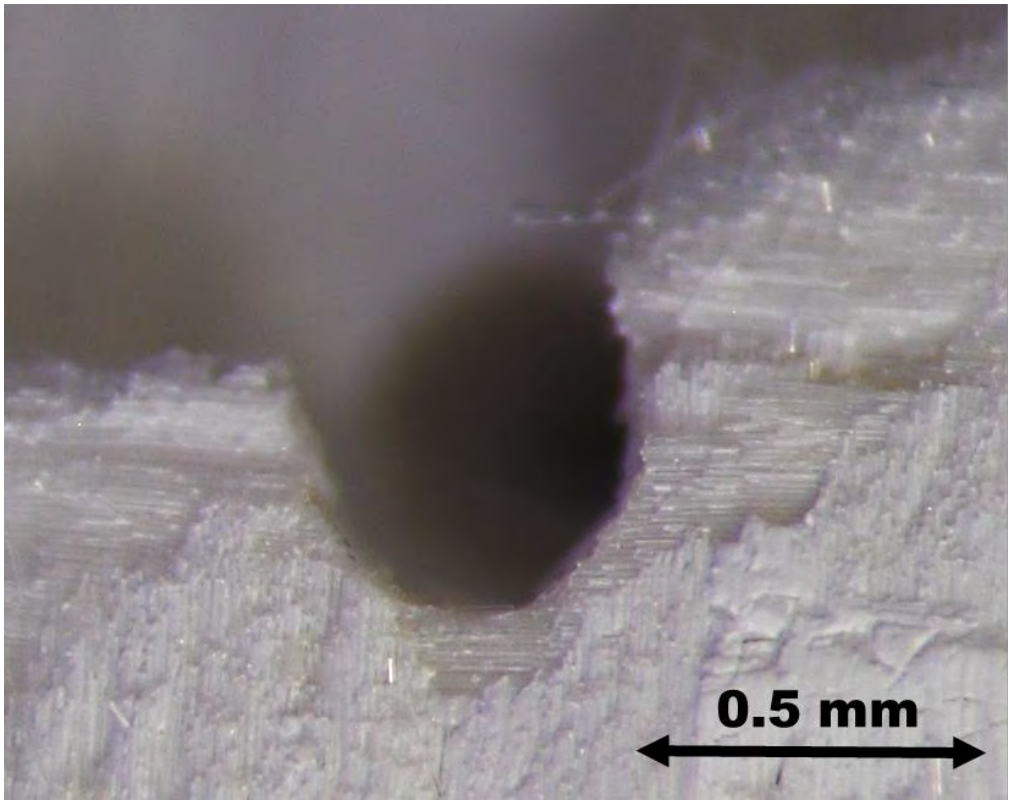


Figure A. 103: Fracture surface obtained for a N720/A specimen with effusion holes in creep at 1200ºC in steam (σ_{cr} = 65 MPa, t_f = 12.44 h).

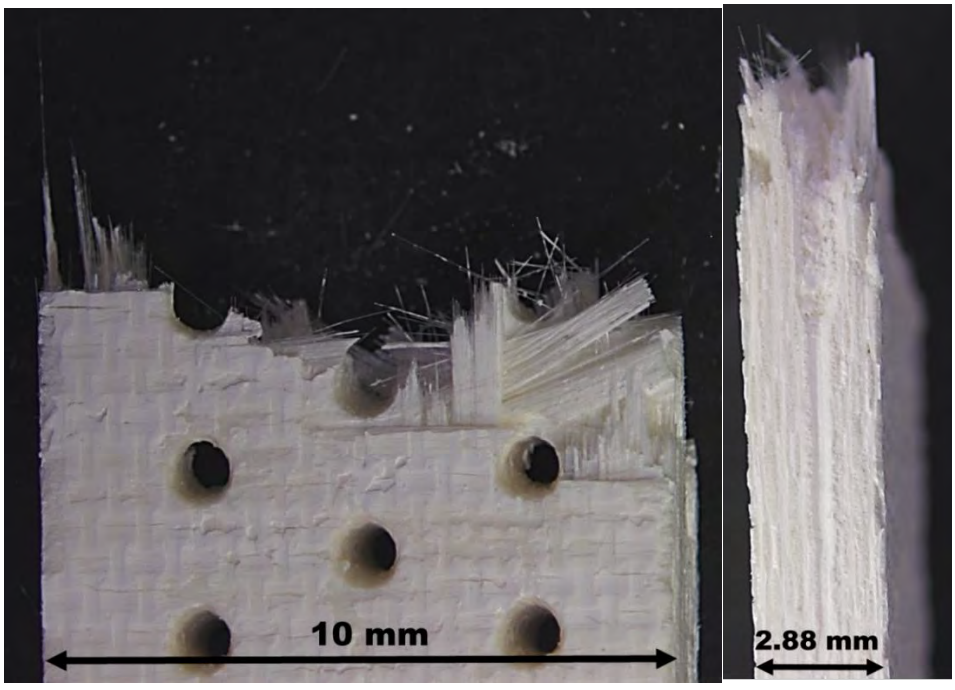


Figure A. 104: Fracture surface obtained for a N720/A specimen with effusion holes in creep at 1200ºC in steam (σ_{cr} = 80 MPa, t_f = 1.605 h).

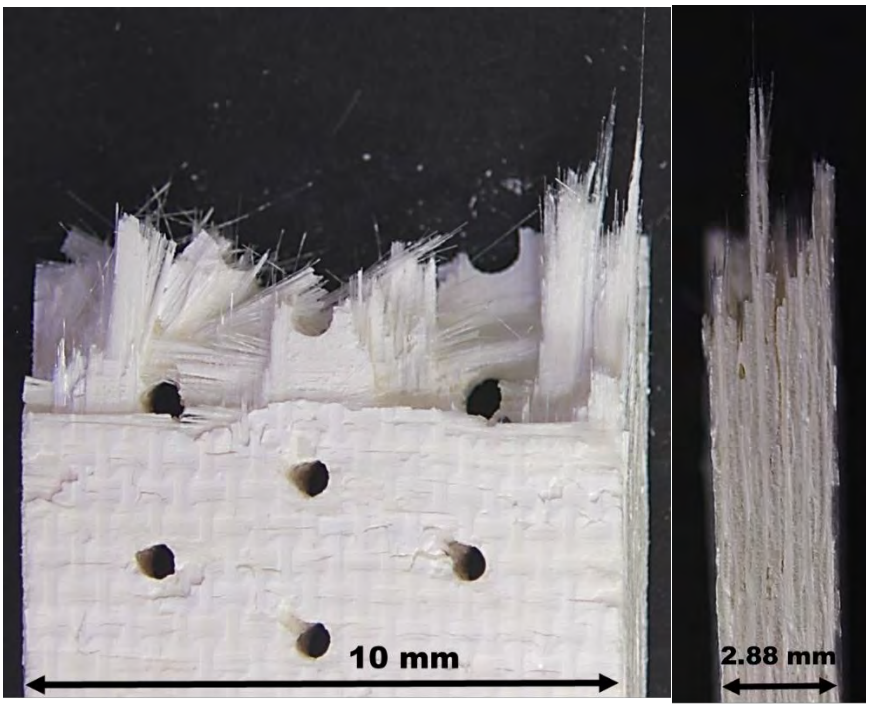


Figure A. 105: Fracture surface obtained for a N720/A specimen with effusion holes in creep at 1200ºC in steam (σ_{cr} = 80 MPa, t_f = 1.605 h).

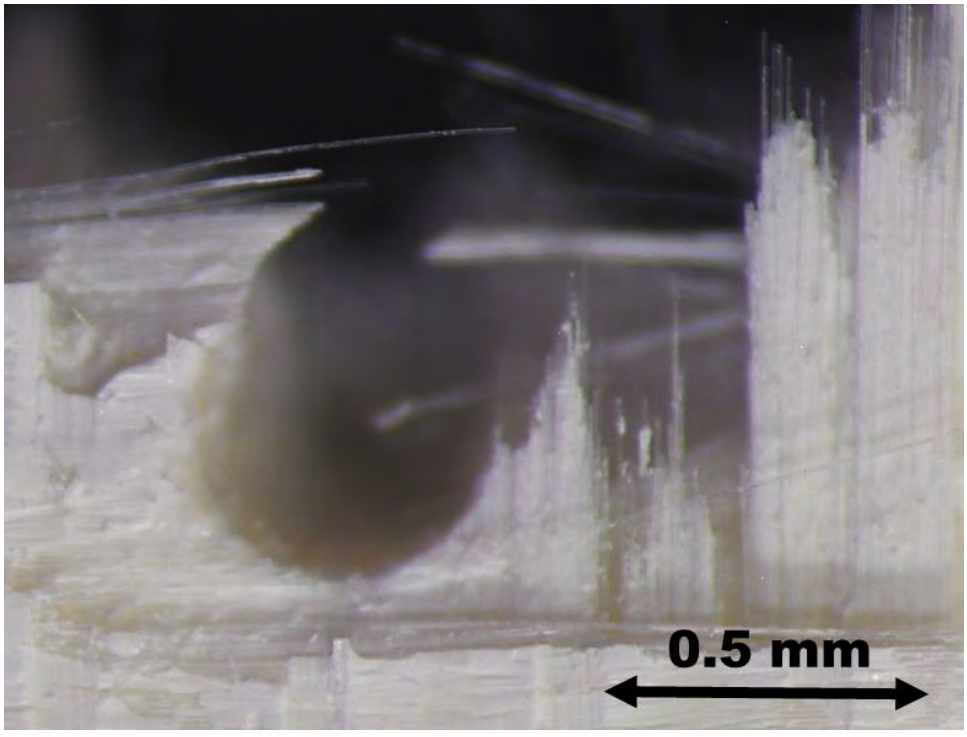


Figure A. 106: Fracture surface obtained for a N720/A specimen with effusion holes in creep at 1200ºC in steam (σ_{cr} = 80 MPa, t_f = 1.605 h).

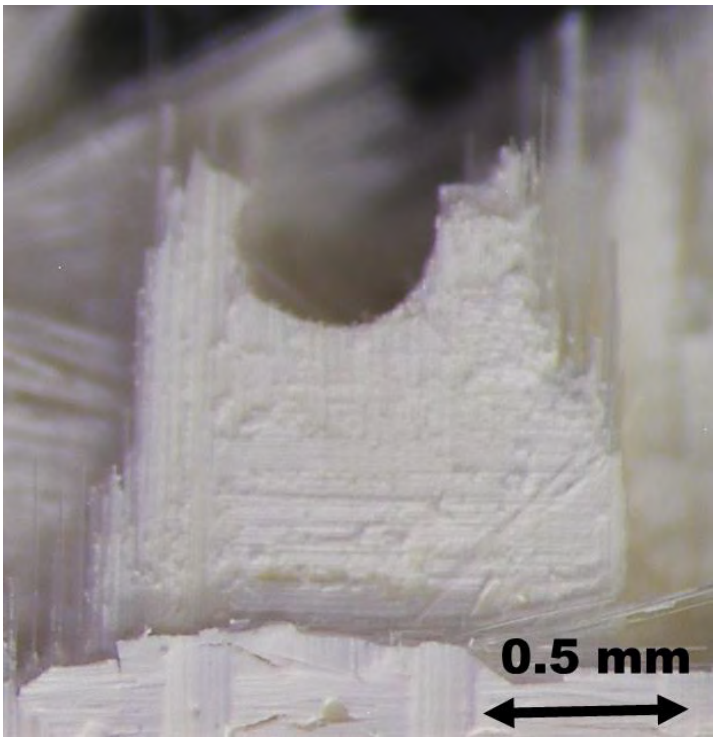


Figure A. 107: Fracture surface obtained for a N720/A specimen with effusion holes in creep at 1200ºC in steam (σ_{cr} = 80 MPa, t_f = 1.605 h).

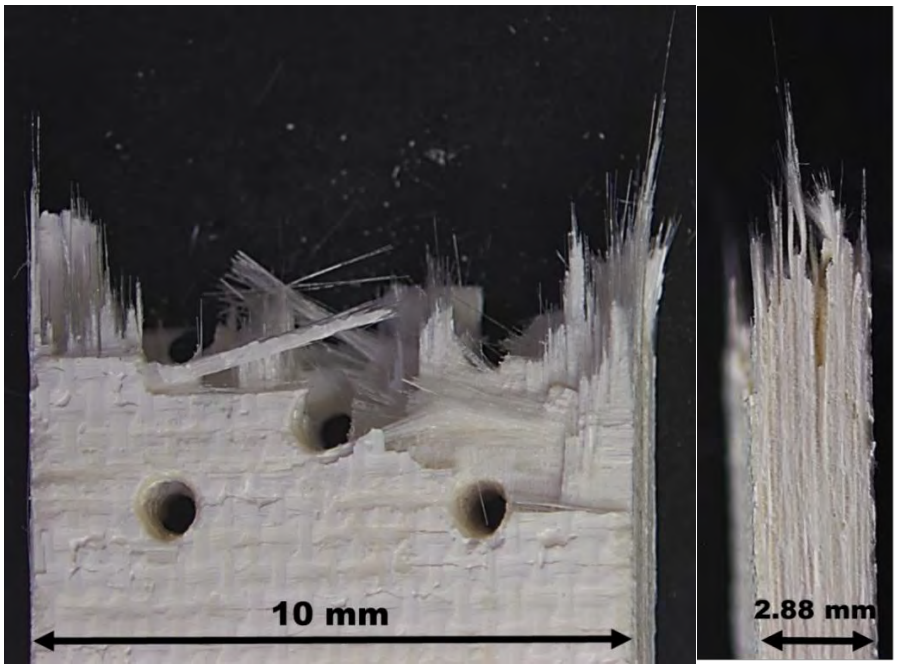


Figure A. 108: Fracture surface obtained for a N720/A specimen with effusion holes in creep at 1200ºC in steam (σ_{cr} = 80 MPa, t_f = 1.605 h).

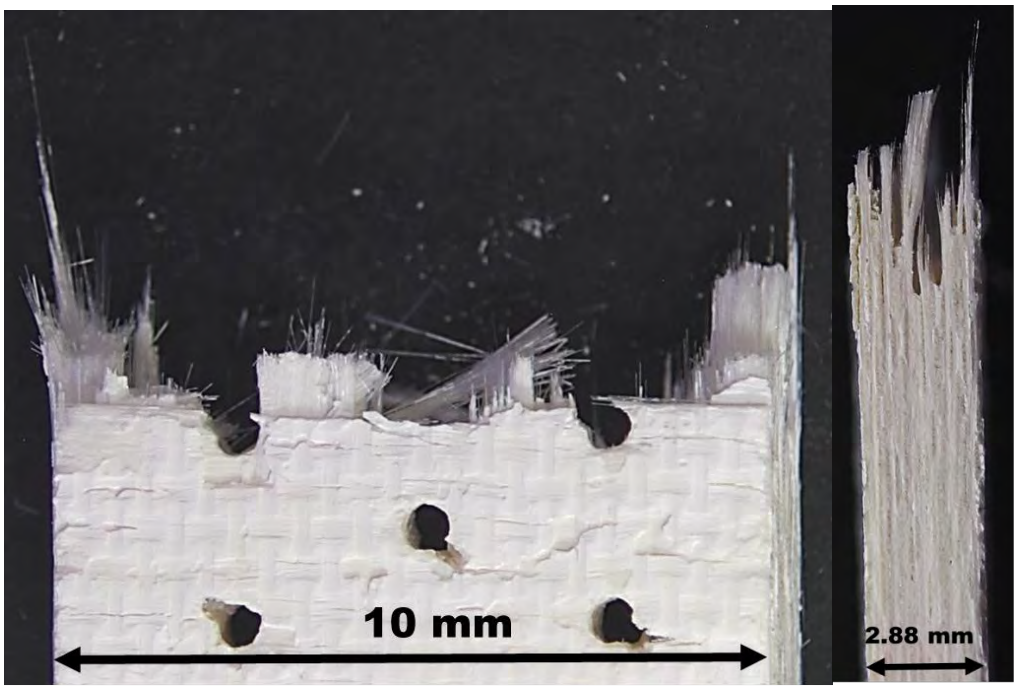


Figure A. 109: Fracture surface obtained for a N720/A specimen with effusion holes in creep at 1200ºC in steam (σ_{cr} = 80 MPa, t_f = 1.605 h).

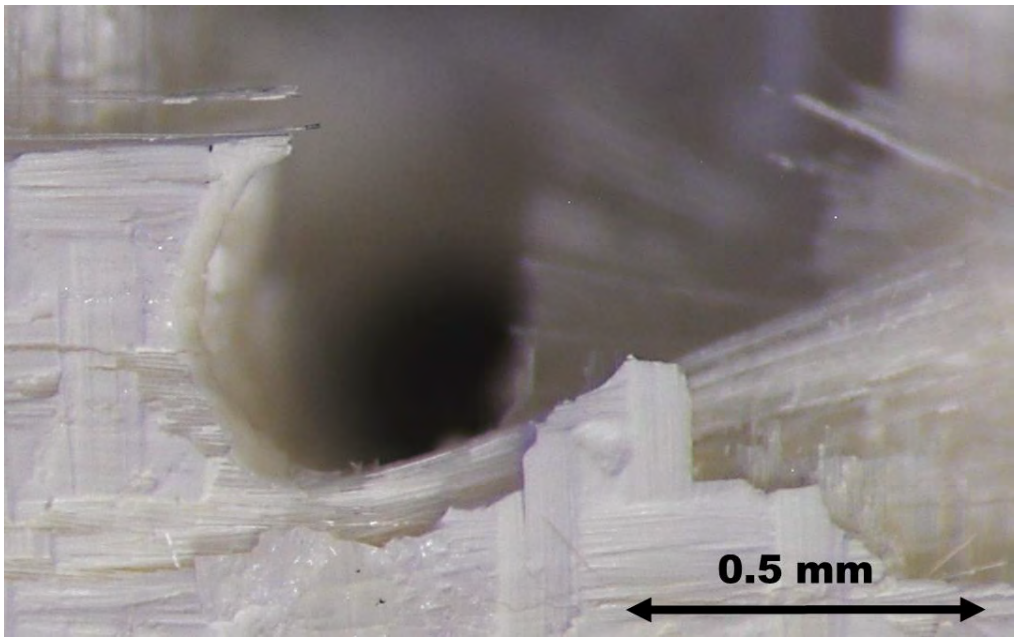


Figure A. 110: Fracture surface obtained for a N720/A specimen with effusion holes in creep at 1200ºC in steam (σ_{cr} = 80 MPa, t_f = 1.605 h).

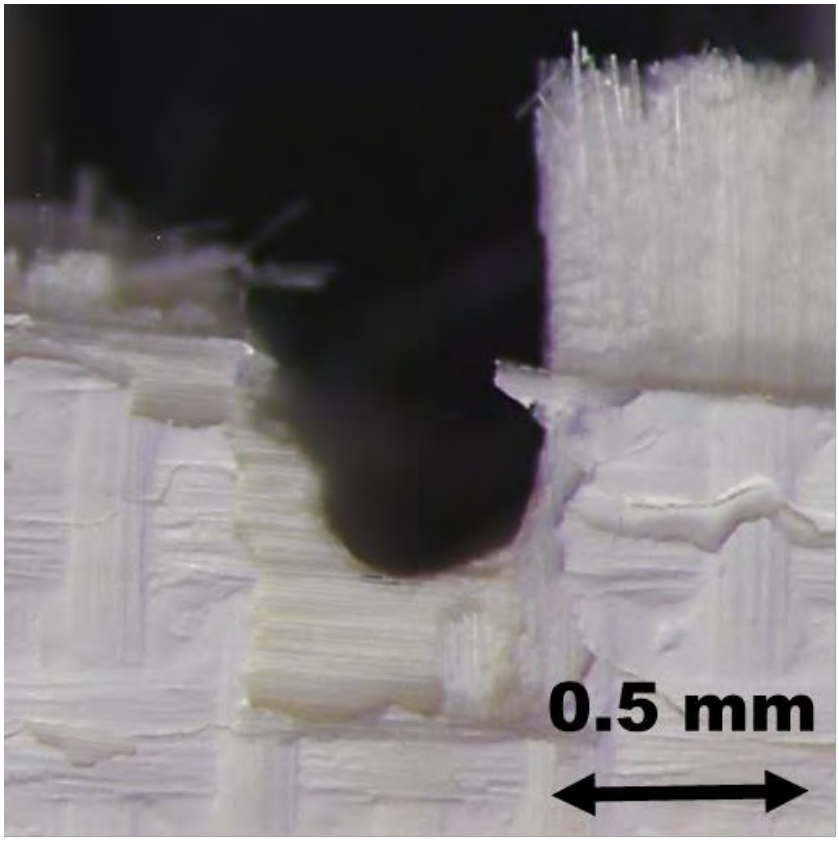


Figure A. 111: Fracture surface obtained for a N720/A specimen with effusion holes in creep at 1200ºC in steam (σ_{cr} = 80 MPa, t_f = 1.605 h).

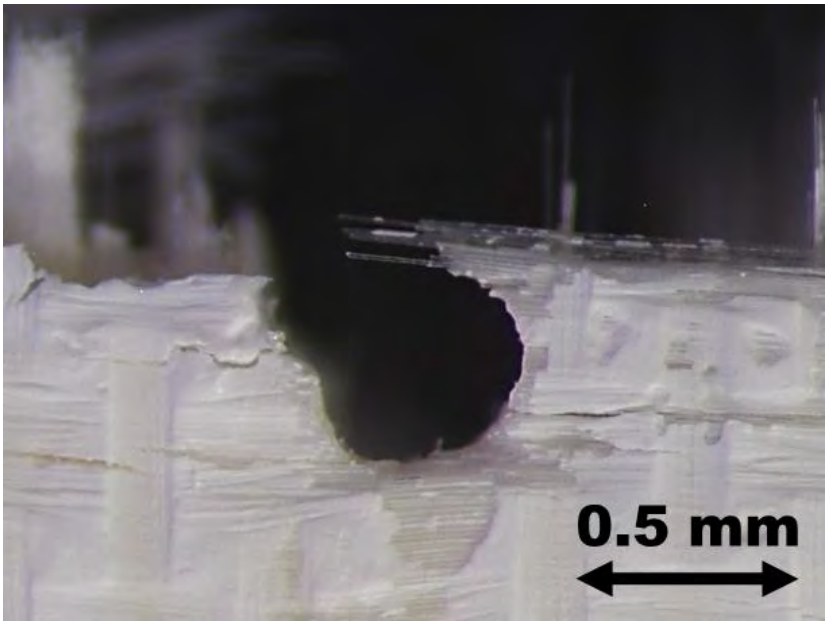


Figure A. 112: Fracture surface obtained for a N720/A specimen with effusion holes in creep at 1200ºC in steam (σ_{cr} = 80 MPa, t_f = 1.605 h).

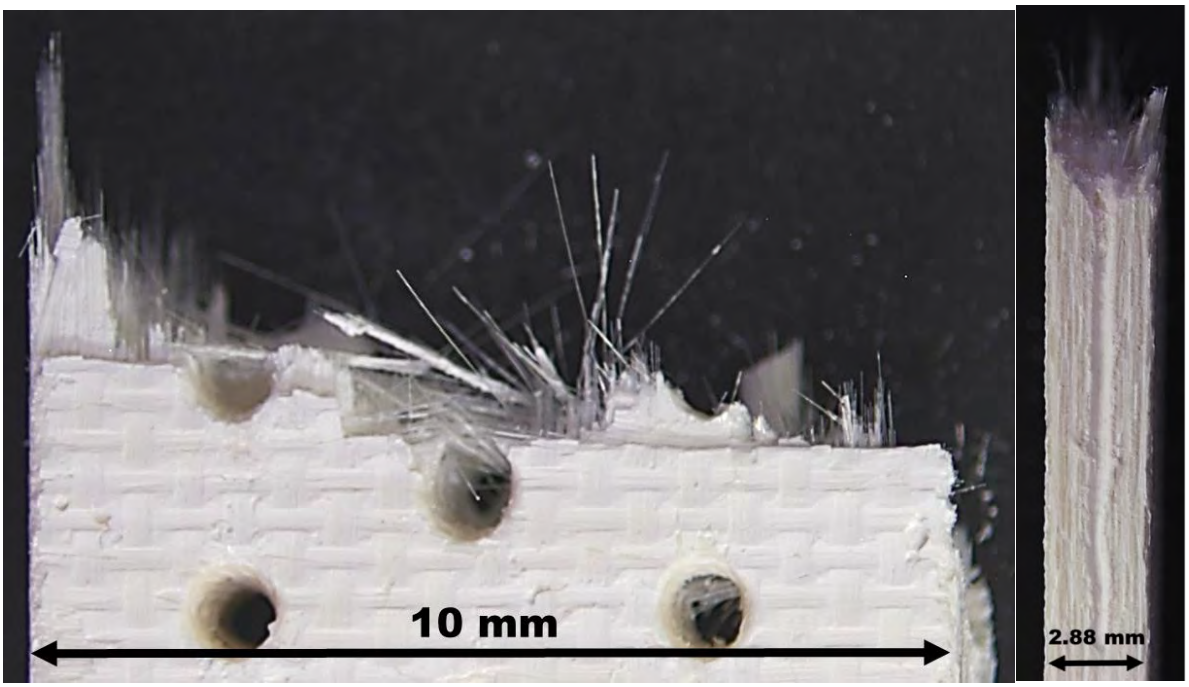


Figure A. 113: Fracture surface obtained for a N720/A specimen with effusion holes in creep at 1200ºC in steam (σ_{cr} = 90 MPa, t_f = 0.572 h).

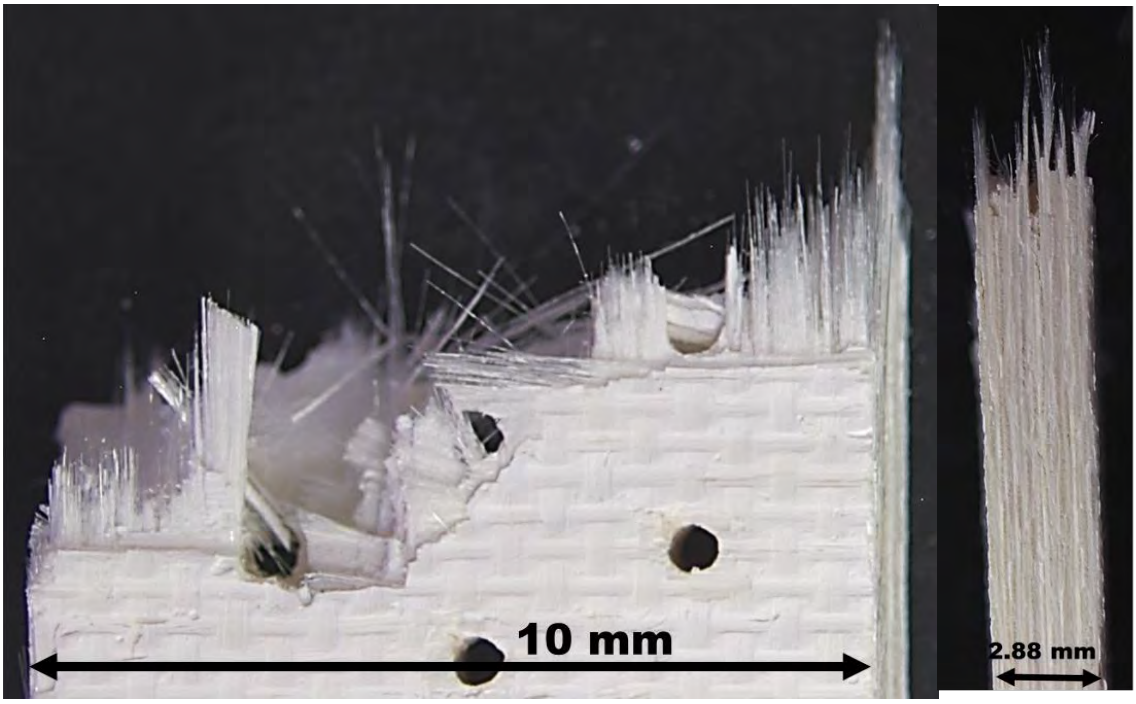


Figure A. 114: Fracture surface obtained for a N720/A specimen with effusion holes in creep at 1200ºC in steam (σ_{cr} = 90 MPa, t_f = 0.572 h).

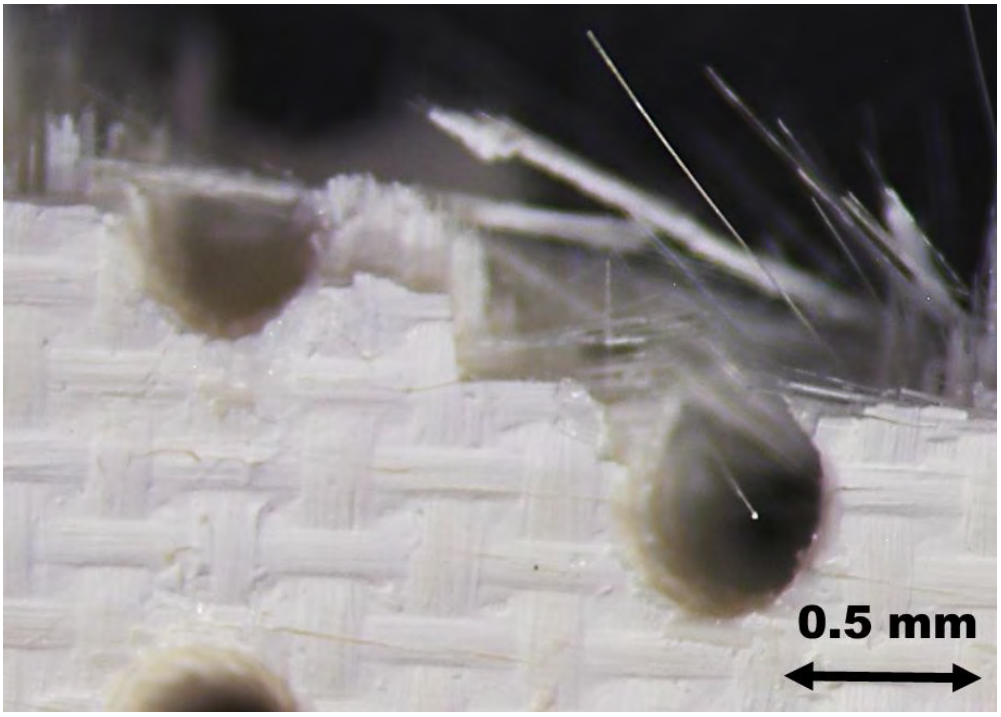


Figure A. 115: Fracture surface obtained for a N720/A specimen with effusion holes in creep at 1200ºC in steam (σ_{cr} = 90 MPa, t_f = 0.572 h).

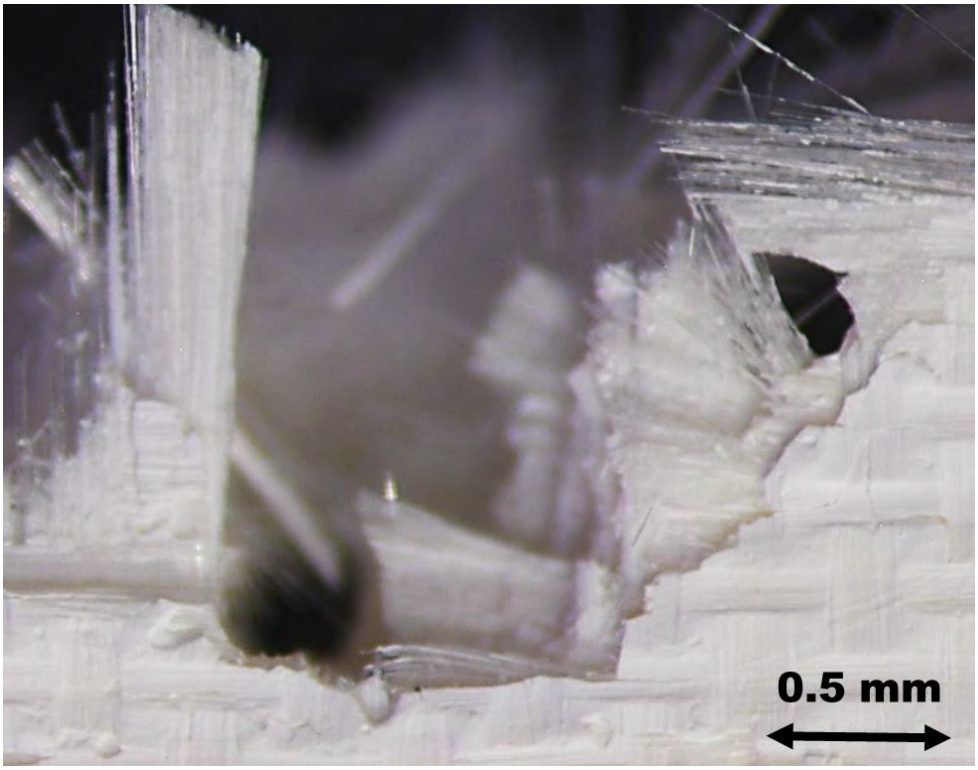


Figure A. 116: Fracture surface obtained for a N720/A specimen with effusion holes in creep at 1200ºC in steam (σ_{cr} = 90 MPa, t_f = 0.572 h).

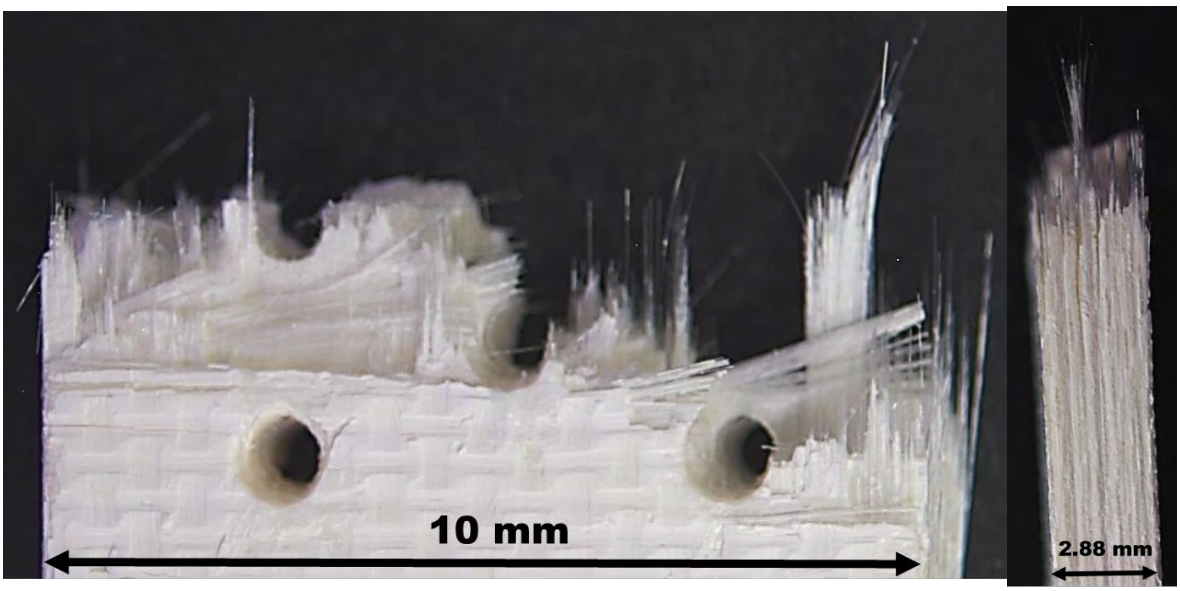


Figure A. 117: Fracture surface obtained for a N720/A specimen with effusion holes in creep at 1200°C in steam (σ_{cr} = 90 MPa, t_f = 0.572 h).

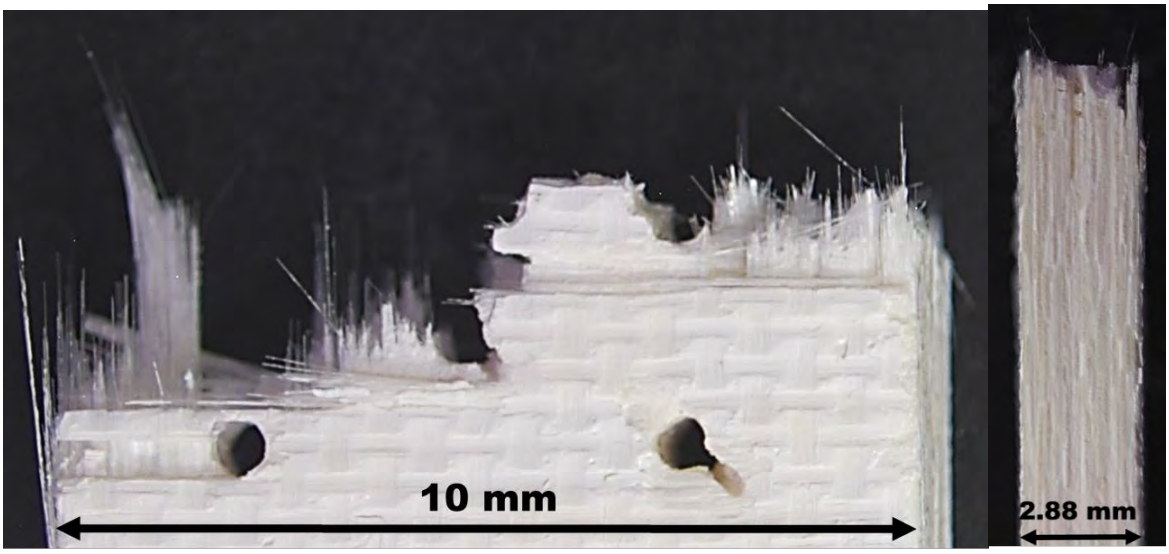


Figure A. 118: Fracture surface obtained for a N720/A specimen with effusion holes in creep at 1200°C in steam (σ_{cr} = 90 MPa, t_f = 0.572 h).

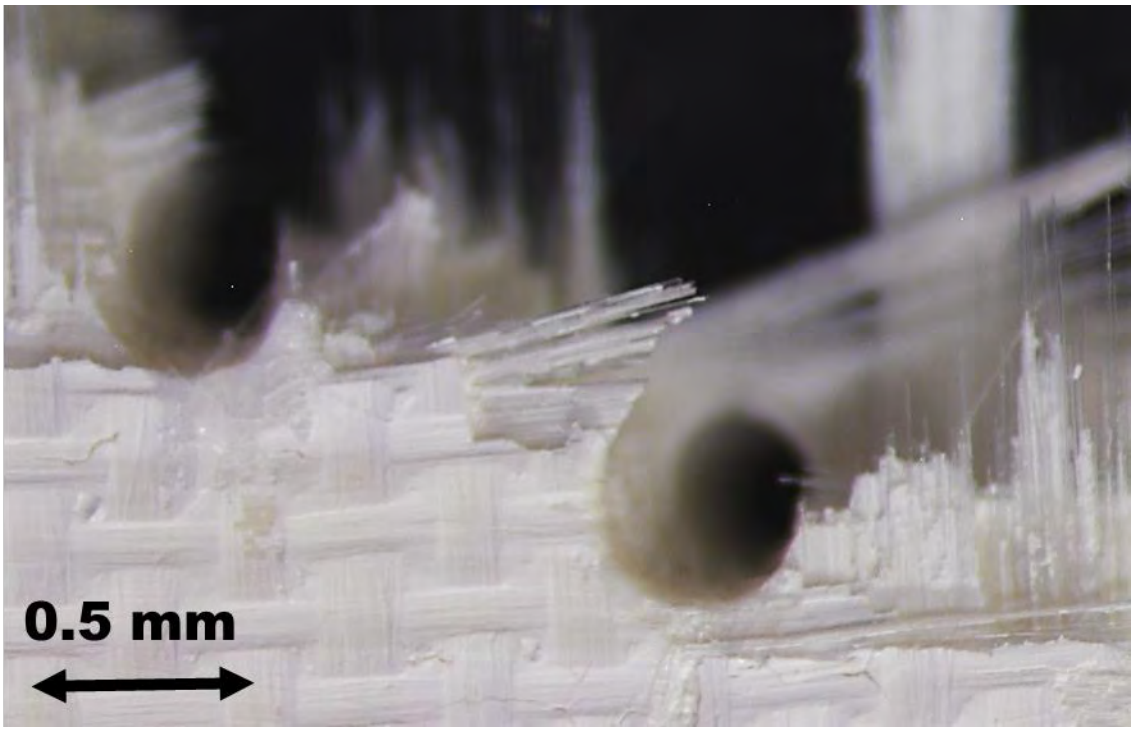


Figure A. 119: Fracture surface obtained for a N720/A specimen with effusion holes in creep at 1200ºC in steam (σ_{cr} = 90 MPa, t_f = 0.572 h).

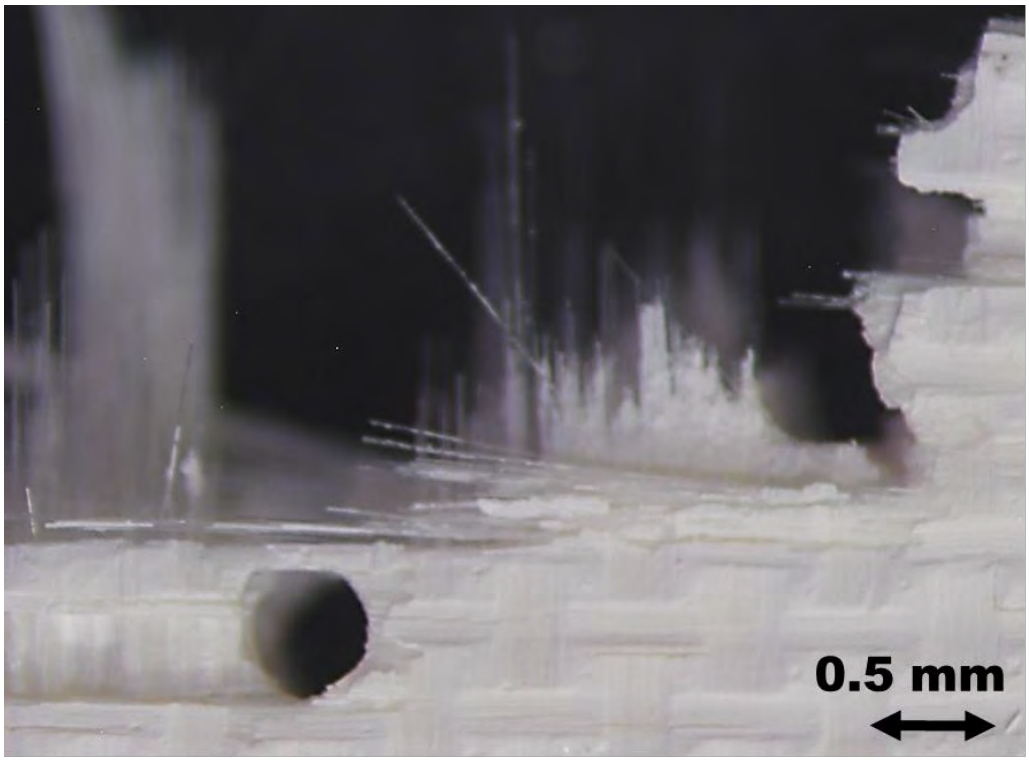


Figure A. 120: Fracture surface obtained for a N720/A specimen with effusion holes in creep at 1200ºC in steam (σ_{cr} = 90 MPa, t_f = 0.572 h).

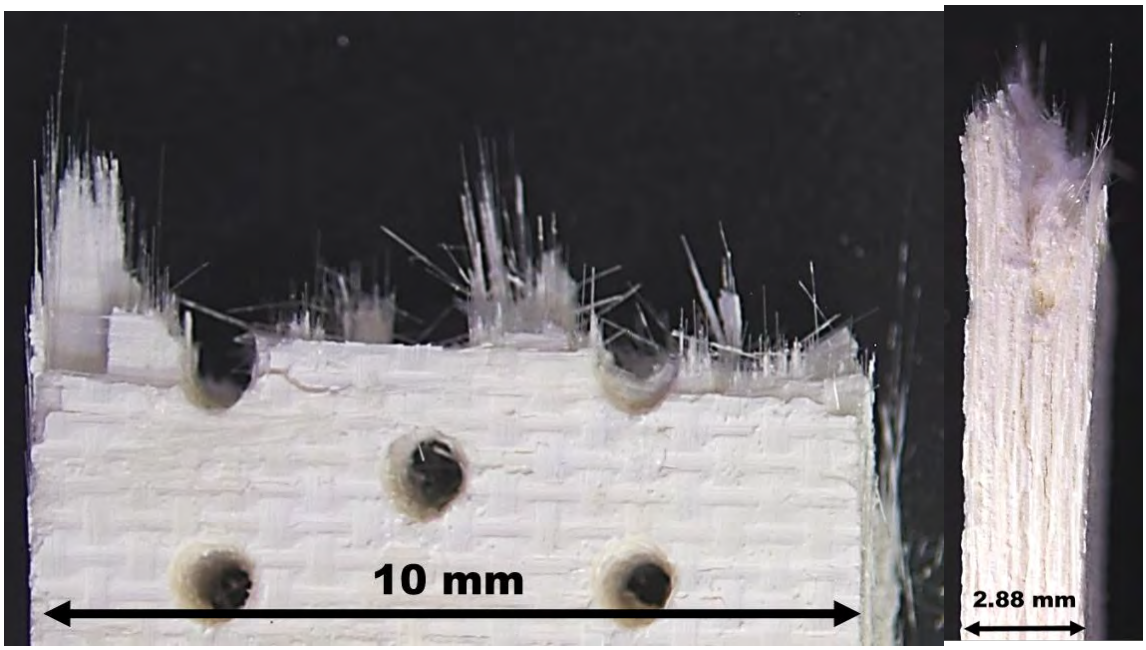


Figure A. 121: Fracture surface obtained for a N720/A specimen with effusion holes in creep at 1200ºC in steam (σ_{cr} = 100 MPa, t_f = 0.141 h).

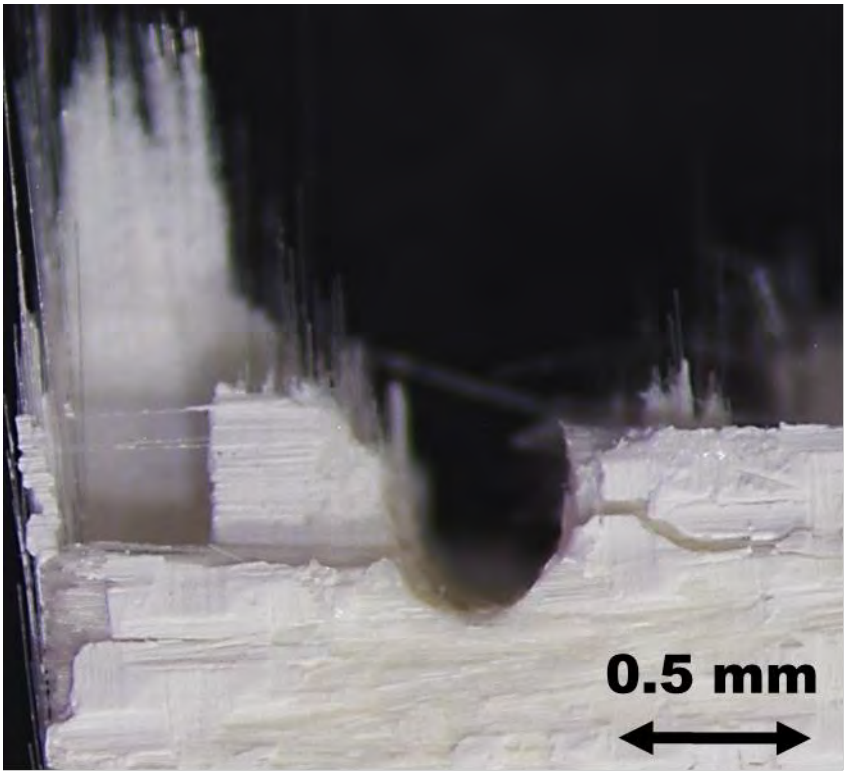


Figure A. 122: Fracture surface obtained for a N720/A specimen with effusion holes in creep at 1200ºC in steam (σ_{cr} = 100 MPa, t_f = 0.141 h).

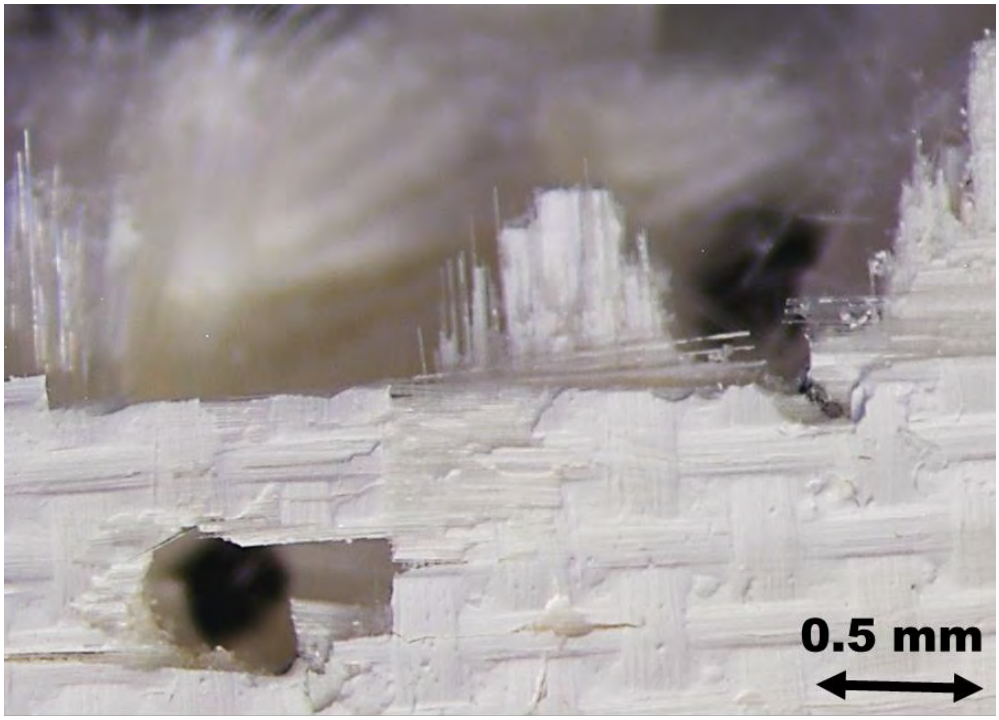


Figure A. 123: Fracture surface obtained for a N720/A specimen with effusion holes in creep at 1200ºC in steam (σ_{cr} = 100 MPa, t_f = 0.141 h).

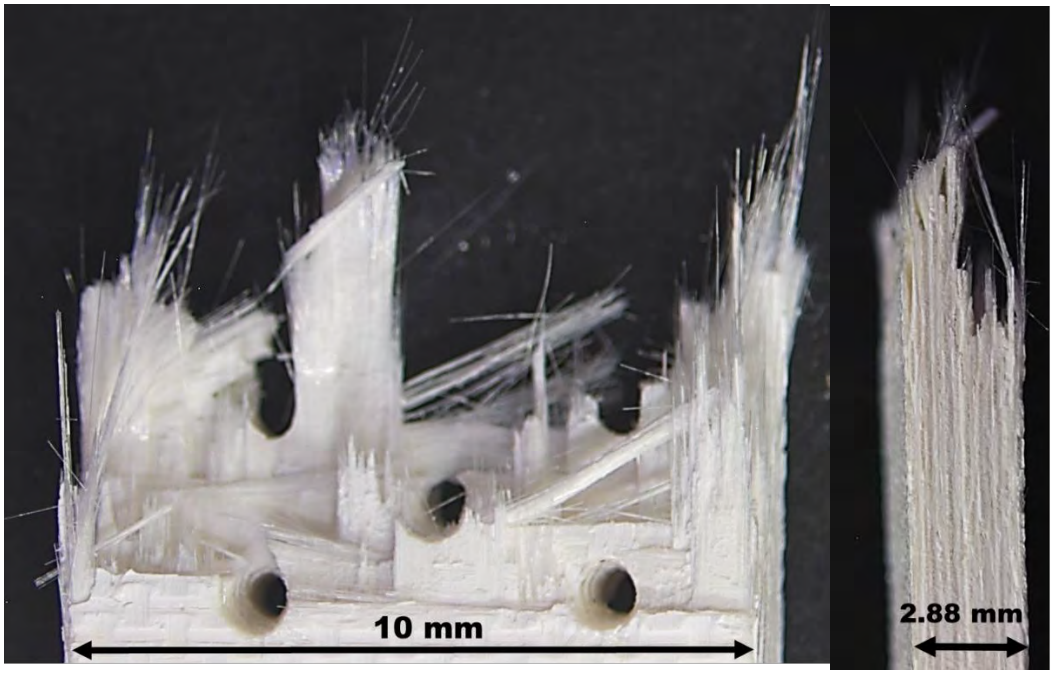


Figure A. 124: Fracture surface obtained for a N720/A specimen with effusion holes in creep at 1200ºC in steam (σ_{cr} = 100 MPa, t_f = 0.141 h).

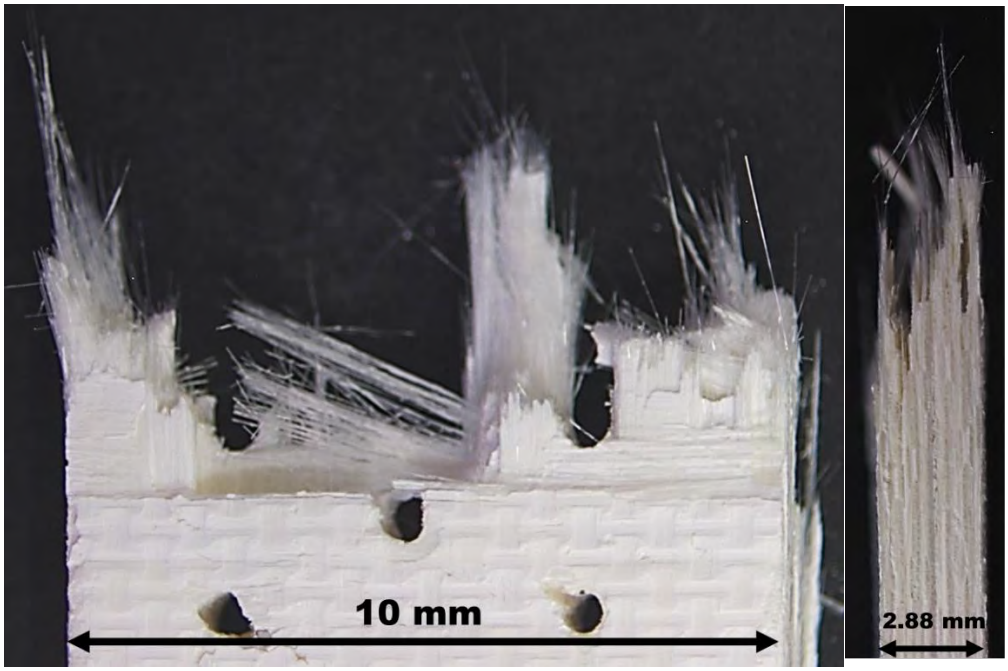


Figure A. 125: Fracture surface obtained for a N720/A specimen with effusion holes in creep at 1200ºC in steam (σ_{cr} = 100 MPa, t_f = 0.141 h).

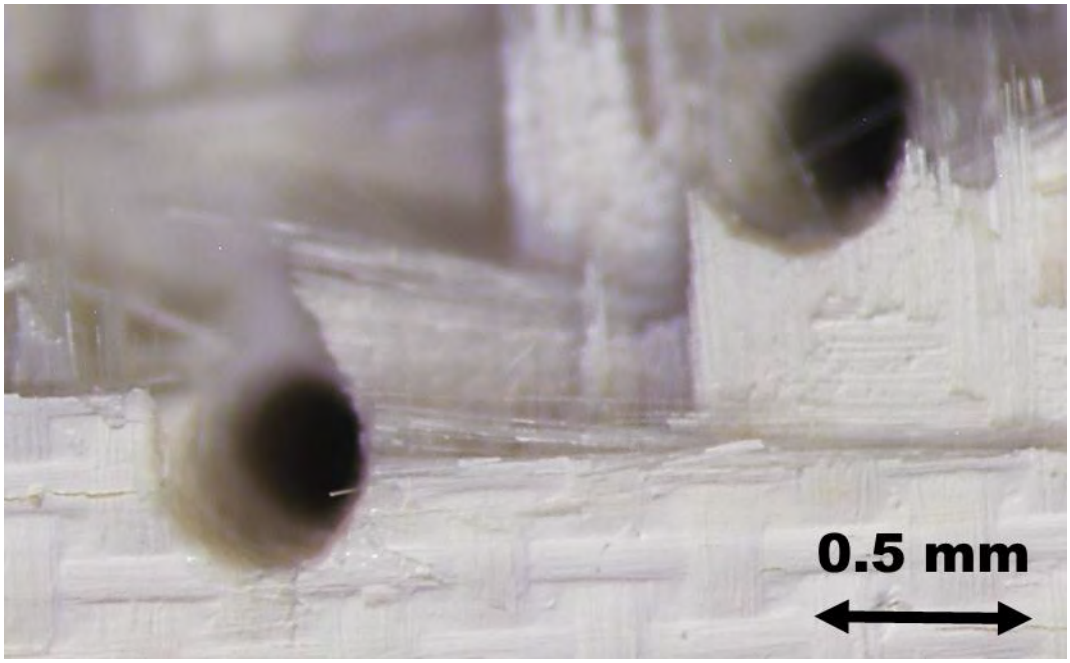


Figure A. 126: Fracture surface obtained for a N720/A specimen with effusion holes in creep at 1200ºC in steam (σ_{cr} = 100 MPa, t_f = 0.141 h).

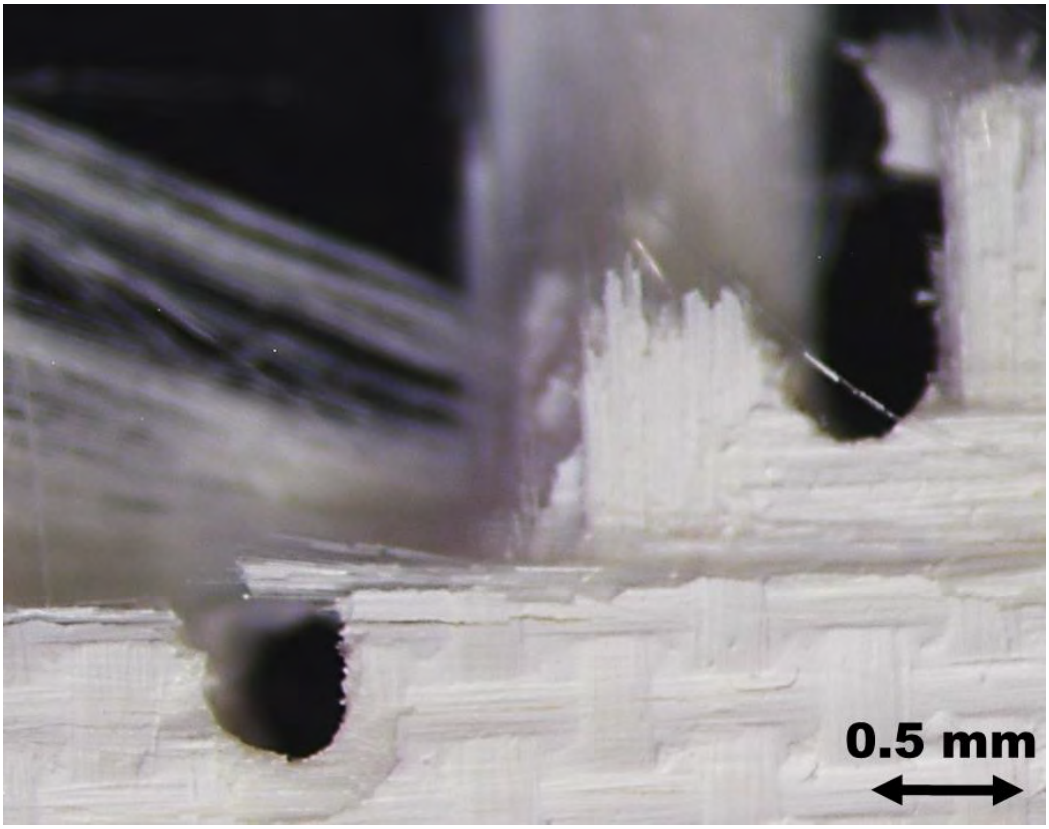


Figure A. 127: Fracture surface obtained for a N720/A specimen with effusion holes in creep at 1200°C in steam (σ_{cr} = 100 MPa, t_f = 0.141 h).

Appendix B. Scanning Electron Microscope Images

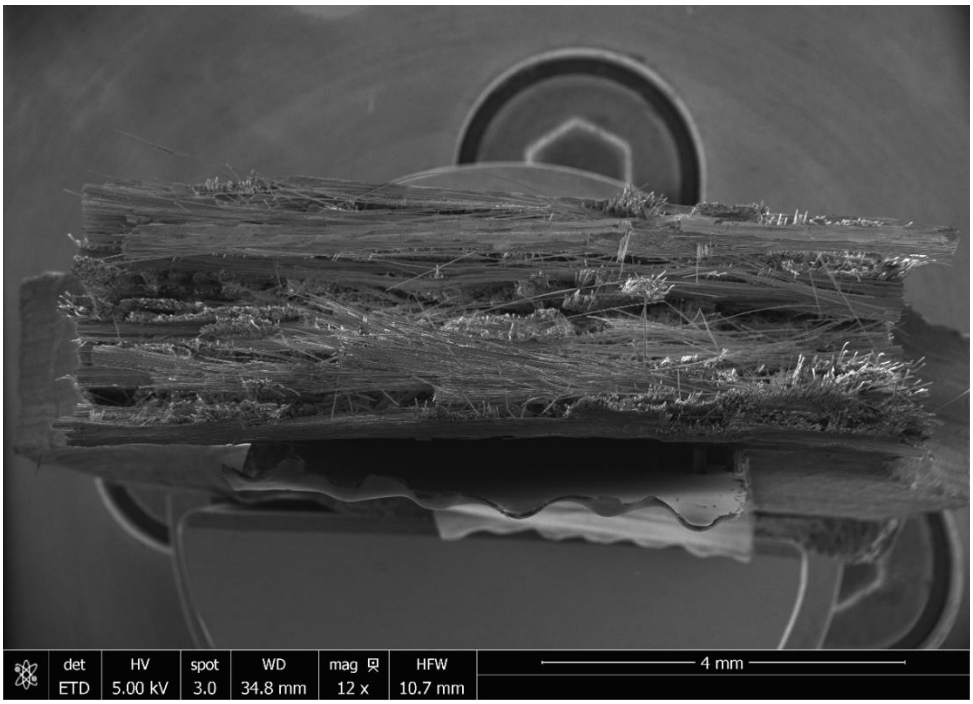


Figure B. 1: Fracture surface obtained for an unnotched N720/A specimen in tension to failure at 1200ºC in air.

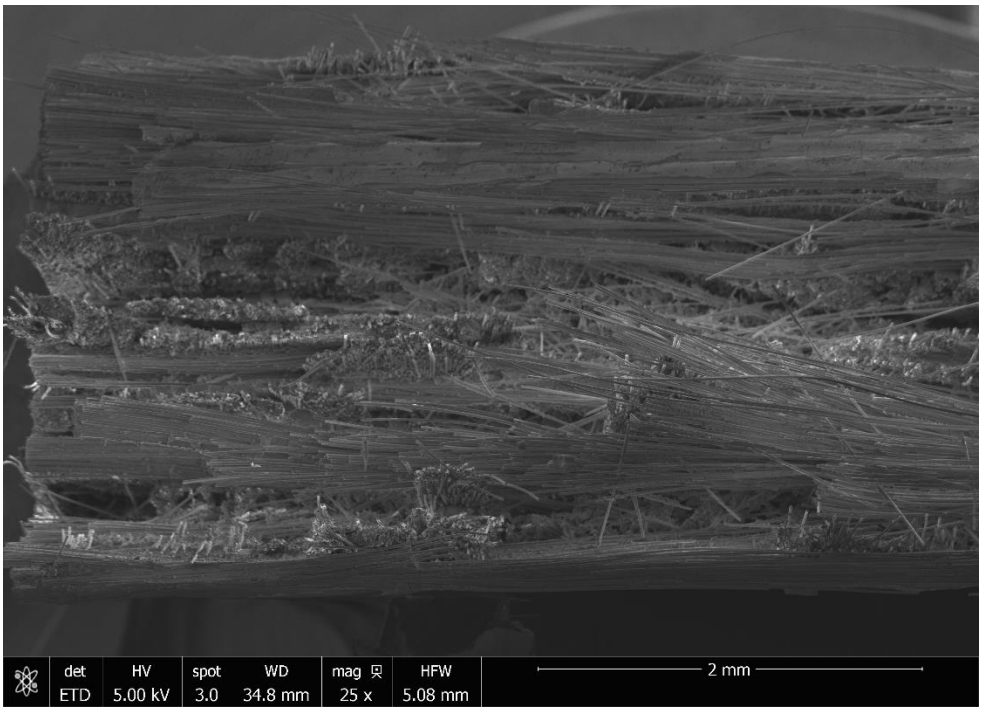


Figure B. 2: Fracture surface obtained for an unnotched N720/A specimen in tension to failure at 1200ºC in air.

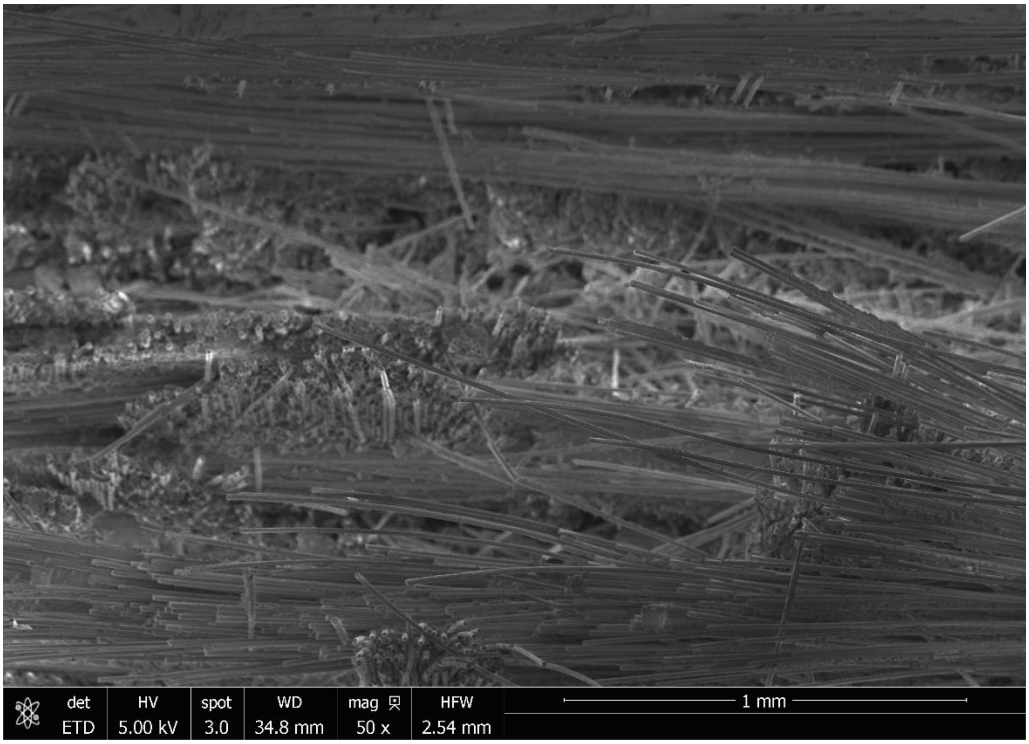


Figure B. 3: Fracture surface obtained for an unnotched N720/A specimen in tension to failure at 1200ºC in air.

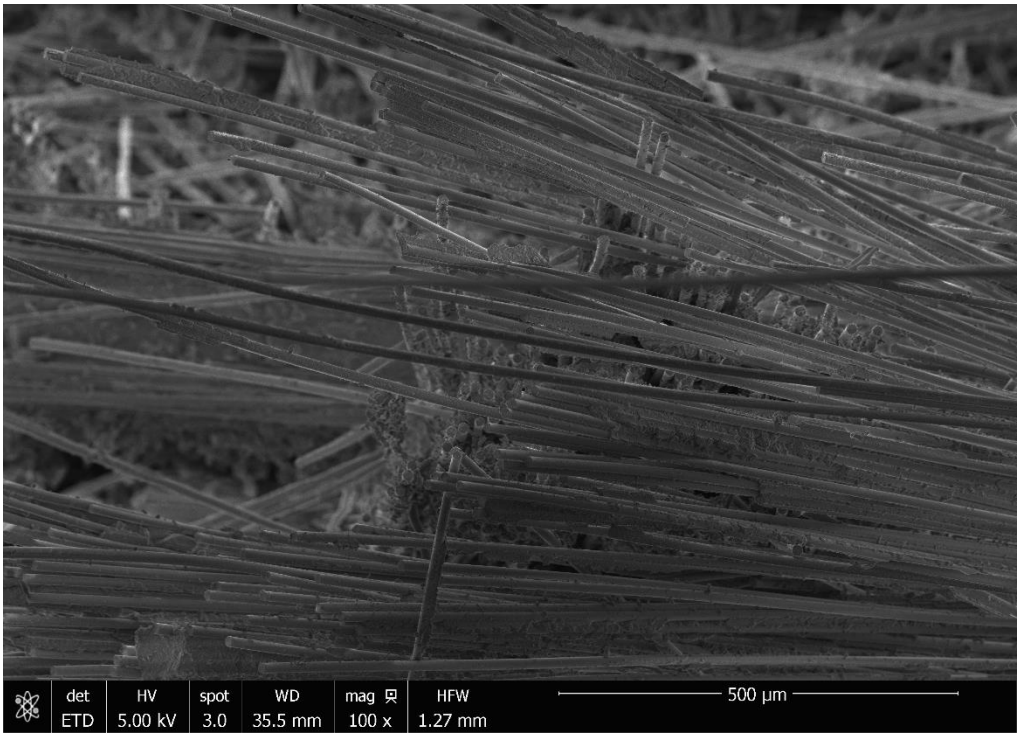


Figure B. 4: Fracture surface obtained for an unnotched N720/A specimen in tension to failure at 1200ºC in air.

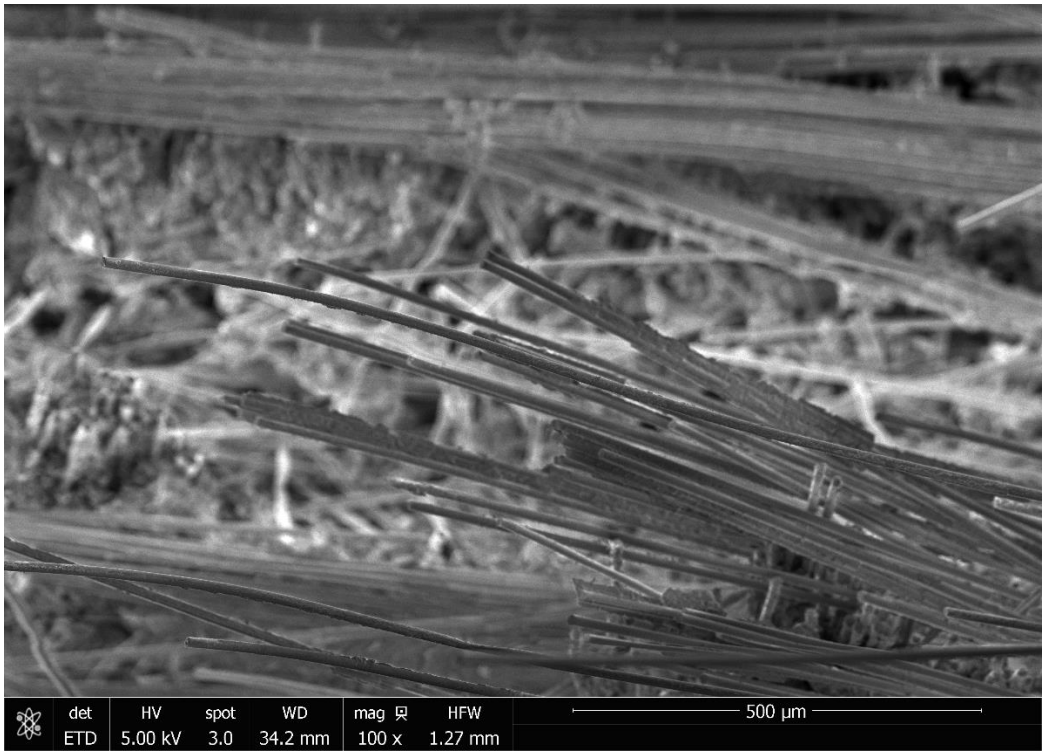


Figure B. 5: Fracture surface obtained for an unnotched N720/A specimen in tension to failure at 1200ºC in air.

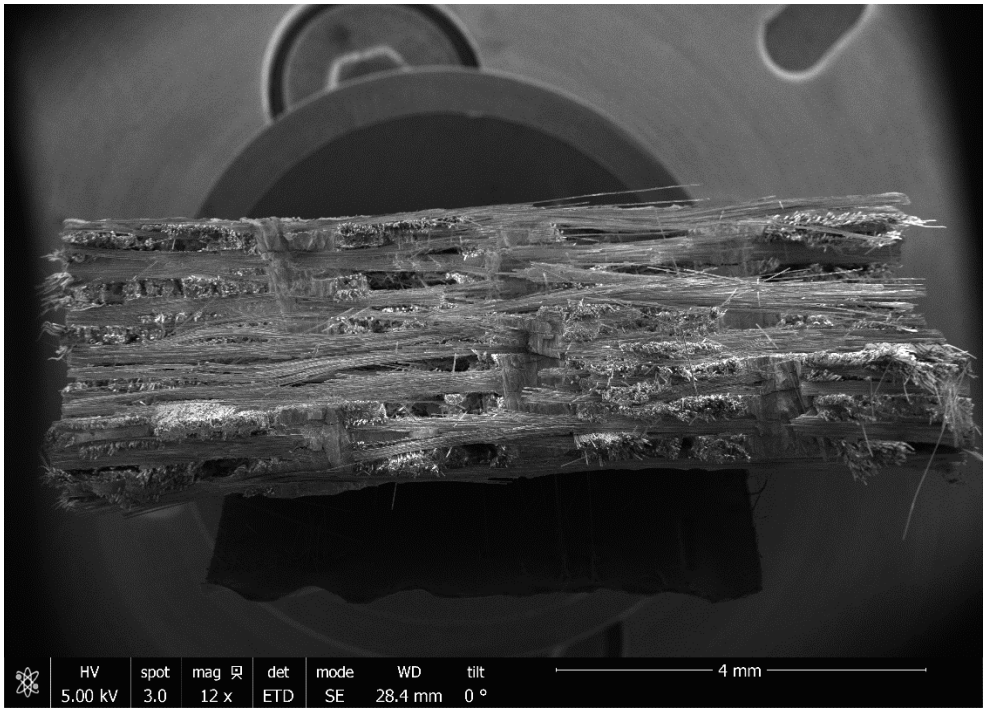


Figure B. 6: Fracture surface obtained for a N720/A specimen with effusion holes in tension to failure at 1200ºC in air.

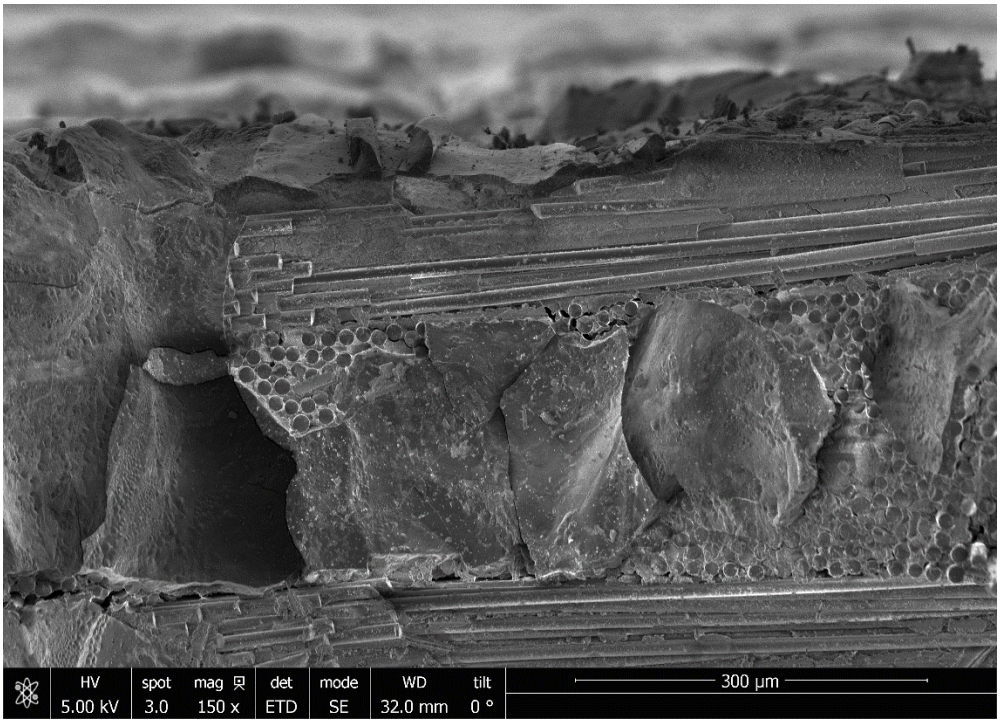


Figure B. 7: Fracture surface obtained for a N720/A specimen with effusion holes in tension to failure at 1200ºC in air.

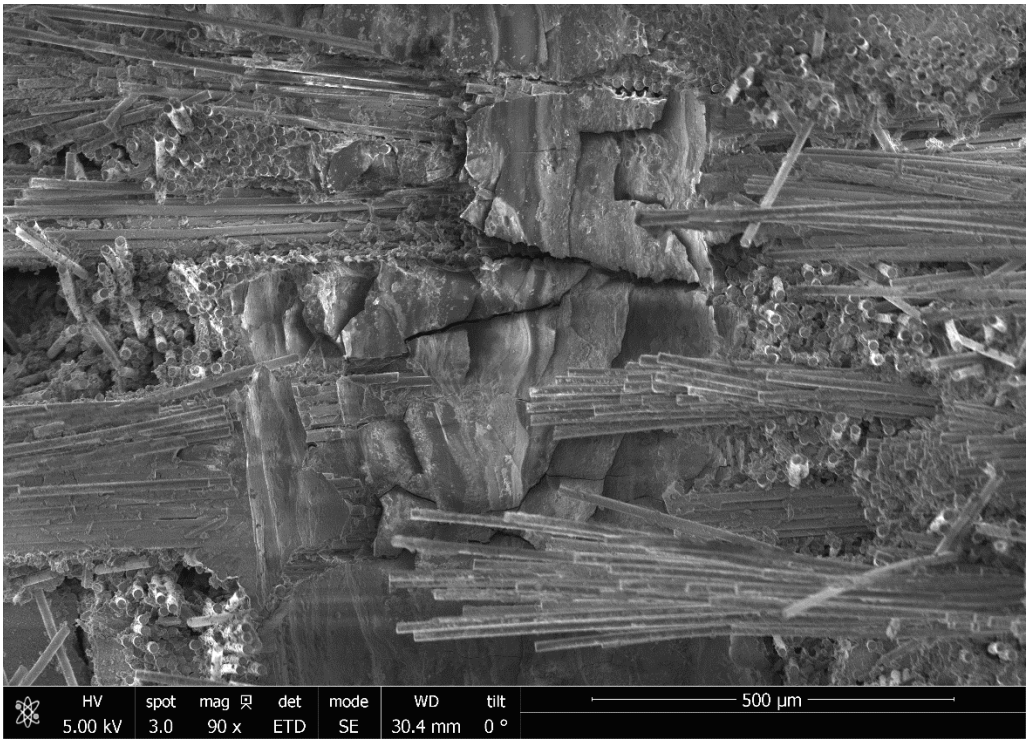


Figure B. 8: Fracture surface obtained for a N720/A specimen with effusion holes in tension to failure at 1200ºC in air.

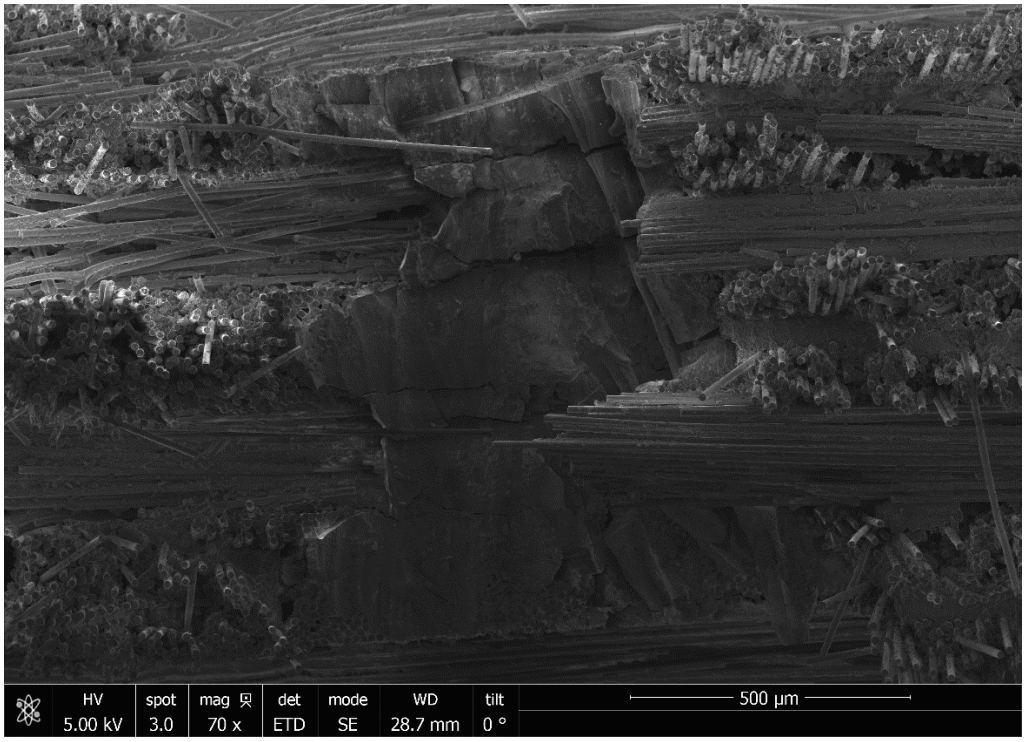


Figure B. 9: Fracture surface obtained for a N720/A specimen with effusion holes in tension to failure at 1200ºC in air.

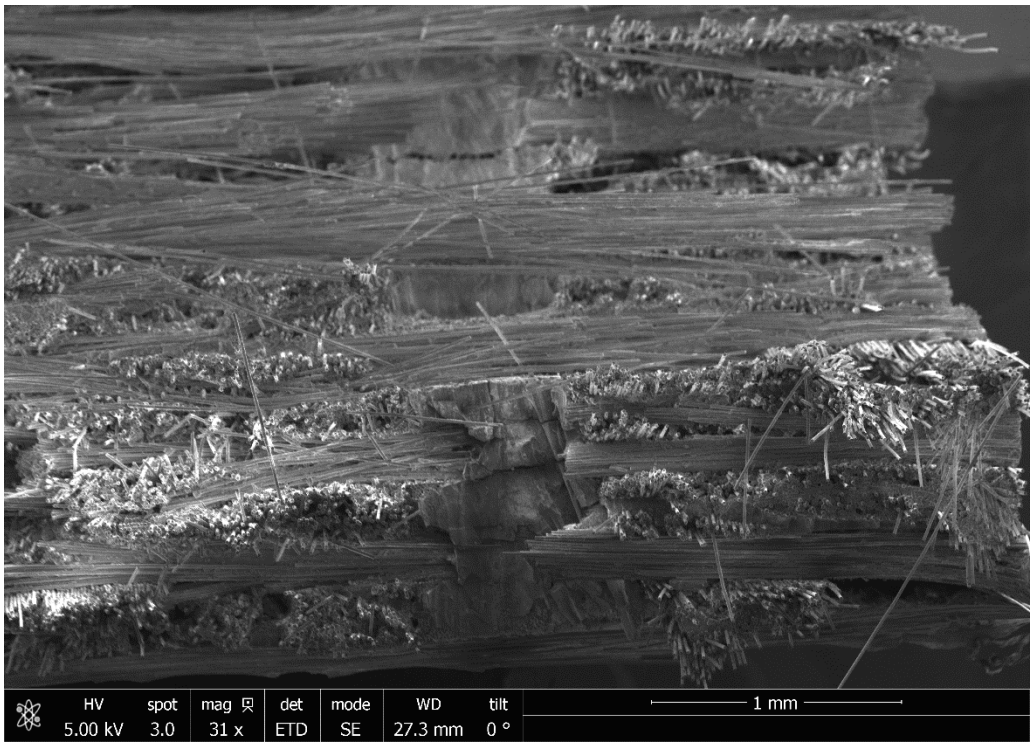


Figure B. 10: Fracture surface obtained for a N720/A specimen with effusion holes in tension to failure at 1200ºC in air.

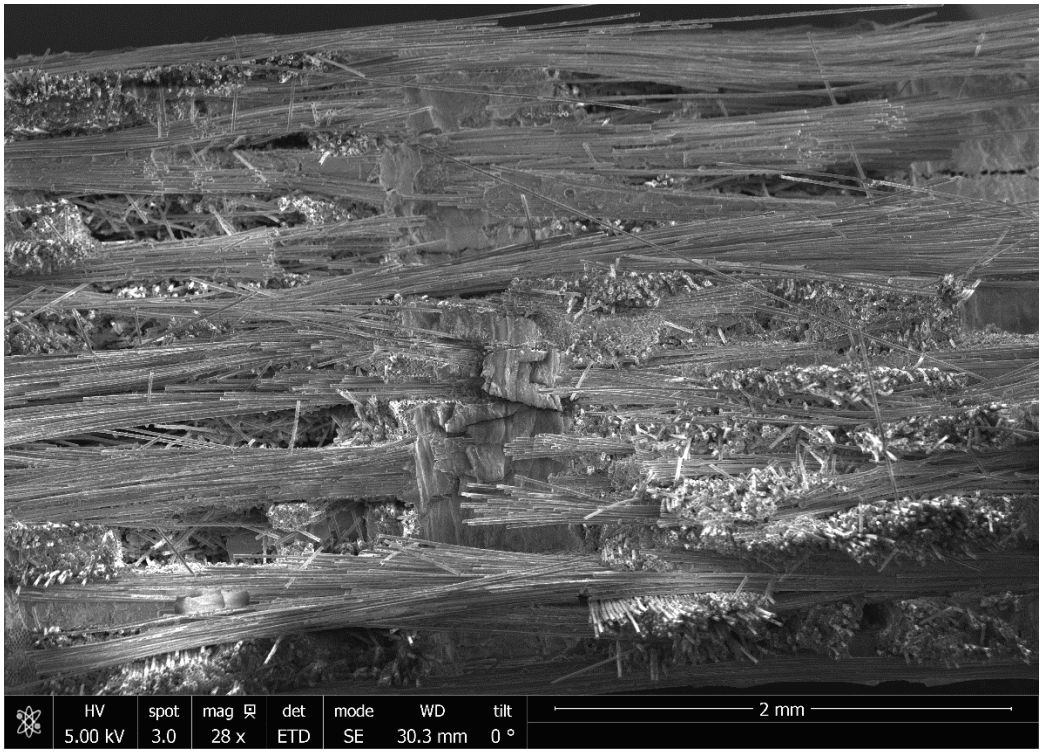


Figure B. 11: Fracture surface obtained for a N720/A specimen with effusion holes in tension to failure at 1200ºC in air.

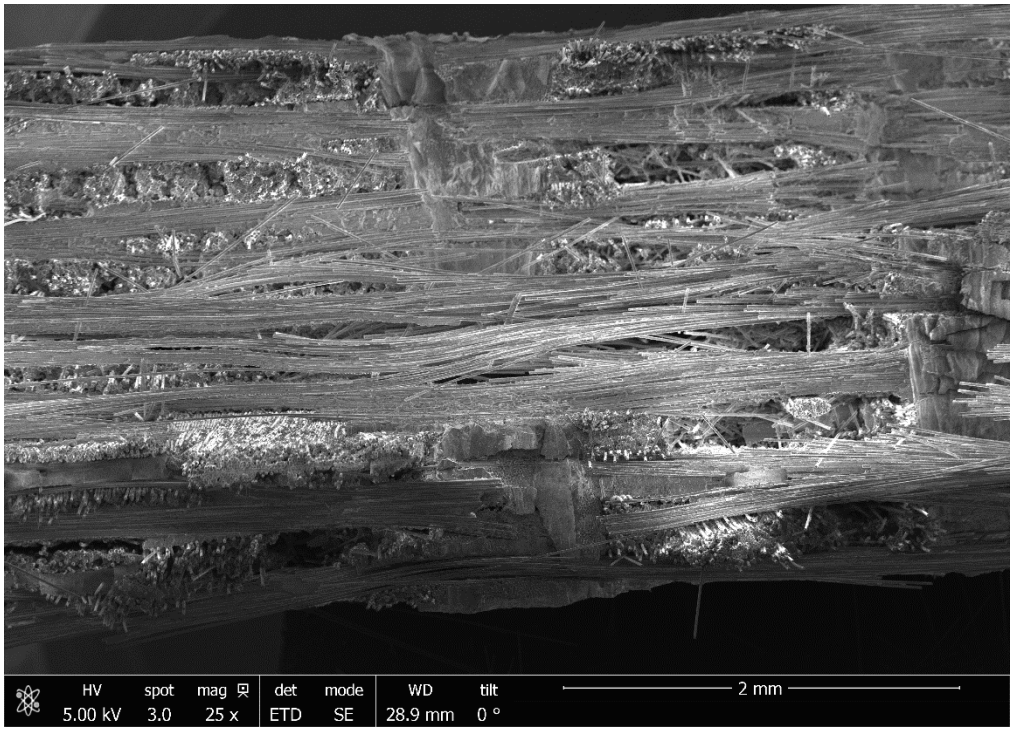


Figure B. 12: Fracture surface obtained for a N720/A specimen with effusion holes in tension to failure at 1200ºC in air.

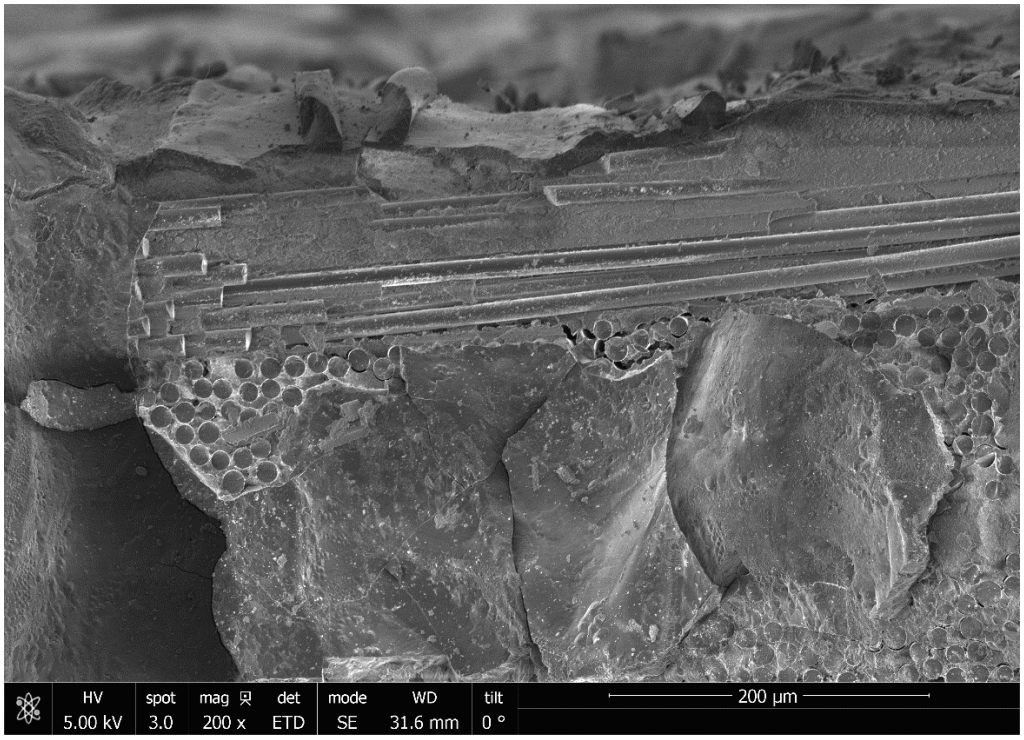


Figure B. 13: Fracture surface obtained for a N720/A specimen with effusion holes in tension to failure at 1200ºC in air.

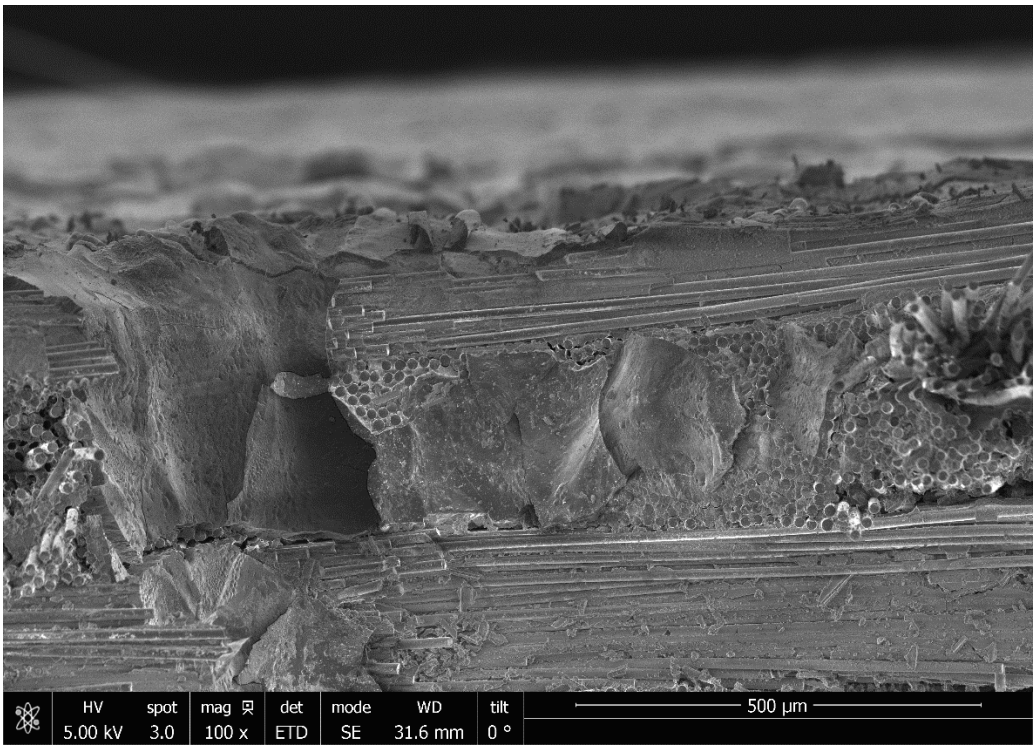


Figure B. 14: Fracture surface obtained for a N720/A specimen with effusion holes in tension to failure at 1200ºC in air.

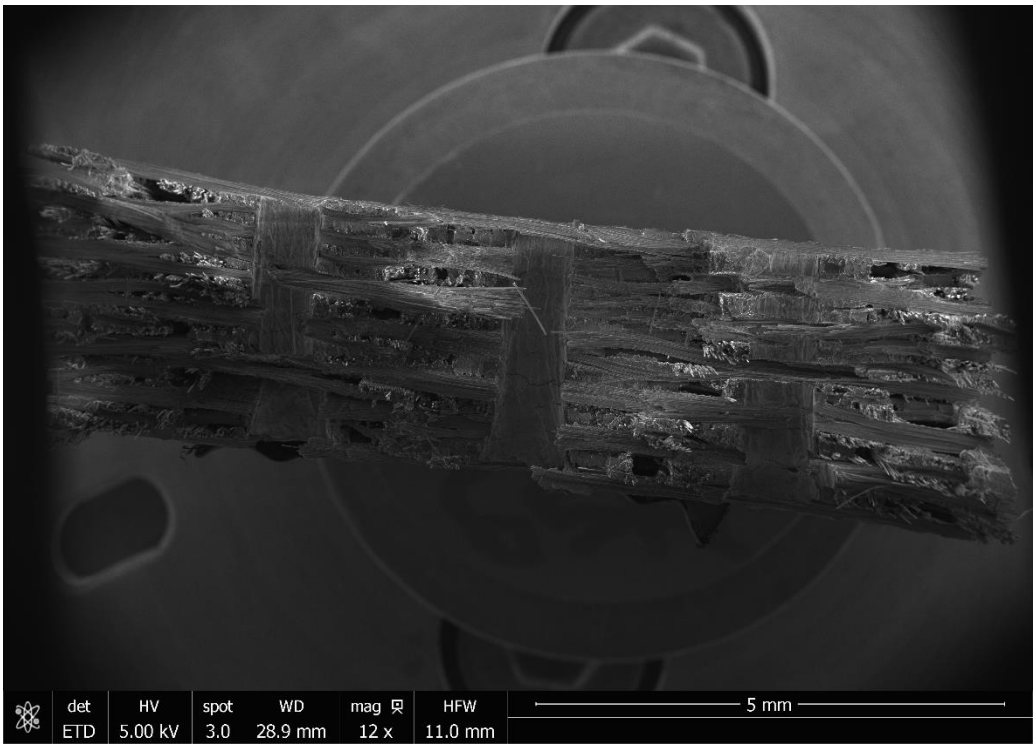


Figure B. 15: Fracture surface obtained for a N720/A specimen with effusion holes in creep at 1200ºC in air (σ_{cr} = 65 MPa, t_f = 58.4 h).

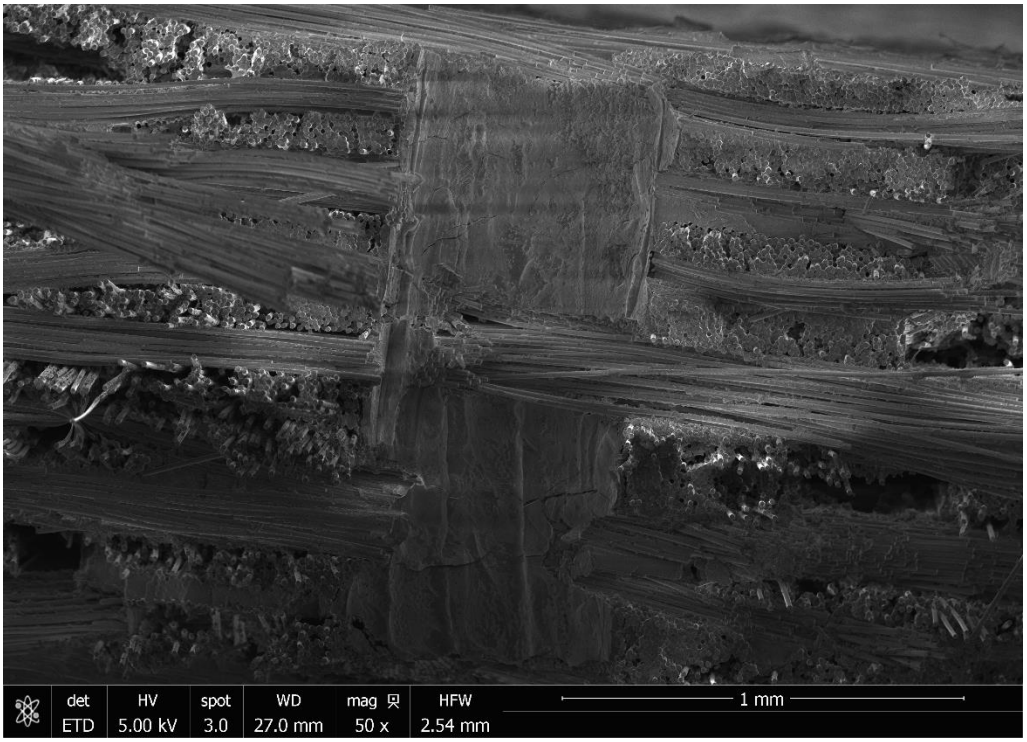


Figure B. 16: Fracture surface obtained for a N720/A specimen with effusion holes in creep at 1200ºC in air (σ_{cr} = 65 MPa, t_f = 58.4 h).

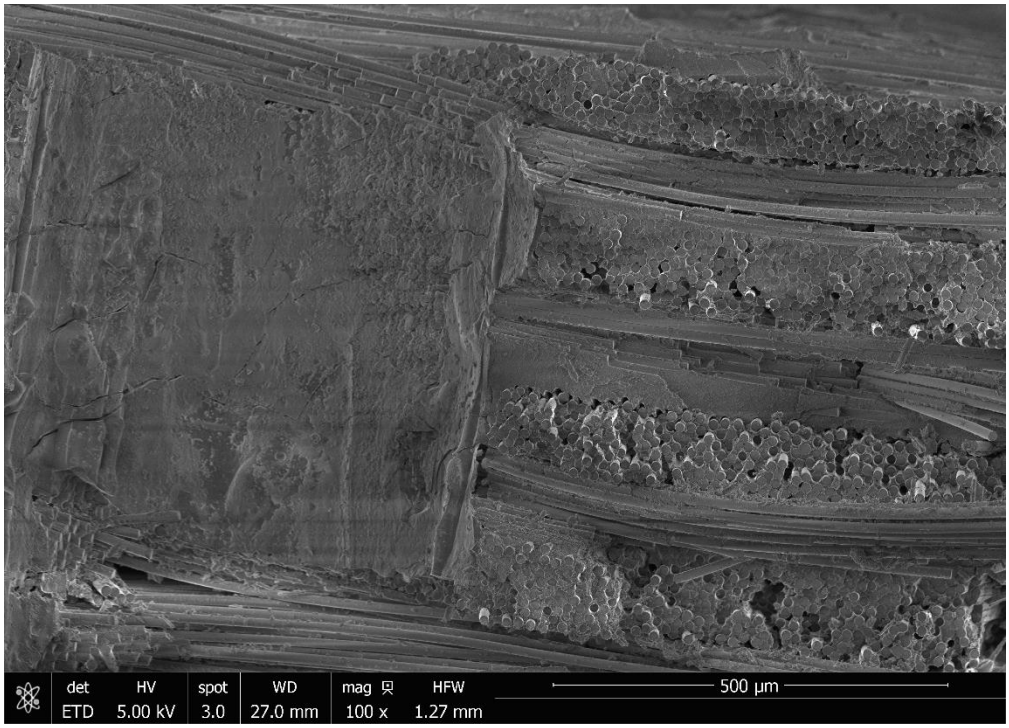


Figure B. 17: Fracture surface obtained for a N720/A specimen with effusion holes in creep at 1200ºC in air (σ_{cr} = 65 MPa, t_f = 58.4 h).

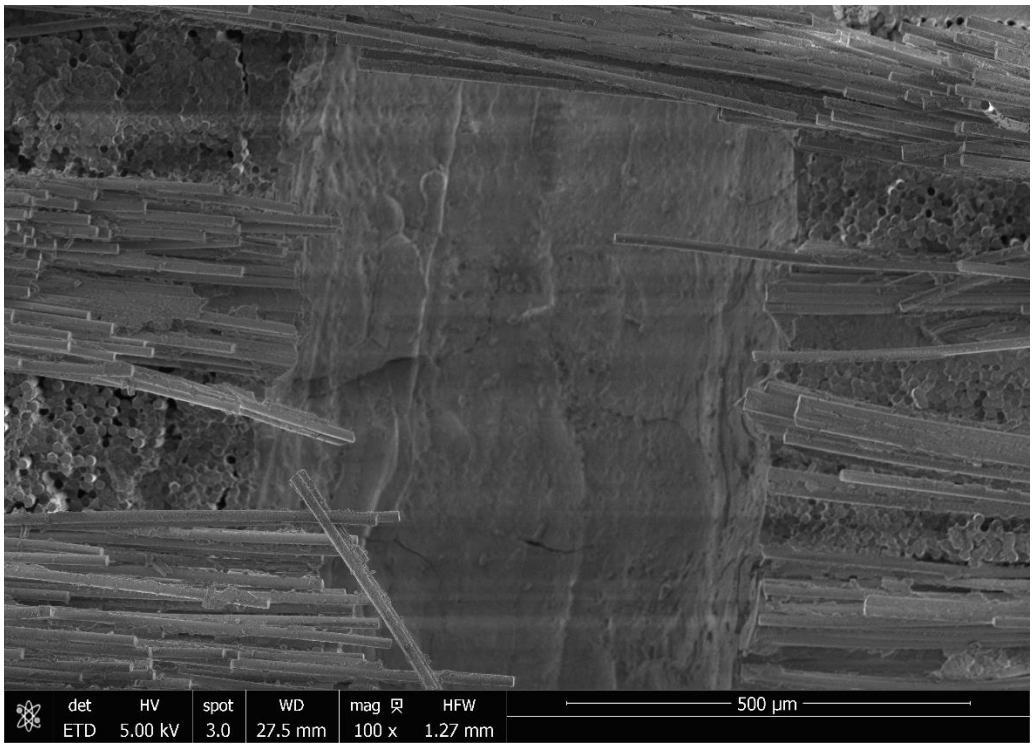


Figure B. 18: Fracture surface obtained for a N720/A specimen with effusion holes in creep at 1200ºC in air (σ_{cr} = 65 MPa, t_f = 58.4 h).

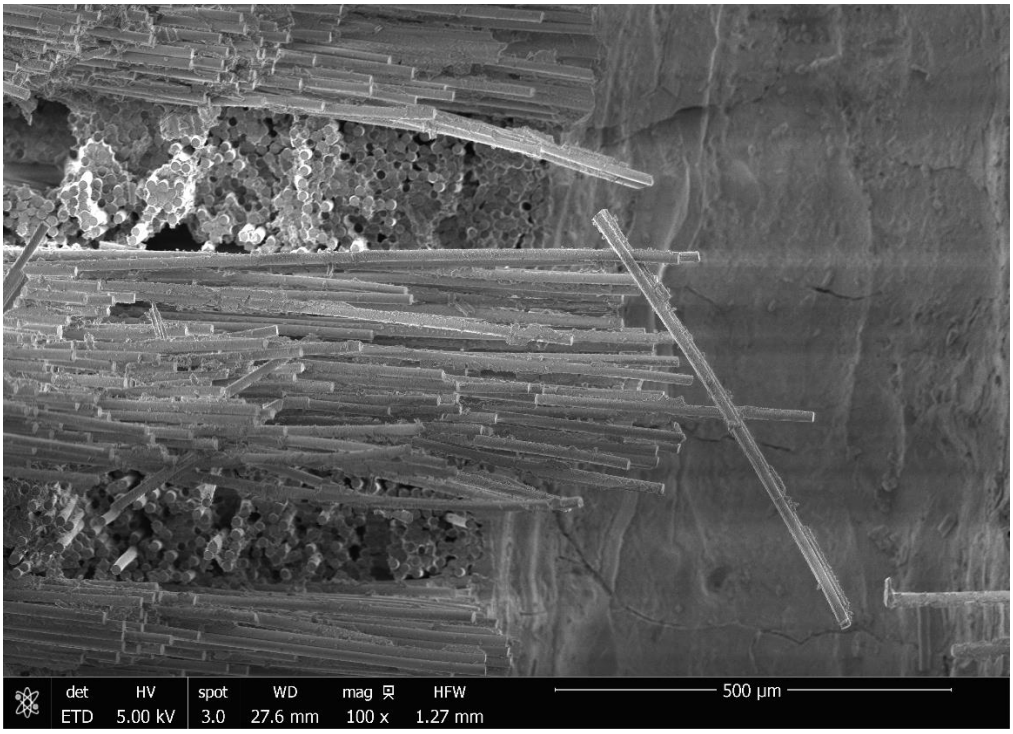


Figure B. 19: Fracture surface obtained for a N720/A specimen with effusion holes in creep at 1200ºC in air (σ_{cr} = 65 MPa, t_f = 58.4 h).

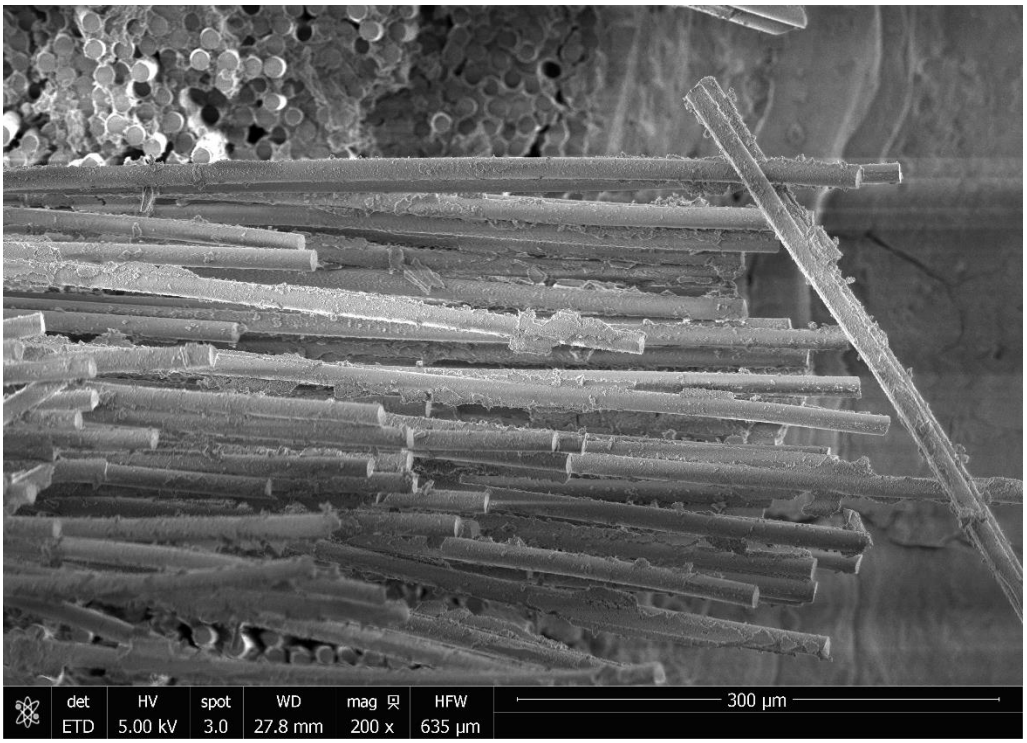


Figure B. 20: Fracture surface obtained for a N720/A specimen with effusion holes in creep at 1200ºC in air (σ_{cr} = 65 MPa, t_f = 58.4 h).

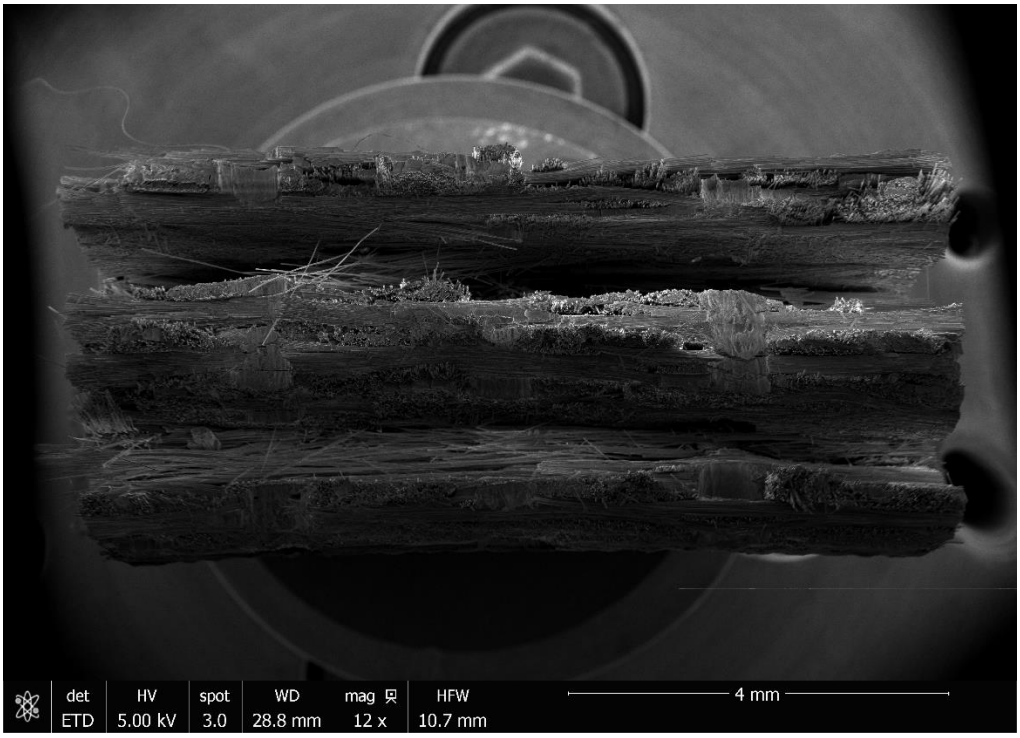


Figure B. 21: Fracture surface obtained for a N720/A specimen with effusion holes in creep at 1200ºC in steam (σ_{cr} = 65 MPa, t_f = 12.44 h).

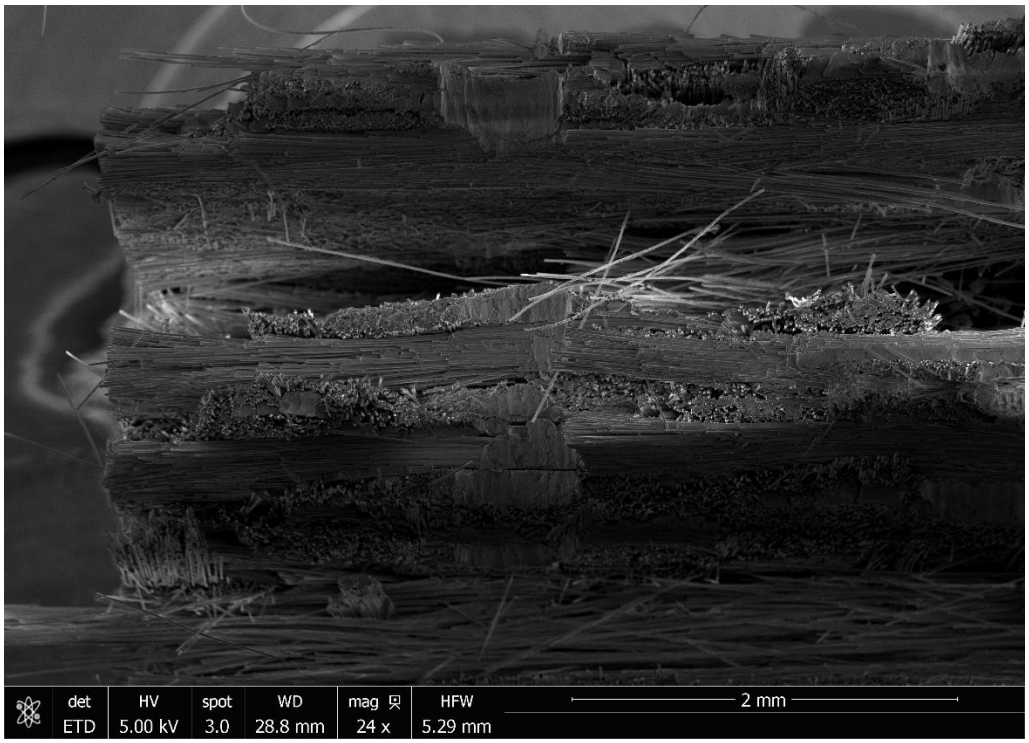


Figure B. 22: Fracture surface obtained for a N720/A specimen with effusion holes in creep at 1200ºC in steam (σ_{cr} = 65 MPa, t_f = 12.44 h).

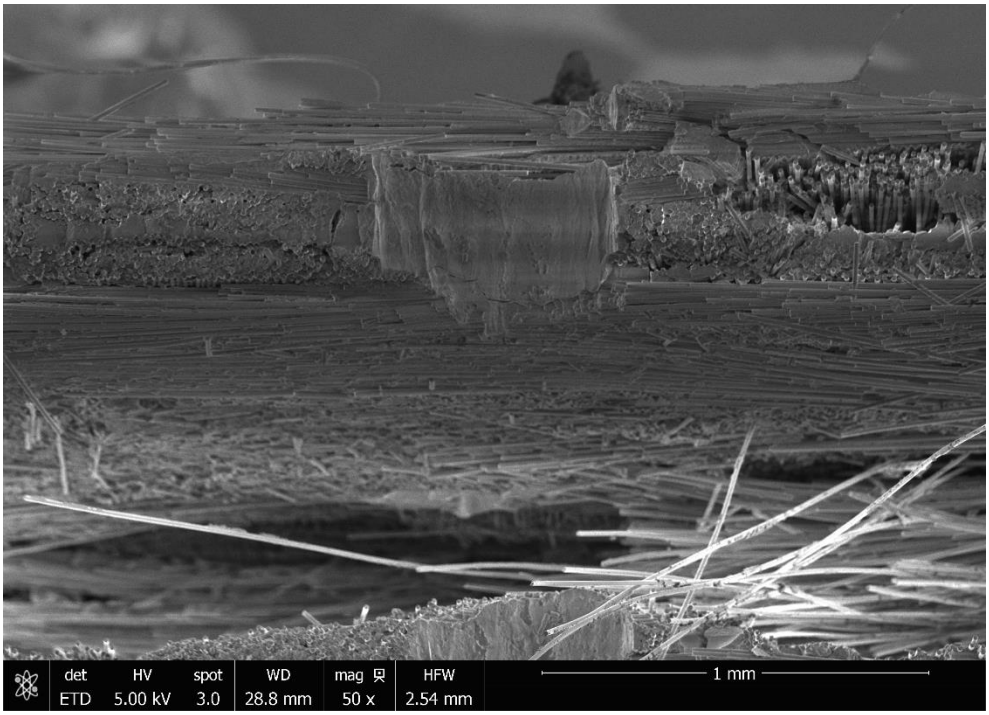


Figure B. 23: Fracture surface obtained for a N720/A specimen with effusion holes in creep at 1200ºC in steam (σ_{cr} = 65 MPa, t_f = 12.44 h).

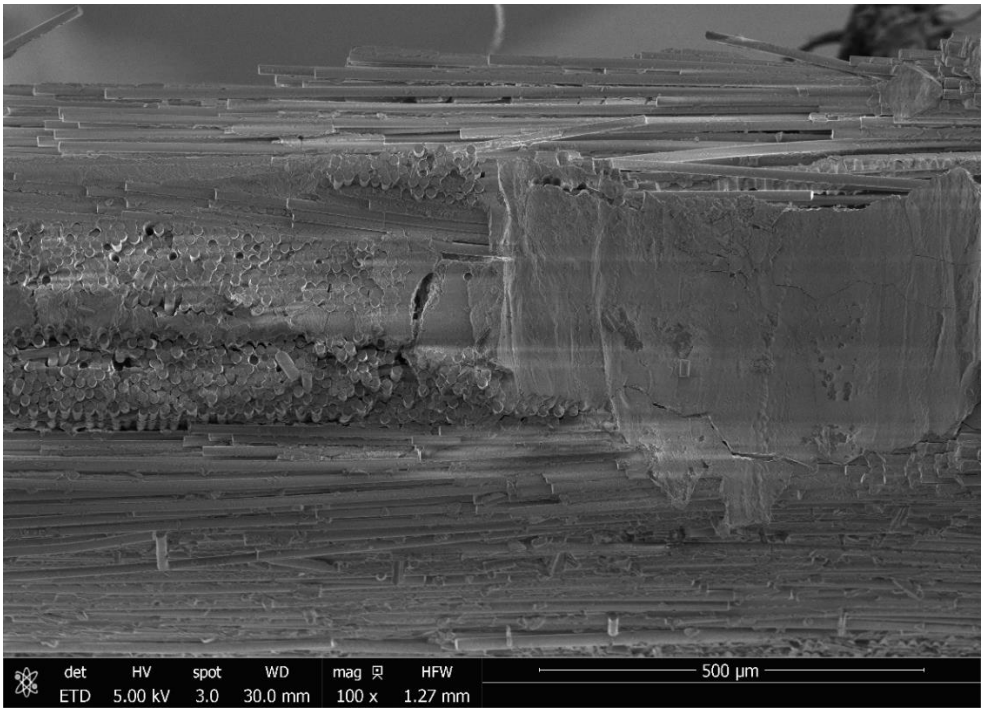


Figure B. 24: Fracture surface obtained for a N720/A specimen with effusion holes in creep at 1200ºC in steam (σ_{cr} = 65 MPa, t_f = 12.44 h).

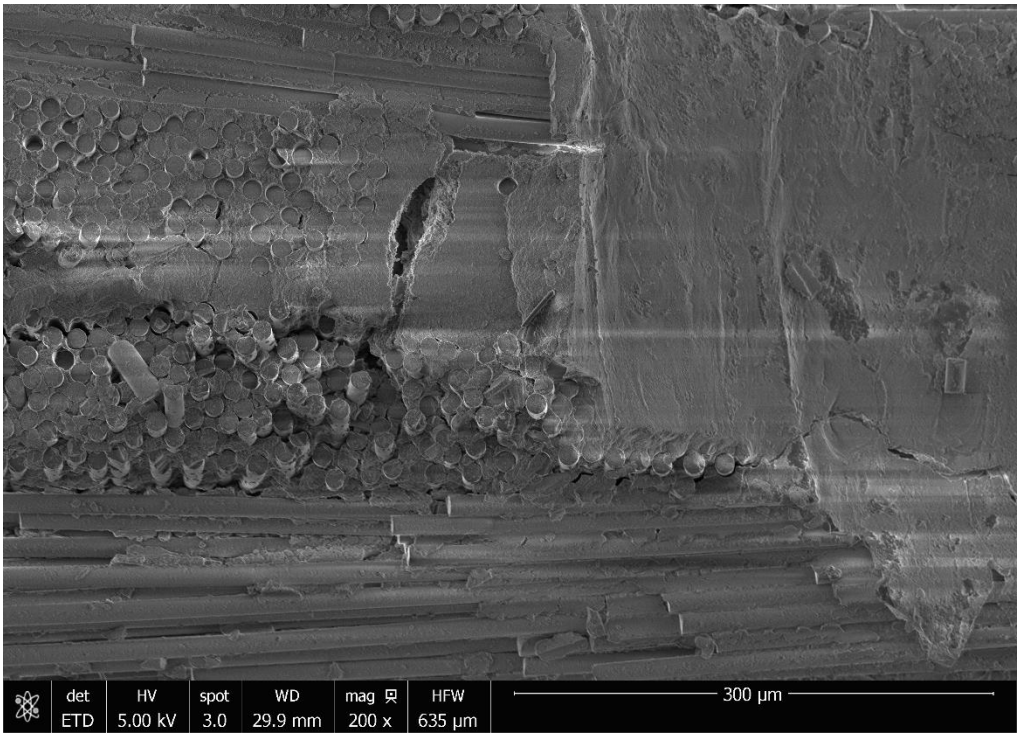


Figure B. 25: Fracture surface obtained for a N720/A specimen with effusion holes in creep at 1200ºC in steam (σ_{cr} = 65 MPa, t_f = 12.44 h).

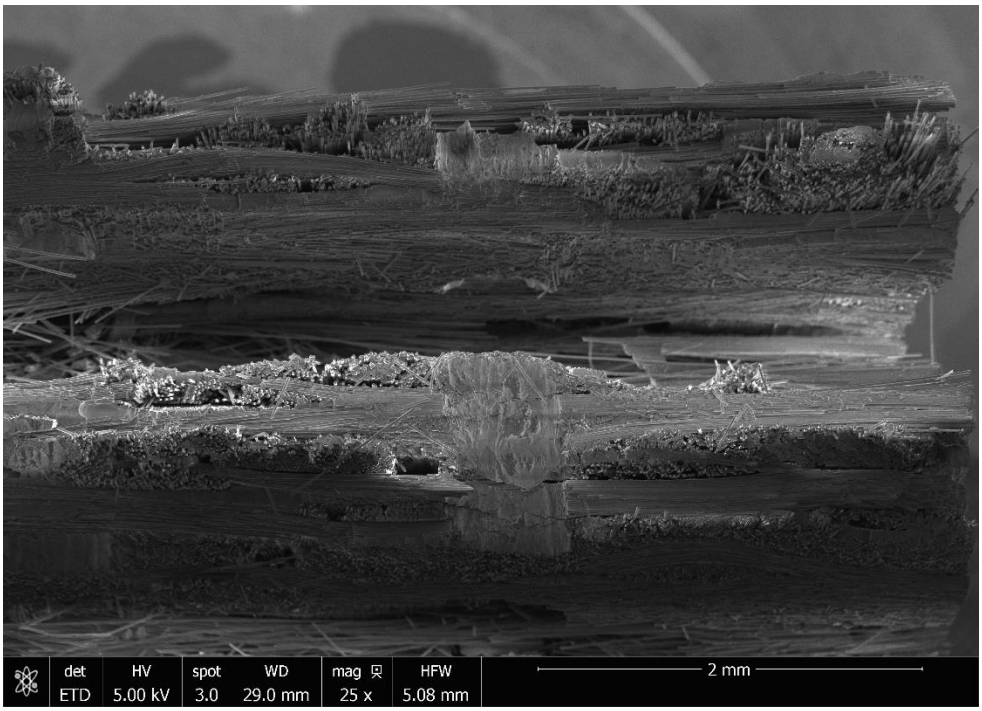


Figure B. 26: Fracture surface obtained for a N720/A specimen with effusion holes in creep at 1200ºC in steam (σ_{cr} = 65 MPa, t_f = 12.44 h).

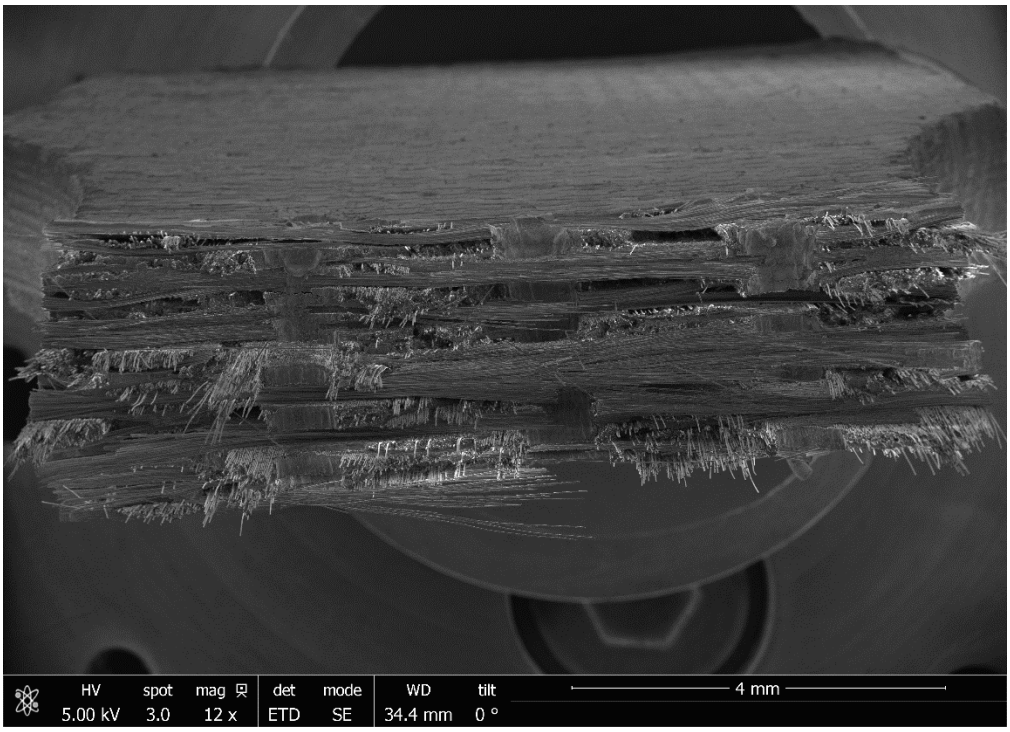


Figure B. 27: Fracture surface obtained for a N720/A specimen with effusion holes in tension to failure following 100 h of creep at 40 MPa at 1200ºC in air.

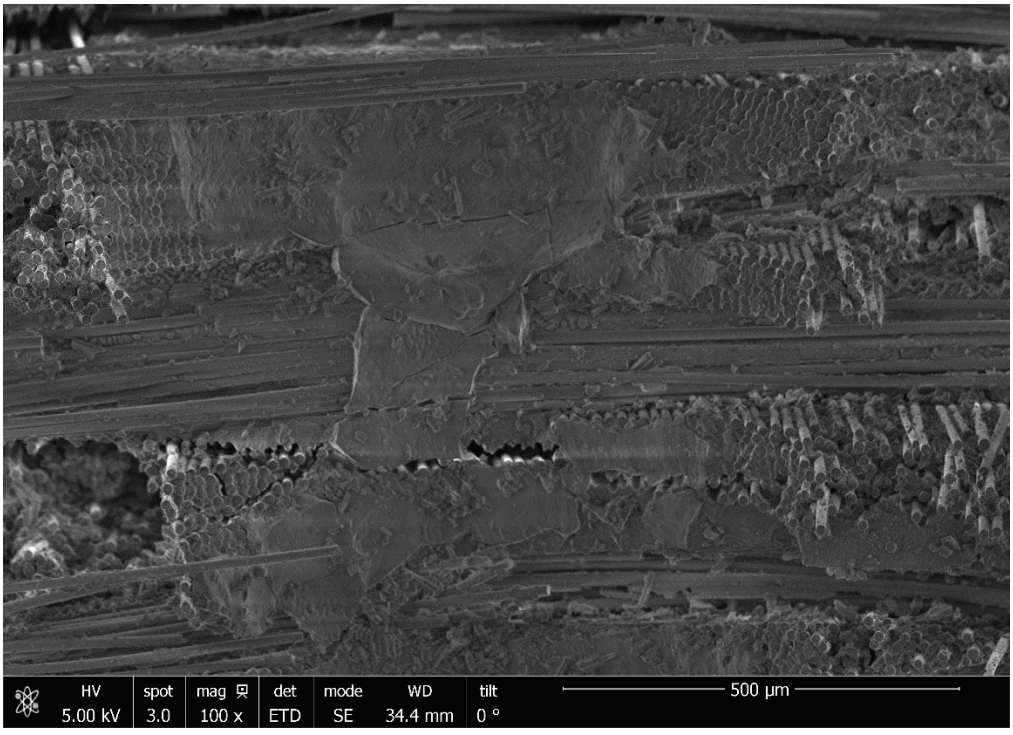


Figure B. 28: Fracture surface obtained for a N720/A specimen with effusion holes in tension to failure following 100 h of creep at 40 MPa at 1200ºC in air.

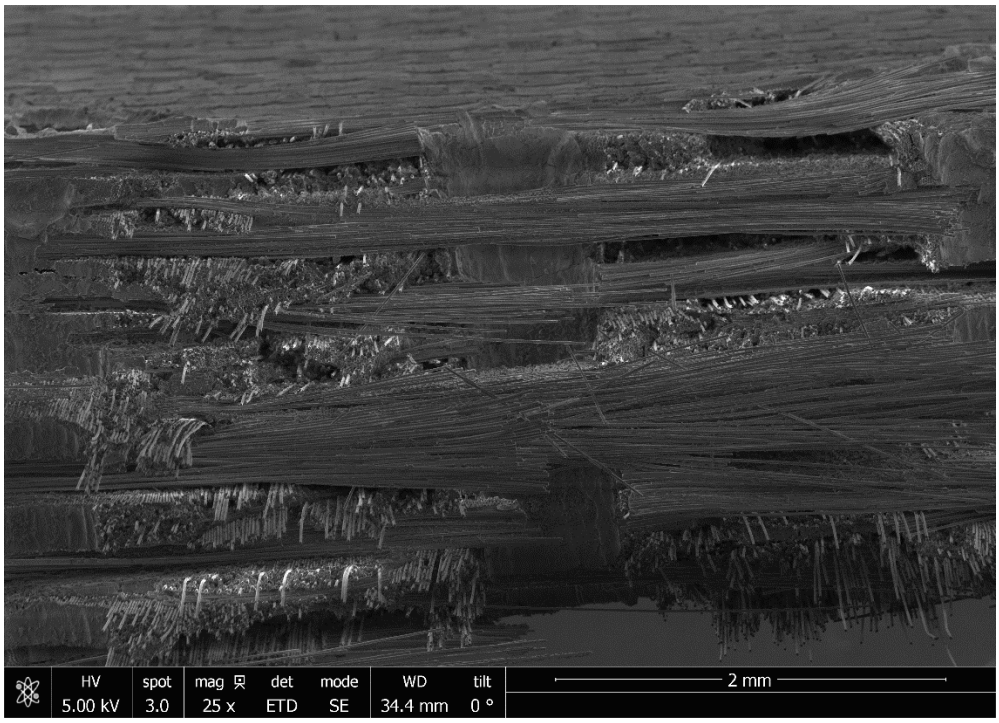


Figure B. 29: Fracture surface obtained for a N720/A specimen with effusion holes in tension to failure following 100 h of creep at 40 MPa at 1200ºC in air.

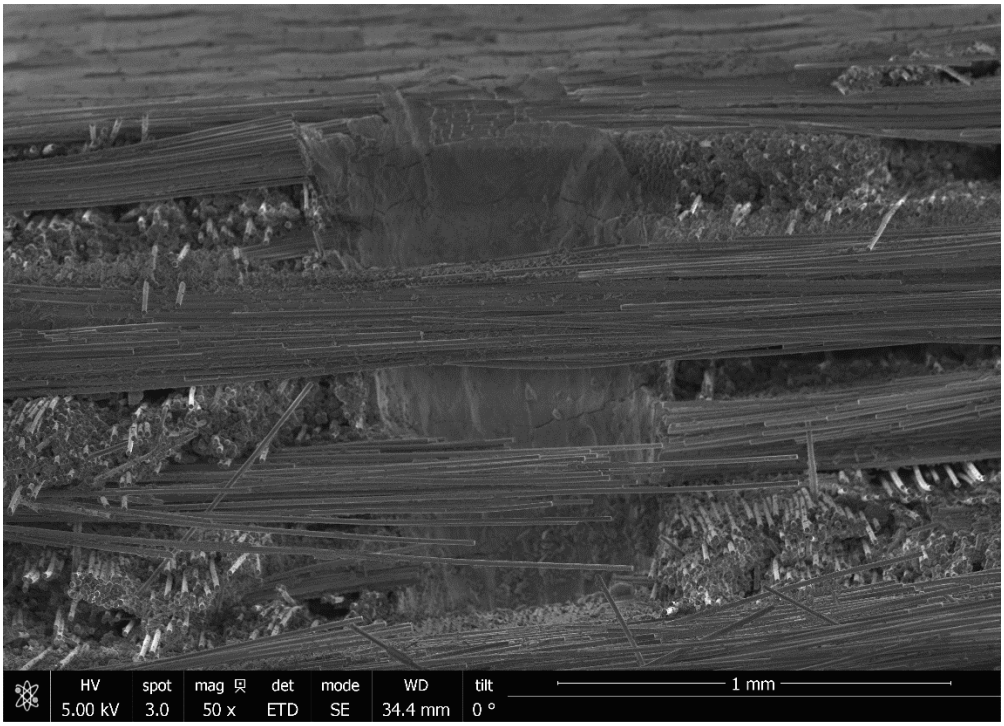


Figure B. 30: Fracture surface obtained for a N720/A specimen with effusion holes in tension to failure following 100 h of creep at 40 MPa at 1200ºC in air.

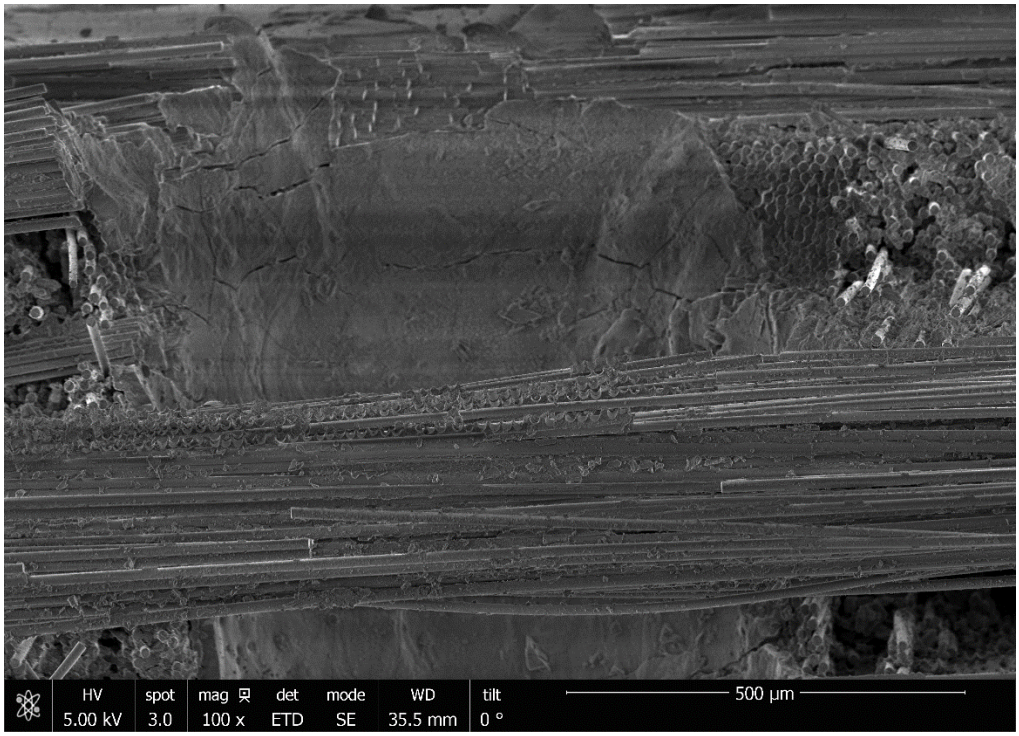


Figure B. 31: Fracture surface obtained for a N720/A specimen with effusion holes in tension to failure following 100 h of creep at 40 MPa at 1200ºC in air.

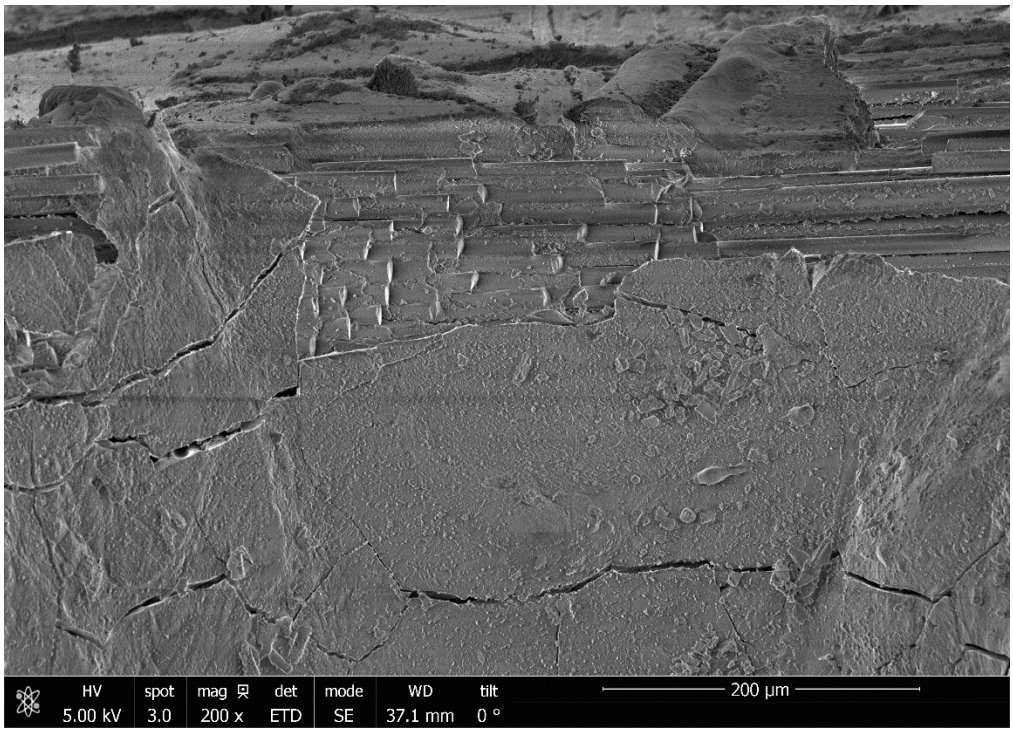


Figure B. 32: Fracture surface obtained for a N720/A specimen with effusion holes in tension to failure following 100 h of creep at 40 MPa at 1200ºC in air.

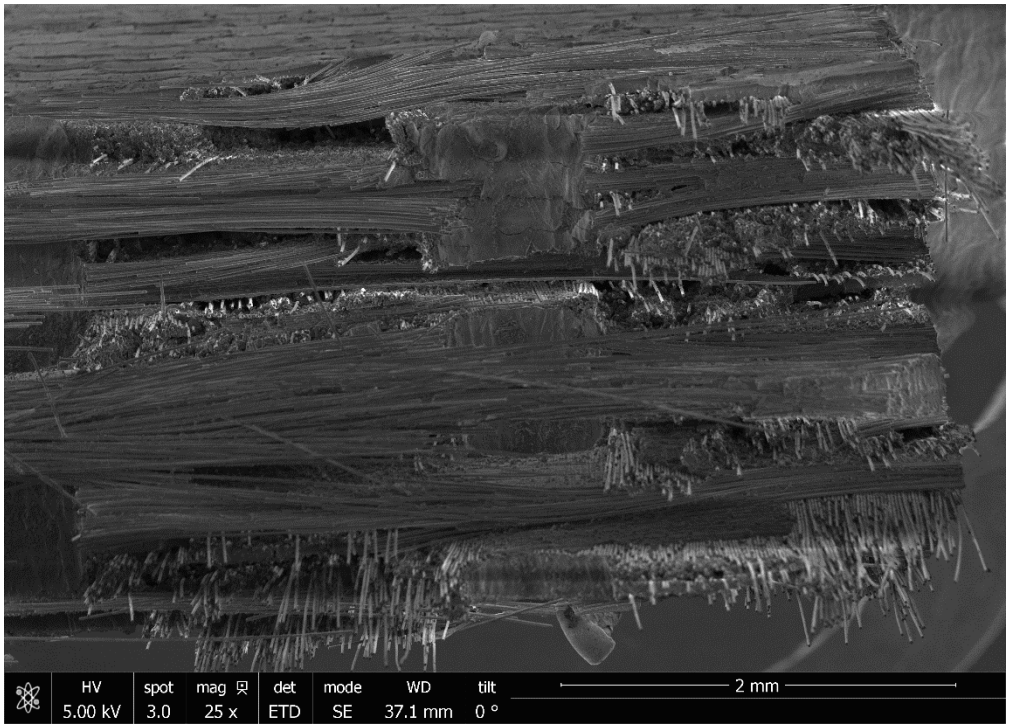


Figure B. 33: Fracture surface obtained for a N720/A specimen with effusion holes in tension to failure following 100 h of creep at 40 MPa at 1200ºC in air.

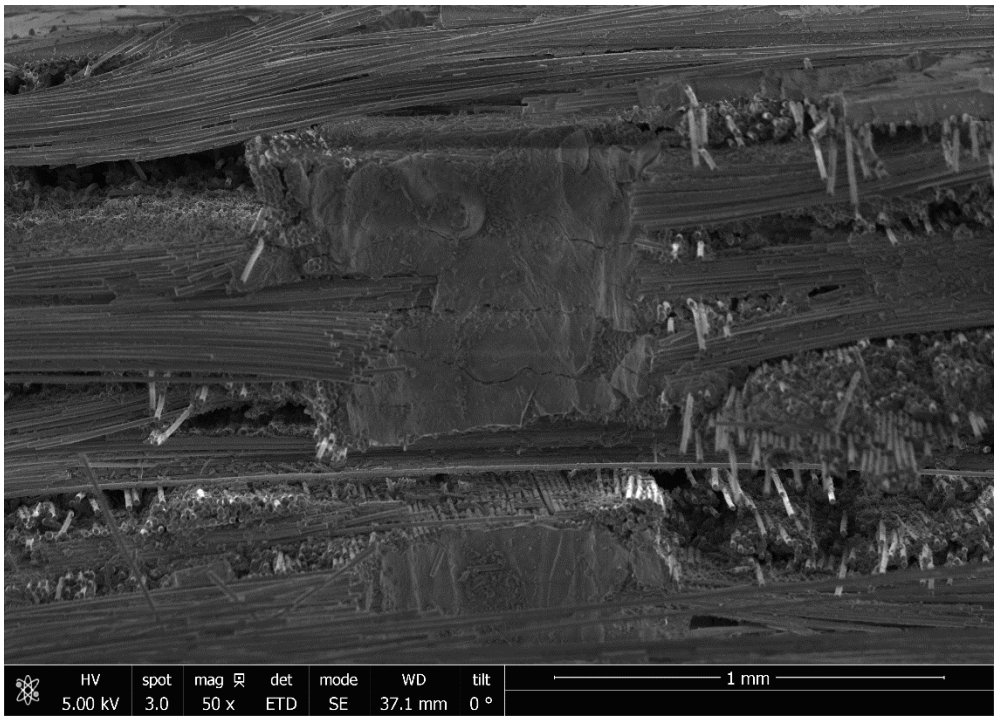


Figure B. 34: Fracture surface obtained for a N720/A specimen with effusion holes in tension to failure following 100 h of creep at 40 MPa at 1200ºC in air.

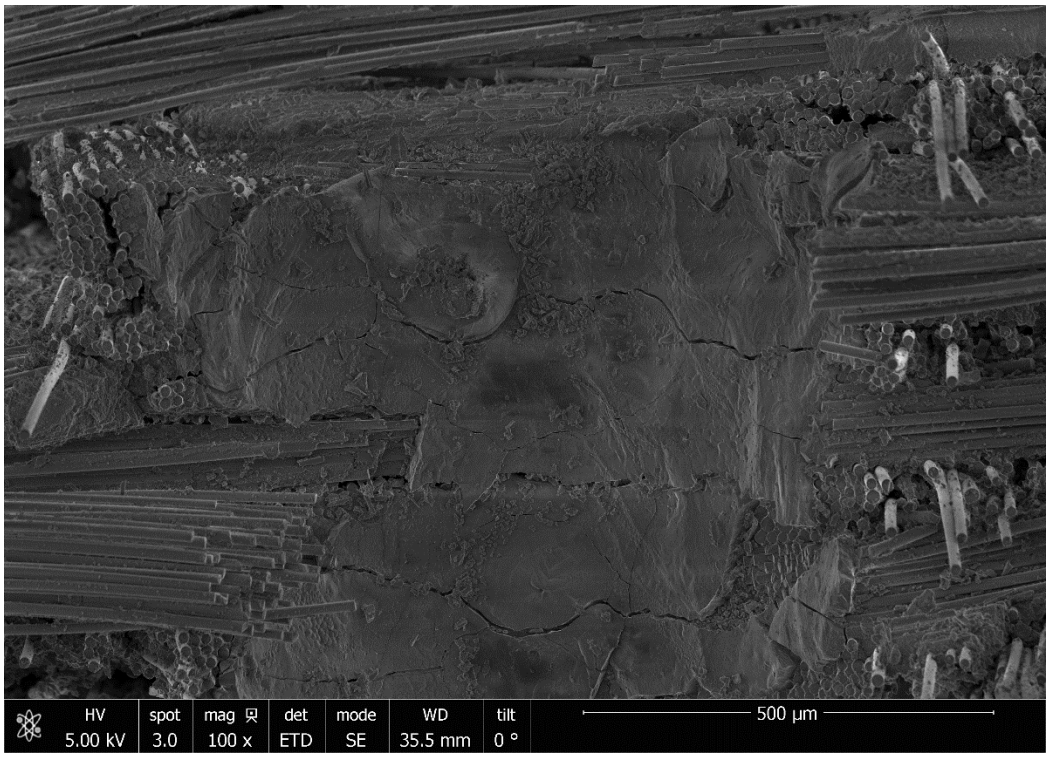


Figure B. 35: Fracture surface obtained for a N720/A specimen with effusion holes in tension to failure following 100 h of creep at 40 MPa at 1200ºC in air.

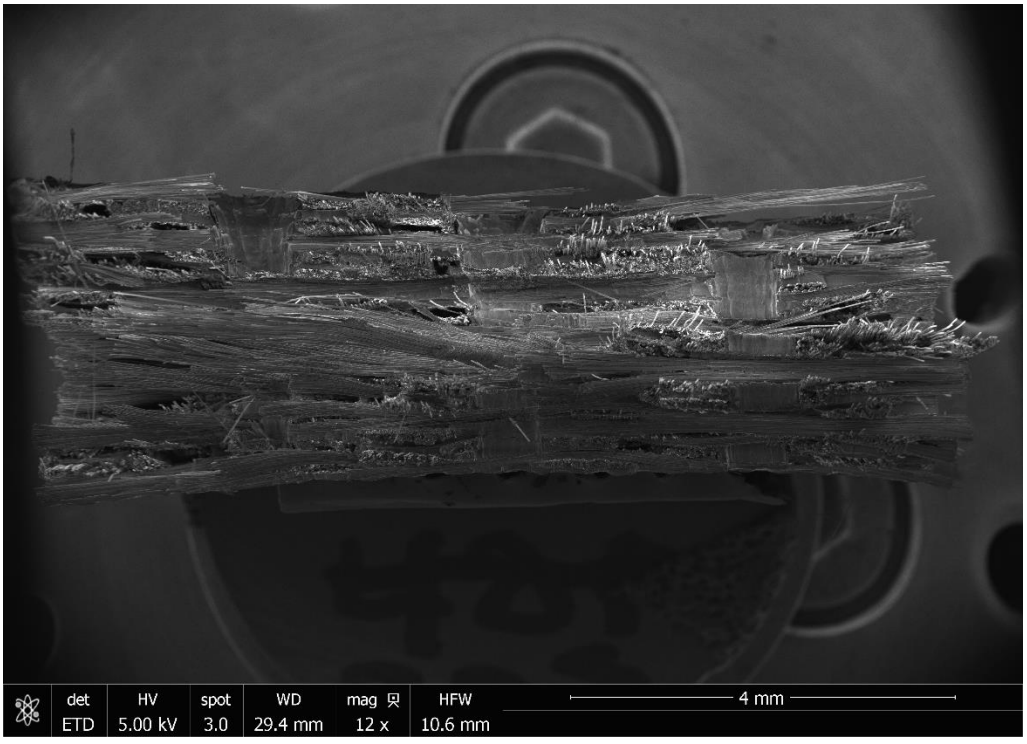


Figure B. 36: Fracture surface obtained for a N720/A specimen with effusion holes in tension to failure following 100 h of creep at 30 MPa at 1200ºC in steam

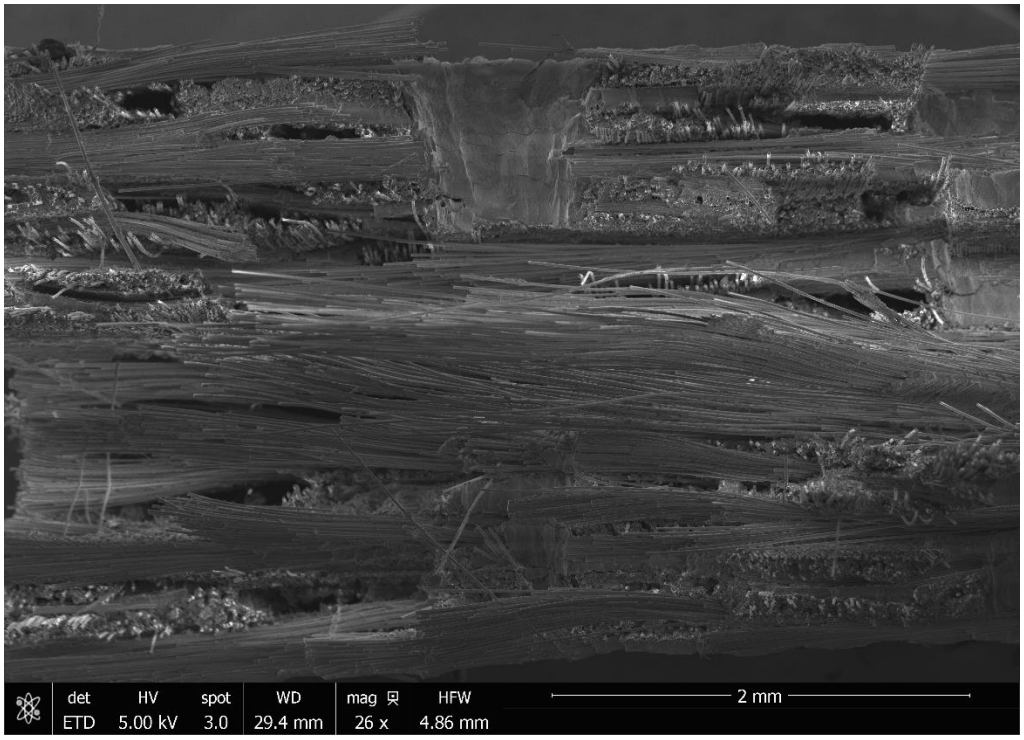


Figure B. 37: Fracture surface obtained for a N720/A specimen with effusion holes in tension to failure following 100 h of creep at 30 MPa at 1200ºC in steam

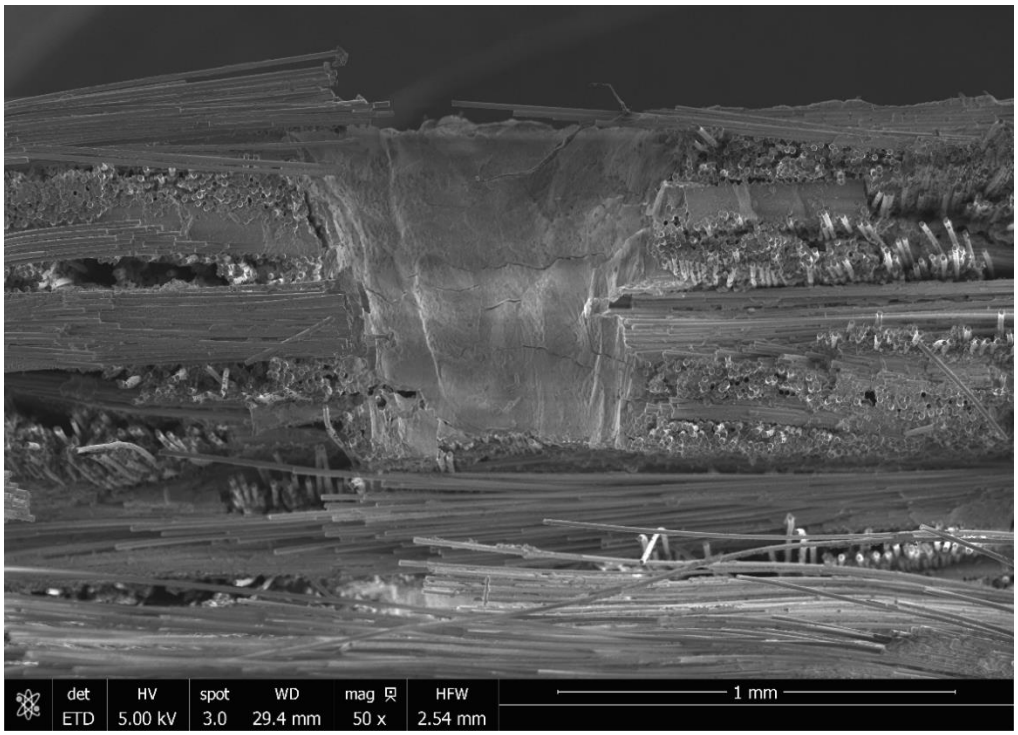


Figure B. 38: Fracture surface obtained for a N720/A specimen with effusion holes in tension to failure following 100 h of creep at 30 MPa at 1200ºC in steam

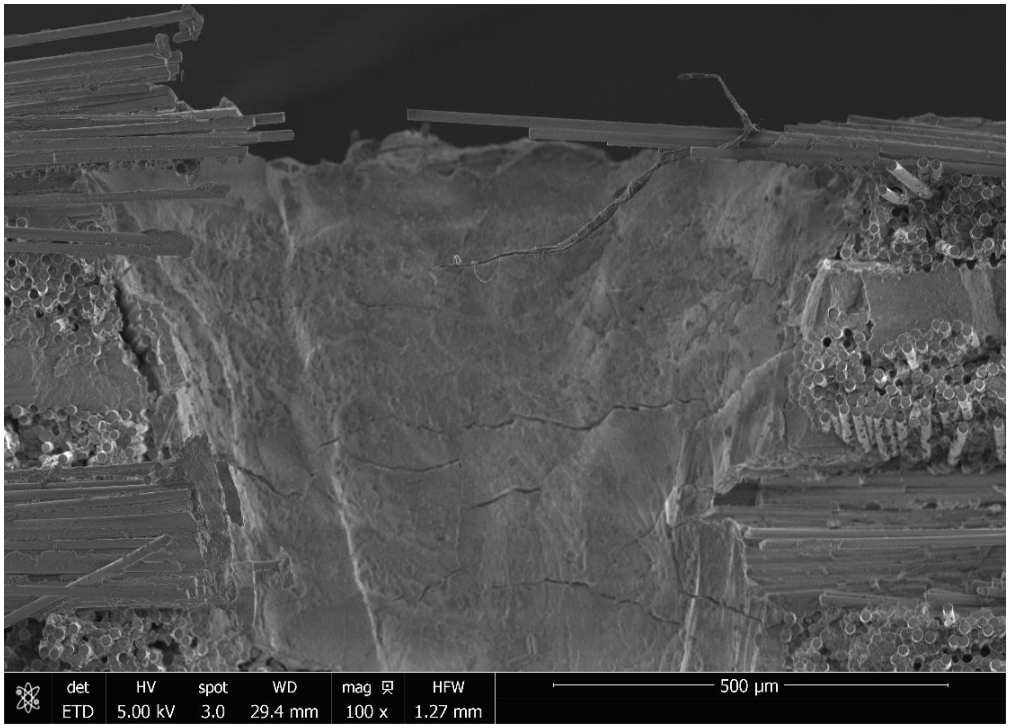


Figure B. 39: Fracture surface obtained for a N720/A specimen with effusion holes in tension to failure following 100 h of creep at 30 MPa at 1200ºC in steam.

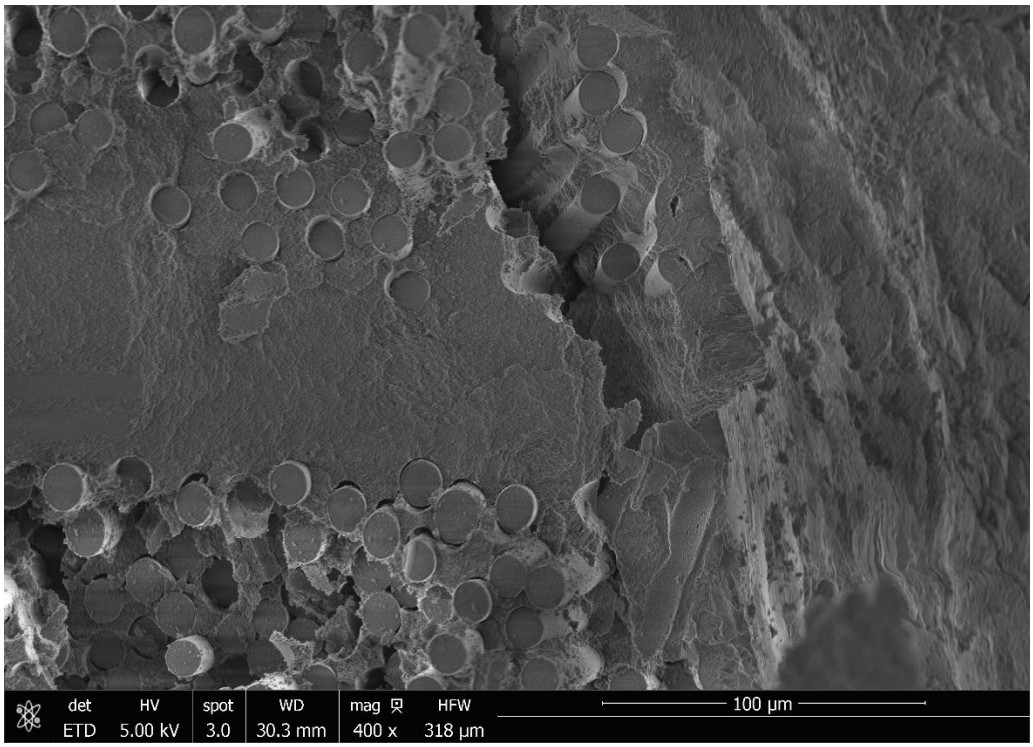


Figure B. 40: Fracture surface obtained for a N720/A specimen with effusion holes in tension to failure following 100 h of creep at 30 MPa at 1200ºC in steam.

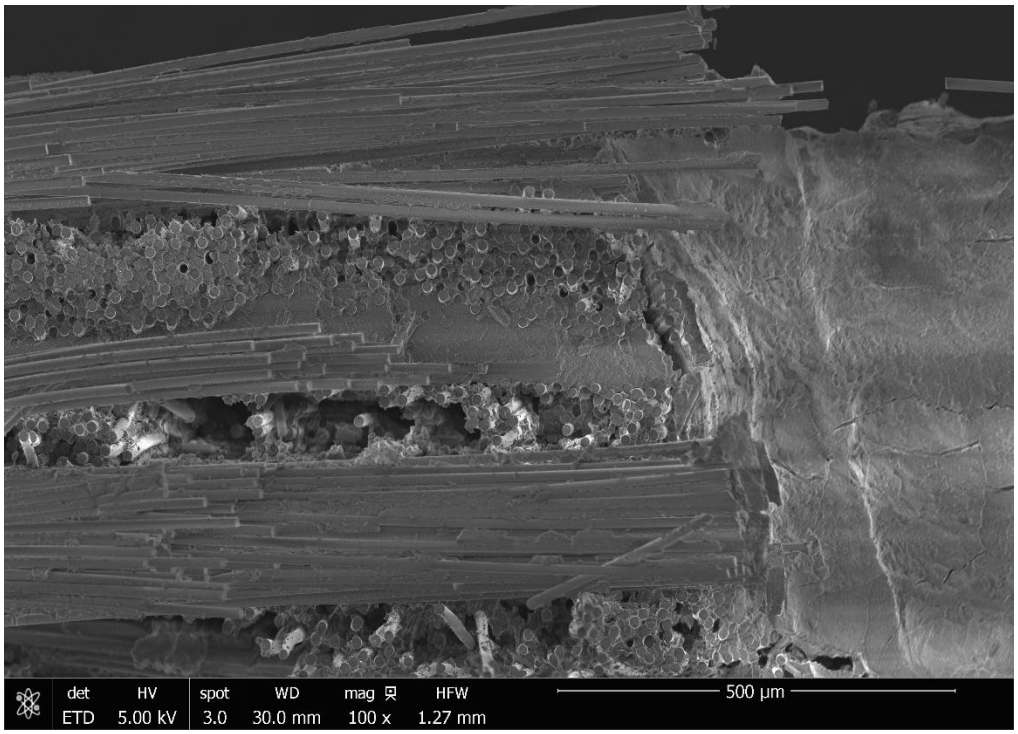


Figure B. 41: Fracture surface obtained for a N720/A specimen with effusion holes in tension to failure following 100 h of creep at 30 MPa at 1200ºC in steam.

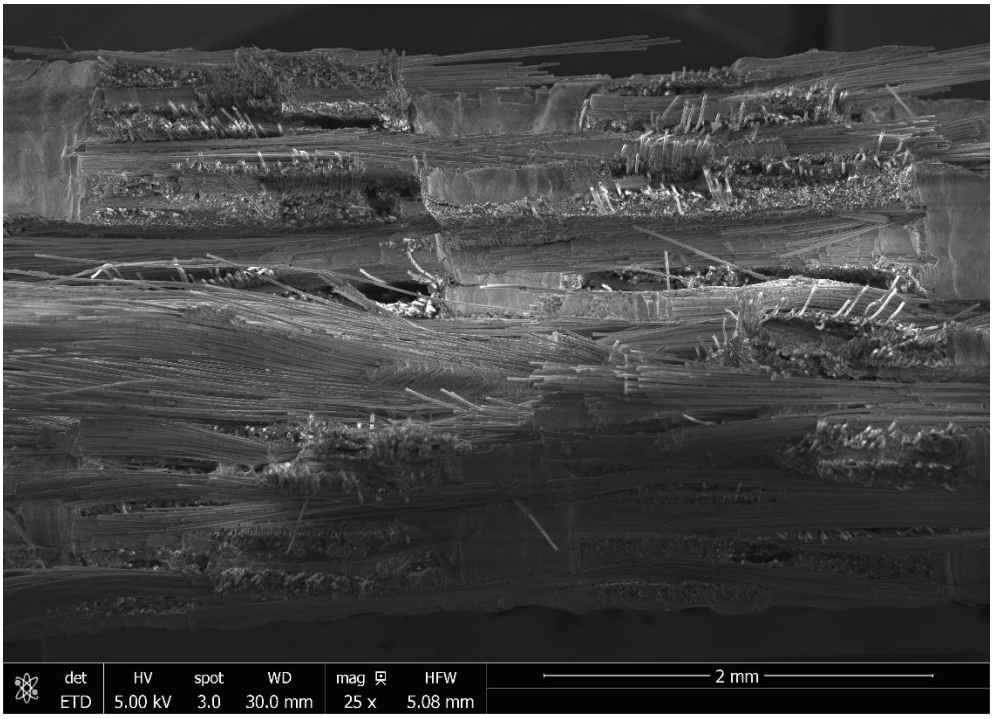


Figure B. 42: Fracture surface obtained for a N720/A specimen with effusion holes in tension to failure following 100 h of creep at 30 MPa at 1200ºC in steam.

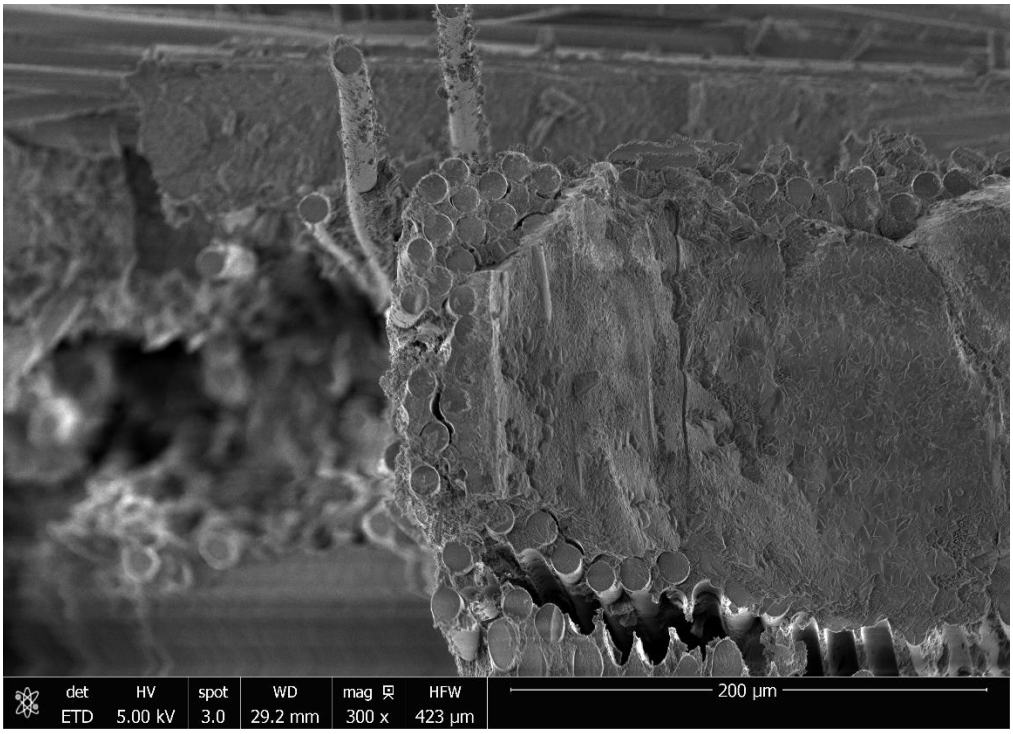


Figure B. 43: Fracture surface obtained for a N720/A specimen with effusion holes in tension to failure following 100 h of creep at 30 MPa at 1200ºC in steam.

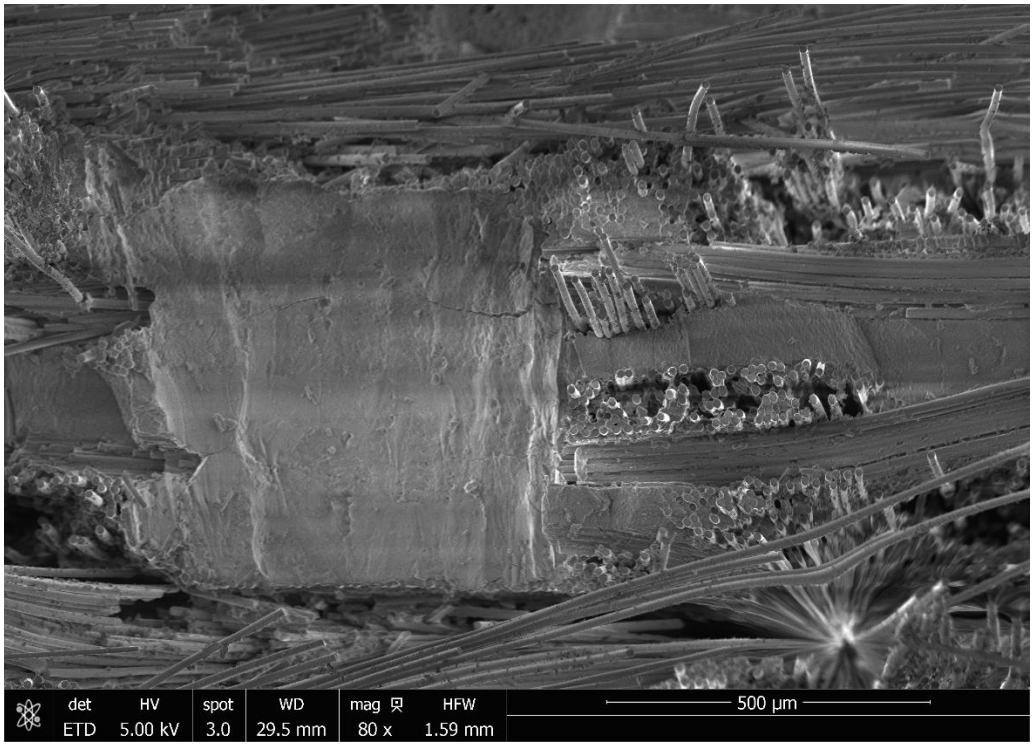


Figure B. 44: Fracture surface obtained for a N720/A specimen with effusion holes in tension to failure following 100 h of creep at 30 MPa at 1200ºC in steam.

Appendix C. Exploration of Hi-Nicalon^{TM} SiC/SiC CMC with an EBC

C.1 Material and Test Specimen

The material studied in this effort was an advanced melt-infiltrated (MI) silicon carbide/silicon carbide (SiC/SiC) CMC. The composite was reinforced with Hi-Nicalon^{TM} fibers woven in a five harness satin weave (5HSW). Laminated fiber preforms were produced from 10 plies of woven fiber fabric in a 0/90 layup. The preforms were coated via chemical vapor infiltration (CVI) with boron nitride (BN). Following the BN coating, a CVI-SiC coating was applied for rigidity. Finally, the composite was completed with a slurry infilatration of SiC particulates and infiltration of molten Si to fill in the remaining porosity. Specimens were machined into dog-bone shaped specimens. Figure C. 1 depicts the specimen geometry.

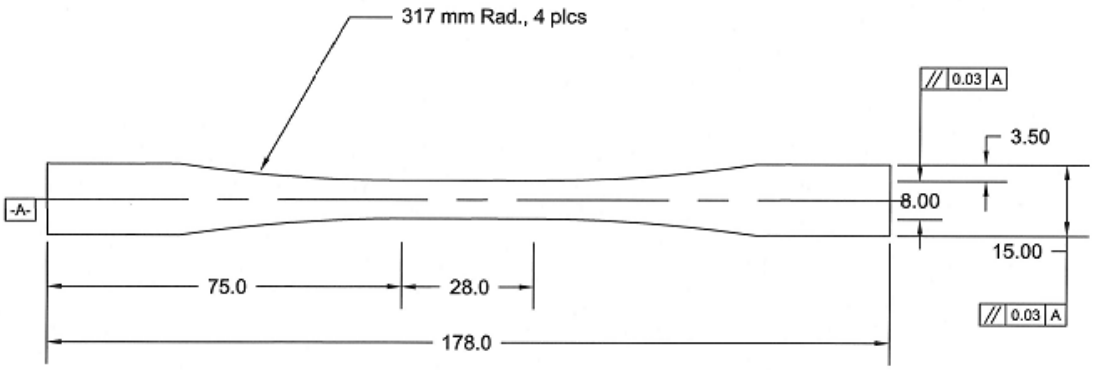


Figure C. 1: Specimen geometry for SiC/SiC CMC. All dimensions are in mm.

After machining, specimens were sent for an environmental barrier coating (EBC). The specimens were first grit blasted to roughen the surface for bonding. A silicon bond-layer ~125 μm thick was placed followed by a 254 μm thick Ytterbium disilicate ($Yb_2Si_2O_7$) top coat. Each layer was placed using air plasma spraying (APS). The final coated specimen is shown below in Figure C. 2.



Figure C. 2: Coated SiC/SiC composite

C.2 Monotonic Tensile Tests

Testing of the SiC/SiC CMC followed the procedures layed out by Ruggles-Wrenn et. Al. [19] and used the same equipment as stated in Section 3.1. Two coated specimens were tested in tension to failure at 1200ºC in laboratory air. The coating thickness was negleted in the stress calculation as it most likely does not carry load. The specimens had an Ultimate Tensile Strength (UTS) of 188 MPa and 218 MPa repectively. Boucher reported a UTS of 239 MPa for the uncoated specimens [20]. This is a 9-21% decrease from the uncoated specimens. It is believed that the grit-blasting during the coating process was the main cause for a decrease in UTS. It has been found previously that grit blasting can reduce the UTS of other materials up to 50%. Specimens were sent for grit-blasting without the top layers and optical images were taken. One such specimen was tensile tested at 1200ºC and the UTS was found to be 182 MPa. This is a 24% decrease in UTS compared to the unblasted specimens and is consistent with what was found from the coated specimens indicating that grit blasting is the cause of the decreased performance. The next step will be to look at the grit blasted specimens closer to determine the exact damage caused by the grit blasting. Since grit blasting has proven to drastically lower the UTS of this material, finding a top coat that does not require the grit blasting processing step could be a useful exploration.

C.3 Pre-Testing Optical Images



Figure C. 3: Pre-Test optical image of coated SiC/SiC.



Figure C. 4: Pre-Test optical image of coated SiC/SiC.



Figure C. 5: Pre-Test optical image of coated SiC/SiC.



Figure C. 6: Pre-Test optical image of coated SiC/SiC.



Figure C. 7: Pre-Test optical image of coated SiC/SiC.

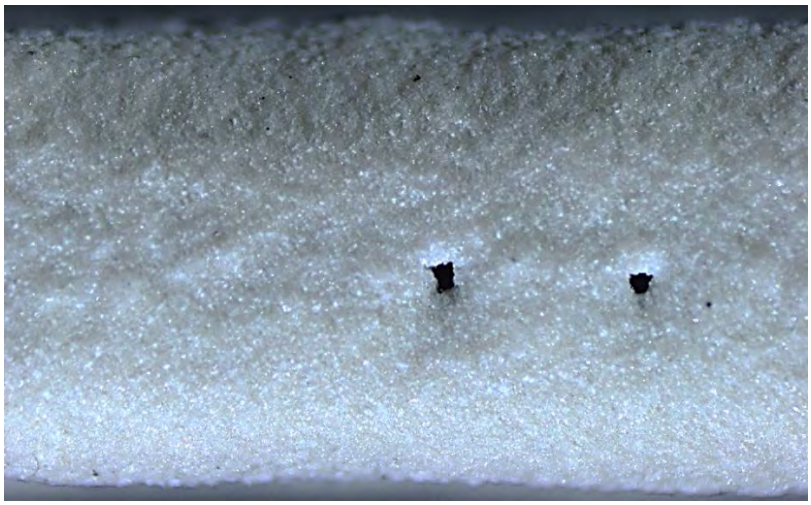


Figure C. 8: Pre-Test optical image of coated SiC/SiC.

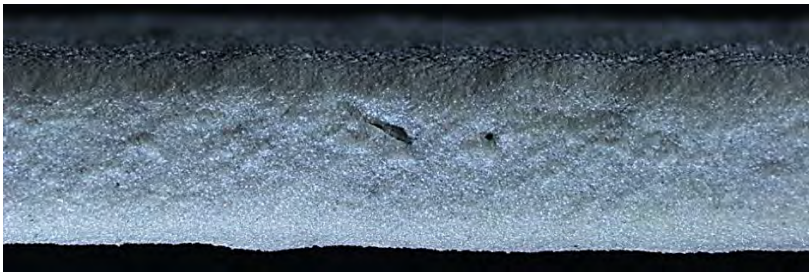


Figure C. 9: Pre-Test optical image of coated SiC/SiC.



Figure C. 10: Pre-Test optical image of coated SiC/SiC.

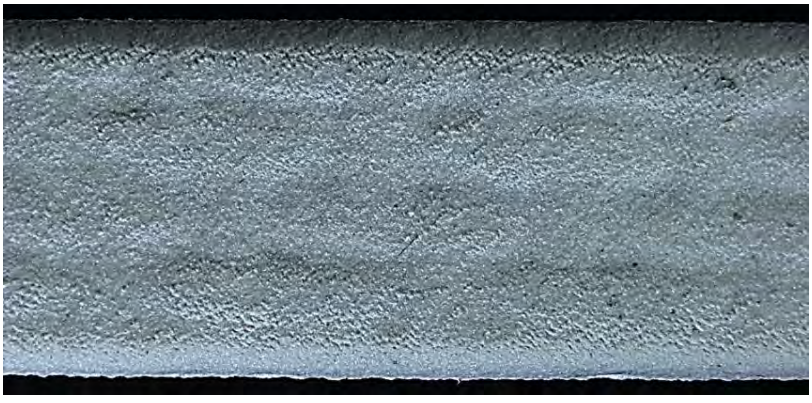


Figure C. 11: Pre-Test optical image of coated SiC/SiC.



Figure C. 12: Pre-Test optical image of coated SiC/SiC.

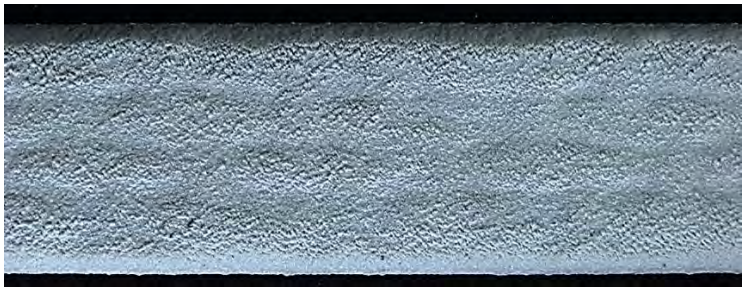


Figure C. 13: Pre-Test optical image of coated SiC/SiC.



Figure C. 14: Pre-Test optical image of coated SiC/SiC.



Figure C. 15: Pre-Test optical image of coated SiC/SiC.



Figure C. 16: Pre-Test optical image of coated SiC/SiC.



Figure C. 17: Pre-Test optical image of coated SiC/SiC.

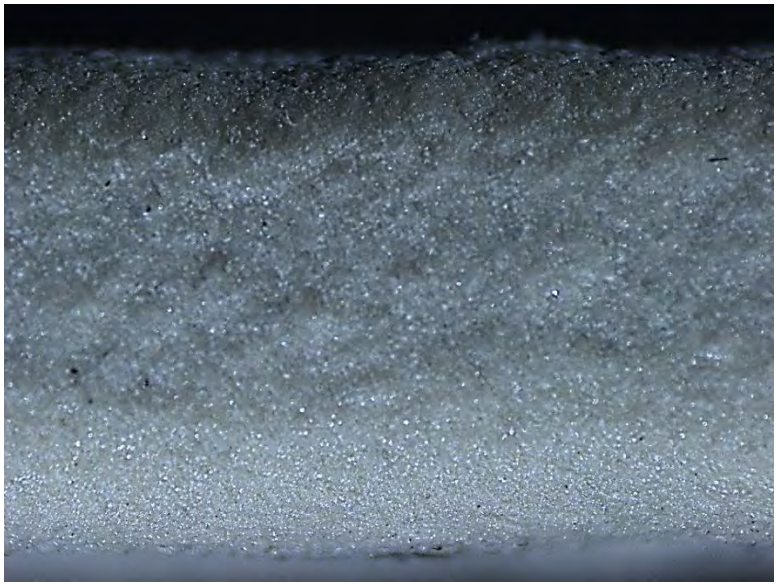


Figure C. 18: Pre-Test optical image of coated SiC/SiC.



Figure C. 19: Pre-Test optical image of coated SiC/SiC.



Figure C. 20: Pre-Test optical image of coated SiC/SiC.



Figure C. 21: Pre-Test optical image of coated SiC/SiC.



Figure C. 22: Pre-Test optical image of coated SiC/SiC.



Figure C. 23: Pre-Test optical image of coated SiC/SiC.

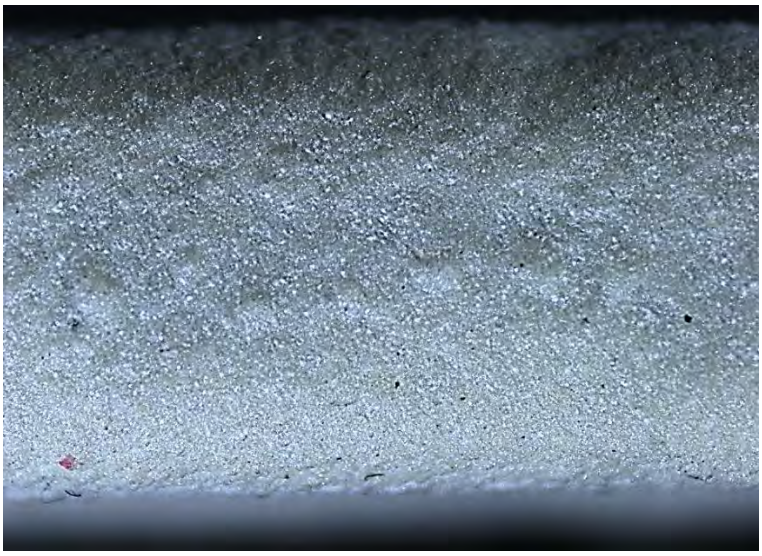


Figure C. 24: Pre-Test optical image of coated SiC/SiC.



Figure C. 25: Pre-Test optical image of coated SiC/SiC.

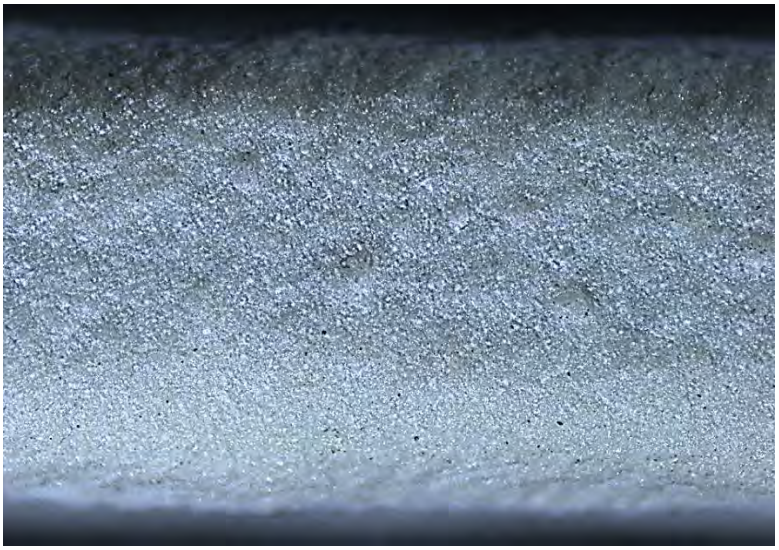


Figure C. 26: Pre-Test optical image of coated SiC/SiC.



Figure C. 27: Pre-test optical image of an SiC/SiC specimen without grit blasting.

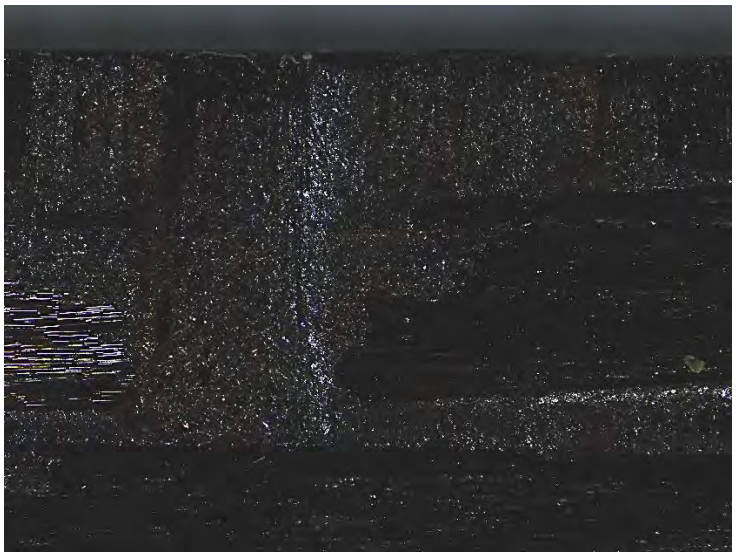


Figure C. 28: Pre-test optical image of an SiC/SiC specimen without grit blasting.



Figure C. 29: Pre-test optical image of an SiC/SiC specimen with grit blasting.

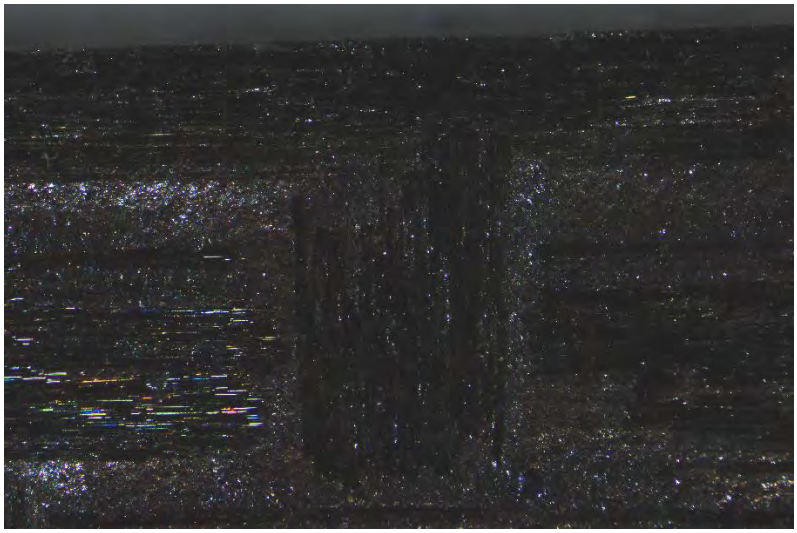


Figure C. 30: Pre-test optical image of an SiC/SiC specimen with grit blasting.

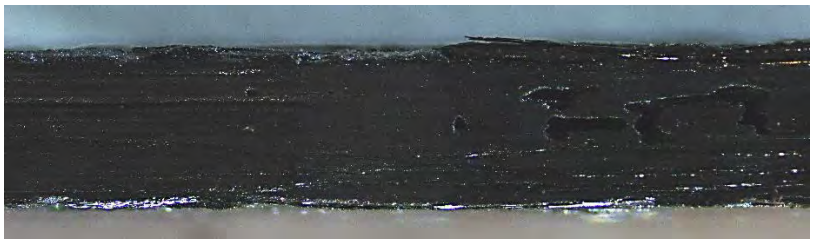


Figure C. 31: Pre-test optical image of an SiC/SiC specimen with grit blasting.

Bibliography

[1] K. K. Chawla, Ceramic Matrix Composites, London: Chapman & Hall, 1993.

[2] K. A. Keller, G. Jefferson and R. J. Kerans, "Oxide-Oxide Composites," in *Ceramic Matrix Composites Materials, Modeling, and Technology*, New Jersey, John Wiley & Sons, Inc, 2015, pp. 236-264.

[3] F. W. Zok, "Developments in Oxide Fiber Composties," *Journal of the American Ceramic Society,* vol. 89, no. 11, pp. 3309-3324, 2006.

[4] "TRUMPF Drilling," TRUMPF, 2018. [Online]. Available: https://www.trumpf.com/en_US/applications/laser-cutting/drilling/. [Accessed 16 January 2018].

[5] J. C. Braun, *Effects of Temperature and Environment on Creep Behavior of an Oxide-Oxide Ceramic Matric Composite,* Wright Patterson Air Force Base, 2007.

[6] G. T. Siegert, *Effect on Environment on Creep Behavior of an Oxide/Oxide CFCC with 45 Fiber Orientation,* Wright Patterson Air Force Base, 2006.

[7] J. M. Mehrman, *Effect of Hold Times on Fatigue Behavior of Nextel 720/Alumina Ceramic Matrix Composite at 1200 C in Air and in Steam Environment,* Wright-Patterson Air Force Base, 2006.

[8] P. A. Koutsoukos, *Effects of Environement on Creep Behavior of Two Oxide-Oxide Ceramic Matrix Composites at 1200 C,* Wright Patterson Air Force Base, 2006.

[9] V. A. Kramb, R. John and L. P. Zawada, "Notched Fracture Behavior of an Oxide/Oxide Ceramic-Matrix Composite," *Journal of the American Ceramic Socitey,* vol. 82, no. 11, pp. 3087-3096, 1999.

[10] D. J. Buchanan, R. John and L. P. Zawada, "Notched Fracture Behavior of Oxide/Oxide Nextel720/AS Composite," in *24th Annual Conference on Composites, Advanced Ceramics, Materials, and Structures:A*, Cocoa Beach, 2000.

[11] R. John, D. J. Buchanan and L. P. Zawada, "Creep Deformation and Rupture Behavior of a Notched Oxide/Oxide Nextel720/AS Compostie," in *24th Annual Conference on Composites, Advanced Ceramics, Materials, and Structures:A*, Cocoa Beach, 2000.

[12] D. J. Buchanan, V. J. Kramb, R. John and L. P. Zawada, "Effect of Small Effusion Holes on Creep Rupture Behavior of Oxide/Oxide Nextel720/AS Composite," in *25th Annual Conference on Composites, Advanced Ceramics, MAterials, and Structures:A*, Cocoa Beach, 2001.

[13] S. Mall and M. A. Sullivan, "Tension-Tension Fatigue Behavior of Notched Nextel720/Alumina (N720/A) at Elevated Temperature," *Science and Engineering of Composite Materials,* vol. 16, no. 4, pp. 235-245, 2009.

[14] U. D. COI Ceramics.

[15] L. B. Harlan, *Creep-Rupture Behavior of an Oxide/Oxide Ceramic Matrix Composite at Elevated Temperatures in Air and Steam Environments,* Wright-Patterson AFB, 2005.

[16] G. Hetrick, *Effects of Frequency and Environment on Fatigue Behavior of an Oxide-Oxide Ceramic Matrix Composite at 1200C,* Wright-Patterson AFB, OH: School of Engineering and Management, Air Force Institute of Technology, 2006.

[17] C. J. Armani, *Creep Perfromance of Oxide Ceramic Figer Materials at Elevated Temperature in Air and in Steam,* Wright-Patterson AFB, OH: Air Force Institute of Technology, 2011.

[18] M. Ruggles-Wrenn and R. Lanser, "Tension-compression fatigue of an oxide/oxide ceramic composite at elevated temperature," *Elsevier,* 2016.

[19] M. Ruggles-Wrenn, N. Boucher and C. Przybyla, "Fatigue of three advanced SiC/SiC ceramic matrix composites at 1200C in air and in steam," *International Journal of Applied Ceramic Technology,* pp. 1-13, 2017.

[20] N. Boucher, "Fatigue Behavior of an Advanced Melt-Infiltrated SiC/SiC Composite at 1200C in air and in steam," Air Force Institute of Technology, WPAFB, 2017.

[21] F. W. Zok and C. G. Levi, "Mechanical Properties of Porous-Matix Ceramic Composties," in *Advanced Engineering Materials*, 2001, pp. 15-23.

REPORT DOCUMENTATION PAGE

Form Approved
OMB No. 0704-0188

The public reporting burden for this collection of information is estimated to average 1 hour per response, including the time for reviewing instructions, searching existing data sources, gathering and maintaining the data needed, and completing and reviewing the collection of information. Send comments regarding this burden estimate or any other aspect of this collection of information, including suggestions for reducing the burden, to Department of Defense, Washington Headquarters Services, Directorate for Information Operations and Reports (0704-0188), 1215 Jefferson Davis Highway, Suite 1204, Arlington, VA 22202-4302. Respondents should be aware that notwithstanding any other provision of law, no person shall be subject to any penalty for failing to comply with a collection of information if it does not display a currently valid OMB control number.

PLEASE DO NOT RETURN YOUR FORM TO THE ABOVE ADDRESS.

1. REPORT DATE *(DD-MM-YYYY)*	2. REPORT TYPE	3. DATES COVERED *(From - To)*
22-02-2018	Master's Thesis	August 2017-March 2018

4. TITLE AND SUBTITLE

Creep of N720/A Ceramic Matrix Composite with Laser Drilled Effusion Holes at 1200°C in Air and in Steam

5a. CONTRACT NUMBER

5b. GRANT NUMBER

5c. PROGRAM ELEMENT NUMBER

6. AUTHOR(S)

Minor, Savannah N, 2d Lt

5d. PROJECT NUMBER

5e. TASK NUMBER

5f. WORK UNIT NUMBER

7. PERFORMING ORGANIZATION NAME(S) AND ADDRESS(ES)

Air Force Institute of Technology
Graduate School of Engineering and Management (AFIT/EN)
2950 Hobson Way, Building 640
WPAFB OH 45433-8865

8. PERFORMING ORGANIZATION REPORT NUMBER

AFIT-ENY-MS-18-M-279

9. SPONSORING/MONITORING AGENCY NAME(S) AND ADDRESS(ES)

AFRL/RXCC
Dr. Craig Przybyla; Craig.Przybyla@us.af.mil
Dr. Eric Jones; Eric.Jones.50@us.af.mil

10. SPONSOR/MONITOR'S ACRONYM(S)

AFRL/RXCC

11. SPONSOR/MONITOR'S REPORT NUMBER(S)

12. DISTRIBUTION/AVAILABILITY STATEMENT

Approved for public release; distribution unlimited.

13. SUPPLEMENTARY NOTES

This material is declared a work of the U.S. Government and is not subject to copyright protection in the United States.

14. ABSTRACT

Creep behavior of an oxide-oxide ceramic matrix composite (CMC) containing an array of effusion holes was investigated at 1200ºC in air and in steam. The composite (N720/A) consisted of a porous alumina matrix reinforced with alumina-mullite NextelTM 720 fibers. Test specimens had an array of 17 effusion holes with 0.5-mm diameter. The effusion holes were drilled through the specimen thickness normal to the specimen surface using a CO2 laser. Effect of the effusion holes on tensile properties was evaluated tension tests to failure at 1200°C in air. Creep of specimens with effusion holes at 1200°C was studied for creep stresses ranging from 40 to 100 MPa in air and from 30 to 90 MPa in steam. Creep run-out was defined as 100 h creep stress. Effect of the laser-drilled effusion holes on creep was assessed by comparing the results of the present study with the results from prior work on unnotched N720/A specimens. The presence of laser-drilled holes significantly reduced creep lifetimes in both air and steam. Post-test microstructure of the composite was examined; damage and failure mechanisms were assessed. Dramatic loss of creep resistance in specimens with holes is due to extensive composite degradation caused by laser drilling.

15. SUBJECT TERMS

Creep of a ceramic matrix composite.

16. SECURITY CLASSIFICATION OF:			17. LIMITATION OF ABSTRACT	18. NUMBER OF PAGES	19a. NAME OF RESPONSIBLE PERSON
a. REPORT	b. ABSTRACT	c. THIS PAGE			Dr. Marina Ruggles-Wrenn
U	U	U	UU	186	19b. TELEPHONE NUMBER *(Include area code)* 864-255-3636 marina.ruggles-wrenn@afit.edu

Reset

Standard Form 298 (Rev. 8/98)
Prescribed by ANSI Std. Z39.18

INSTRUCTIONS FOR COMPLETING SF 298

1. REPORT DATE. Full publication date, including day, month, if available. Must cite at least the year and be Year 2000 compliant, e.g. 30-06-1998; xx-06-1998; xx-xx-1998.

2. REPORT TYPE. State the type of report, such as final, technical, interim, memorandum, master's thesis, progress, quarterly, research, special, group study, etc.

3. DATES COVERED. Indicate the time during which the work was performed and the report was written, e.g., Jun 1997 - Jun 1998; 1-10 Jun 1996; May - Nov 1998; Nov 1998.

4. TITLE. Enter title and subtitle with volume number and part number, if applicable. On classified documents, enter the title classification in parentheses.

5a. CONTRACT NUMBER. Enter all contract numbers as they appear in the report, e.g. F33615-86-C-5169.

5b. GRANT NUMBER. Enter all grant numbers as they appear in the report, e.g. AFOSR-82-1234.

5c. PROGRAM ELEMENT NUMBER. Enter all program element numbers as they appear in the report, e.g. 61101A.

5d. PROJECT NUMBER. Enter all project numbers as they appear in the report, e.g. 1F665702D1257; ILIR.

5e. TASK NUMBER. Enter all task numbers as they appear in the report, e.g. 05; RF0330201; T4112.

5f. WORK UNIT NUMBER. Enter all work unit numbers as they appear in the report, e.g. 001; AFAPL30480105.

6. AUTHOR(S). Enter name(s) of person(s) responsible for writing the report, performing the research, or credited with the content of the report. The form of entry is the last name, first name, middle initial, and additional qualifiers separated by commas, e.g. Smith, Richard, J, Jr.

7. PERFORMING ORGANIZATION NAME(S) AND ADDRESS(ES). Self-explanatory.

8. PERFORMING ORGANIZATION REPORT NUMBER. Enter all unique alphanumeric report numbers assigned by the performing organization, e.g. BRL-1234; AFWL-TR-85-4017-Vol-21-PT-2.

9. SPONSORING/MONITORING AGENCY NAME(S) AND ADDRESS(ES). Enter the name and address of the organization(s) financially responsible for and monitoring the work.

10. SPONSOR/MONITOR'S ACRONYM(S). Enter, if available, e.g. BRL, ARDEC, NADC.

11. SPONSOR/MONITOR'S REPORT NUMBER(S). Enter report number as assigned by the sponsoring/ monitoring agency, if available, e.g. BRL-TR-829; -215.

12. DISTRIBUTION/AVAILABILITY STATEMENT. Use agency-mandated availability statements to indicate the public availability or distribution limitations of the report. If additional limitations/ restrictions or special markings are indicated, follow agency authorization procedures, e.g. RD/FRD, PROPIN, ITAR, etc. Include copyright information.

13. SUPPLEMENTARY NOTES. Enter information not included elsewhere such as: prepared in cooperation with; translation of; report supersedes; old edition number, etc.

14. ABSTRACT. A brief (approximately 200 words) factual summary of the most significant information.

15. SUBJECT TERMS. Key words or phrases identifying major concepts in the report.

16. SECURITY CLASSIFICATION. Enter security classification in accordance with security classification regulations, e.g. U, C, S, etc. If this form contains classified information, stamp classification level on the top and bottom of this page.

17. LIMITATION OF ABSTRACT. This block must be completed to assign a distribution limitation to the abstract. Enter UU (Unclassified Unlimited) or SAR (Same as Report). An entry in this block is necessary if the abstract is to be limited.